PRODUCTION OF ANTIBACTERIAL HYDROXYAPATITE

by

Mehmet İPEKOĞLU

B.S., Mechanical Engineering, Boğaziçi University, 2001

M.S., Mechanical Engineering, Boğaziçi University, 2004

Submitted to the Institute for Graduate Studies in
Science and Engineering in partial fulfillment of
the requirements for the degree of
Doctor of Philosophy

Graduate Program in Mechanical Engineering

Boğaziçi University

2011

To my dear grandmother, Emine İPEKOĞLU
Always remembering with love and pride
how much I owe her
not only for her infinite and embracing love and compassion
but also for enlightening for me the way
towards being a good man
and leading a life I can be proud of

and

To my dear uncle, Selçuk BATUR
For being my exemplary idol
of a true and noble man
living an honest and fruitful life

Wish they were here with me…

ACKNOWLEDGEMENTS

I would like to express my sincere gratitude to my thesis supervisor and "Doktorvater" Prof. Dr. Sabri ALTINTAŞ for his irreplaceable advice, guidance, support and tolerance throughout this study. He was not only a wonderful supervisor and an inspiring mentor paving the way for his student but I have also learned invaluable lessons from him about being a visionary scientist, a dedicated teacher and a life-long learner. Without his help no single word of this work would exist.

I am very grateful to Prof. Dr. Mahmut Ahsen SAVAŞ for his supporting guidance, positive motivation and illuminating instructions all the time and Prof. Dr. Gökhan BAYKAL for his encouragement, support and enlightening discussions. They are precious role models not only as valuable scientists but also as devoted teachers.

I am very thankful to Assoc. Prof. Dr. Mehmet Ali GÜLGÜN from the Materials Science and Engineering Department of Sabanci University and, Prof. Dr. Selim KÜSEFOĞLU and his assistant Dr. Cem ÖZTÜRK from the Chemistry Department of Boğaziçi University for their valuable support and sincere help.

I am very much indebted to my dear friends and colleagues Dr. Nazım MAHMUTYAZICIOĞLU, Dr. Önder ALBAYRAK and İlker ÖZDEN not only for their fruitful scientific and technical discussions but also for their precious friendship and profound support.

I want to thank all the academic members of the Mechanical Engineering Department of Boğaziçi University, the academic members of the Chemical and Metallurgical Engineering Faculty of Istanbul Technical University and the administrative staff of the Mechanical Engineering Department of Boğaziçi University.

I would like to sincerely thank all my dearest friends and brothers in-heart Can YALÇIN, Dr. Tulga ERSAL, Özgün ÖZIŞIKYILMAZ and Dr. Arsun ARTEL very much

for being with me and being there for me throughout my life all the way in the good and hard times. They are of so great significance to me.

I am grateful to my dear wife and best friend Ayşe Mine ÇELEBİ İPEKOĞLU first of all for her unconditional and unlimited love from the beginning on and for her understanding, tolerance, patience, support and help in all circumstances, no matter what, not only throughout my studies but all the way throughout our life together. With her existence I have always felt myself complete as a whole. My deep love supersedes my sincere thankfulness.

I am thankful to my dear grandmother Fatma BATUR, my dear aunt Dr. Ayfer ÇOKUĞRAŞ, my dear cousin Dr. Zeynep Aslı BATUR ÇALIŞ and my dear cousin prospective Dr. Işıl ÇOKUĞRAŞ who has always been and always will be a true sister to me and my best friend than a cousin and never ever lets me down no matter what happens. I have always felt being wrapped up with their love. They are not only my family but they are my ties I hang on to life with. I love them from the bottom of my heart.

And last, but not least, all my grateful and sincere thanks and all my deepest love goes to my dear father, Şeref Aydın İPEKOĞLU, and my dear mother, Prof. Dr. Nursen Adile İPEKOĞLU. No word can express how thankful, happy and proud I am for them being my parents and for me being their child. They have always done much more than any parent could do for their children. They have done more than anything and everything a parent is capable of to help me reach where now I am. I am aware of their enormous sacrifices and I wish I could do the slightest of these for them. I would be the happiest person on earth if I could make them smile and honor them even a little bit with what I have become and achieved in life so far. I owe them everything I am and everything I will be, everything I have done and everything I will do in the future. Without them I could not exist in any terms and I could not be here. All these years of hard work and study, their scientific value and their contributions to my personal progress put aside, are so much worth for giving me the humble opportunity to write just this one single paragraph. They are my true joy, my inner treasure and my sound backbone. I love them so deeply…

FOREWORD

The author particularly would like to thank The Scientific and Technological Research Council of Turkey (Türkiye Bilimsel ve Teknolojik Araştırma Kurumu, TÜBİTAK) for its financial support through the 2211 - Ph.D. Fellowship for Domestic Students Program (2211 - Yurt İçi Doktora Burs Programı) during this study.

This work was financially supported in part by The Scientific and Technological Research Council of Turkey (Türkiye Bilimsel ve Teknolojik Araştırma Kurumu, TUBİTAK) through the project 107M556, State Planning Organization (Devlet Planlama Teşkilatı, DPT) through the project 03K120250, and by Boğaziçi University Scientific Research Projects (Boğaziçi Üniversitesi Bilimsel Araştırma Projeleri, BAP) through the project 08HA601D.

ABSTRACT

PRODUCTION OF ANTIBACTERIAL HYDROXYAPATITE

Hydroxyapatite was produced by rapid microwave synthesis method. Effects of microwave power and duration were examined on the powder morphology of the hydroxyapatite powder during the synthesis process and microwave aging was found to be an effective method to produce hydroxyapatite. Silver was added in different amounts to calcium deficient and stoichiometric hydroxyapatite during the synthesis process using microwave, the antibacterial activities of the powders produced were analyzed and silver addition was found to impart antibacterial properties to hydroxyapatite. Hydroxyapatite powders containing different amounts of silver were heat treated at temperatures between 900-1100 °C, the decomposition of the powders were analyzed using XRD and FTIR analysis, the increasing heat treatment temperature and increasing silver amount were found to negatively effect the decomposition of the powders. The hydroxyapatite powders produced which do and do not contain silver were used to produce coatings on titanium substrates, hydroxyapatite decomposition at high sintering temperatures was effectively inhibited by the use of titanium dioxide inner layer. The effects of coating voltage and coating duration of the titanium dioxide inner layer on the mechanical properties of the coatings were examined, use of lower voltage and shorter coating times for the titanium dioxide inner layer were found to increase the mechanical strength of the coated hydroxyapatite.

Keywords: Hydroxyapatite, silver, antibacterial, titanium, coating, sintering.

ÖZET

ANTİBAKTERİYEL HİDROKSİAPATİT ÜRETİMİ

Mikrodalga yardımıyla hidroksiapatit sentezlenmiştir. Sentezlenme sırasında uygulanan mikrodalga gücü ve süresinin elde edilen tozların morfolojisi üzerindeki etkileri incelenmiş ve mikrodalga yaşlandırma işleminin hidroksiapatit üretiminde etkili bir yol olduğu sonucuna ulaşılmıştır. Mikrodalga ile sentezleme işlemi sırasında üretilen kalsiyum eksik ve stokiyometrik hidroksiapatite farklı oranlarda gümüş ilave edilmiş, bu şekilde üretilen tozların antibakteriyel etkinlikleri incelenmiş ve eklenen gümüşün hikdroksiapatite antibakteriyel etkinlik kazandırdığı belirlenmiştir. Farklı oranlarda gümüş içeren tozlar 900-1100 °C arasında ısıl işleme tabi tutulmuş, tozların bozunması XRD ve FTIR analizi yardmıyla incelenmiş ve artan ısıl işlem sıcaklığı ve artan gümüş ilavesi miktarının tozların bozunma karakteristiklerini olumsuz yönde etkilediği sonucuna ulaşılmıştır. Gümüş katkılı ve gümüş katkısız olarak üretilen tozlar titanyum altlıklar üzerine kaplanmış, yüksek sinterleme sıcaklıklarında meydana gelen hidroksiapatit bozunması titanium dioksit ara tabaka uygulaması ile önlenmiştir. Titanyum dioksit ara tabaka kaplama gerilimi ve süresinin kaplamaların mekanik dayanımlarına etkileri incelenmiş, düşük gerilim ve kısa kaplama süreleri uygulanmasıyla kaplanan hidroksiapatitin mekanik dayanımlarının arttırılabildiği gözlemlenmiştir.

Anahtar kelimeler: Hidroksiapatit, gümüş, antibakteriyel, titanyum, kaplama, sinterleme.

TABLE OF CONTENTS

LIST OF FIGURES

LIST OF TABLES

LIST OF SYMBOLS

a	Representative coefficient
A	Area
b	Broadening of the diffraction peak at half of its maximum intensity
c	Concentration
C_S	Average crystallite size
d	Distance
E	Strength of the electric field
K	Shape factor
M	Mass
q	Surface charge density
t	Time
ε	Dielectric constant
η	Viscosity of the liquid medium
λ	Wavelength of x-rays
μ	Electrophoretic mobility
θ	Diffraction angle
ζ	Zeta potential (Electrokinetic potential)

LIST OF ABBREVIATIONS

10CDHA	Calcium deficient hydroxyapatite with Ag:Ca ratio of 1.0 %
15CDHA	Calcium deficient hydroxyapatite with Ag:Ca ratio of 1.5 %
3SHA	Hydroxyapatite (stoichiometric) with Ag:Ca ratio of 0.3 %
5CDHA	Calcium deficient hydroxyapatite with Ag:Ca ratio of 0.5 %
6SHA	Hydroxyapatite (stoichiometric) with Ag:Ca ratio of 0.6 %
9SHA	Hydroxyapatite (stoichiometric) with Ag:Ca ratio of 0.9 %
CDHA	Calcium deficient hydroxyapatite
Cfu	Colony forming unit
CH	Calcium hydroxide
DAHP	Diammonium hydrogen phosphate
FTIR	Fourier transform infrared
HA	Hydroxyapatite (stoichiometric)
Rpm	Revolutions per minute
SEM	Scanning electron microscope
SCDHA	Silver substituted calcium deficient hydroxyapatite
SHA	Silver substituted hydroxyapatite
TCP	Tricalcium phosphate
UV	Ultraviolet
Wt.	Weight
XRD	X-ray diffraction
β-TCP	Beta tricalcium phosphate

1. INTRODUCTION

Hydroxyapatite [HA; $Ca_{10}(PO_4)_6(OH)_2$], being a biocompatible ceramic material, has been studied for many years as filling material for bone and tooth defects, as raw material for bone grafts, and as coating material for metallic implants due to its close similarity in chemical composition to and high biocompatibility with natural bone tissue [1, 2]. HA can be synthetically produced from various calcium and phosphate containing chemicals as well as derived from bone and tooth being the major inorganic constituent of both [3-6]. Whereas the first method is suitable for the production of nano sized powders the latter one results in micron and submicron sized particles. Recent studies have shown that nano sized HA has superior characteristics with respect to the cell attachment, proliferation and differentiation [7].

According to the Agency for Healthcare Research and Quality, the number of knee surgeries climbed by 69 %, from 328,800 in 1997 to 555,800 in 2005 alone in the United States [8]. In the same time period, the number of hip replacements rose 32 % from 290,700 to 383,500 [8]. Hospital stays for orthopedic procedures cost $31.5 billion in total which corresponds to 11 % of all hospital patient-care costs and medical care paid nearly 60 % of all knee surgeries and 64 % of all hip replacements [8]. The increasing number of patients who need joint replacements and the enormous related costs which need to be covered by the patients and medical care services underlines the necessity of successful implantation of joint replacements.

Preventing infection on the implantation site is of extreme importance for a successful implantation. Infections resulting from implanted biomaterials are reported as one of the important causes of revisional surgery [9]. Loading the implant material with antibiotics may be a solution to the problem. However, the amount of antibiotics loaded must be high enough to prevent bacterial infection. At the same time, the antibiotic loading must be below critical levels such that it does not result in systemic toxicity. On the other hand, studies have shown that silver has low toxicity against mammalian cells [10]. Therefore, incorporation of silver, which is shown to have antibacterial effects [11], into implant materials, may be an alternative approach to prevent biomaterial-based infections.

Accordingly, Chung et al. were able to synthesize micron sized HA between 3-10 μm with silver addition via sol-gel route and have demonstrated its antibacterial properties [12].

Success and long-term survival of a biomedical implant depends on the presence of the bacteria surrounding the implants [13]. Implant associated infections, which are some of the most frequent complications connected with the use of biomaterials, are considered to be serious and common complications in orthopedic surgery, and the problem usually requires removal of the prosthesis [14, 15]. The infection in the presence of implant materials is not only detrimental to the host, but also tends to scathe the implant itself [14].

Depending on the type of implant, infection rates associated with prosthetic joints range between 1-9 % which makes implant related infections the second reason, next to the aseptic ones, for revision surgery in the case of total hip replacements [16, 17]. This not only results in dangerous complications which increases morbidity but also elevates medical costs. Infection rates after surgery revision are even higher by 40 % than after primary replacement [18]. The estimated average total cost associated with an infected implant case range between $15,000 and $30,000 which indicates an increase of approximately 3 times than the initial procedure [19]. Due to the implant related infection, the patients spent on average 14 extra days in the hospital after readmission [19].

Complications resulting from an implant associated infection in the case of dental implants are not as severe as in the case of joint implants and do not usually require patient hospitalization. However, they decrease the patient's quality of life and satisfaction as a result of early failures due to poor osseointegration and late failures [20].

The objective of this study is to produce silver substituted hydroxyapatite powder as a potential antibacterial bioceramic material via a microwave assisted rapid synthesis method. The antibacterial activity of the produced powders was determined and use of the powders as a coating material for titanium substrates by electrophoretic deposition method was investigated.

2. LITERATURE REVIEW

2.1. Biomaterials

Materials substituting parts of the human body were used throughout the history of human civilization. In the last century specifically designed and produced materials, called biomaterials, have found wide applications in the replacement of damaged hard and soft tissues [21]. By definition, a biomaterial is a material which can function in intimate contact with the living tissue, neither causing adverse reaction nor rejected by the host organism [22, 23].

Use of various materials in vivo for different purposes may result in certain reactions by the host body which makes the scientist question the compatibility of the particular material. This in turn, gives rise to the term “biocompatibility”. Biocompatibility may be defined as the acceptance of an artificially implanted material by the surrounding tissue which it is in contact with and the host body as a whole. More specifically, it is the ability of a material to perform its designated function with a predictable and acceptable host response [22, 23]. Biocompatibility has a broader meaning than simply being inert, or more specifically bioinert. A biocompatible material must be able to interact with the contacting tissues and organs in a nontoxic manner and not destroy cellular constituents of the body fluids it interfaces [24]. This requires bioactivity meaning formation of bonds between the biomaterial implanted and the surrounding tissues [25, 26].

Although, emphasis is on the bioinertness and bioactivity by definition, biocompatibility is not limited to biological and chemical acceptability of a material by living tissue. A biocompatible material must also be mechanically and structurally acceptable by the host organism.

Biomaterials can be classified into four categories, similar to the classification of engineering materials, which are ceramics, metals, polymers and composites.

Table 2.1. Strengths, weaknesses and applications areas of various biomaterials [23, 27].

Material Type	Strengths	Weaknesses	Applications
Ceramics			
Hydroxyapatite	Bioinertness	Density	Tooth
Tricalcium phosphate	Biocompatibility	Resilience	Coatings
Aluminum oxide	Corrosion resistance	Reliability	Hip prosthesis
Zirconium oxide	Compressive strength	Brittleness	Transcutaneous devices
		Fabrication	
Metals			
Titanium	Ductility	Density	Nails
Titanium alloys	Toughness	Biocompatibility	Wires
Stainless steel	Wear resistance	Corrosion resistance	Plates
Co-Cr alloys	Tensile strength	Mechanical mismatch	Screws
Gold			Root implants
			Joint implants
Polymers			
Silicone	Density	Strength	Ear
Dacron	Resilience	Deformation	Nose
Nylon	Fabrication	Degradability	Tendon
Teflon			Sutures
			Soft tissues
			Blood vessels
Composites			
Carbon-polymer	Tailor-made	Fabrication	Heart valve
Carbon-carbon	Tensile strength		Knee implants
	Biocompatibility		
	Corrosion resistance		

Historically, stainless steel which was used as a biometal has greatly been replaced by titanium and its alloys, especially Ti6Al4V, in biomedical implant applications. The relatively higher degree of bioinertness of titanium as compared to stainless steel renders it as a good biometal candidate in comparison to stainless steel. Moreover, the relatively high

strength-to-weight ratio of titanium and its alloys compared to stainless steel enhances the practical use of titanium and titanium alloys as compared to stainless steel.

Pure Ti and Ti6Al4V with a higher yield strength posses the necessary bioinertness which makes these metals an excellent choice as a biometal. The stable TiO_2 formed on the metal surface gives superior corrosion resistance to the metal. The TiO_2 film is also thought to enhance the osseointegration of the implant with the surrounding hard tissue [25]. However, to improve the process of healing to a level fast enough in terms of integration of the implant with the surrounding tissues implants produced from biometals are coated by bioceramics not only to enhance the osseointegration but also to protect the metal from corrosion in vivo.

2.2. Bioceramics

Ceramics have found wide applications in the industry due to their inertness to various chemicals which may be deteriorative for other materials, their high compressive strength and their desirable appearance.

Similarly, bioceramics show chemical and biological inertness to the highly corrosive environment in vivo and their appearance makes them suitable materials for applications where aesthetics is of concern. Therefore, they have been widely used to replace hard tissues such as bone and teeth. Their high compressive strength may be less meaningful in certain cases since the loading scenarios in a living body may also be torsional and tensile in nature than compressive alone. Implants constituting entirely of bioceramics are used where mechanical loading is not the main design parameter or the loading scheme is more compressive than tensile or torsional. Dental applications are good examples where bioceramics may be used to produce the whole implant which is mostly loaded in compression.

However, in specific applications where the loading type may be other than compressive metals have several advantages. In such cases, however, bioceramics are employed to produce coating layers on top of the metals used to produce the implant in order to increase the biocompatibility of the implant overall and to increase the

bioinertness of the implant in the chemically hostile environment in the living organism which cannot easily tolerated by metals. These coating layers may be produced porous or dense depending on the requirements of the specific implant application and on the method applied to produce the coating [28].

Bioceramics may be classified into four different categories ranging from completely bioinert to completely bioactive, namely; inert, allowing ingrowth, bioactive and resorbable. These four different types of bioceramics exert different mechanisms of implant fixation in vivo [22, 25, 26, 29].

Nonporous, dense and nearly inert bioceramics attach by bone growth into surface irregularities by cementing the implant into the tissues or by fitting the implant into the defect which is designated as morphological fixation. Porous and inert bioceramics allow bone ingrowth which mechanically attaches the implant material to the hard tissue resulting in biological fixation. Bioactive fixation occurs when dense, nonporous surface-reactive bioceramics directly attach to the hard tissue by chemical bonding. Dense and resorbable bioceramics can slowly be replaced by the surrounding hard tissue which allows production of resorbable implants.

Several different bioceramics such as hydroxyapatite, beta tricalcium phosphate (β-TCP), aluminum oxide (Al_2O_3, alumina), zirconium dioxide (ZrO_2, zirconia), titanium dioxide (TiO_2, titanium (IV) oxide, titania) have been and still are in common use where the specific biomedical application necessitates use of ceramic materials for their various properties. Among those bioceramics alumina has better mechanical characteristics such as a high Young's modulus and higher compressive strength accompanied with low coefficient of friction and wear rate which renders the material as an excellent choice for bearing surfaces in joint replacements [25]. On the other hand, zirconia is preferred in the production of the articulating ball in the hip prosthesis due to its advantages in lower modulus of elasticity and high strength [2]. Titanium dioxide is especially preferred due to its photocatalytic effect [30]. TiO_2, being a strong photocatalyst, can generate an oxidizing effect on the microbes and molds which are in contact with the TiO_2 surface [31, 32].

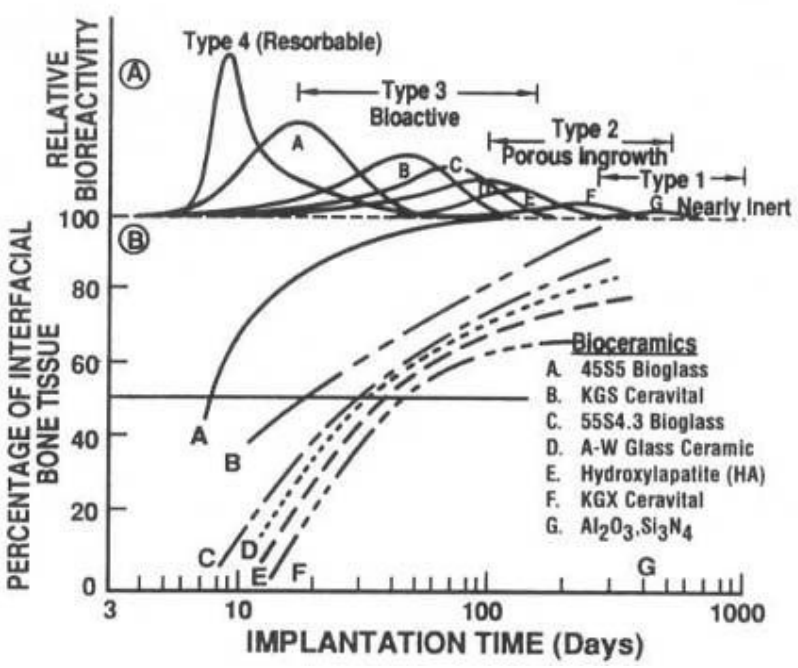

Figure 2.1. Bioactivity spectra for various bioceramic implants
(a) relative rate of bioactivity,
(b) (b) time dependence of formation of bone bonding at an implant interface [22].

2.3. Calcium Phosphates

The idea of using materials which are chemically similar to the hard tissues such as bone and tooth resulted in the production of calcium phosphate based bioceramics [2, 23]. Calcium phosphates are widely used in implant applications due to their established history of biocompatibility and safety [1, 33, 34]. Their use enables a better control of the bioresorption and hard tissue substitution [35] which makes calcium phosphates the mostly used bioceramic material for over three decades both in granular and solid forms.

Depending on the starting materials and the production method the properties of the calcium phosphates may be altered to obtain bioceramics with specific properties ranging from bioresorbable to bioinert. This makes the production of tailor-made bioceramics to fit the requirements of the specific biomedical application possible. The Ca/P ratio of the calcium phosphate to be produced, addition of several elements in relatively small amounts, presence of water during the production and the final thermal treatment determine the characteristics of the end product such as relatively high humidity and low

temperature during the production favors formation of hydroxyapatite whereas use of a dry atmosphere and high temperatures result in the formation of β-TCP [22, 23].

In body fluids and at body temperature two distinct calcium phosphates are stable. At pH values lower than 4.2 dicalcium phosphate is the stable phase whereas at pH values higher than 4.2 hydroxyapatite is the only stable calcium phosphate phase. Unhydrated calcium phosphates such as β-TCP tend to interact with water to form hydroxyapatite in body fluids at 37 °C while producing HPO_4^{2-} anions. The resulting HPO_4^{2-} anions decrease the pH of the solution which further increases the solubility of β-TCP. In this manner, the solubility of β-TCP approaches the solubility of hydroxyapatite [22]. The increased degradation rate of β-TCP compared to hydroxyapatite due to its lower Ca/P ratio [23, 36] enables progressive digestion of the material by living tissue which in turn can promote its ingrowth enhancing tissue-implant attachment and results in implant fixation [37, 38].

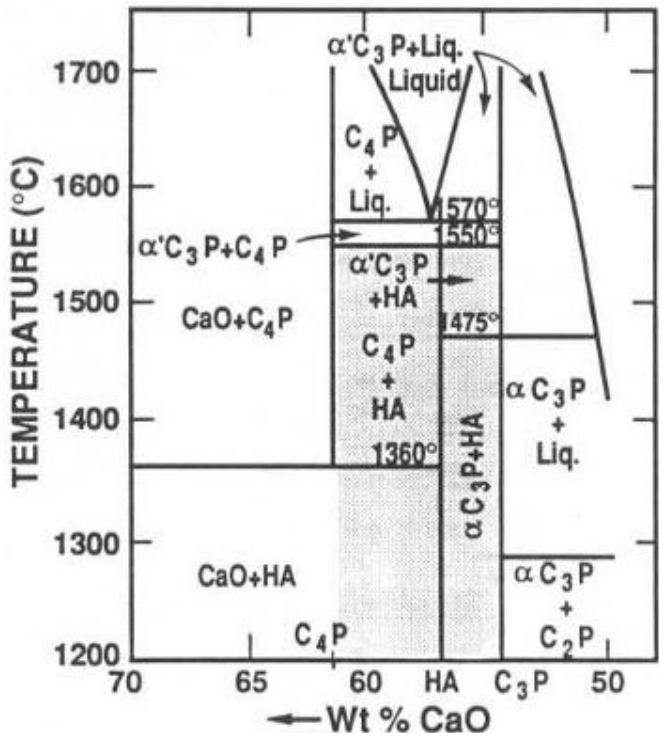

Figure 2.2. Phase equilibrium diagram of calcium phosphates in a water atmosphere (Shaded area is processing range to yield hydroxyapatite-containing implants) [22].

Sintering of calcium phosphates occur at high temperatures ranging from 1000 to 1500 °C where the formed phases not only depend on the temperature but also on the partial pressure of water. Under sufficiently humid conditions hydroxyapatite can remain stable up to 1360 °C [22].

Major drawbacks of calcium phosphates, and of all bioceramics in general, are their brittleness and low tensile strengths. Having outstanding compressive strength they tend to fail under tensile and torsional loading conditions [25, 39]. The relatively small Weibull factor of hydroxyapatite in physiological solutions indicates low reliability under tensile loads. Therefore calcium phosphates are used in powder form as filler material, in small and unloaded implants, for low loaded porous implants where bone growth acts as a reinforcing factor and as coating material for metal implants to enhance hard tissue fixation where the underlying metal substrate is supposed to carry the load [22, 25].

2.4. Hydroxyapatite

The stoichiometric ratio of calcium:phosphorus (Ca/P) in HA is 10:6 and its calculated density 3.219 g/cm^3. Apatites, having the chemical formula $A_{10}(BO_4)_6X_2$, crystallize into hexagonal rhombic prisms having unit cell dimensions of a = 0.9432 nm and c = 0.6881 nm.

Properties of the final product greatly changes by the variation of the polycrystalline structure in calcium phosphates which is a direct result of the manufacturing parameters and conditions. HA appears in crystalline and amorphous forms and its crystalline structure may be altered by subsequent thermal treatments [28]. In particular, thermal treatment of the product changes the hydroxyapatite and β-TCP composition found in the final product.

HA has been widely used as a bioceramic material in biomedical implant applications due to its close resemblance to the mineral part of hard tissues such as bone and tooth. Its excellent biocompatibility allows formation of direct chemical bonds between the implant and the surrounding tissues. Bond formation between HA and hard tissue is a direct result of the physicochemical interaction between HA and the interfacial fluid in the form of dissolution/resorption which is followed by epitaxial growth [40]. A

cellular bone matrix consisting of differentiated osteoblasts appear at the surface of HA implant producing a narrow amorphous electron-dense band of 3-5 μm thickness. Bone mineral crystals are identified in this amorphous area and collagen bundles are observed between this area and the cells. The bonding zone shrinks to a thickness of 0.05-0.20 μm while the bonding site matures resulting in the attachment of healthy bone tissue to the implant through a thin epitaxial bonding layer. Analyses of the hydroxyapatite bone interfaces reveal almost perfect epitaxial alignment of some of the growing bone crystallites with the apatite crystallites in the implant [23].

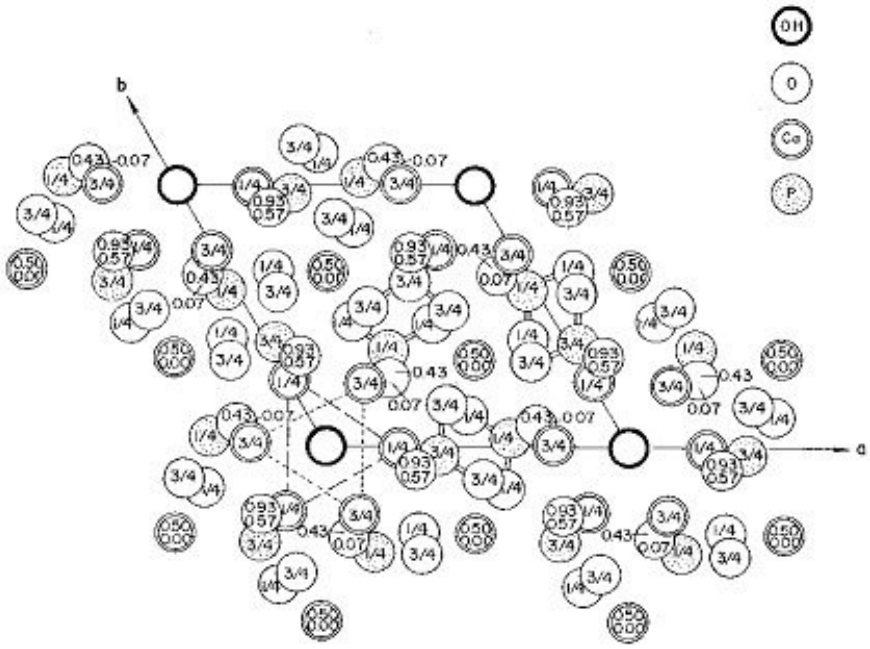

Figure 2.3. Hydroxyapatite structure projected down the c axis onto the basal plane [23].

Biodegradation/resorption behavior of HA is mainly governed by three different factors first of which being the physicochemical dissolution which depends on the solubility product of HA and the local pH of the environment. Physicochemical dissolution results in the formation of new surface phases such as amorphous calcium phosphate, dicalcium phosphate dehydrate octacalcium phosphate, and anionic-substituted hydroxyapatite. The second factor is the physical disintegration into small particles as a result of preferential chemical attack of grain boundaries. And the final one is the biological factor, such as phagocytosis, which decreases the local pH [23].

The rate of biodegradation increases with the increasing surface area and the decreasing crystallinity, crystal perfection, and crystal and grain sizes. Similarly, biodegradation is enhanced due to ionic substitutions with the exception of fluoride substituting hydroxide ions which gives greater chemical stability due to the closer coordination of fluorine as compared to hydroxyl by the nearest calcium atom.

HA can be produced by three different methods the first one being the processing of hydroxyapatite containing hard tissue such as bone and tooth [41-44]. Tas states that bone mineral obtained from hard tissue which is commonly referred as hydroxyapatite is in fact is a defective and complex substance doped with several cations [45]. Using natural resources to obtain hydroxyapatite is a simple and inexpensive method due to the ease of the calcination process to remove the soft tissue and to the economics and availability of raw material. However, preparing the obtained powder for further use requires grinding of the material obtained from processed hard tissue and the particle size possible to obtain through the grinding process is limited to several microns [41].

Another method is obtaining hydroxyapatite through the reaction of calcium containing natural resources such as coral and egg shell with ammonium containing chemicals [46]. Similar to the method noted above, this method has advantages of being economic and availability of the raw material. However, complete control over the properties of the final product is not possible due to the varying properties of the raw material used.

The final, and widely applied, production method is chemical synthesis which is based on using various calcium and phosphorus containing reactants to obtain hydroxyapatite. The method allows close control of the process parameters as well as tailoring the properties of the end product. Hydroxyapatite with varying Ca/P ratios and with various ionic substitutions may be produced and crystallinity and the particle size of the end product may be controlled by simply controlling the chemical reaction.

Researchers have been working on different synthesis techniques of hydroxyapatite production such as solid-state reaction, mechanochemical reaction, emulsion, sol-gel and

precipitation methods [47, 48]. However, three distinct methods have gained significant application due to the possibility of the control of product parameters.

Dry methods are based on the formation of the desired lattice through solid state diffusion of the constituent ions when heated to an optimum temperature. Calcium and phosphorus ions containing constituents are reacted under humid conditions. Dry methods which are able to produce perfectly stoichiometric hydroxyapatite are, however, expensive due to the necessity of high processing temperatures between 1000-1400 °C [49].

Wet methods are based on the idea of precipitating hydroxyapatite from the reaction of a calcium ion and a phosphorus ion source. The process requires control of the reaction pH since the reaction requires pH values above 9 to be completed. Through varying the amount of the calcium and phosphorus ions resources hydroxyapatite with varying Ca/P ratios may be obtained [46]. Based on the choice of the precursor materials as the calcium and phosphorus sources wet methods may be economic and simplicity of the precipitation reaction does not involve use of high temperatures and pressures.

Hydrothermal methods may be used to obtain precipitates of crystals of dimensions larger than those possible to obtain through wet methods by the application of high temperatures. Pressures higher than atmospheric pressure to increase the boiling point of the precipitating medium are necessary to increase the overall temperature of the reactants. High crystallinity and product purity can be obtained through the use of the hydrothermal methods however, the process is not inexpensive due to the high temperature and pressure requirements.

Recently, microwave irradiation has been used in order to synthesize ceramic materials, in particular calcium phosphate ceramics and hydroxyapatite, and for their sintering [50-53]. The microwave assisted production of hydroxyapatite is a promising technique due to its rapid nature. It is a time saving and energy efficient method since aging and crystallization of the produced powder occurs under microwave in a very short time period [54-56]. The microwave assisted method goes to completion under 650 to 1300 W microwave power in 15 to 30 min as compared to acid-base method which requires 24 to 48 h at 30 to 85 °C [57], to calcium acetate method which requires 3 h at 40 °C [58] and

metathesis method which requires 3 h at boiling temperature followed by a up to 20 days long aging process [58]. The technique also allows control of the crystallite size of the produced powder by varying the microwave parameters such as microwave treatment time and microwave power. In addition to that, the specific choice of precursor materials in this work simplifies the production process by guaranteeing that the pH value remains above 9 throughout the reaction without use of any additional chemicals, e.g. ammonium hydroxide.

Being a biocompatible ceramic material HA has numerous uses in its powder form, in its sintered form and as a coating material. Many products in granular forms or blocks, such as Bonfil®, Bonetite®, and Apaceram® from Pentax Co., Boneceram® from Sumitomo Osaka Cement Co. and Neobone® from Mitsubishi Ceramics Co., are available for commercial use, all of which are officially approved either for orthopedic or dental use [59].

Mazor et al. used HA bone cement for sinus floor augmentation and concluded that HA bone cement holds great promise as a grafting alloplastic material for sinus floor augmentations [60]. Yamamoto et al. used variously shaped pieces of HA as a bone filling material after excision of benign bone tumors by curettage [61]. They found out that the applied HA powder was well incorporated into the surrounding host bone tissue in all the followed patients without any local pain at the final follow-up. In addition to these, they observed bone remodeling and new bone formation at the implantation site. Similar to them, Reddy and Natarajan obtained successful results by using bovine HA as a filling material after curettage of benign bone tumors [62, 63]. De Almeida et al. compared in vivo performances of titanium dental implants either coated with HA by electrophoretic deposition or uncoated [64]. They concluded that the HA coated implants had better performance regarding the bone-implant contact area than the uncoated implants. Similarly, Darimont et al. observed that HA coated implants result in more bone contact than titanium plasma spray implants [65]. De Sena et al. successfully obtained calcium deficient HA coatings on titanium via electrophoretic deposition [66].

2.5. Electrophoretic Deposition Coating

2.5.1. Techniques for the Production of Bioceramic Coatings on Metallic Implants

Hydroxyapatite, being a ceramic material, has satisfactory mechanical properties where compression is the primary type of loading. However, the loading conditions in a human body may vary greatly and tensile and torsional types of loading come into the picture. To take advantage of the high biocompatibility and osseointegrative characteristics of hydroxyapatite and to be able to withstand tensional and torsional loads at the same time hydroxyapatite has been widely used as a coating material on metallic implant materials such as stainless steel and various titanium alloys to produce implants. This approach makes use of the superficial mechanical characteristics [67] of metallic implant materials and of the biocompatibility of hydroxyapatite [68, 69] while preventing on-site corrosion of metallic implants in vivo.

Various techniques have been developed for coating metallic surfaces with ceramic materials which have wide industrial use. Among those different techniques dip coating, sputter coating, biomimetic coating, plasma spraying, electrochemical deposition and electrophoretic deposition have proven especially suitable for coating of biomedical implant with bioceramics.

Dip coating involves dipping the metallic implant material into a suspension prepared using the ceramic particles to be coated and an appropriate binder [58]. Following the dipping process, the coated metallic surfaces are sintered at elevated temperatures. Due to the thermal expansion coefficient mismatch between the metallic substrate and he ceramic coating during the cooling period after the sintering stage surface cracks may form leading to severe damage of the coating layer.

Sputter coating is based on the deposition of ejected atoms from a source surface by high energy ion bombardment under vacuum conditions [58]. Resultingly, a dense coating with high purity coating can be achieved. However, due to the limitations of the technique, coating of complex shapes is not possible.

In biomimetic coating, an active apatitic layer is formed on a metallic implant surface by immersion into a supersaturated calcium and phosphate solution [70]. Homogenous nucleation of hydroxyapatite from the solution onto the metallic surface results in a bioceramic coating. The process leads to the decrease of ion concentrations in the solution which requires renewal of the solution. Long processing times and the necessity to replenish the supersaturated solution are the major drawbacks of the technique.

Plasma spraying is a fast and economical coating technique based on the deposition of hydroxyapatite particles injected into a high temperature plasma jet produced using a direct current with various gases such as argon, nitrogen or helium onto metallic substrates [58]. Although the substrates are kept at relatively low temperatures HA particles face very high temperatures. These elevated temperatures result in the decomposition of hydroxyapatite into tri- and tetracalcium phosphates [58]. The obtained coatings are relatively weak and the coating of complex shaped surfaces is not possible [58].

Electrochemical deposition is a rapid coating technique [71] which is based deposition of calcium phosphate using aqueous electrolytes containing calcium and phosphate ions [72]. Although precise control of the processing parameters is possible [71] the resulting coating has relatively low strength [73].

Electrophoretic deposition technique is a colloidal process based on the movement of charged hydroxyapatite particles under the influence of an applied electric field. The metallic substrate which is going to be coated acts as an electrode on which the charged particles deposit [57]. Electrophoretic deposition is an economically efficient and simple process which enables coating of complex shaped structures. However, surface cracks may form during the drying and the sintering of the coated surface.

Coatings can be produced using electrophoretic deposition in relatively short times with a high level of control of the deposit morphology by controlling the process parameters such as time, voltage, electrode distance and suspension concentration. However, weak adhesion of the deposited particles and the necessity of the application of low sintering temperatures to preserve the mechanical properties of the underlying metal substrate act as factors limiting of the process.

2.5.2. Particle Suspension and Suspension Stability

"Phoresis" is the Greek word for "being carried" hence, the term electrophoresis denotes the process of transmitting of electrically charged particles suspended in a fluid in response to an applied electric field. The process itself is basically separation of electrically charged particles based on their movement under the influence of an electric field towards oppositely charged surfaces which act as electrodes such that negatively charged particles move towards the positive electrode, the anode, and the positively charged particles move towards the negatively charged electrode, the cathode [74].

The spatial stability of the colloidal particles suspended in liquid medium prepared for the coating process is of great importance [75]. Colloidal particles with a diameter of ~1 μm or less tend to remain suspended in the liquid medium due to Brownian motion thus, forming a stable suspension. On the other hand, particles with a diameter larger than ~1 μm tend to settle decreasing the suspension concentration which further requires continuous agitation of the suspension [75]. However, in case of the suspension is too stable the repulsive forces between the particles may not be overcome by the electric field thus, particle movement and deposition is not possible [58].

2.5.3. Particle Charging Mechanisms

Two separate particle charging mechanism may act considering ceramic suspensions. The first one is the selective adsorption of ions from the liquid phase onto the ceramic particles based on chemical binding or physical adsorption and the next one is the dissociation of ions from the ceramic particles into the liquid based on the ionization of surface groups [57, 76]. The polarity of the net charge acquired by the suspended particles depends not only on the charge of the ions involved in the process but also on which mechanism dominates. While in water most ceramic particles acquire a negative charge in organic fluids the charge acquired may either be negative or positive [58].

2.5.4. Formation of an Electrical Double Layer

The distribution of the electrical charges around the solid particle in a suspension is not uniform [58]. Resulting the acquired net charge of the particles in the suspension the suspended particles are surrounded by an ion cloud of opposite charge [77] forming an electrical double layer at the separation between the two phases, namely the solid-liquid interface. This double layer exists at all solid-liquid interfaces such that it forms at the surface of colloidal particles [58]. Formation of an electrical double layer plays an important role in the stability of colloidal suspensions and their electrokinetic properties by keeping the suspended particles apart. Smaller electrical double layers result in decreased repulsive forces such that the particles attract each other by van der Waals forces further decreasing the suspension stability [78]. On the other hand, larger electrical double layers result in increased repulsive forces which cannot be overcome by van der Waals forces further enhancing particle separation and increasing suspension stability.

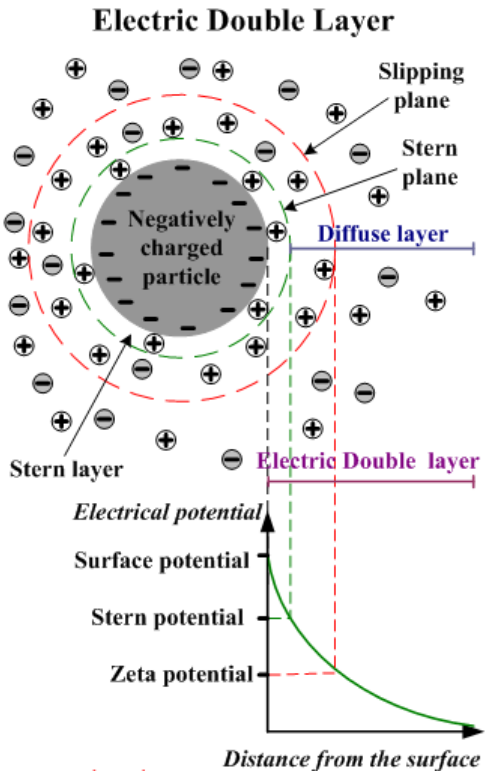

Figure 2.4. Electrical double layer formation around a particle with net negative surface charge [80].

The electrical double layer can be considered as consisting of two regions, an inner and an outer region. The inner region includes the adsorbed ions onto the particle surface and a diffuse region in which ions are distributed due to the influence of electrical attractive forces and random thermal motion [79]. The charge density of the so formed ionic layer, which is tightly bonded to the particle surface, further attracts a layer of ions of opposite charge which form the outer region. The net collective charge of the ions in the outer region balances the charge density of the inner region. Suspended articles having similar electrical double layers can form a stable suspension by the retardation of the flocculation process [80].

2.5.5. Electrokinetic Potential

Electrokinetic (zeta) potential is the voltage difference between the surface of a particle in a suspension and the surrounding electrolytic solution and thus a measure of the effective electrical charge on a colloidal particle [57]. The electrokinetic behavior of a particle depends on the electrokinetic potential on the shear surface between the particle surface and the electrolytic solution and therefore, this potential is a measurement of the strength of particle interactions in a suspension. Since electrokinetic potential can be related to suspension stability [81] it can be used as parameter characterizing the colloid [75] by providing a measure of the level of surface charge and serving as an indicator of the relative magnitude of the repulsive forces between the solid particles in a liquid medium. Being related to the suspension stability the zeta potential provides information about the agglomeration characteristics of a suspension.

2.5.6. Factors Influencing the Electrophoretic Deposition Process

The Dutch scientist Hugo Christiaan Hamaker formulated the mass of material which can be deposited in a certain amount of time as:

$$M = \int_0^t (a \cdot A \cdot c \cdot \mu \cdot E) \cdot dt \tag{2.1}$$

where;

M: mass of material deposited (kg)

a: representative coefficient for the fraction of particles near the electrode which are deposited

A: electrode area (m^2)

c: concentration of the suspension (kg/m^3)

μ: electrophoretic mobility ($m^2/V{\cdot}s$)

E: strength of the electric field (V/m)

t: time of deposition (s)

The electrophoretic mobility, μ, can be calculated using the equation by Marian Smoluchowski, a Polish physicist, [58]:

$$\mu = \frac{\varepsilon \cdot \zeta}{4 \cdot \pi \cdot \eta} \tag{2.2}$$

where;

ε: dielectric constant of the liquid medium

ζ: electrokinetic (zeta) potential of the material in that medium

η: viscosity of the liquid medium

For small particles in non-ionizing medium, use of the equation by Erich Hückel, a German physical chemist, is more convenient [58]:

$$\mu = \frac{\varepsilon \cdot \zeta}{6 \cdot \pi \cdot \eta} \tag{2.3}$$

The electrokinetic potential is obtained as:

$$\zeta = \frac{4 \cdot \pi \cdot q \cdot d}{\varepsilon} \tag{2.4}$$

where;

q: surface charge density

d: distance of separation

ε: dielectric constant of the medium between the layers

Therefore, the amount of material deposited during an electrophoretic deposition process mainly depends on the electrokinetic potential and so, on the surface charge density, on the distance between the electrodes and the electrode area, the dielectric constant of the medium, viscosity of the medium, concentration of the suspension, strength

of the electric field, thus, the applied voltage, and on the time of the deposition process. However, due to sensitivity of the process, parameters such as pH and temperature of the medium, and surface characteristics of the particles also play an important role in the amount of the deposited material [57, 58].

Especially important to note is the effect of the suspension pH on the success of the electrophoretic deposition process. pH value is an indirect measurement of the ionic strength of a suspension which in turn is related to the electrical conductivity of the suspension. Therefore pH value of a suspension determines its electrical conductivity. In case of a low ionic concentration there will be insufficient amount of ions available which adhere onto the particle surface and drive the particle motion towards the oppositely charged electrode. On the other hand, in case of a high ionic concentration the amount of ions will so much that the ions themselves act as electrical carriers thus, the particle motion is hindered. A similar effect of suspension concentration on the electrophoretic yield is observed. At low concentrations the conductivity decreases such that the yield of the process is insufficient to obtain satisfactory deposition [82]. On the other hand, increasing the suspension concentration increases the viscosity of the suspension such that particle motion is obstructed [79].

Increasing the suspension temperature decreases the suspension viscosity thus, promoting particle motion [57]. Opposite to that, an increase in particle size decreases the particle mobility [79]. For particles occupying the same volume particle symmetry effects the particle mobility such that an increase in the particle asymmetry increases the resistance of the particles to move.

2.5.7. Production of Hydroxyapatite Coatings on Metal Substrates by Electrophoretic Deposition

Using electrophoretic deposition technique to obtain HA coatings on metal substrates is an emerging area of application for the production of biomedical implants. The electrophoretic deposition method draws particular attention due to its economics, simplicity and high level of control of the end product qualities together with the ability of producing thin and even coating layers on irregular and porous surfaces [58].

Electrophoretic deposition of HA on metal substrates such as stainless steel and titanium and its alloys is generally performed in organic media such as ethyl alcohol (ethanol) [66, 83-85] and isopropyl alcohol (isopropanol) [86, 87]. Dispersion of the solid particles in the suspension is a necessary condition for successful electrophoresis. Towards this purpose, small particle size accompanied with high electrokinetic potential was found to result in good dispersion of the particles in the medium [67]. Magnitude of the deposition voltage and the duration of the deposition process are factors effecting the preferential deposition of particles. Smallest particles reach the highest electrokinetic mobility and therefore, deposit first on the metal substrate. Choosing a higher deposition voltage and longer deposition duration results in an increase of the size of the deposited particles since larger and larger particles can gain electrokinetic mobility with the increasing voltage and deposit on the electrode with the extended time [88]. However, in order to form deposit surfaces using particles larger than 1μm adequate stirring may be necessary for successful dispersion of the particles and higher voltages may be needed to electrokinetically move the large particles. However, use of high coating voltages was found to result in hydrogen evolution at the cathode at which HA coating was supposed to be achieved which increases the coating porosity [89].

Due to the relatively low bonding strength of HA particles on the metal surface immediately after the deposition subsequent sintering is required to improve densification of the coating layer, to improve particle adhesion on the surface and to increase the bond strength. However, the sintering process itself is coupled with several difficulties resulting in the decrease of the quality of the final product.

Use of elevated temperatures to achieve successful sintering results in the deterioration of the underlying metal substrate due to surface oxidation, phase transformation and enhanced grain growth. This problem may be overcome by keeping the sintering temperature as low as possible and by conducting the sintering process under inert or vacuum atmosphere to eliminate the oxidative effect of the atmospheric air. On the other hand, high sintering temperatures also result in partial decomposition of HA, which is a hydrated phase, into β-TCP, which is an unhydrated phase and, which possesses higher biodegradability. The decomposition is based on the enhanced ion migration from the metal surface into the ceramic coating layer. Use of a humid sintering atmosphere may

slow the decomposition process preserving the HA composition in the coating layer [22, 23] however, can have negative effects on the substrate metal. On the other hand, studies have shown that application of an interlayer between the metal substrate and the HA coating can successfully hinder HA decomposition due to ion migration. For this purpose, Wei has used a dual coating approach consisting of two consecutive HA coating layers the first of which is in direct contact with the metal surface serving as an ion barrier and the second forms the actual HA coating [58]. To achieve the same goal, Albayrak has successfully incorporated a TiO_2 interlayer between the metal substrate and the HA coating layer [57].

Using nanosized HA particles results in more uniform and faster migration of the particles such that enhanced packing and thus, a high density coating may be achieved at relatively low sintering temperatures [83, 86, 88, 89]. Prior calcination of HA enhances the deposition characteristics of the powder and results in the formation of dense coating layers [90-92].

Shrinkage observed in the coating layer immediately after the deposition due to the evaporating suspension medium and densification of the coating layer obtained during the sintering process together with the differences in the thermal expansion coefficients of the underlying metal substrate and the HA forming the coating layer result in crack formation in the coating.

Table 2.2. Thermal expansion coefficients of HA, TiO_2 and potential metallic substrate candidates [93].

Material	**Thermal Expansion Coefficient ($x10^{-6}$ K^{-1})**
HA	11 - 14
TiO_2	8.6 - 9.0
Ti	8.7 - 10.1
Ti6Al4V	8.7 - 9.8
316L stainless steel	16.0 - 19.0

Shrinkage during the drying of the coated samples is inevitable and may only be slightly controlled by the retardation of the drying process. The effect of the mismatching thermal expansion coefficients of the metal substrate and the ceramic coating may partially be negated by applying relatively low heating and cooling rates during the sintering step. However, most significantly, the choice of the substrate metal determines the crack susceptibility of the coating layer during the cooling stage after sintering. The difference in the thermal expansion coefficients is mostly irrelevant during the heating stage of the sintering process since complete bonding is not achieved until the dwelling temperature is reached. However, once complete bonding took place after the dwell time and the metallic substrate with HA coating is subjected to decreasing temperature during the cooling stage of the sintering process the underlying titanium or titanium alloy, having a slightly lower thermal expansion coefficient, exerts tensile stress on the HA which has a higher thermal expansion coefficient resulting in the formation of cracks in the coating layer. In case of using a stainless steel substrate, on the other hand, the HA layer is conversely subjected to compressive stress which tends to constrain the crack formation. However, particular choice of the substrate material is a subject matter of other factors such as biocompatibility which favors use titanium and its alloys instead of stainless steel.

Cracks formed due to the densification of the HA layer have a deleterious effect on the mechanical properties of the produced coating. Again, use of the dual coating layer approach which employs a dense interlayer consisting of TiO_2 or HA limits the crack occurrence in the outer HA layer by allowing gradual expansion and contraction of the coating layers. Important to note is the necessity of applying the sintering process in a single step after coating of both the interlayer and outside coating layer in order to minimize the negative effect of the elevated temperatures due to subsequent sintering steps on the mechanical properties of the metal substrate.

2.6. Physiology of Bacteria

2.6.1. Classification of Living Cells

Two basic cell types have appeared during the evolution, namely procaryotic (Greek “pro”, before and “karyon”, nucleus) and eucaryotic (Greek “eu”, true or good) cells.

These cell types primarily differ in their complexity of their cell structure. In general, procaryotic cells are smaller than eucaryotic cells and they lack special structures such as nucleus and small organs, called organelles. Organelles are small cell stuctures bound to the membrane and perform specific functions in eucaryotic cells [94].

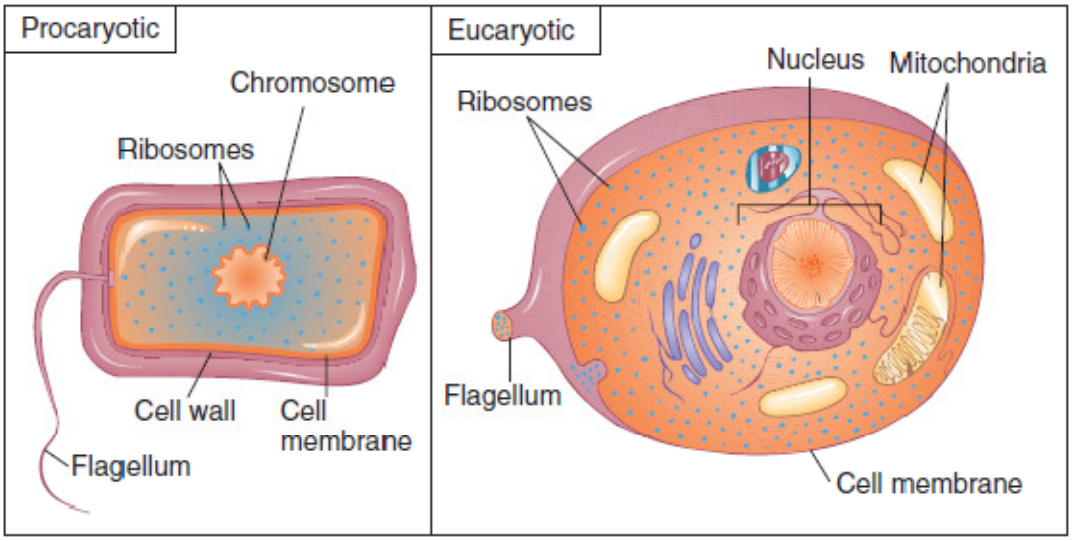

Figure 2.5. Comparative schematic diagrams of prokaryotic and eukaryotic cells [94].

Historically, scientists classified the living organisms in two distinct classes, plants and animals. In time, it became clear that certain newly discovered organisms, mainly starting with use of microscopy as a method of research of living organisms, do not truly fit in either of these classes. So, a third class, namely protists, which were thought of lacking tissue differentiation, was proposed. However, sigficant differences arose among the protists themselves such that a fourth class, bacteria, and a fitfth class, fungi, were recognized [94].

Although, the use of the traditional Whittaker system consisting of five different classes representing all the existing living organisms was a valuable and practical method of classification recent studies in the molecular biology have provided a more accurate view of the relationships and origins of cells. It has been determined that certain types of molecules in cells, called ribosomal ribonucleic acids (rRNA), provide a solid record of the evolutionary history of living cells. Analyses of these molecules in the prokaryotic and eukaryotic cells have shown that a certain type of cells is so different from the prokaryotic

and eukaryotic cells such that it would be logical to constitute a third group called archaea, or archaeabacteria [94].

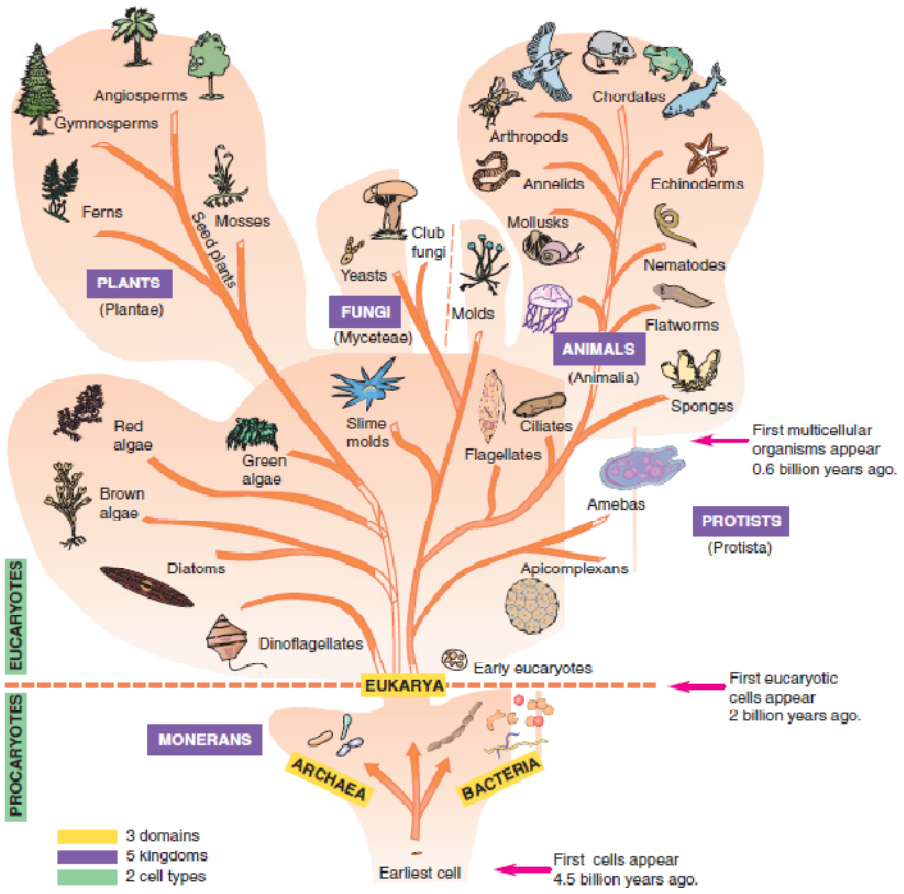

Figure 2.6. Traditional Whittaker system of classification of living cells [94].

The new established system of classification of cells contains two different cell types, prokaryotic and eukaryotic, and three different groups.

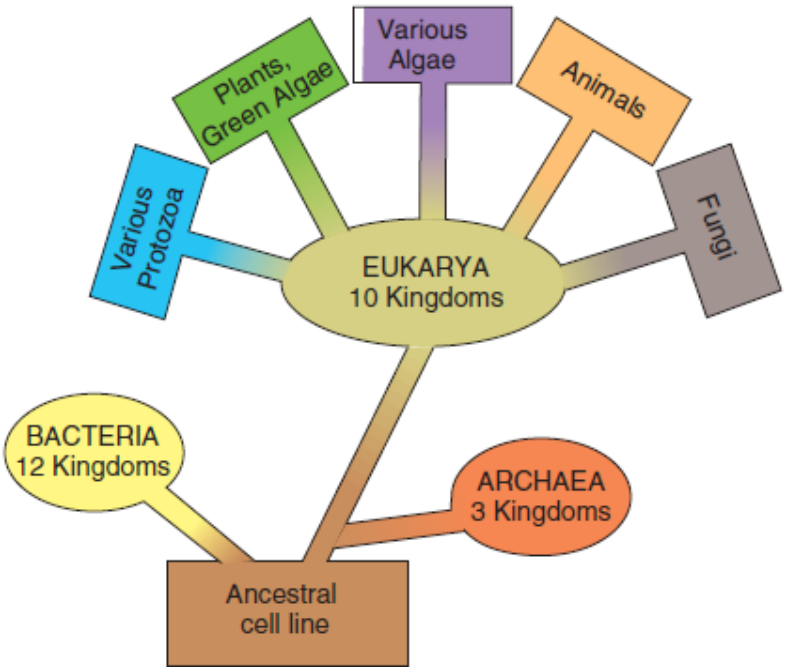

Figure 2.7. Schematic presentation of the origins of cell lines and major groups as proposed by Carl Woese and colleagues, also referred as the Woese system [94].

2.6.2. Features of Bacteria

The evolutionary history of procaryotic cells back at least 3.5 billion years. These organisms have endured for so long in such a variety of habitats indicative of a cellular structure and function which are amazingly versatile and adaptable.

Bacteria may come in a great many sizes and several shapes. Most bacteria range from 0.2 to 2.0 µm in diameter and 2 to 8 µm in length. Three distinctive basic shapes are common; spherical coccus (plural: cocci, meaning berries), rod-shaped bacillus (plural: bacilli, meaning little staffs), and spiral [95].

Table 2.3. Cellular organization of a prokaryotic cell [94].

Cytoplasma	Cell envelope	Appendages
Cell pool	Glycocalyx (capsules, slime layers)	Flagella/periplasmic flagella
Ribosomes		Pili
Granules	Cell wall	Fimbriae
Nucleoid/chromosome	Cell membrane	

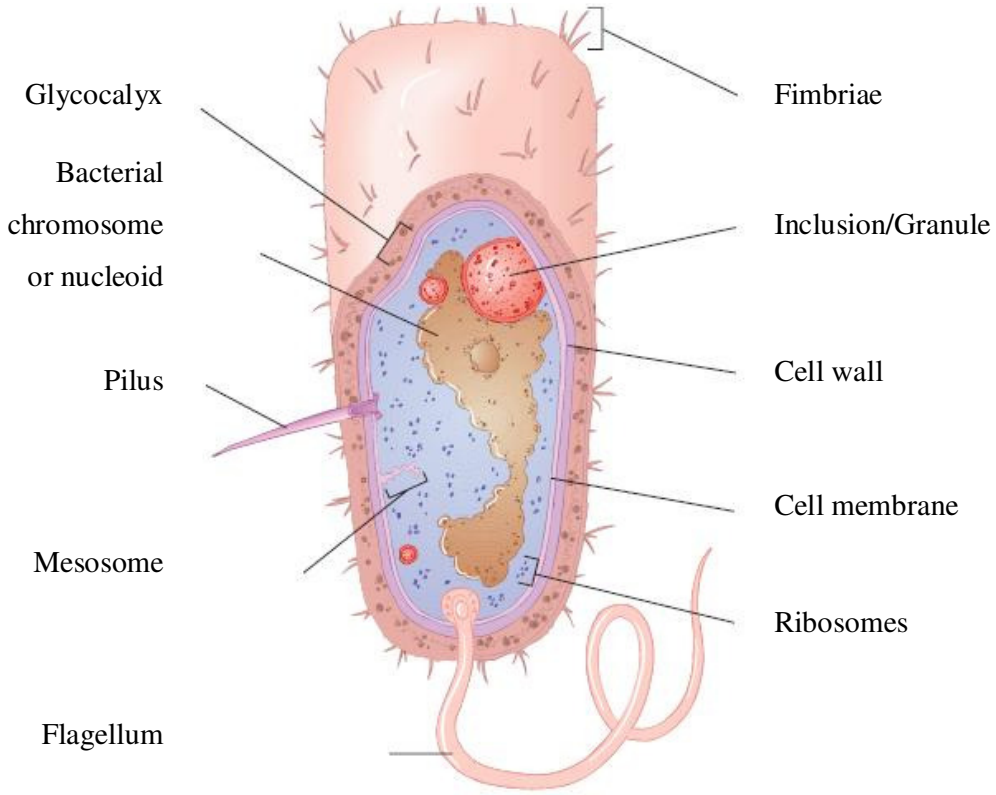

Figure 2.8. Structure of a prokaryotic cell [94].

Glycocalyx is a coating or layer of molecules external to the cell wall. It serves protective, adhesive, and receptor functions. Bacterial chromosome or nucleoid is the site where the large DNA molecule is condensed into a packet. DNA is the code that directs all genetics and heredity of the cell. Pilus is an elongate, hollow appendage used in transfers

of DNA to other cells and in cell adhesion. Mesosome is an extension of the cell membrane that folds into the cytoplasm and increases surface area. Flagellum is specialized appendage attached to the cell by a basal body that holds a long rotating filament. The movement pushes the cell forward and provides motility. Fimbriae are fine, hair like bristles from the cell surface that help in adhesion to other cells and surfaces. Inclusion/Granule is stored nutrients such as fat, phosphate, or glycogen deposited in dense crystals or particles that can be tapped into when needed. Cell wall is a semi rigid casing that provides structural support and shape for the cell. Cell membrane is a thin sheet of lipid and protein that surrounds the cytoplasm and controls the flow of materials into and out of the cell pool. Ribosomes are tiny particles composed of protein and RNA that are the sites of protein synthesis.

2.6.3. Gram Staining to Differentiate Bacteria

In 1884, Hans Christian Gram developed a staining technique which can be used to make bacteria in specimens more visible. The Gram staining technique consists of a timed, sequential application of crystal violet (the primary dye), Gram's iodine (IKI, the mordant), an alcohol rinse (decolorizer), and a contrasting counterstain. Gram originally used yellow or brown as counterstain which was replaced by the red dye, safranin. Since this substitution, bacteria that stained purple are called Gram positive [Gram (+)], and those that stain red are called Gram negative [Gram (-)]. The terms Gram negative and Gram positive do not indicate electrical charge of cells or dyes but whether or not a cell retains the primary dye-iodine complex after decolorization. The different results in the Gram stain are due to differences in the structure of the cell wall and how it reacts to the series of reagents applied to the cells.

In the first step, crystal violet is attracted to the cells in a smear and stains them all the same purple color. The second and differentiating step is the addition of the mordant (Gram's iodine) which is a stabilizer that causes the dye to form large crystals in the peptidoglycan meshwork of the cell wall. Because the peptidoglycan layer in Gram positive cells is thicker, the entrapment of the dye is far more extensive in them than in Gram negative cells. Application of alcohol in the third step dissolves lipids in the outer membrane and removes the dye from the peptidoglycan layer and the Gram negative cells.

In contrast to the Gram negative bacteria, the crystals of dye tightly embedded in the peptidoglycan of Gram positive bacteria are relatively inaccessible and resistant to removal. Because Gram negative bacteria are colorless after decolorization, their presence is demonstrated by applying the counterstain safranin in the final step.

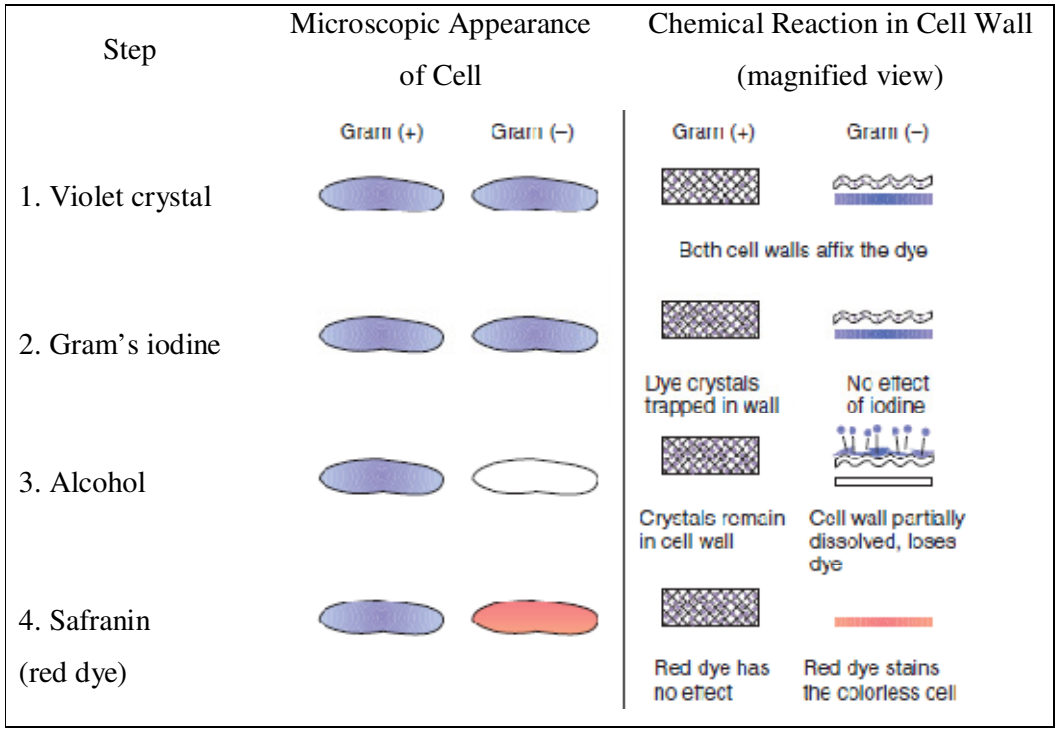

Figure 2.9. Step-by-step view of Gram staining technique [94].

The differences between Gram positive and Gram negative bacteria are evident in the physical appearance of their cell envelopes. In Gram positive cells, a microscopic section resembles an open-faced sandwich with two layers: the thick outer cell wall, composed primarily of peptidoglycan, and the cell membrane. A similar section of a Gram negative cell envelope shows a complete sandwich with three layers: the cell wall, composed of an outer membrane and a thin layer of peptidoglycan, and the cell membrane.

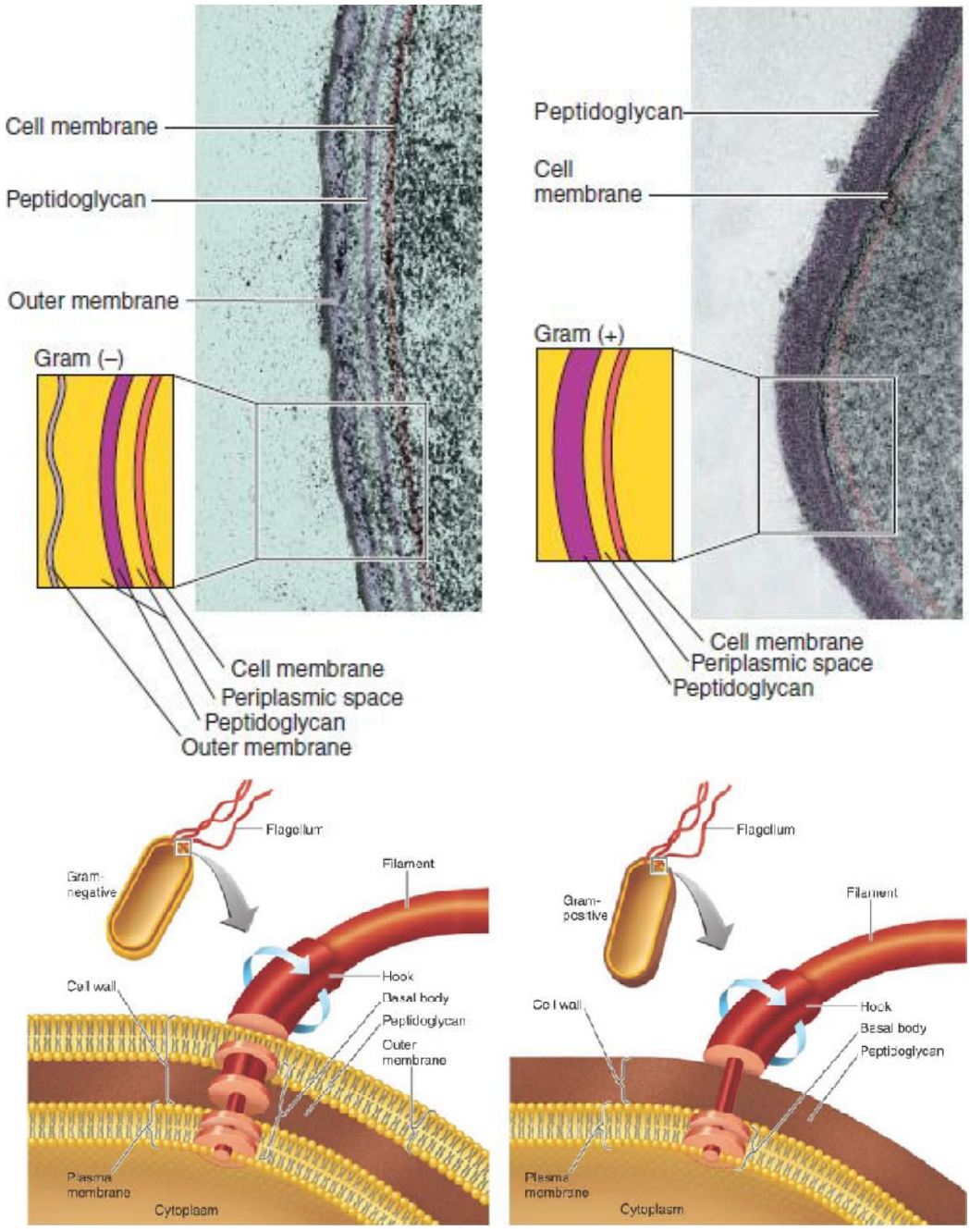

Figure 2.10. Cell wall and flagellum of Gram negative (left) and Gram positive bacteria (right) [95].

This old staining method remains the basis for bacterial classification and identification. It allows differentiation of four major categories based on coloring reaction and shape: Gram positive rods, Gram positive cocci, Gram negative rods, and Gram negative cocci. The Gram stain can be used as a practical and easy-to-apply method to aid

in diagnosing infection and in guiding following drug treatment. For example, Gram staining a fresh urine or throat specimen can help to identify the possible cause of infection and in some cases it is possible to begin drug therapy on the basis of this stain. Even in this day of elaborate and expensive medical technology Gram stain still remains an important and unbeatable first tool in diagnosis.

2.7. Prevention of Infection

2.7.1. Implant Based Infection

The genus Staphylococcus is the major organism causing infection based on implant applications and use of medical devices employed in operational surgery [96]. The Staphylococcus genus is divided into two groups, the virulent Staphylococcus aureus (S. aureus) and the non-virulent Staphylococcus epidermidis (S. epidermidis). Staphylococcus cells are Gram positive bacteria and due to their anaerobic metabolism they can survive oxygen absent environments by sugar fermentation resulting in lactic acid.

A healthy human body is familiar with the Staphylococcus species which exist in normal flora where they live as commensal organism. Commensalism is a special form of parasitism which causes neither any benefit nor any harm to the host organism. Staphylococcus species are widely found especially in mucous membranes in a healthy human-being where skin, conjunctivae, nasal cavity, mouth, intestinal tract, anus, vagina and urethra are the most commonly tissues hosting Staphylococcus species.

Among the Staphylococcus species S. aureus is well known for its aggressive tendency to invade healthy tissues and causing serious infections. S. aureus produces a very strong toxin known as toxic shock syndrome toxin which can reach different organs in the body through abrasions in mucous membranes causing severe infections, likely resulting in death. S. aureus is known to cause half of the cases of bacterial endocarditis and is also responsible for pericarditis, cellulitis, impetigo, abscesses, boils and less dangerous skin infections [96]. The opportunistic nature of Staphylococcus infections renders this organism the most common organism encountered in implant related infections such as observed in catheter and artificial joint applications [96]. Due to several

adhesins the organism can facilitate bacterial adhesion to hard tissues such as bone and result in orthopedic infections [97].

2.7.2. Mechanisms of Infection

Infection occurs through formation and adhesion of biofilms on the implant surface which contain bacterial organisms. In the first place, many factors such as dispersion, polarity and hydrogen bonding, van der Walls forces and, hydrostatic and electrostatic interactions play important roles as physicochemical factors in bacterial adhesion on a surface [98]. Next step of infection is related to the characteristics of bacteria which adhere onto the surface and is mostly based on cellular and molecular interactions and the proteins present on the target surface [99, 100].

Implantation of any biomaterial results in formation of a conditioning layer of blood proteins and cells on its surface. The existence of these proteins are thought to influence the potential risk of bacterial attachment onto the implant surfaces by two distinctive ways first of which is the non-specific masking of direct interaction between the adhesive bacterial surface components and the material surface. Next one is more specifically increasing the attractiveness of the artificial surfaces for the organisms by presenting suitable binding sites for the organisms. The result is formation of strong biofilms on the implant surfaces which enables a suitable environment for communication and material exchange for the bacteria. Once the biofilm reaches its mature state most antibiotics become ineffective to eradicate the dense biofilm structure [101]. Bacterial organisms in a biofilm can exist in a web of entangled polysaccharide fibers which do not only bind the organism together but also responsible for attachment onto the implant surfaces through glycocalyx formation. Nutrients delivery and toxin removal takes place which also prepares suitable conditions for other bacterial organisms to exist in an already established microcosmos resulting in various infections. The glycocalyx matrix serves as a matrix protecting and isolating the bacteria from defensive mechanisms of the host organism and external antimicrobial agents. Although a bacterium isolated from biofilm may be susceptible to a certain level of an antibiotica the glycocalyx formation increases the resistance of the bacteria present in the matrix [102].

2.7.3. Controlling Bacterial Activity

Controlling the bacterial activity is a broad term related to controlling the number of living bacteria forming a colony or a biofilm. In this sense, sterilization is destruction of all existent bacteria whereas disinfection means reducing the number of bacteria to a level at which they pose no risk of disease formation. Bacterial control activities are based on elimination of disease forming bacteria at the first place by cell death and by taking necessary measures in order to prevent further reproduction and proliferation at the second. Bacterial cell death is, by definition, altering the state of bacterium such that it is no longer able to divide to produce new cells and substantially form a colony or a biofilm.

Methods to control bacterial activity can be subdivided into three groups, namely physical control, chemical control and control by chemotherapeutic agents. Physical and chemical controlling methods are extensively used to ensure bacteria free implantation of a biomaterial into the host organism whereas control by chemotherapeutic agents is employed as a cure for disease control and prevention.

The first and most prominent method of physical control is removal of existing bacteria by physical ways such as washing, filtration and limiting bacterial transfer by using surgical gloves, masks and clothing. Heating, cooling, desiccation, UV radiation and increasing the osmotic pressure to cause cell rupture are other ways of physical control of bacterial activity.

Table 2.4. Physical controlling methods of bacterial activity [95].

Method	Mechanism
Filtration	Separation of bacteria from suspending liquid
Heat	
- Boiling steam	Protein denaturation
- Flowing steam	
- Autoclaving	Protein denaturation
- Pasteurization	Protein denaturation
- Direct flaming	Burning to ashes
- Incineration	Burning to ashes
- Hot-air sterilization	Oxidation
Cold	
- Refrigeration	Decreased chemical reactions and possible changes in proteins
- Deep-freezing	Decreased chemical reactions and possible changes in proteins
- Lyophilization	Decreased chemical reactions and possible changes in proteins
High Pressure	Alteration of molecular structure of proteins and carbohydrates
Osmotic Pressure	Plasmolysis
Desiccation	Disruption of metabolism
Radiation	
- Ionizing	Destruction of DNA
- Nonionizing	Damage to DNA

Chemical controlling methods are mostly involved with the inhibition or denaturation of lipid or protein structures of bacteria such as plasma membrane, enzymes and essential proteins.

Table 2.5. Chemical controlling methods of bacterial activity [95].

Method	Mechanism
Phenols and Phenolics	
- Phenols	Disruption of plasma membrane, denaturation of enzymes
- Phenolics	Disruption of plasma membrane, denaturation of enzymes
- Bisphenols	Disruption of plasma membrane
Biguanides (chlorhexidine)	Disruption of plasma membrane
Halogens	Protein inhibition, oxidization
Alcohols	Protein denaturation, lipid dissolution
Heavy metals and their compounds	Denaturation of enzymes, denaturation of essential proteins
Surface active agents	
- Soaps and detergents	Mechanical removal of microbes
- Acid-anionic sanitizers	Enzyme inactivation or disruption
- Quaternary ammonium compounds (cationic detergents)	Enzyme inhibition, protein denaturation, disruption of plasma membranes
Chemical Food Preservatives	
- Organic acids	Metabolic inhibition
- Nitrates/nitrites	Enzyme inhibition

Chemotherapeutic agents, widely known as antibiotics, are used for treatment of the bacteria related infections. These antimicrobial drugs are either bactericidial, killing bacteria directly, or bacteriostatic, preventing bacteria from growing and multiplying. The major mechanisms of action of the antimicrobial drugs are inhibition of cell wall, proteins, nucleic acids and essential metabolites and, disruption of plasma membrane.

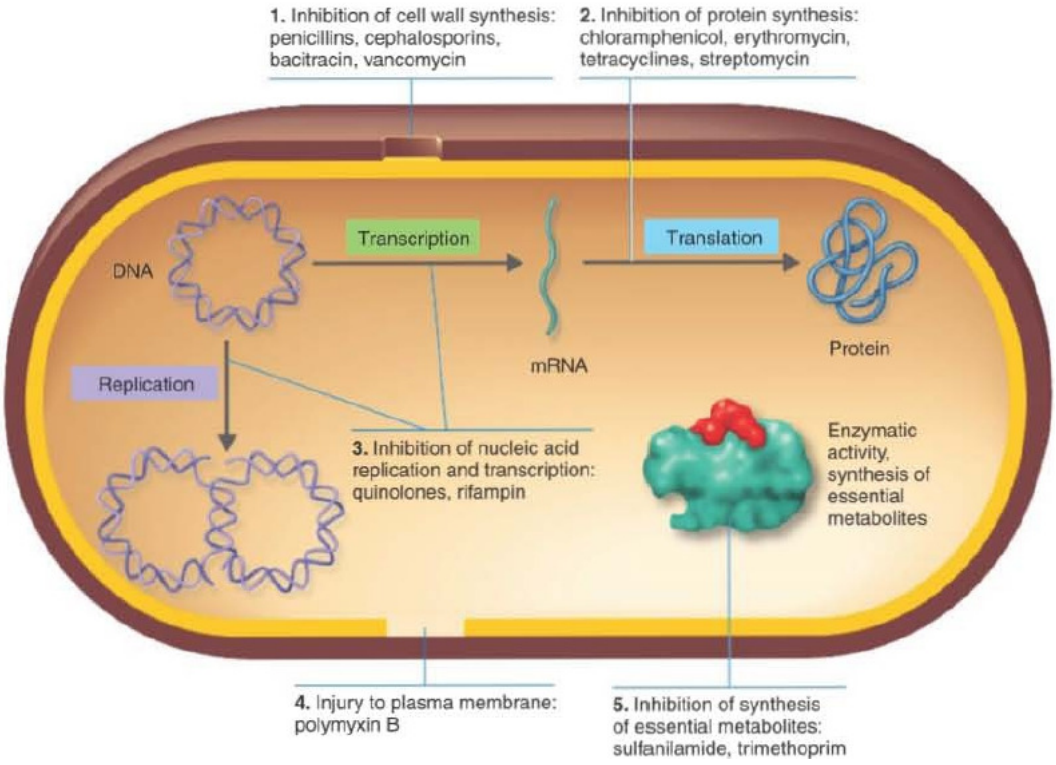

Figure 2.11. Mechanisms of action of antibiotics [95].

2.8. Silver as an Antibacterial Material

Success of an orthopedic or dental implant is mainly measured by the success of the osseointegration which is the integration of the surfaces of the implant material and the implanted bone in short term and the survival of the implant in long term.

The fixation of implant with the surrounding bone is linked with the bone-to-implant contact, and higher percentage of bone contact results in better stabilization of the implant [103]. When bone healing is associated with infection, the healing process becomes more complicated and the implant failure is expected since the implant becomes loosened due to the formation of bacteria colony on the implant surfaces [14]. Studies on the effects of interaction of organisms such as S. epidermidis on bioactive ceramics have revealed that microbial induced degradation occurred in vitro. The presence of bacteria (S. epidermidis and S. aureus) significantly increased the levels of calcium in the media [14].

Bacterial activity on the implantation site is a rising complication in the wide use of implant and can effect both the short and long term success of implant. Therefore, considerable attention is on the effect of implant surface properties on bacterial adhesion [104]. Bacterial infection after implant placement is a significant rising complication and the infection rates of total joint hip arthroplasties range between 0.5 and 3.0 % in primary total hip arthroplasty [13]. Infection leading to implant failure accounts for an enormous medical cost, an increase in morbidity and a decrease in patient satisfaction [13, 105].

Several methods have been developed to avoid bacterial activity on hydroxyapatite surfaces. Some scientists have tried to inhibit bacterial activity by using antibacterials. For this purpose antibacterial agent impregnated hydroxyapatite has been used. This method has been proven to be successful up to a certain extent since controlled delivery of the antibacterial agent on the implantation site is quite a problem. The main point here is to control the release of the agent on a timely basis and deliver the necessary amount of agent when needed. It is also necessary to be able to continue the delivery until the agent is no more needed. To be able to load the hydroxyapatite with as much antibacterial agent as needed large surface areas are needed. This can be achieved by various production methods. However, extensive control of the release agent still remains a challenge to be solved by the scientists.

Another direction of research is to avoid bacterial activity just before it occurs. This is a more proactive approach since it tries to avoid the bacterial activity before it spreads out as opposed to the antibacterial agent treatment which tries to inhibit the bacterial growth after the activity has already took place. The underlying logic of this proactive method is to render the hydroxyapatite surface such as it is impossible for the bacteria to adhere onto the implant surface, to grow and to multiply on it.

Towards this purpose, use of various heavy metal ions such as Ag^{+}, Cu^{2+}, Zn^{2+} and photocatalysts such TiO_2 have been trialed for their antibacterial effectiveness in hydroxyapatite [94, 95, 106].

The antibacterial effectiveness of metal ions, such as silver and copper, has been well known for centuries [94, 95]. Silver has been widely used as an antiseptic in form of

diluted silver nitrate solution [95]. Silver-impregnated dressings that slowly release silver ions have proven especially useful against antibiotic-resistant bacteria [95]. Silver can be incorporated into indwelling catheters, which are a common source of hospital infections, and in wound dressings to prevent bacterial infections [95].

Among all the metal ions silver has outstanding importance due to its highest toxicity for microorganisms and least toxicity to animal cells [107, 108]. It has a very broad antimicrobial spectrum, including Gram negative enterobacteria and Gram positive cocci [107]. In addition to its antibacterial characteristics silver is also known to have antiviral effects against poliovirus, adenovirus, bovine rotavirus, herpes, and vaccine virus. Studies also report antialgal activities associated with silver [107].

In a study conducted by Feng et al., silver has been found to inhibit bacterial growth mechanism [109]. The underlying reasons are reported for this behavior of silver. First, as reaction against the denaturation effects of silver ions, DNA molecules become condensed and lose their replication abilities. And next, silver ions interact with functional groups such as sulfhydryl, thiol, hydroxyl, amine and phosphate, in protein which induces the inactivation of the bacterial proteins resulting in denaturation [95]. As a result, the bacterial activity comes to a standstill resulting in bacterial death in relatively short time of 1-48 h [94, 95].

In using silver as an antibacterial agent, the mostly encountered problem is the determination of the correct silver ion concentration which will be effective enough to have an antibacterial effect but will cause no harm to the host organism. Unfortunately, the problem is merely solved by the fact that an antibacterial activity can be achieved at concentrations of ng/ml whereas connective tissue damage starts to occur at concentrations of the order of magnitude of mg/ml [110].

The critical fatal dose of silver has been reported to be relatively high. For an acute toxic reaction 10 g of silver are found to be critical whereas recovery from much higher dosages is also reported. For chronic toxicity to occur the critical intake is between 1-30 g. Following oral or inhalation exposure to silver compounds, humans excrete silver primarily in the feces and only very minor amounts in the urine. Excretion rate in the

mammalian organism is very high and between 90-99 % and the excretion is completed between 2-30 days from exposure to silver [111].

Three distinctive ways of silver incorporation into hydroxyapatite have been followed by various researchers. The first and more obvious method is to mix hydroxyapatite powder with silver particles.

Asmus et al. have prepared hydroxyapatite-silver oxide composites in a fractional range of silver up to 40 %. They have found out that silver has greatly improved the mechanical properties of hydroxyapatite and that the high thermal expansion coefficient of silver (higher than hydroxyapatite) implies, that compressive stresses are operative on the hydroxyapatite matrix after cooling down from a sintering process [112].

Zhang and his team have followed a similar procedure which has yielded hydroxyapatite-silver oxide composites with concentrations of silver oxide up to 30 %. They have found out that a sintered mixture which contains 30 % silver oxide has a toughness which is 3.5 times higher than that of hydroxyapatite [113].

Manjubala and Sampath Kumar have tried to produce functionally graded bioceramics by spreading TiO_2-Ag_2O mixture on the surface of hydroxyapatite ceramics [114].

Another method of incorporating silver into hydroxyapatite is by ion exchange. Kim et al. have prepared solutions of $AgNO_3$, $Cu(NO_3)_2{\cdot}3H_2O$ and, $Zn(NO_3){\cdot}6H_20$ into which $Ca(OH)_2$ was added. Drop wise addition of H_3PO_4 into the prepared solution resulted in Ag substituted hydroxyapatite. They have concluded that only the samples prepared with $AgNO_3$ have remarkable antibacterial properties whereas Cu and Zn ions have not shown any significant effect towards the elimination of bacterial activity [106].

Interestingly, Shirkhanzadeh et al. have noticed that even very small concentrations of silver ions incorporated into apatite coatings may have a profound effect on the formation of new carbonated apatite in simulated body fluid solution. Thus, they have

concluded that silver ions enhance the bone-bonding properties of these coatings in vivo [115].

On the other hand, to reach an alternative use of silver doped hydroxyapatite, Yang and his colleagues have used the ion exchange method to incorporate silver into hydroxyapatite to produce porous ceramics for separation and elimination of microorganisms [116].

The most sophisticated method for using antibacterial effects of silver along with hydroxyapatite is incorporation of silver into hydroxyapatite by substitution during the synthesis stage. Towards this purpose, Chung et al. have prepared hydroxyapatite powder with silver addition via a sol-gel route [12] and Rameshbabu et al. have prepared nanosized hydroxyapatite powder with varying amounts of silver added [56]. Conclusively, they have found out that even low silver content was effective in eliminating bacteria active on the samples with excellent osteoblast adherence [56]. Addition of silver to the powder during the precipitation reaction, which decreases the production time and simplifies the production process as compared to an ion exchange procedure [14] which can alternatively be used to incorporate silver.

3. MATERIALS AND METHODS

3.1. Synthesis of Nanosized Calcium Deficient Hydroxyapatite by Microwave

3.1.1. Powder Preparation

Calcium deficient hydroxyapatite (CDHA) with the calcium:phosphorus ratio of 1.6, which is below the stoichiometric ratio of 1.67, was synthesized using microwave irradiation.

The main purpose of the microwave irradiation is to benefit from the crystallizing and aging effect of microwave on the CDHA produced. The exact time to microwave exposure and the microwave power are the parameters that affect the properties of CDHA powder.

Analytical grade calcium hydroxide [CH, $Ca(OH)_2$] (Merck, Calciumhydroxide, 1.02047.1000) was chosen as the calcium source and analytical grade diammonium hydrogen phosphate [DAHP, $(NH_4)_2HPO_4$] (Merck, di-Ammoniumhydrogenphosphate, 1.01207.0500) was chosen as the phosphate source in order to prepare calcium deficient hydroxyapatite [CDHA, $Ca_{10-x}(HPO_4)_x(PO_4)_{6-x}(OH)_{2-x}$] with the calcium:phosphorus ratio equal to 1.6.

The chemical formula of the produced calcium deficient hydroxyapatite is:

$$Ca_{10-x}(HPO_4)_x(PO_4)_{6-x}(OH)_{2-x}$$

where $0 < x \leq 1$ and the precipitation reaction to produce calcium deficient hydroxyapatite is as follows:

$$(10\text{-}x)\ Ca(OH)_2 + 6\ (NH_4)_2HPO_4 \rightarrow$$
$$Ca_{10-x}(HPO_4)_x(PO_4)_{6-x}(OH)_{2-x} + (6\text{-}x)\ H_2O + 12\ NH_4^+ + 12\ OH^-$$

In the conducted study the calcium:phosphorus ratio was chosen to be 1.6. Therefore, x turns out to be 0.4 in order to be able to produce calcium deficient hydroxyapatite with the calcium:phosphorus ratio of 1.6.

There are other routes and reagents used in the literature to produce hydroxyapatite. However, the specific choice of reagents preferred in this study ensures the presence of hydroxide ions (OH^-) which in turn ensures maintenance of the pH condition for the synthesis without any ammonium hydroxide addition, which is generally added to maintain the pH above 9 which is necessary for successful production of hydroxyapatite by precipitation.

The molecular masses of the incorporated molecules in the above reaction are:

M_{CH} = 40.078 + 2 * (15.9994 + 1.00794) = 74.09268 g/mol

M_{DAHP} = 2 * (14.0067 + 4 * 1.00794) + 1.00794 + 30.973762 + 4 * 15.9994
= 132.056222 g/mol

Setting x = 0.4 to obtain the calcium:phosphorus ratio of 1.6

M_{CDHA} = (10 – 0.4) * 40.078 + 0.4 * (1.00794 + 30.973761 + 4 * 15.9994) + (6 – 0.4) *
(30.973761 + 4 * 15.9994) + (2 – 0.4) * (15.9994 + 1.00794)
= 982.19188 g/mol

In order to determine the suitability of microwave irradiation for the production of hydroxyapatite 0.3 M CH and 0.3 M DAHP solutions are prepared. The concentrations of the solutions are kept low for successful mixing. For this purpose;

0.3 M * 74.09268 g/mol = 22.227804 g/l
→ 22.227804 g → 22,227 g of CH is dissolved in 1 l deionized water

0.3 M * 132.056222 g/mol = 39.168666 g/l
→ 39.168666 g → 39,168 g of DAHP is dissolved in 1 l deionized water

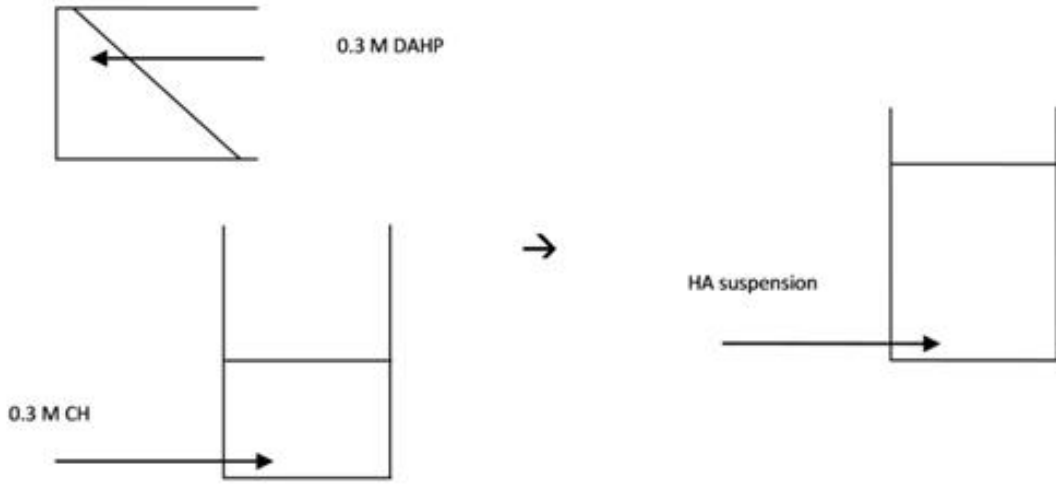

Figure 3.1. Schematic view of the calcium deficient hydroxyapatite production process.

The weight measurements are accomplished by an electronic scale (Precisa XB220A). Deionized water (Sartorius arium 611DI) has been used throughout the experiments. All the experimental equipments were first cleaned with commercial kitchen detergent and thoroughly rinsed with grid water. Following this, all the equipment was thoroughly rinsed with deionized water for 3 times.

0.3 M DAHP solution was added drop wise into the 0.3 M CH solution by a burette. The volumetric ratio of the reagent solutions were set such that the calcium:phosphorus ratio of the final product is 1.6. The rate of addition of the diammonium hydrogen phosphate solution to the calcium hydroxide suspension was chosen to be 5 ml/min to ensure successful reaction. Thereby the mixture was magnetically stirred vigorously at 350 rpm and held at 30 °C. The stirring continued further after all of the DAHP solution is poured into the CH solution for 1 min.

During the experiments, the pH value of the CH solution was monitored to be 13.28 and of the DAHP solution to be 8.03 before mixing both solutions. The pH value after mixing both solutions was observed to be 10.88. While adding the pH 8.03 DAHP solution to the pH 13.28 CH solution the pH value of the mixture continuously dropped and finally reached 10.88, never dropping below pH 9. However, since the pH value never got below pH 9 no additional pH regulation was necessary to keep the pH value above 9. The pH

measurements were done by a Thermo Orion 4 Star after calibrating the device with solutions of known pH values of 4.01, 7.00 and 10.01.

Mixing of the suspensions was accomplished at constant temperature (30 °C) in a magnetic stirrer with varying speeds (IKA Works, Inc., Yellowline MSC basic C). The stirrer has an integrated heater which allows heating the mixture and keeping the temperature at the desired value. The device is capable to apply and control temperatures up to 450 °C and speeds up to 1200 rpm. The solutions were heated to 30 °C before reaction and kept at 30 °C to overcome changes in the ambient temperature depending on seasonal variations throughout the study.

3.1.2. Microwave Treatment

The resulting mixture of solutions was immediately placed into a commercial microwave oven in an open glass beaker. The microwave oven chosen for this purpose was a 2400 W commercial microwave oven (Beko Turkey intellowave MD1585, 2.45 GHz, 1300 W). The microwave oven has preset microwave powers of 100, 400, 650 and 1300 W and can be programmed up to 60 min.

The beaker containing the mixed reactants was held in the microwave oven for 30 min, and the microwave power was selected as 1300 W. After the microwave irradiation the HA suspension processed in the microwave oven was taken out of the microwave oven and left to cool in open atmosphere. It was further centrifuged at 3000 rpm for 5 min to remove the impurity ions resulting from the chemical reaction. To ensure complete removal of the impurity ions in the slurry the centrifugation process was repeated for 5 times. The filtration of the slurry after the microwave treatment stage was conducted using a centrifuge (Hettich Zentrifugen, Rotina 38).

3.1.3. Powder Drying

The following wet sludge was placed into the drying oven (Elektromag M 420 P) for final drying at 60 °C for 72 h. The dried powder taken out of the drying oven was ground

using an agate mortar and pestle by hand, and placed in a dark colored, closed sample bottle, and stored in a desiccator until further analysis.

3.1.4. Preparation of Control Sample

A control sample was also prepared using the above described procedure but without any subsequent exposure to microwave irradiation. For this purpose, the obtained precipitate was immediately centrifuged after the mixing of the reagent solutions without further aging.

3.1.5. Characterization Techniques

The powder samples were characterized by X-ray diffraction (XRD, Rigaku D/Max-Ultima+/) for the existing phases and crystallite sizes where data was collected over the 2θ range of 10°-70° with a step size of 0.02° and step time of 2 s. The particle sizes of the produced powders with and without using microwave were determined by a particle size measurement device (Malvern Instruments Nano ZS). Scanning electron microscope (SEM, Philips XL ESEM-FEG&EDAX) micrographs were obtained at 150000x and 300000x to determine powder size and morphology.

3.2. Synthesis of Silver Substituted Nanosized Calcium Deficient Hydroxyapatite by Microwave

3.2.1. Powder Preparation

Analytical grade calcium hydroxide [$Ca(OH)_2$, Merck] and analytical grade diammonium hydrogen phosphate [$(NH_4)_2HPO_4$, Merck] were chosen for the preparation of CDHA. In order to produce silver substituted calcium deficient hydroxyapatite (SCDHA) extra pure silver nitrate [$AgNO_3$, Merck] was used as the silver source. The specific choice of precursor materials guarantees that the pH is approximately 10.5 throughout the reaction which is well above 9 such that there is no need to regulate the pH by adding any other chemical, e.g. ammonium hydroxide.

Calcium deficient hydroxyapatite was prepared without any silver addition which will further be denoted as CDHA as described earlier. To produce CDHA the amount of the reactants was calculated based on the Ca:P molar ratio of 1.6. Regarding the substitution of calcium by silver in SCDHA [$Ca_{10-x-y}Ag_y(HPO_4)_x(PO_4)_{6-x}(OH)_{2-x}$] powders with varying silver content were prepared where the (calcium+silver):phosphate molar ratio was fixed at 1.6. Three different compositions of silver SCDHA were prepared where y is set to 0.05, 0.10 and 0.15. These compositions will further be referred as 5SCDHA, 10SCDHA and 15SCDHA according to their silver content, respectively.

To prepare SCDHA, 0.25 M suspension of calcium hydroxide and 0.25 M solutions of diammonium hydrogen phosphate and silver nitrate were prepared using deionized water at 30 °C. The silver nitrate solution was slowly added to the calcium hydroxide suspension under stirring conditions while the temperature of the calcium hydroxide suspension was kept constant at 30 °C. The diammonium hydrogen phosphate solution was slowly added at the rate of 5 ml/min to the silver nitrate dissolved calcium hydroxide aqueous suspension. To prepare CDHA, the step of silver nitrate addition was omitted while the other parameters and the procedure were kept the same.

3.2.2. Microwave Treatment

After the addition of the reactants under vigorous stirring conditions the resulting suspension was immediately placed into a commercial microwave oven (Beko Turkey intellowave MD1585, 2.45 GHz, 1300 W) with adjustable microwave power settings to achieve rapid aging and crystallization of the produced powder. After microwave processing the precipitate was thoroughly washed via centrifugation using deionized water for 5 times to remove impurity ions resulting from the reaction. The slurry was oven dried in glass beakers at 40 °C for 96 h. The dried powder was ground using an agate mortar and pestle by hand and stored in a desiccator in dark colored glass bottles wrapped in aluminum foil.

To determine the effect of varying microwave power and time of exposure to microwave irradiation on the crystallite size of the powders and the phase formations four different batches of 15SCDHA powder were prepared using two different microwave

powers (650 and 1300 W) and two different durations of exposure to microwave (15 min and 30 min).

3.2.3. Calcination

In order to determine the effect of calcination CDHA, 5SCDHA, 10SCDHA and 15SCDHA samples prepared using microwave irradiation of 1300 W for 30 min were calcined at 700 °C for 1 h. The CDHA sample was also calcined at 600 and 800 °C for 1 h for comparison purposes. These samples were calcined in a furnace at a heating rate of 5 °C/min, held at the calcination temperature for 1 h and left in the oven to cool down to room temperature.

3.2.4. Characterization Techniques

The powder samples were characterized by X-ray diffraction (XRD, Rigaku D/Max-Ultima+/) for the existing phases and crystallite sizes where data was collected over the 2θ range of 10°-70° with a step size of 0.02° and step time of 2 s. Fourier transform infrared (FTIR, Perkin Elmer Spectrum One) analyses were conducted for the determination of the functional groups and scanning electron microscope (SEM, Philips XL ESEM-FEG&EDAX) micrographs were obtained to determine powder size and morphology.

The intensity of (221) lattice plane of β-TCP on the XRD patterns were used as an indicator of its purity. Therefore, the ratios of the peak intensities $I_{TCP(221)}/I_{HA(002)}$ were calculated for those samples for which β-TCP peaks were observed using the peak intensities of the (221) lattice plane for β-TCP and the (002) lattice plane for HA obtained by the XRD analysis.

The crystallite sizes of the powders were determined using the Scherrer's formula at the isolated diffraction peak at around 25.9°

$$C_S = \frac{K \cdot \lambda \cdot \cos\theta}{b} \quad (3.1)$$

where;

C_S: average crystallite size (nm)

K: shape factor (K = 0.9)

λ: wavelength of x-rays (λ = 0.154056 nm for Cu Kα radiation)

θ: diffraction angle (degree)

b: broadening of the diffraction peak at half of its maximum intensity (radian).

Two different methods were utilized to determine the diffraction angle of the indicated diffraction peak and the broadening of the diffraction peak at half of its maximum intensity. The first method was measuring the diffraction angle and the peak broadening on the XRD graphs of the samples, whereas the second method was finding the requested parameters by interpolation using the raw data of the XRD analysis. Both methods were found successful in terms of reflecting the relative relationship between the samples and therefore, each method was correct and consistent in itself. However, calculations showed that using measurements made on the graphs resulted in crystallite sizes consistently higher 5 to 10 % than the crystallite sizes obtained by using interpolation on the raw data. Although, these differences were not significant in terms of comparing the crystallite sizes of the samples relative to each other they were thought to result first, from the possible errors resulting from the measurement procedure and then, from using interpolation on the raw data.

3.2.5. Antibacterial Assessment

The antibacterial effect of silver addition was assessed against Escherichia coli [IFO 3972] (E. coli) and Staphylococcus aureus [IFO 12-732] (S. aureus) bacteria after 30 min and 24 h. For this purpose bacterial solution with a concentration of $1x10^6$ cfu/ml (colony forming unit/ml) was prepared using 1/500 nutrient broth. 100 mg of sample powder was mixed with 10 ml bacterial solution and shaken for 30 min using a shaker. The initial response to the powders was detected right after the shaking (30 min). To determine the response after 24 h of contact time the samples were incubated at 37 °C for 24 h and then the colony formation was evaluated (24 h). The experiments were repeated in two different

laboratory settings using the same set of parameters and powders to check the consistency of the results.

3.3. Synthesis of Silver Substituted Nanosized Stoichiometric Hydroxyapatite by Microwave

3.3.1. Powder Preparation

As similar to the preparation of nanosized calcium deficient hydroxyapatite, analytical grade calcium hydroxide [$Ca(OH)_2$, Merck] and analytical grade diammonium hydrogen phosphate [$(NH_4)_2HPO_4$, Merck] were chosen for the preparation of stoichiometric hydroxyapatite (HA). In order to produce silver substituted stoichiometric hydroxyapatite (SHA) extra pure silver nitrate [$AgNO_3$, Merck] was used as the silver source.

To produce SHA the amount of the reactants was calculated based on the Ca:P molar ratio of 10:6. Regarding the substitution of calcium by silver in SHA [$Ca_xAg_y(PO_4)_6(OH)_2$] powders with varying silver content were prepared where the (calcium+silver):phosphate molar ratio was fixed at 10:6 such that (x+y) always kept constant accordingly. Three different compositions of silver SHA were prepared where y is set to 0.03, 0.06 and 0.09. These compositions will further be referred as 3SHA, 6SHA and 9SHA according to their silver content, respectively.

To prepare SHA, 0.25 M suspension of calcium hydroxide and 0.25 M solutions of diammonium hydrogen phosphate and silver nitrate were prepared using deionized water at 30 °C. The silver nitrate solution was slowly added to the calcium hydroxide suspension under stirring conditions while the temperature of the calcium hydroxide suspension was kept constant at 30 °C. The diammonium hydrogen phosphate solution was slowly added at the rate of 5 ml/min to the silver nitrate dissolved calcium hydroxide aqueous suspension. To prepare SHA, the step of silver nitrate addition was omitted while the other parameters and the procedure were kept the same.

3.3.2. Microwave Treatment

After the addition of the reactants under vigorous stirring conditions the resulting suspension was immediately placed into a commercial microwave oven (Beko Turkey intellowave MD1585, 2.45 GHz, 1300 W) with adjustable microwave power settings to achieve rapid aging and crystallization of the produced powder. After microwave processing at 650 W for 15 min the precipitate was thoroughly washed via centrifugation using deionized water for 5 times to remove impurity ions resulting from the reaction. The slurry was oven dried in glass beakers at 40 °C for 96 h. The dried powder was ground using an agate mortar and pestle by hand and stored in a desiccator in dark colored glass bottles wrapped in aluminum foil.

3.3.3. Compaction and Sintering

SHA, 3SHA, 6SHA and 9SHA powders were calcined at 900 °C for 1 h at a heating rate of 5 °C/min and left to cool down in the oven to room temperature. Pellet samples were prepared from the calcined powders using 0.5 g of sample powder. Powders were first compacted in a stainless steel die (Figure 3.2) with a diameter of 10 mm using a manually operated uniaxial press under 80 MPa. The formed pellets were further cold isostatically pressed under 350 MPa. In order to determine the effect of sintering temperature on the densification of the powders HA and 3SHA pellet samples were sintered at 900, 1000 and 1100 °C for 1 h at a heating rate of 10 °C/min and a slower cooling rate of 5 °C/min to avoid cracking of the sintered pellets.

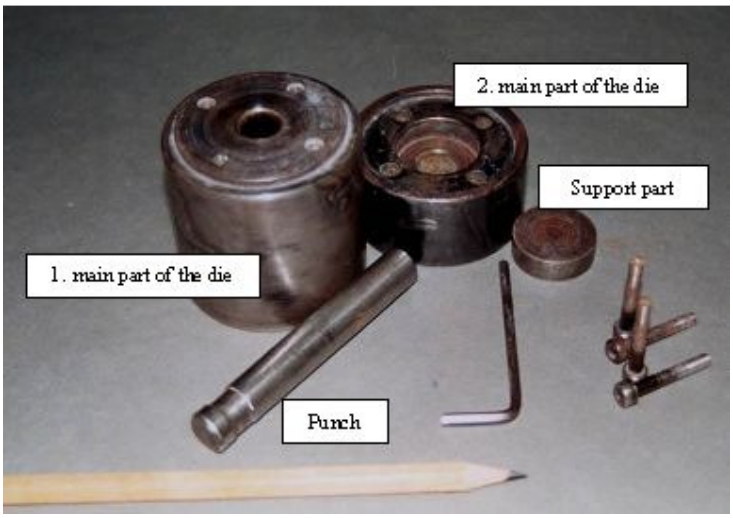

Figure 3.2. Stainless steel die used to prepare the pellet specimens [117].

3.3.4. Characterization Techniques

The powder samples were characterized by X-ray diffraction (XRD, Rigaku D/Max-Ultima+/) for the existing phases where data was collected over the 2θ range of 10°-70° with a step size of 0.02° and step time of 2 s. Fourier transform infrared (FTIR, Perkin Elmer Spectrum One) analyses were conducted for the determination of the functional groups. Scanning electron microscope (SEM, Philips XL ESEM-FEG&EDAX) micrographs were obtained for the pellets to determine the effect of sintering temperature on the densification behavior of the powders.

3.3.5. Antibacterial Assessment

Similar to the antibacterial assessment of the silver substituted calcium deficient hydroxyapatite, the antibacterial effect of silver addition was assessed against Escherichia coli [IFO 3972] (E. coli) and Staphylococcus aureus [IFO 12-732] (S. aureus) bacteria after 30 min and 24 h 100 mg of sample powder was mixed with 10 ml bacterial solution of a concentration of $1x10^6$ cfu/ml which was prepared using 1/500 nutrient broth and shaken for 30 min in a shaker. The initial bacterial response to the prepared powders was detected right after the shaking (30 min). To determine the response after 24 h of contact time the samples were incubated at 37 °C for 24 h following which the colony formation was evaluated (24 h).

3.4. Production of Silver Substituted Hydroxyapatite Coatings on Titanium Substrates by Electrophoretic Deposition

3.4.1. Preparation of Titanium Substrates for Coating by Electrophoretic Deposition

The titanium substrates (Grade 4, pure Ti) were ground using 240-1000 grid grinding paper. The ground substrates were held in ultrasonic bath first using deionized water and a commercial detergent for 30 min and then using acetone for 15 min for cleaning. The cleaned substrates were passivated in 25 % nitric acid (69.0-71.0 % Merck, Germany) by volume for 12 h and finally thoroughly cleaned using deionized water.

Substrates of different geometries were prepared for SEM imaging, XRD analysis and mechanical tests. Substrate dimensions were tabulated and substrate geometries were given (Table 3.1).

Table 3.1. Dimensions of substrates prepared for various tests.

Substrate type	Height (mm)	Width (mm)	Thickness (mm)
SEM imaging	25	15	1
XRD analysis	25	15	1
Antibacterial test	30	25	1
Mechanical test*	5	25	3

* distance of the center of hole to the nearest end: 14 mm, hole diameter: 12 mm

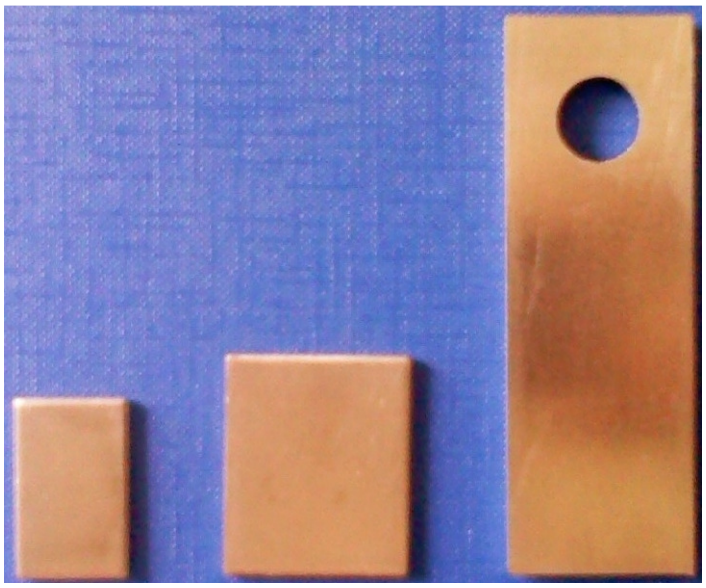

Figure 3.3. Types of prepared substrates for SEM imaging and XRD analysis (left), antibacterial test (middle), and mechanical testing (right).

3.4.2. Coating of Silver Substituted Nanosized Stoichiometric Hydroxyapatite on Titanium Substrates by Electrophoretic Deposition

Silver containing HA (9SHA) powders were used to prepare coatings on titanium substrates. For this purpose, 9SHA powders were calcined at 900 °C in open atmosphere for 1 h and ground by hand using an agate mortar and pestle. Suspensions were prepared by adding 1.0 g of calcined 9SHA powder into 100 ml ethanol (Merck 96 %, Germany). The prepared suspensions were magnetically stirred for 20 min (IKA MSC Basic C) and dispersed in an ultrasonic bath (Everest Elektromekanik, Turkey) at 30 °C for 30 min. The suspensions were left to rest for a following 30 min to eliminate agglomerated particles. After decantation the remaining suspensions were further dispersed ultrasonically for 30 min and used for electrophoretic deposition after adjusting the initial pH value of the suspension to pH 3.8 by drop wise addition of 1 M HCl (Merck, HCl, 1 M, Germany) according to the performed zeta potential measurements.

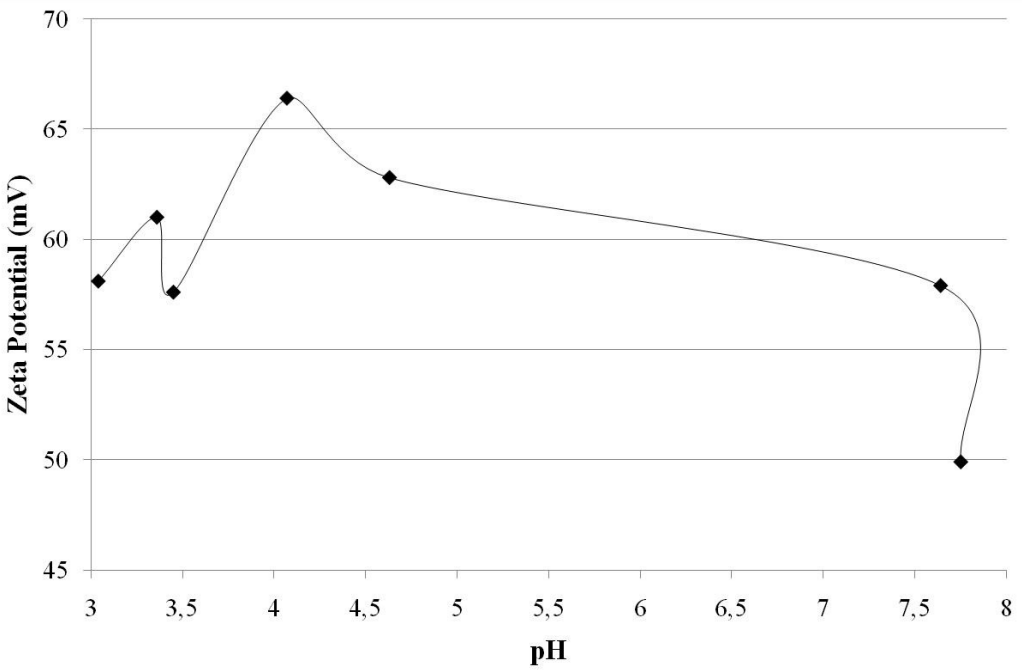

Figure 3.4. Zeta potential values of the 9SHA powder in ethanol suspension (1.0 g/100 ml) as a function of pH value of the suspension.

Electrodes consisting of titanium substrates were placed in 9SHA suspension parallel to each other with a separation of 10 mm (Figure 3.5) and electrophoretic deposition took place at constant voltages of 100 and 200 V for 1 min. The obtained coated specimen were sintered in a vacuum furnace under $1x10^{-5}$ mbar at 800 and 900 °C for 1 h at a heating rate of 100 °C/h and a cooling rate of 50 °C/h to prevent crack occurrence in the coating layer.

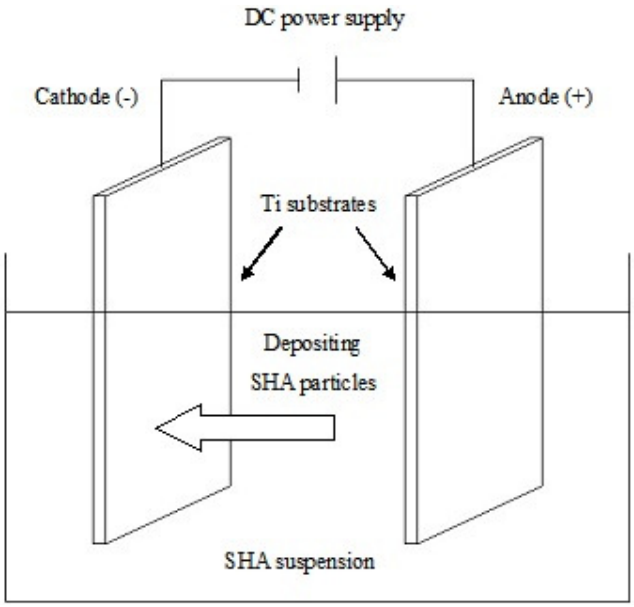

Figure 3.5. Schematic view of the electrophoretic deposition process setup.

3.4.3. Controlling the Decomposition of Silver Substituted Stoichiometric Hydroxyapatite Coatings by the Use of Titanium Dioxide Inner Layer Application

TiO_2 inner layer coatings were performed to prevent 9SHA decomposition resulting from ion transfer from the underlying titanium substrate into the HA coating layer. For this purpose the titanium substrates were first coated using TiO_2 (Alfa Aesar, Titanium (IV) oxide, anatase, 99.9 %, Germany) having an average particle size of 35 nm. TiO_2 suspensions were prepared using the same procedure and parameters as previously described for the preparation of 9SHA suspensions the only difference being the suspension pH which was adjusted to pH 3 by the zeta potential measurements of the TiO_2 suspension. Titanium substrates prepared as described previously were first coated with TiO_2. The TiO_2 coated samples were dried at 40 °C in open atmosphere for 24 h. The dried samples were then coated by 9SHA using electrophoretic deposition and sintered in a vacuum furnace. The sintering stage took place in a single step after coating the substrates both with TiO_2 inner layer and 9SHA layer to prevent the negative effect of the sintering on the mechanical properties of the titanium substrates due to the elevated sintering temperatures.

Titanium substrates were first coated with TiO_2 at 20, 40 and 50 V for 60 s and then with 9SHA at 80 and 200 V for 60 s. Also samples were prepared without any TiO_2 inner layer by coating of 9SHA at 100 V. The obtained coated samples were sintered in a vacuum furnace under $1x10^{-5}$ mbar at temperatures 800, 900, and 1000 °C for 1 h at a heating rate of 100 °C/h and a cooling rate of 50 °C/h. XRD analysis was performed to determine the effect of TiO_2 inner layer on the decomposition characteristics of 9SHA coatings.

The set parameters of parameters used to determine the effect of TiO_2 inner layer on the decomposition characteristics of 9SHA coatings were tabulated (Table 3.2).

Table 3.2. Parameters of the samples prepared to determine the effect of TiO_2 inner layer on the decomposition characteristics of 9SHA coatings.

TiO_2 inner layer coating		9SHA coating		Sintering	
Voltage (V)	Duration (s)	Voltage (V)	Duration (s)	Temperature (°C)	Duration (h)
-	-	100	60	90	1
-	-	100	60	1000	1
20	60	80	60	900	1
20	60	80	60	1000	1
40	60	80	60	900	1
40	60	80	60	1000	1
50	60	200	60	800	1
50	60	200	60	900	1

Samples prepared for the XRD analysis of the outer layer in order to determine the effects of TiO_2 coating voltage and the sintering temperature on the 9SHA decomposition were presented in Figure 3.6.

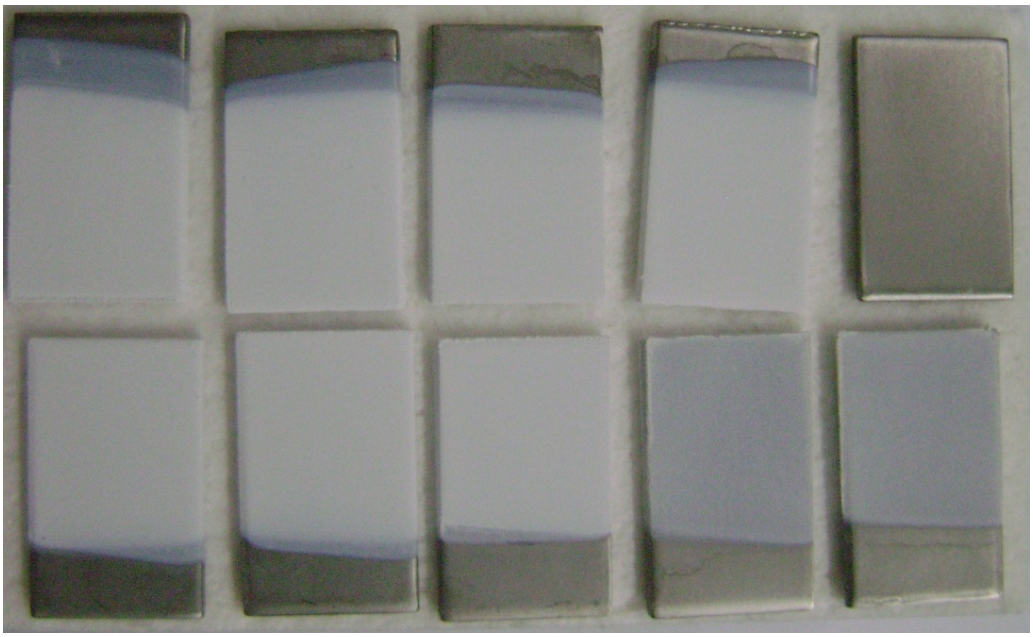

Figure 3.6. XRD samples prepared to determine the effects of TiO_2 coating voltage and sintering temperature on 9SHA decomposition (light grey areas: TiO_2 coating; white areas: 9SHA coating; right most sample in the upper row: titanium substrate without coating).

3.4.4. Determination of the Effect of Titanium Dioxide Inner Layer Application on the Sintering Characteristics of Silver Substituted Stoichiometic Hydroxyapatite Coatings

Titanium substrates were first coated with TiO_2 at 20 and 40 V for 60 s and then with 9SHA at 80 and 200 V for 60 s. The obtained coated samples were sintered in a vacuum furnace under $1x10^{-5}$ mbar at temperatures 900 and 1000 °C for 1 h at a heating rate of 100 °C/h and a cooling rate of 50 °C/h SEM analysis was performed to determine the effect of TiO_2 inner layer on the sintering characteristics of 9SHA coatings.

The set parameters of parameters used to determine the effect of TiO_2 inner layer on the sintering characteristics of 9SHA coatings were tabulated (Table 3.3).

Table 3.3. Parameters of the samples prepared to determine the effect of TiO_2 inner layer on the sintering characteristics of 9SHA coatings.

TiO_2 inner layer coating		9SHA coating		Sintering	
Voltage (V)	Duration (s)	Voltage (V)	Duration (s)	Temperature (°C)	Duration (h)
20	60	200	60	800	1
20	60	200	60	900	1
20	60	80	60	900	1
20	60	80	60	1000	1
40	60	80	60	900	1
40	60	80	60	1000	1

3.4.5. Mechanical Strengths of the Coatings Produced by the Electrophoretic Deposition of Silver Substituted Stoichiometric Hydroxyapatite on Titanium Substrates with the Use of Titanium Dioxide Inner Layer Application

A test setup was prepared to determine the shear strength of the produced coatings. For this purpose an attachment was produced which allows vertical alignment of the test sample. A coated sample was glued on an uncoated sample (Figure 3.6) by using an epoxy resin (DP100, 3M, USA) according to ASTM F1044-99 [118] and the coated side of the sample was fixed in the attachment using a pin allowing horizontal movement. The uncoated side of the sample was fixed in the lower jaw of the testing machine (Z100, Zwick Roell, Germany). Titanium substrates were first coated with TiO_2 at 10, 20 and 50 V for 30 and 60 s and then with 9SHA at 200 V for 60 s. The obtained coated samples were sintered in a vacuum furnace under $1x10^{-5}$ mbar at temperatures 900 and 1000 °C for 1 h at a heating rate of 100 °C/h and a cooling rate of 50 °C/h. Mechanical tests were conducted to determine the effect of TiO_2 inner layer coating parameters and the sintering temperature on the shear strengths of 9SHA coatings. The mechanical tests were conducted using a universal mechanical testing device with a 100 kN load cell and a cross head speed of 1 mm/min.

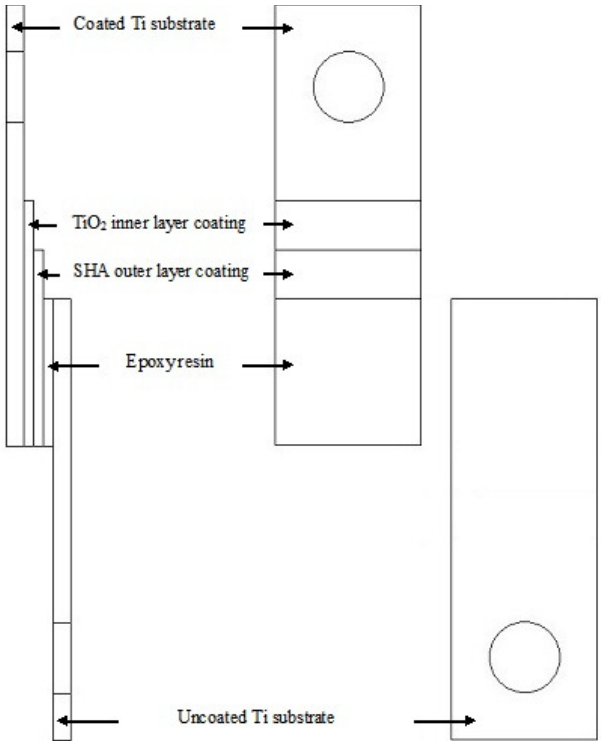

Figure 3.7. Schematic view of the mechanical test sample.

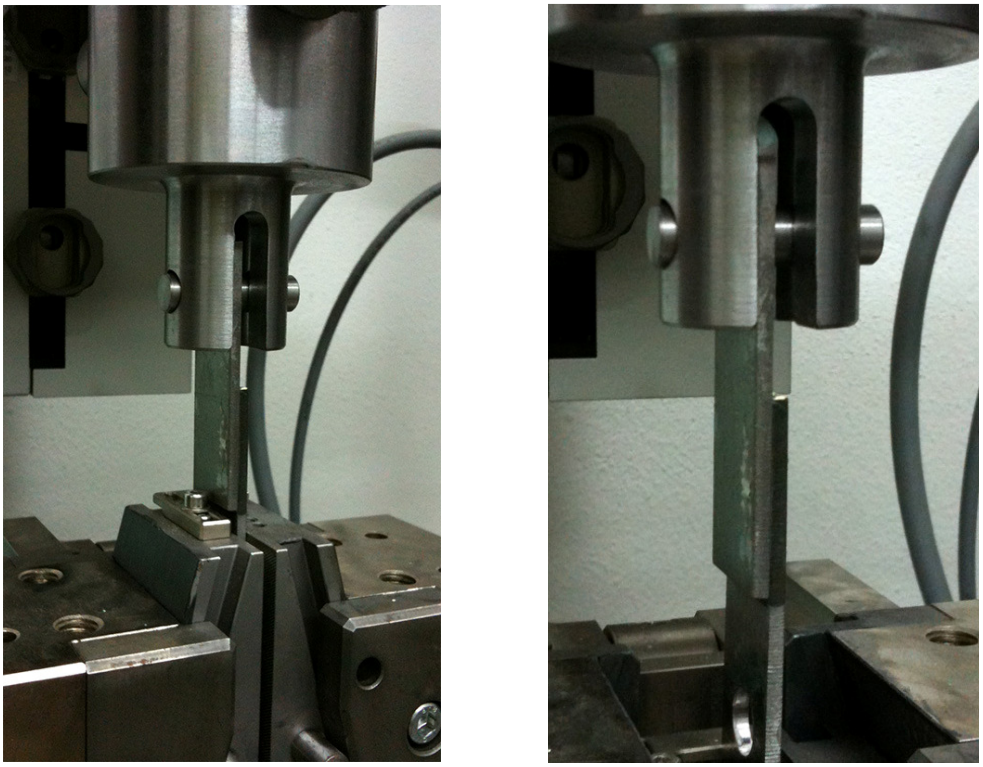

Figure 3.8. Experimental setup and produced attachment to test the shear strength of the coated samples.

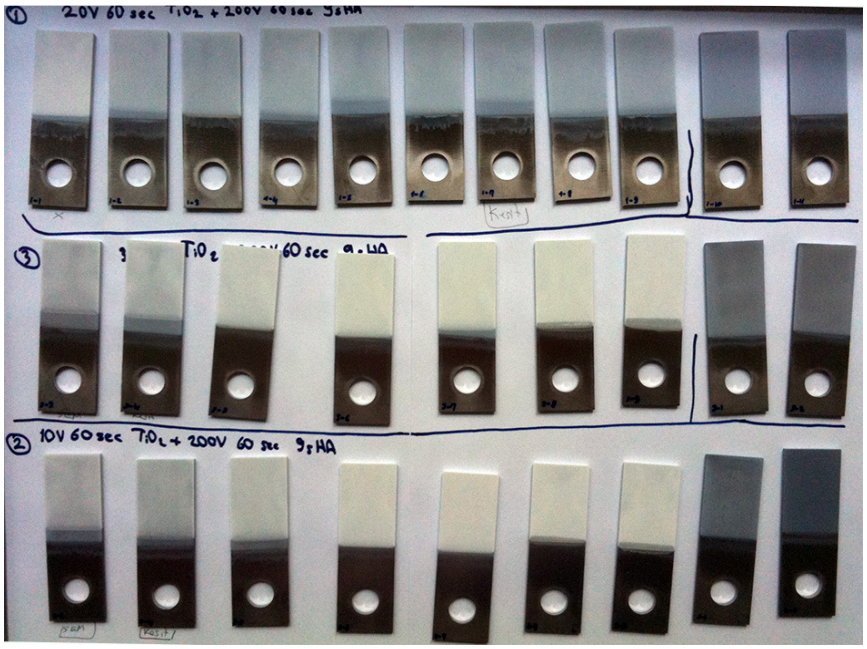

Figure 3.9. Samples prepared for testing the mechanical strength of the coatings produced by the electrophoretic deposition of 9SHA on titanium substrates with the use of TiO_2 inner layer application.

The set of parameters used to determine the shear strengths of the 9SHA coatings prepared with the application of TiO2 inner layer by electrophoretic deposition were tabulated (Table 3.4).

Table 3.4. Samples prepared to determine the effect of TiO_2 inner layer coating parameters on the mechanical strength of 9SHA coatings.

TiO_2 inner layer coating		9SHA coating		Sintering	
Voltage (V)	Duration (s)	Voltage (V)	Duration (s)	Temperature (°C)	Duration (h)
50	60	200	60	900	1
50	60	200	60	1000	1
20	60	200	60	900	1
20	60	200	60	1000	1
10	60	200	60	900	1
20	30	200	60	900	1

4. RESULTS AND DISCUSSION

4.1. Synthesis of Nanosized Calcium Deficient Hydroxyapatite by Microwave

4.1.1. XRD Study of Nanosized Calcium Deficient Hydroxyapatite Produced with and without Use of Microwave

Both of the samples prepared using microwave irradiation and the sample prepared without microwave application were found to be hydroxyapatite. The XRD spectra (Figures 4.1-4.2) of both samples were in close agreement with "JCPDS 86-0740" and no peaks other than hydroxyapatite were observed.

The difference between the two samples was that the peaks of the microwave treated sample were more distinctive. This leads to the fact that the sample prepared using microwave irradiation was more crystallized than the sample prepared without microwave application which in turn indicates that application of microwave irradiation had a positive effect on the crystallization of the produced calcium deficient hydroxyapatite. Thus, microwave irradiation was found to be an efficient method for the crystallization of the precipitated powder.

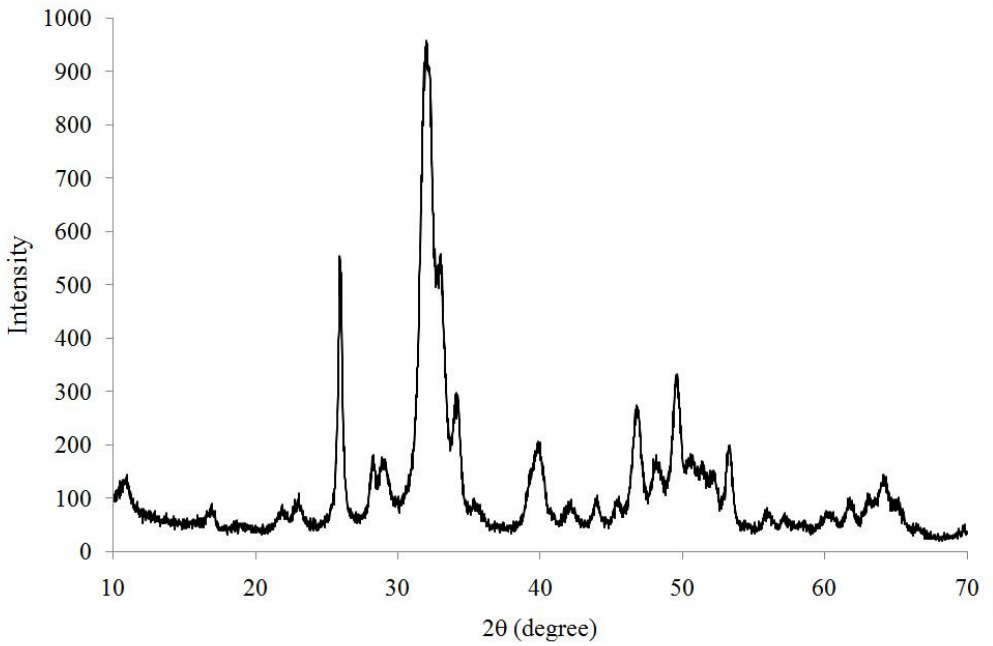

Figure 4.1. XRD spectrum of the calcium deficient hydroxyapatite powder sample prepared without microwave irradiation.

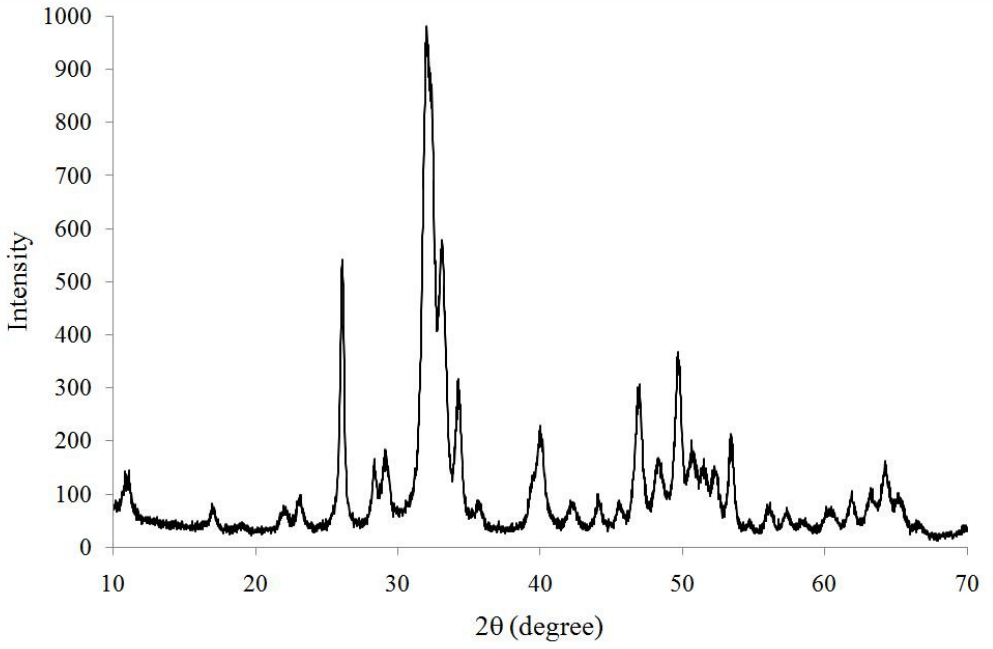

Figure 4.2. XRD spectrum of the calcium deficient hydroxyapatite powder sample prepared using microwave irradiation (1300 W, 30 min).

4.1.2. Effect of Microwave Application on the Particle Morphology of Nanosized Calcium Deficient Hydroxyapatite Powder

The investigation of the SEM images of the samples prepared with (Figures 4.3-4.5) and without (Figures 4.6-4.8) microwave treatment revealed that both processes resulted in the precipitation of rod like hydroxyapatite particles. However, the particles prepared using microwave irradiation were slightly smaller than the particles prepared without microwave application. This observation supported the results of the XRD study and showed that microwave treatment enhanced the crystallization of hydroxyapatite.

Rod like calcium deficient hydroxyapatite particles with 90-110 nm length and 20-30 nm width were obtained using microwave treatment at 1300 W microwave power for 30 min.

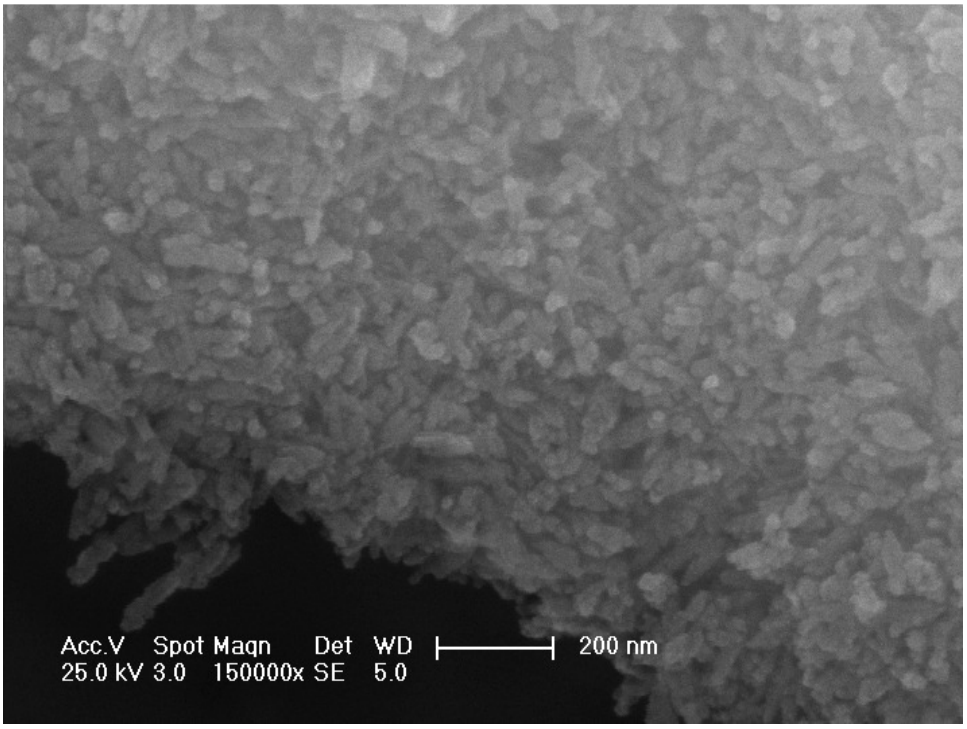

Figure 4.3. SEM image of the calcium deficient hydroxyapatite powder sample prepared using microwave irradiation (1300 W, 30 min, 150000x).

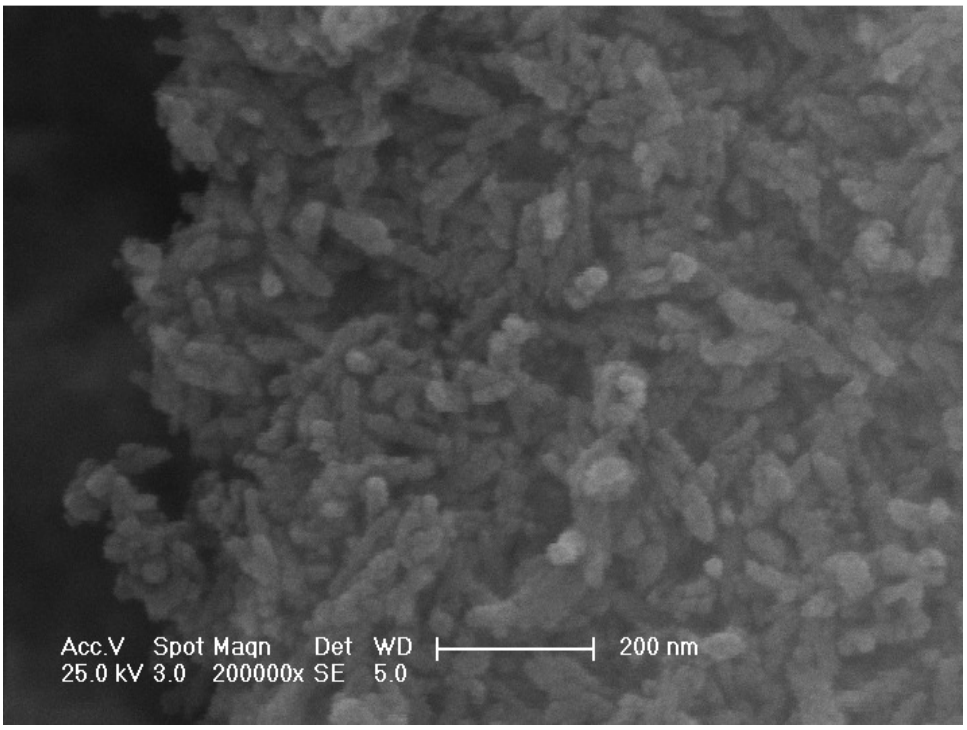

Figure 4.4. SEM image of the calcium deficient hydroxyapatite powder sample prepared using microwave irradiation (1300 W, 30 min, 200000x).

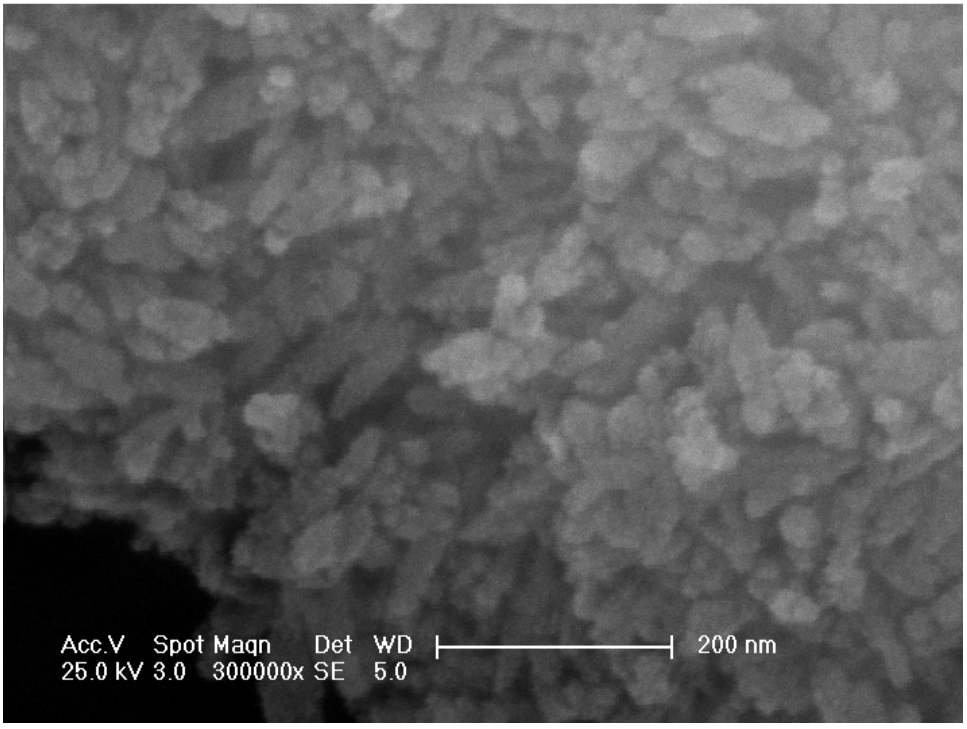

Figure 4.5. SEM image of the calcium deficient hydroxyapatite powder sample prepared using microwave irradiation (1300 W, 30 min, 300000x).

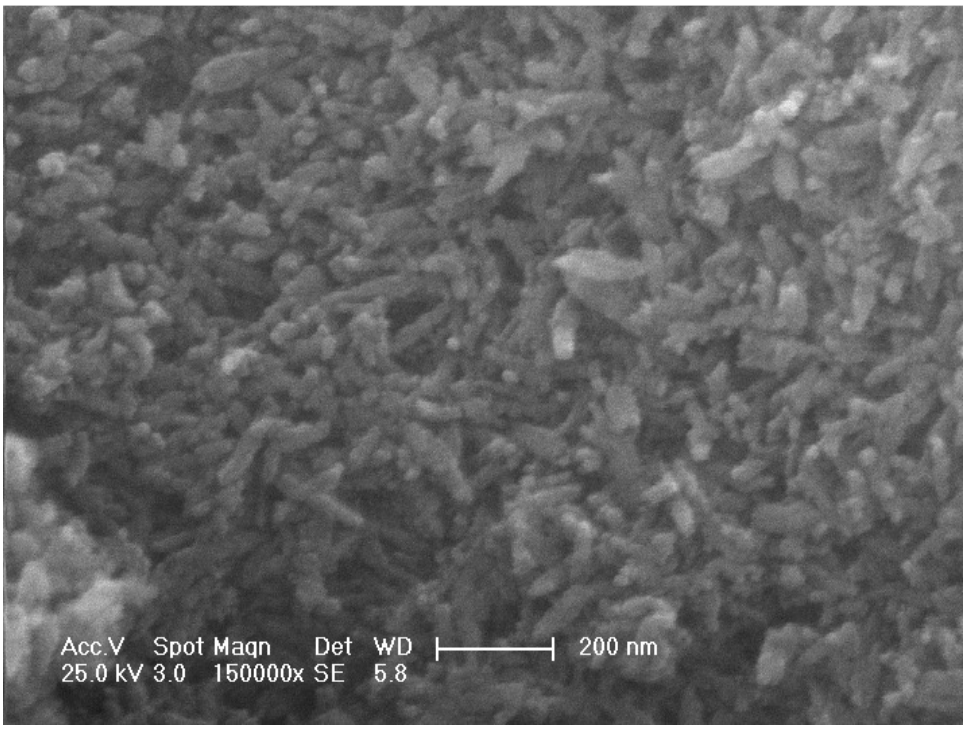

Figure 4.6. SEM image of the calcium deficient hydroxyapatite powder sample prepared without microwave irradiation (150000x).

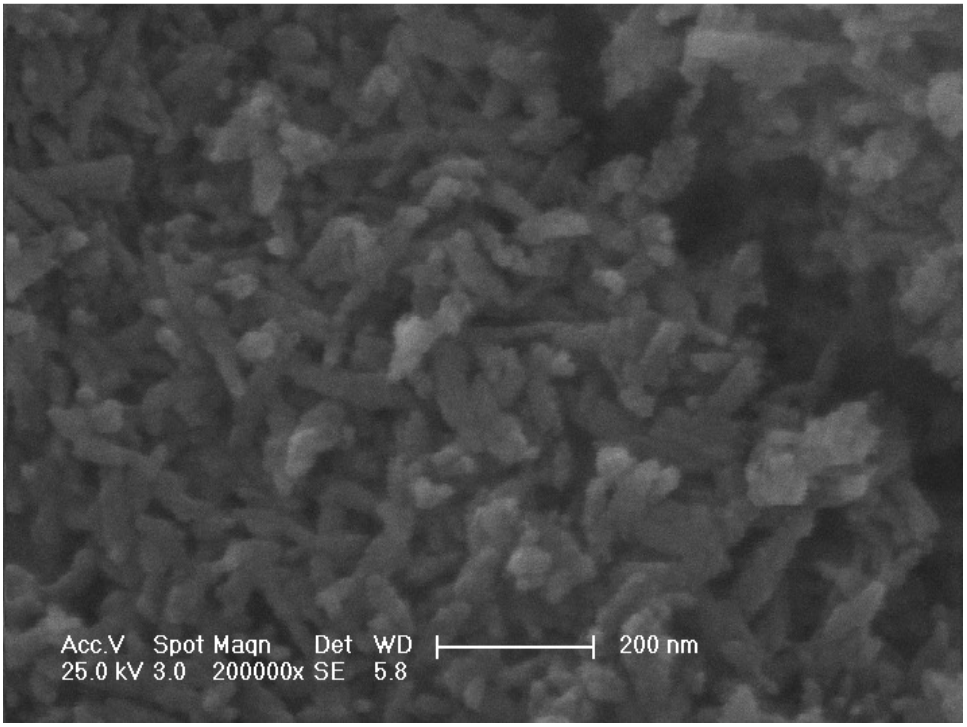

Figure 4.7. SEM image of the calcium deficient hydroxyapatite powder sample prepared without microwave irradiation (200000x).

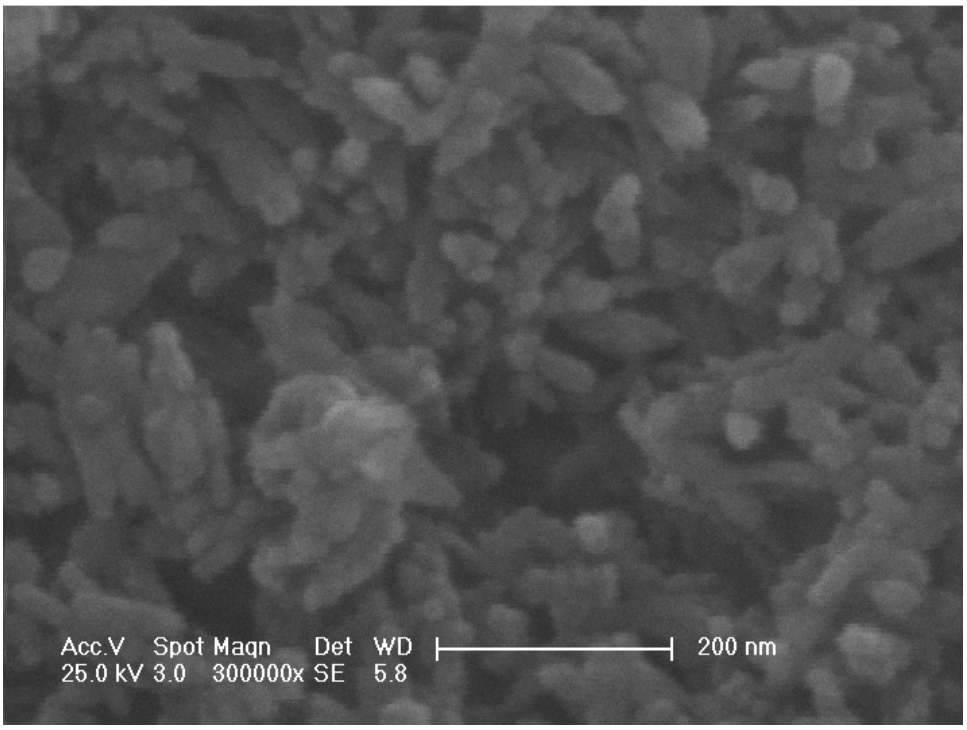

Figure 4.8. SEM image of the calcium deficient hydroxyapatite powder sample prepared without microwave irradiation (300000x).

4.1.3. Effect of Microwave Application on the Agglomeration Characteristics of Nanosized Calcium Deficient Hydroxyapatite Powder

50 mg of both of the prepared powders were dispersed in 50 ml of ethyl alcohol at ambient temperature. The suspensions were tested to determine the particle sizes of the dispersed powders using a particle size analyzer. Three consecutive particle size measurements were taken for each suspension with a time interval of 1 min to determine the time dependency of the agglomeration behavior of the powders (Figures 4.9-4.10).

Both of the powders showed a tendency to agglomerate as compared to the SEM images. The agglomerate sizes of the microwave treated sample turned out to increase with time being between 200-300 nm. On the other hand, the agglomerate size of the powder sample prepared without microwave treatment was found to be more stable at around 200 nm.

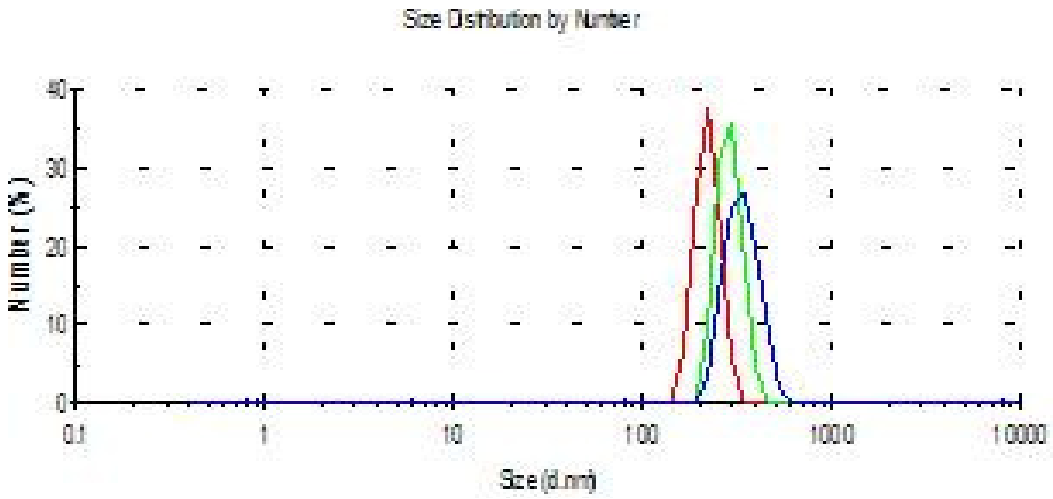

Figure 4.9. Particle size measurements of calcium deficient hydroxyapatite powder prepared using microwave irradiation (1300 W, 30 min) (measurements taken with a time interval of 1 min from left to right).

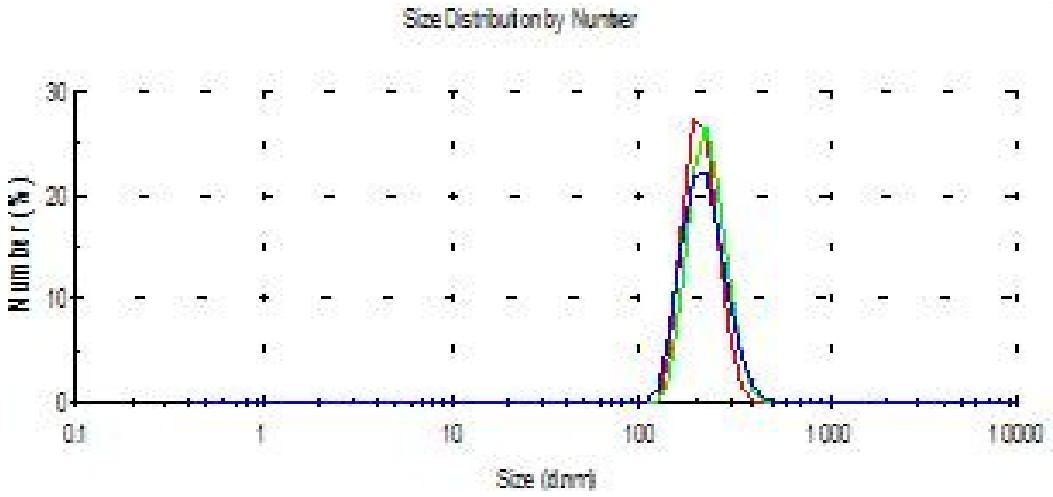

Figure 4.10. Particle size measurements of calcium deficient hydroxyapatite powder prepared without using microwave irradiation (1300 W, 30 min) (measurements taken with a time interval of 1 min from left to right).

Similar results were obtained in the particle size measurement tests conducted using acetone as medium. The starting agglomerate sizes of both powders were same while the agglomerate size of the microwave treated sample increased with time while the agglomerate size of the powder prepared without microwave irradiation remained stable during the experiments.

4.2. Synthesis of Silver Substituted Nanosized Calcium Deficient Hydroxyapatite by Microwave

4.2.1. XRD Study of Nanosized Calcium Deficient Hydroxyapatite with and without Silver Substitution

4.2.1.1. Effect of Microwave Treatment and Calcination on the Crystallite Size and β-TCP Formation of CDHA. The XRD patterns of both the microwave treated and not treated CDHA samples correspond to that of hydroxyapatite and no other peaks were observed (Figures 4.11 and 4.12) where the peaks became more distinctive by microwave treatment indicating better crystallinity. The microwave treated sample had well resolved peaks because of its improved crystallinity due to the subsequent microwave treatment. This leads to the fact that microwave treatment is an efficient method for the crystallization of CDHA.

The microwave process increased the average crystallite size of the powder from 19.9 to 22.5 nm (Table 4.1) on average, as calculated using Scherrer's formula (Eq. 3.1) at the isolated diffraction peak at around 25.9°.

The calcination study of the microwave treated CDHA sample showed that the powder was thermally stable at 700° C (Figure 4.14) whereas formation of the β-TCP peaks was observed at 800° C (Figure 4.15).

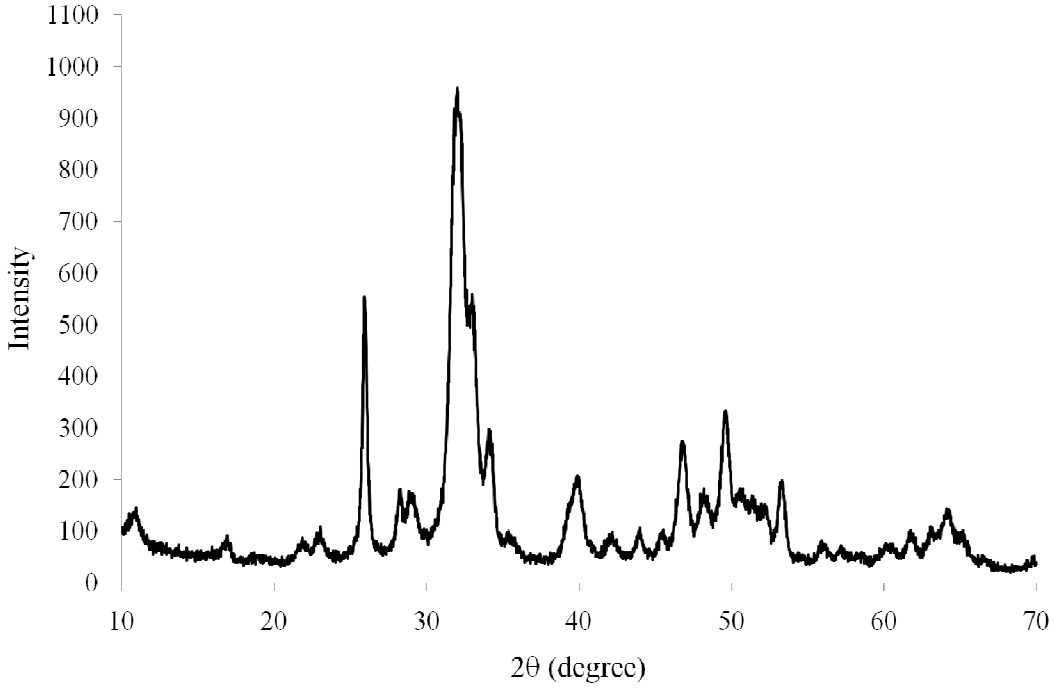

Figure 4.11. XRD spectrum of CDHA sample produced without microwave treatment.

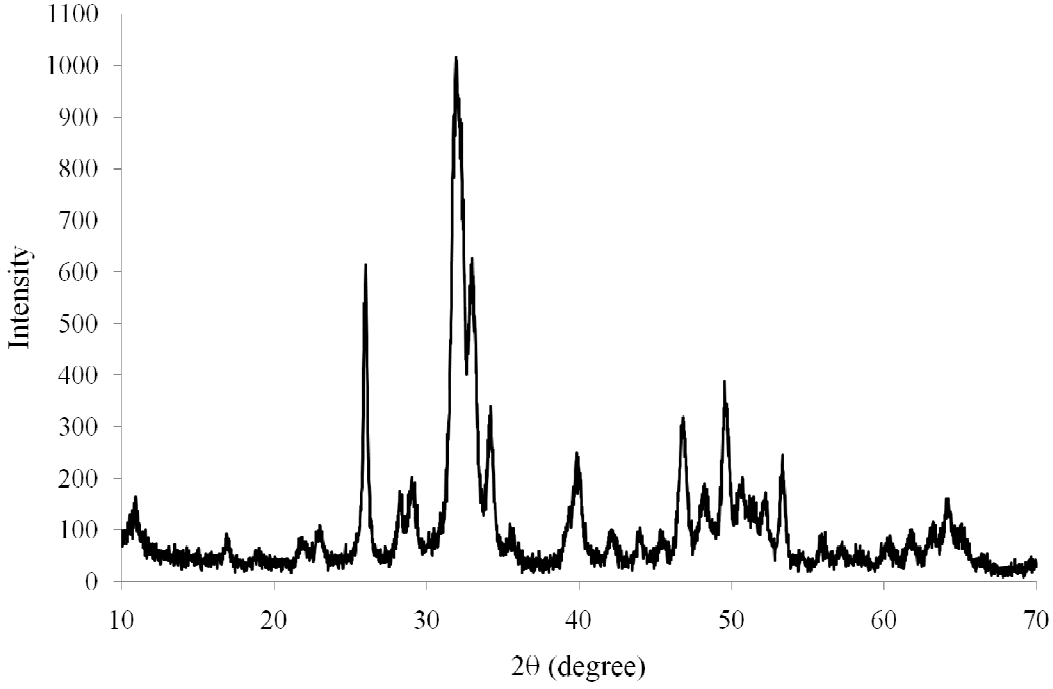

Figure 4.12. XRD spectrum of CDHA sample produced with microwave treatment at 1300 W for 30 min.

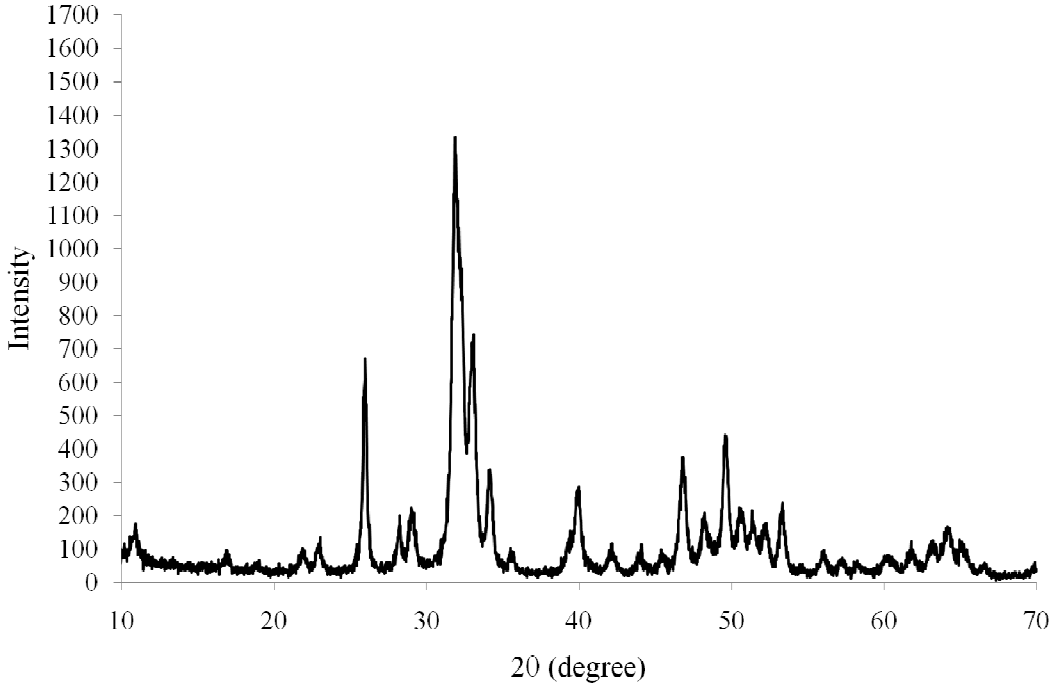

Figure 4.13. XRD spectrum of CDHA sample produced with microwave treatment at 1300 W for 30 min and calcined at 600 °C.

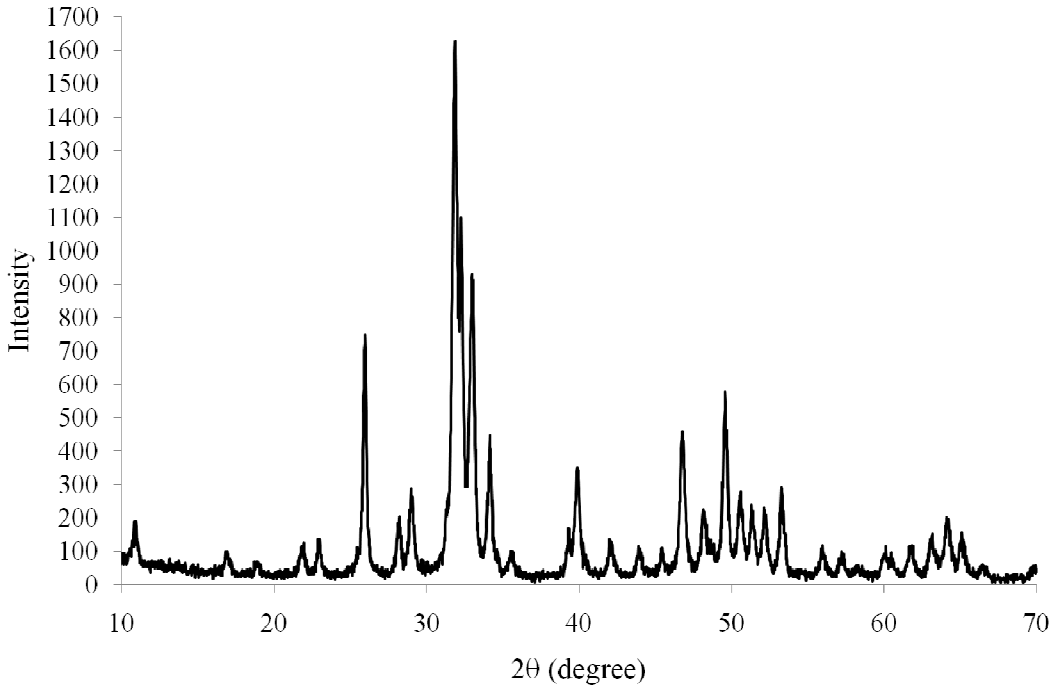

Figure 4.14. XRD spectrum of CDHA sample produced with microwave treatment at 1300 W for 30 min and calcined at 700 °C.

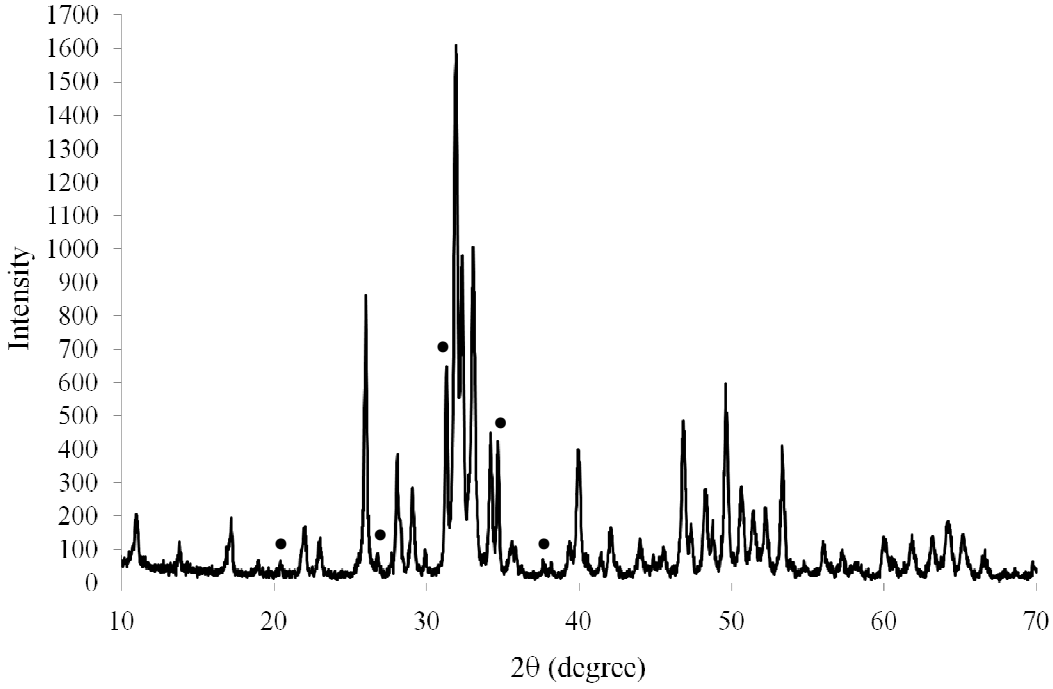

Figure 4.15. XRD spectrum of CDHA sample produced with microwave treatment at 1300 W for 30 min and calcined at 800 °C (•: β-TCP).

Table 4.1. Crystallite sizes and $I_{TCP(221)}/I_{HA(002)}$ ratios (where applicable) of CDHA powders produced using different microwave power and duration and at different calcination temperatures.

Sample	Microwave Power (W)	Microwave Time (min)	Calcination Temperature (°C)	$I_{TCP(221)}/I_{HA(002)}$ (for samples with β-TCP peaks)	Crystallite Size (nm)	
					Exp. Set #1	Exp. Set #2
CDHA	-	-	-	-	19.9	-
CDHA	1300	30	-	-	21.5	23.5
CDHA	1300	30	600	-	26.6	-
CDHA	1300	30	700	-	27.7	-
CDHA	1300	30	800	0.752	33.7	-

4.2.1.2. Effect of Microwave Treatment on the Crystallite Sizes of SCDHA Samples. The microwave power and duration influenced the crystallite size of the powders, calculated using the Scherrer's formula and the XRD data (Table 4.2). The crystallite size increased with decreasing microwave power and increasing microwave duration. However, the effect of the microwave power was more pronounced than the duration of the applied microwave process. More specifically, doubling the microwave duration had a minor effect on the crystallite size for both the microwave powers. However, doubling the microwave power had a greater effect on the decrease of the crystallite size for both durations.

This observation leads to the idea that crystallization under microwave was primarily controlled by the microwave power and not the duration. The decrease of the crystallite size with increasing microwave power from 650 W to 1300 W may be explained by two counteracting phenomenon as explained by Bouyer et al. [119]. An increase in temperature due to microwave processing increases the crystallinity which is thermally activated. However, the increase in temperature limits the tendency of the crystal growth following the c-axis. Since a slow increase in temperature can be achieved using a low microwave power the crystallite size of the powders prepared using a lower microwave power are greater. These results can be used to produce CDHA and SCDHA with desired crystallite size within a reasonable range by varying the microwave power and duration accordingly.

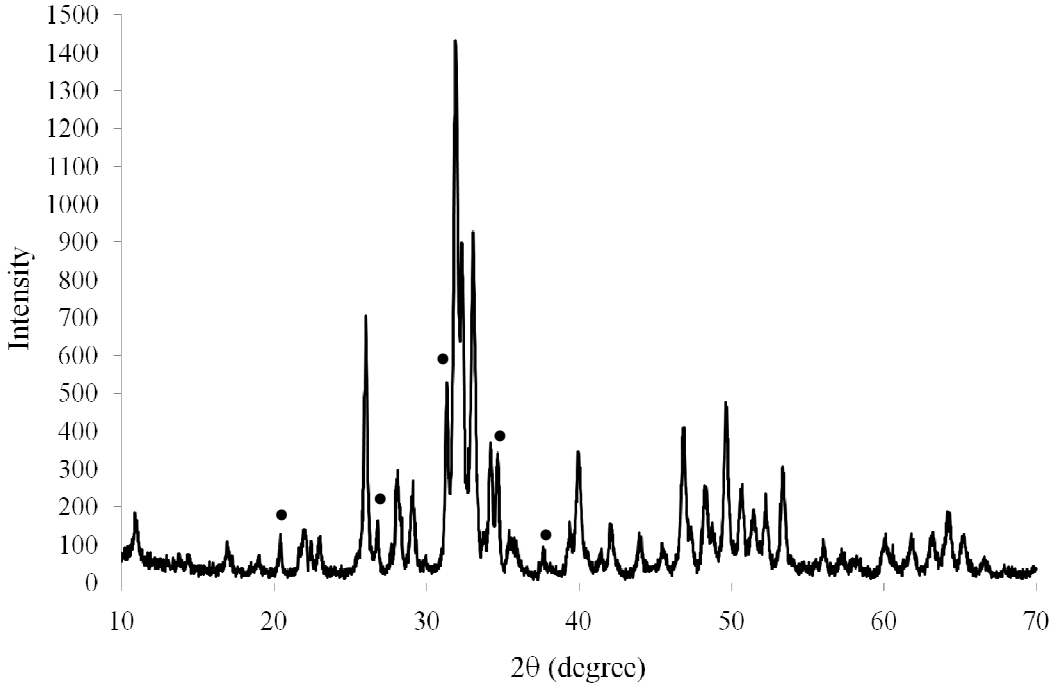

Figure 4.16. XRD spectrum of 15SCDHA sample produced with microwave treatment at 650 W for 15 min and calcined at 700 °C (•: β-TCP).

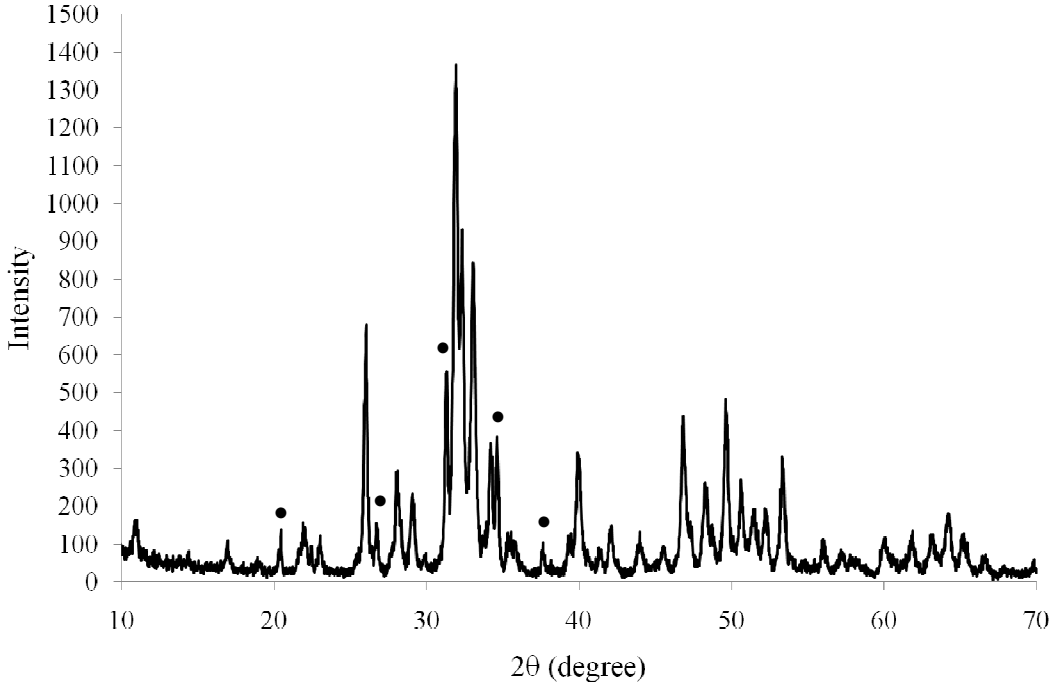

Figure 4.17. XRD spectrum of 15SCDHA sample produced with microwave treatment at 650 W for 30 min and calcined at 700 °C (•: β-TCP).

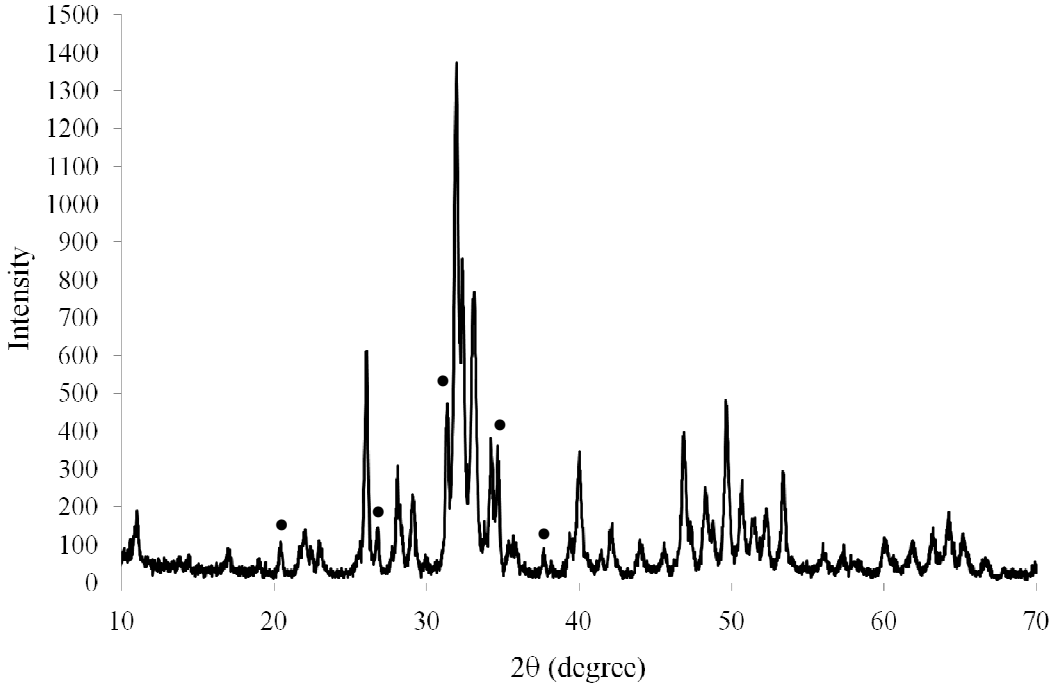

Figure 4.18. XRD spectrum of 15SCDHA sample produced with microwave treatment at 1300 W for 15 min and calcined at 700 °C (•: β-TCP).

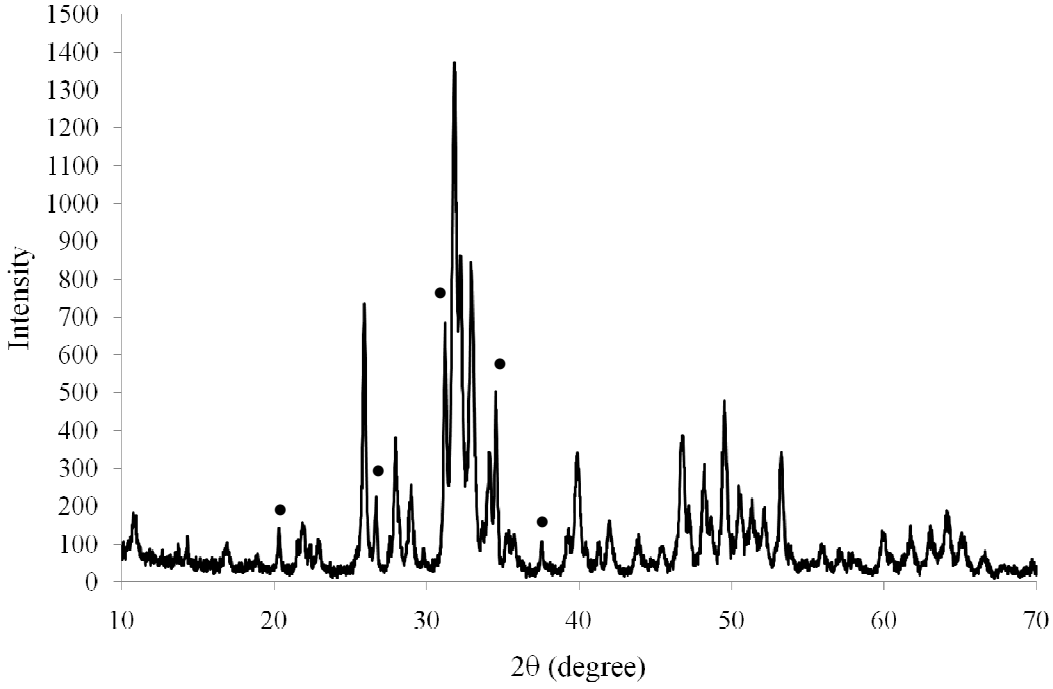

Figure 4.19. XRD spectrum of 15SCDHA sample produced with microwave treatment at 1300 W for 30 min and calcined at 700 °C (•: β-TCP).

4.2.1.3. Effect of Calcination on the Crystallite Sizes of SCDHA Samples. The calcination process increased the crystallite sizes of the samples (Table 4.2). With the increasing silver content added by the substitution process the crystallite sizes of the produced powders increased having a direct relationship with the added silver content. The calcination process had a similar effect regarding the crystallite size on all the samples regardless of the silver content, almost a 20 % increase of the crystallite sizes with respect to their uncalcined states were detected for all the samples. Therefore, the relationship of the crystallite sizes with respect to the silver content remained unchanged even after calcination.

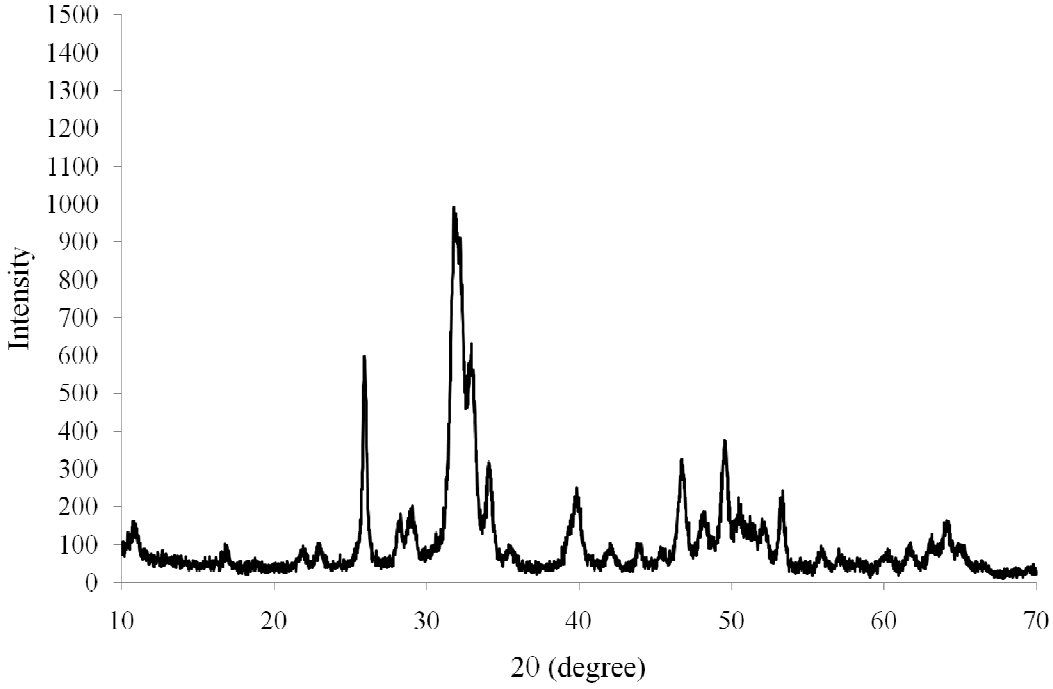

Figure 4.20. XRD spectrum of the 5SCDHA sample prepared with microwave treatment at 1300 W for 30 min.

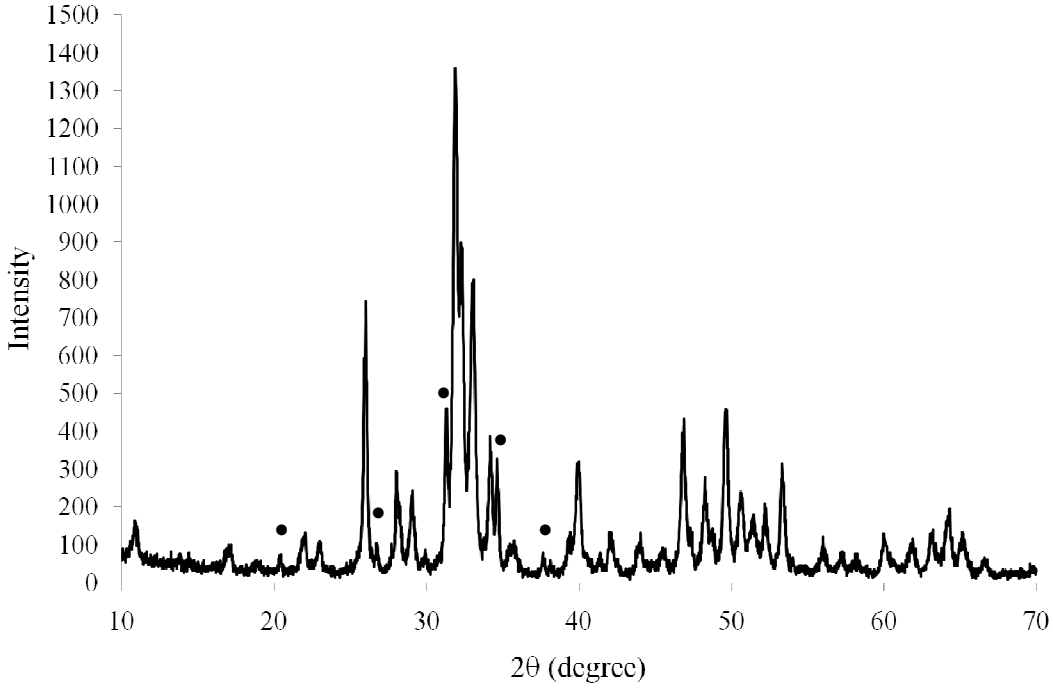

Figure 4.21. XRD spectrum of the 5SCDHA sample prepared with microwave treatment at 1300 W for 30 min and calcined at 700 °C (•: β-TCP).

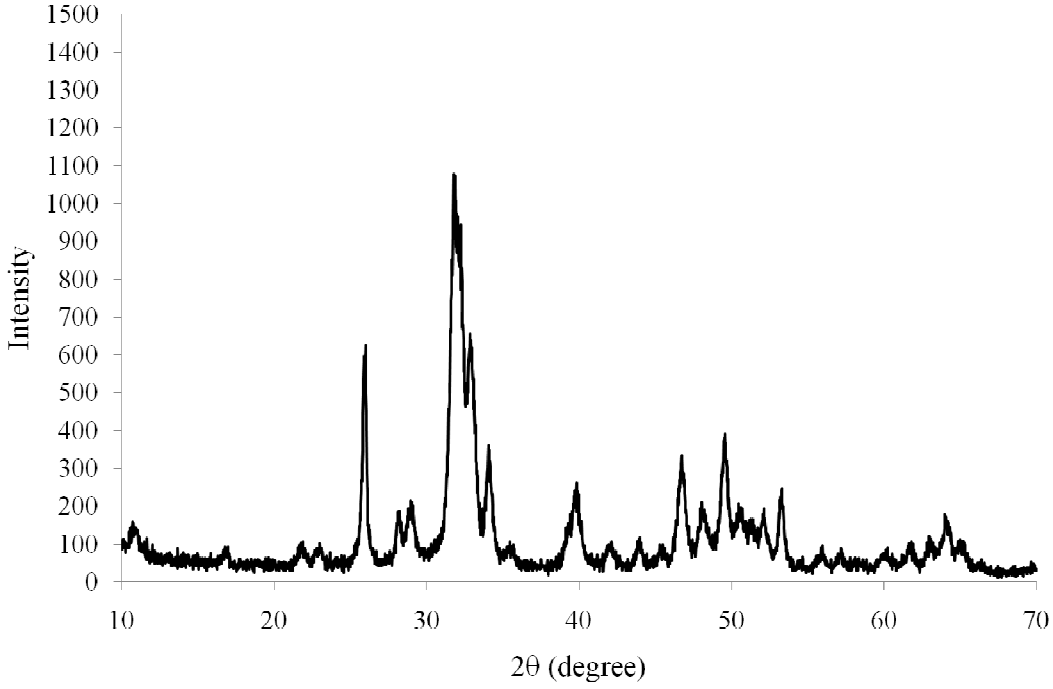

Figure 4.22. XRD spectrum of the 10SCDHA sample prepared with microwave treatment at 1300 W for 30 min.

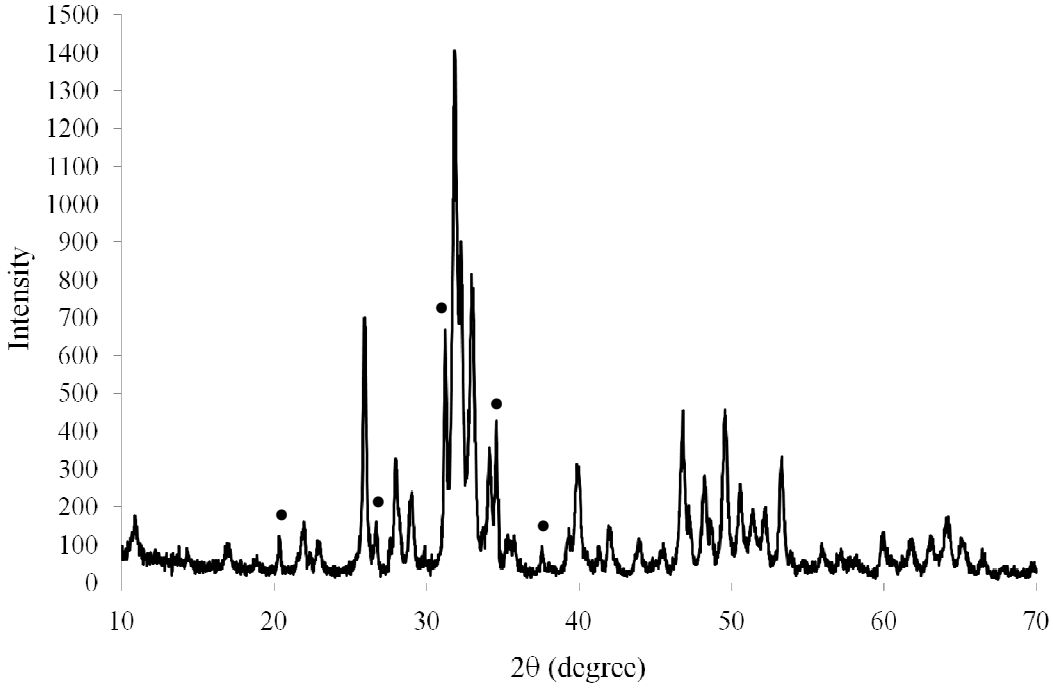

Figure 4.23. XRD spectrum of the 10SCDHA sample prepared with microwave treatment at 1300 W for 30 min and calcined at 700 °C (•: β-TCP).

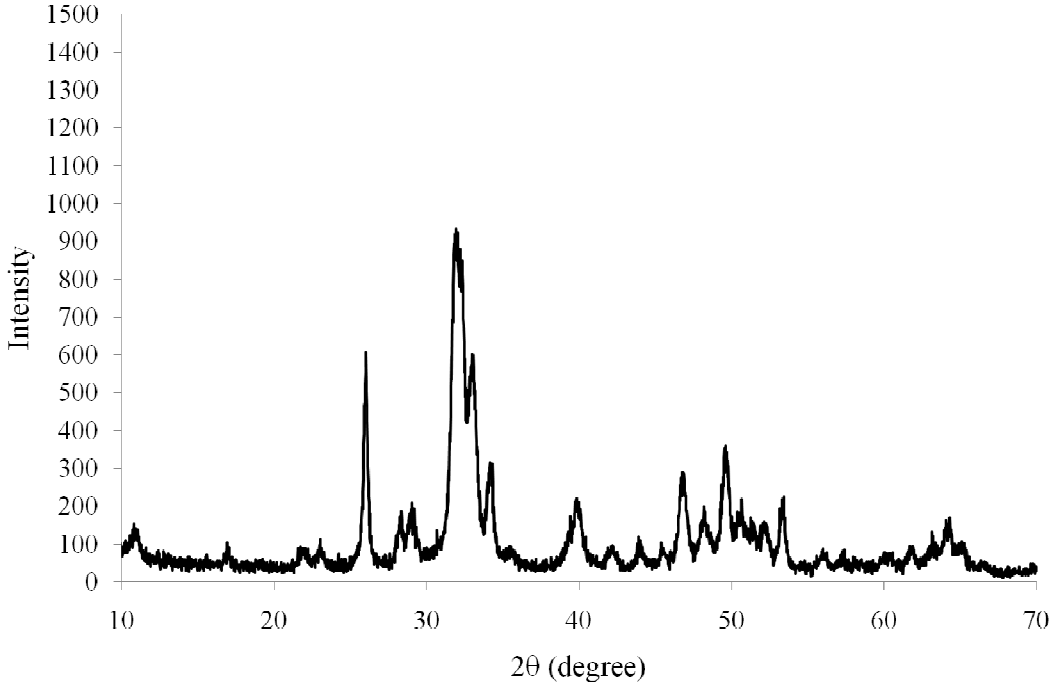

Figure 4.24. XRD spectrum of the 15SCDHA sample prepared with microwave treatment at 1300 W for 30 min.

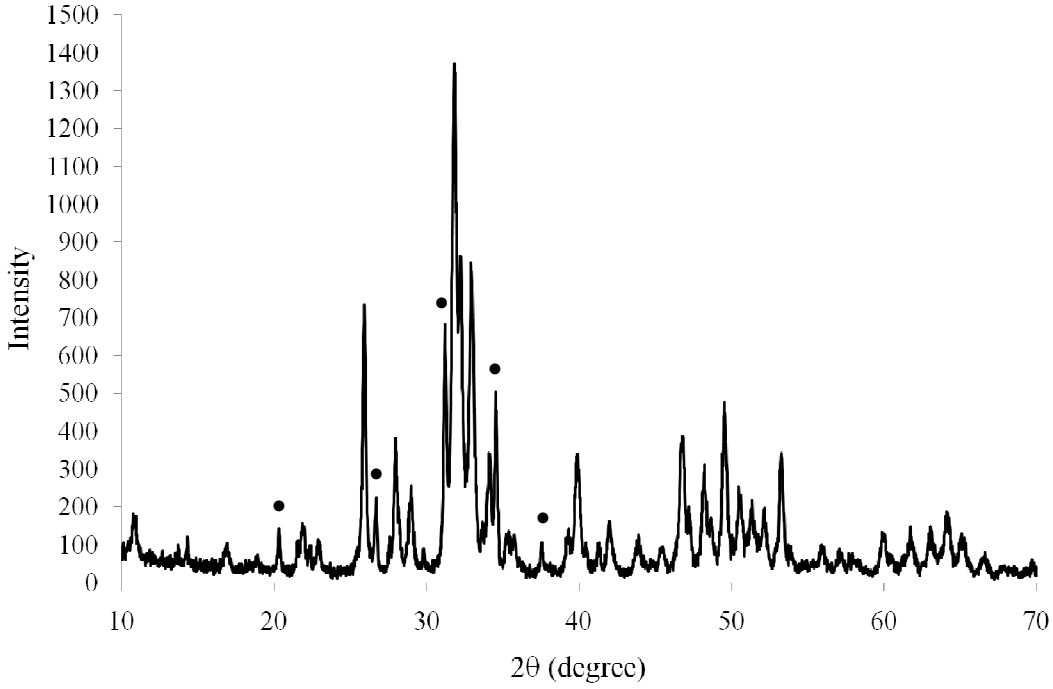

Figure 4.25. XRD spectrum of the 15SCDHA sample prepared with microwave treatment at 1300 W for 30 min and calcined at 700 °C (•: β-TCP)
(Figure 4.15 repeated for the sake of completeness).

4.2.1.4. Effect of Calcination on the β-TCP Formation of SCDHA Samples. The XRD patterns of all the uncalcined SCDHA samples with varying silver content were free of phases other than hydroxyapatite (Figures 4.20, 4.22 and 4.24). None of the SCDHA samples exhibited silver phosphate (Ag_3PO_4) peaks in their XRD analysis before and after the calcination. Similarly, no free silver peaks were detected in the XRD patterns of the SCDHA samples before and after the calcination process. These observations lead to the idea that all of the used silver successfully substituted calcium ions in the apatite such that no silver reacted with the phosphate ions to form silver phosphate which would further exhibit silver phosphate peaks or silver peaks after calcination due to decomposition.

After calcination β-TCP peaks were observed in the XRD patterns (Figures 4.21, 4.23 and 4.25) of the SCDHA samples such that even the lowest silver concentration resulted in obvious β-TCP peaks. The peaks became more pronounced with the increasing silver content. The CDHA was found to be stable at 700° C (Figure 4.14) and β-TCP peaks were observed at 800° C (Figure 4.15) whereas the β-TCP formation already took place in

the SCDHA samples at 700° C (Figures 4.21, 4.23 and 4.25). The observation that the SCDHA samples show β-TCP formation at a lower temperature than the CDHA sample may be attributed to the vacancy at the hydroxyl site resulting from the charge imbalance caused by Ag^{+} for Ca^{2+} ions and also, to the difference of ionic radii of Ag^{+} for Ca^{2+} ions.

The β-TCP formation was also apparent in the four different batches of 15SCDHA prepared using two different microwave powers (650 and 1300 W) and under two different microwave durations (15 and 30 min) and calcined at 700 °C for 1 h afterwards (Figures 4.16-4.19). β-TCP peaks were seen after calcination in all these samples. Although, the final phases after calcination seemed to depend more on the calcination process itself than the microwave parameters such as power and duration it can be noted that the microwave parameters influenced the intensities of the β-TCP peaks. The β-TCP peak intensities seemed to increase with increasing microwave power as well as duration.

The intensity of (221) lattice plane of β-TCP on the XRD patterns is used as a direct indicator of its purity in the literature [120]. The ratios of the peak intensities $I_{TCP(221)}/I_{HA(002)}$ were calculated for XRD patterns of those samples for which β-TCP peaks were observed (Table 4.2). Obviously, the ratio of the peak intensities $I_{TCP(221)}/I_{HA(002)}$ after calcination increased with the increasing amount of the silver. Thereby, the microwave power and duration applied before the calcination process seemed to alter the ratio of the peak intensities and thus, these parameters may effectively be used to regulate the β-TCP formation in the produced SCDHA powders.

Table 4.2. Crystallite sizes and $I_{TCP(221)}/I_{HA(002)}$ ratios (where applicable) of SCDHA powders produced using different microwave power and duration and at different calcination temperatures.

Sample	Microwave		Calcin.	$I_{TCP(221)}/I_{HA(002)}$	Crystallite	
	Power (W)	Time (min)	Temp. (°C)	(for samp. with β-TCP peaks)	Size (nm) interp.	measure.
5SCDHA	1300	30	-		23.1	-
5SCDHA	1300	30	700	0.617	28.5	-
10SCDHA	1300	30	-		24.7	-
10SCDHA	1300	30	700	0.952	27.7	29.3
15SCDHA	1300	30	-		24.1	25.4
15SCDHA	1300	30	700	0.993	27.7	30.8
15SCDHA	1300	15	700	0.772	27.6	30.4
15SCDHA	650	30	700	0.819	29.6	32.2
15SCDHA	650	15	700	0.752	29.9	31.9

4.2.2. FTIR Study of Nanosized Calcium Deficient Hydroxyapatite with and without Silver Substitution

FTIR spectra of the CDHA and 15SCDHA powders were obtained both for their uncalcined and calcined states (Figures 4.26-4.29). All of the samples have characteristic υ_3 PO_4^{3-} bands for HA between 1027 and 1032 cm^{-1} [121]. This result agrees with the data obtained from XRD. The intensity of the phosphate peak slightly increased after calcination of the same sample (Figures 4.26-4.27 and Figures 4.27-4.28). Calcination results in a hydroxyl peak at around 3660 cm^{-1} for the CDHA sample. The hydroxyl peaks around 3660 cm^{-1} are more pronounced for the 15SCDHA sample in its both states. The υ_2

mode near 900 cm^{-1} and the υ_3 mode near 1400 cm^{-1} for carbonate were observed for the 15SCDHA sample before and after calcination [69, 122-124]. The peaks around 2970 cm^{-1} and 2900 cm^{-1} corresponded to the hydrogen-bonded O–H group stretch of HA and water [125]. The decrease of those peaks after calcination indicated the removal of absorbed water. The bands at around 1250 cm^{-1} were due to P–O and P=O stretching of phosphate group [126]. The peaks observed for the uncalcined 15SCDHA sample decreased after calcination.

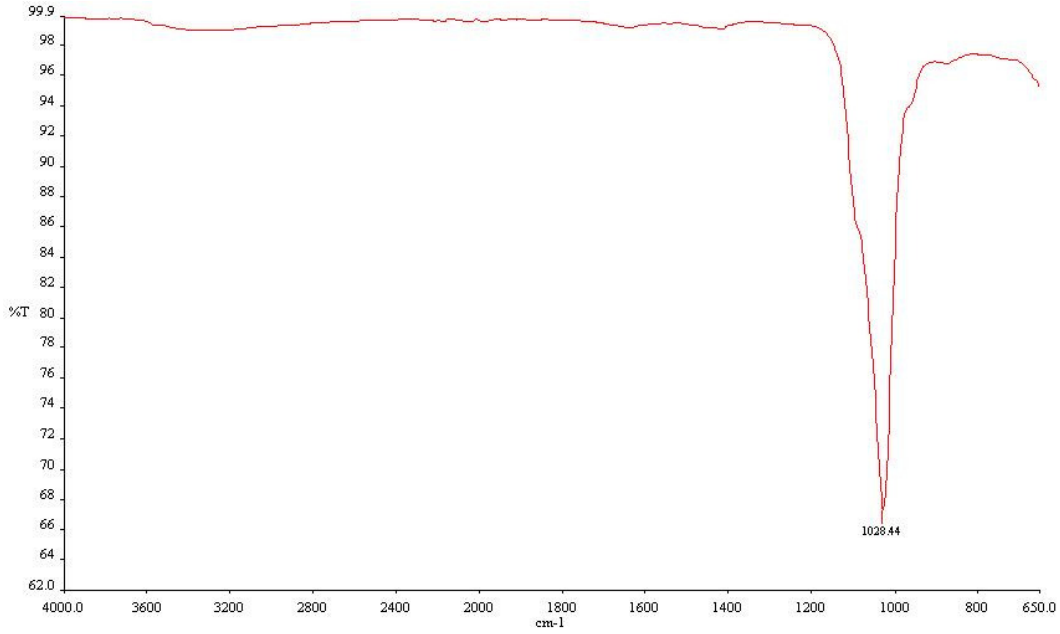

Figure 4.26. FTIR spectrum of the CDHA sample prior to calcination.

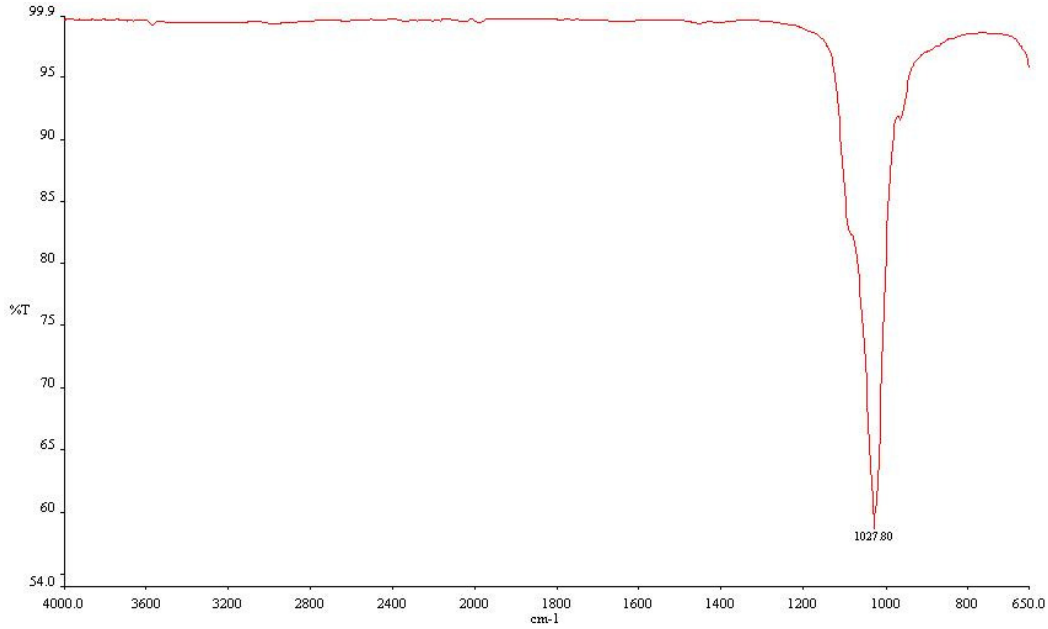

Figure 4.27. FTIR spectrum of the CDHA sample after calcination at 700 °C.

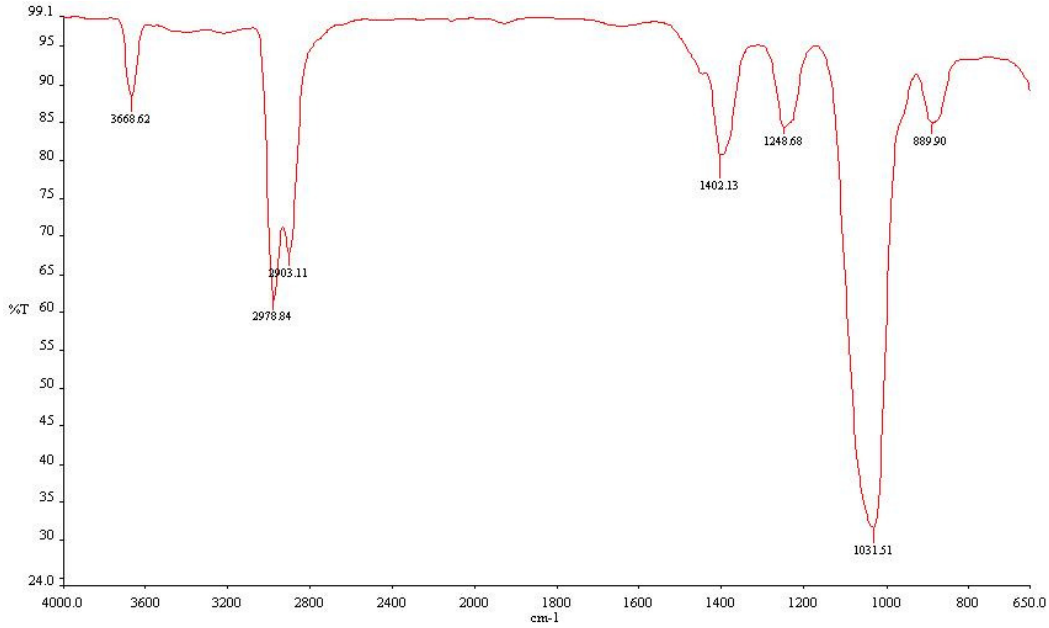

Figure 4.28. FTIR spectrum of the 15SCDHA sample prior to calcination.

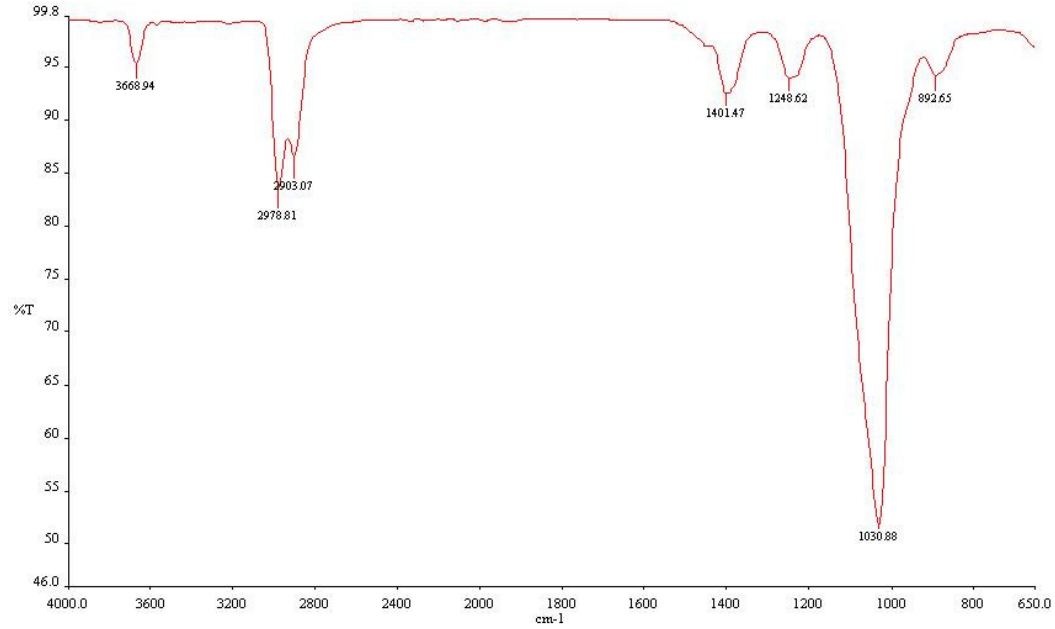

Figure 4.29. FTIR spectrum of the 15SCDHA sample after calcination at 700 °C.

4.2.3. Particle Size and Morphology of Nanosized Calcium Deficient Hydroxyapatite with and without Silver Substitution

According to the SEM images the produced powders with (Figures 4.34-4.37) and without (Figures 4.30-4.33) silver addition were of nano size with needle like shapes of 20-25 nm width and 70-90 nm length. Particles of both powders strongly tend to agglomerate. Apparently, the silver added by the substitution reaction had no effect on the particle size and morphology. However, the calcination process greatly effected the particle morphology as well as their size. The shapes of the particles changed from needle-like to nodular-like with sharper contours than their as-synthesized counterparts. Also, an increase in particle size was noticeable resulting in particles of 30-45 nm in width and 100-120 nm in length.

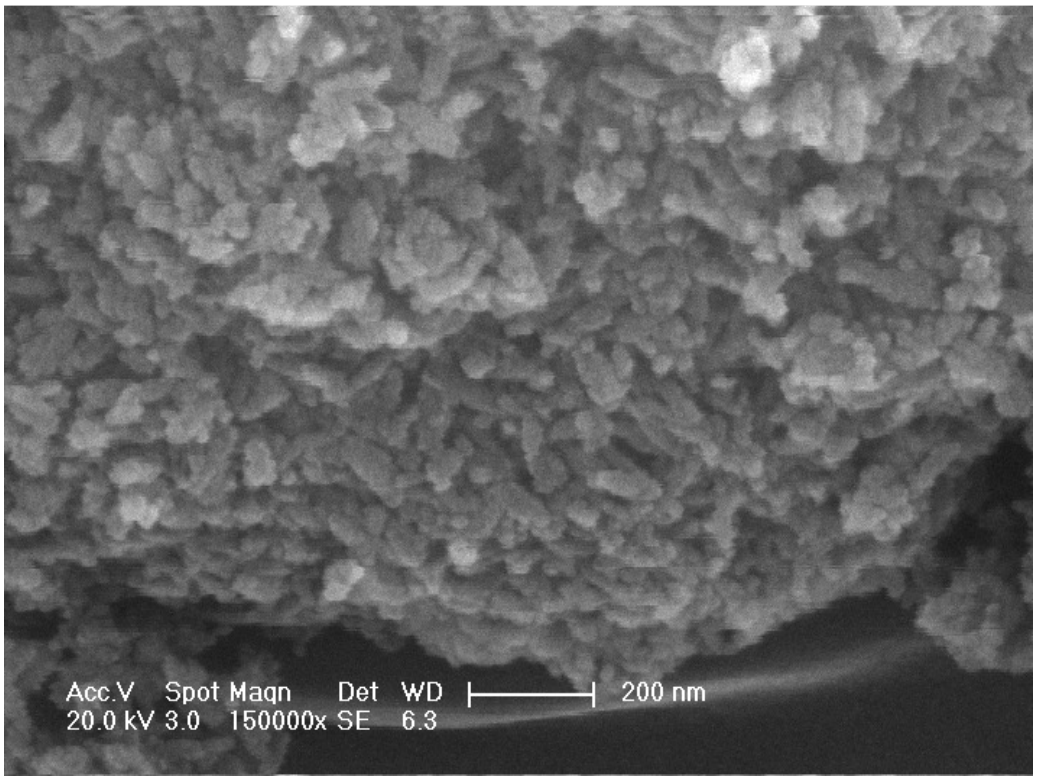

Figure 4.30. SEM image of the CDHA sample prior to calcination (150000x).

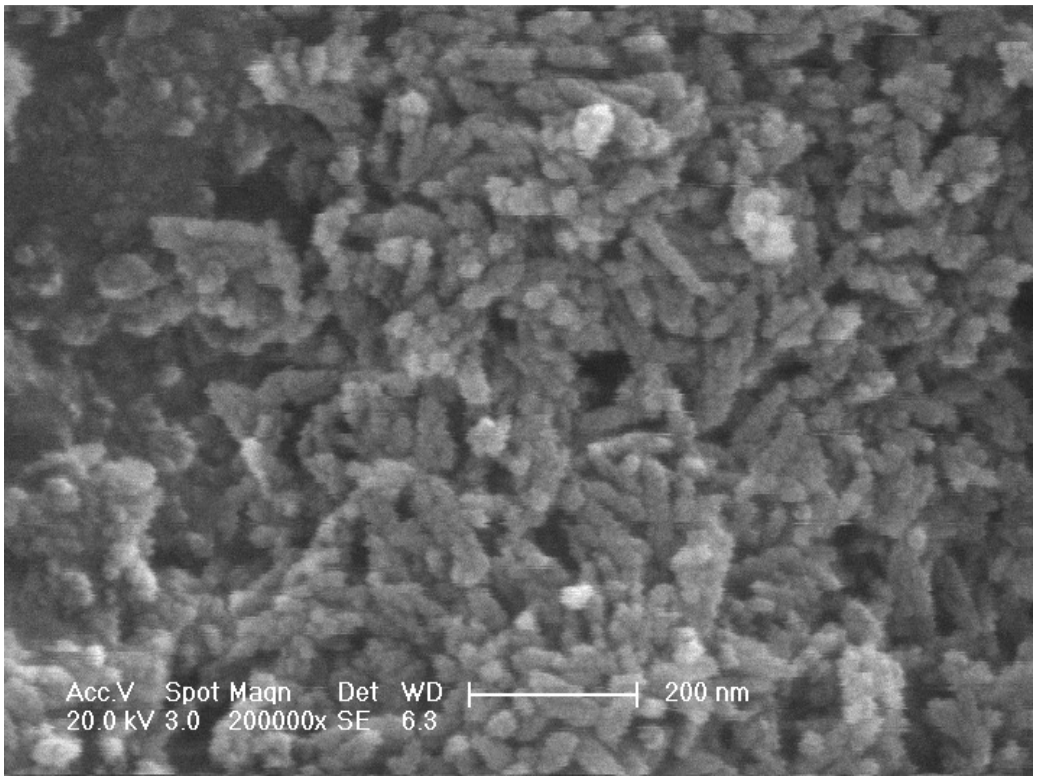

Figure 4.31. SEM image of the CDHA sample prior to calcination (200000x).

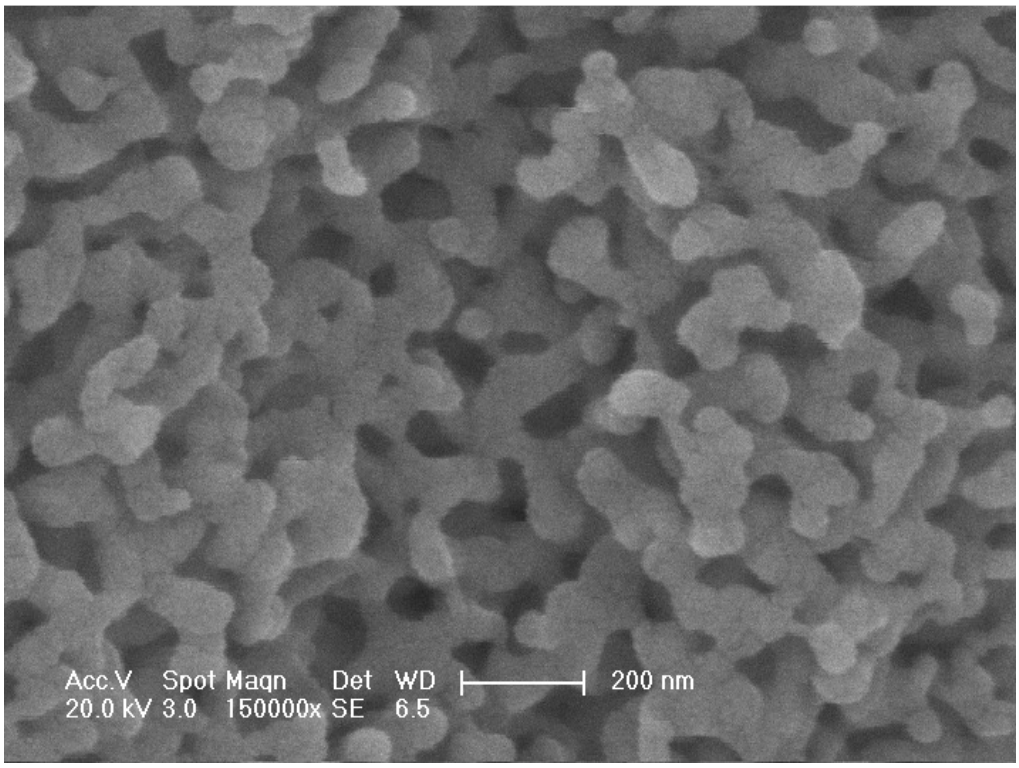

Figure 4.32. SEM image of the CDHA sample after calcination at 700 °C (150000x).

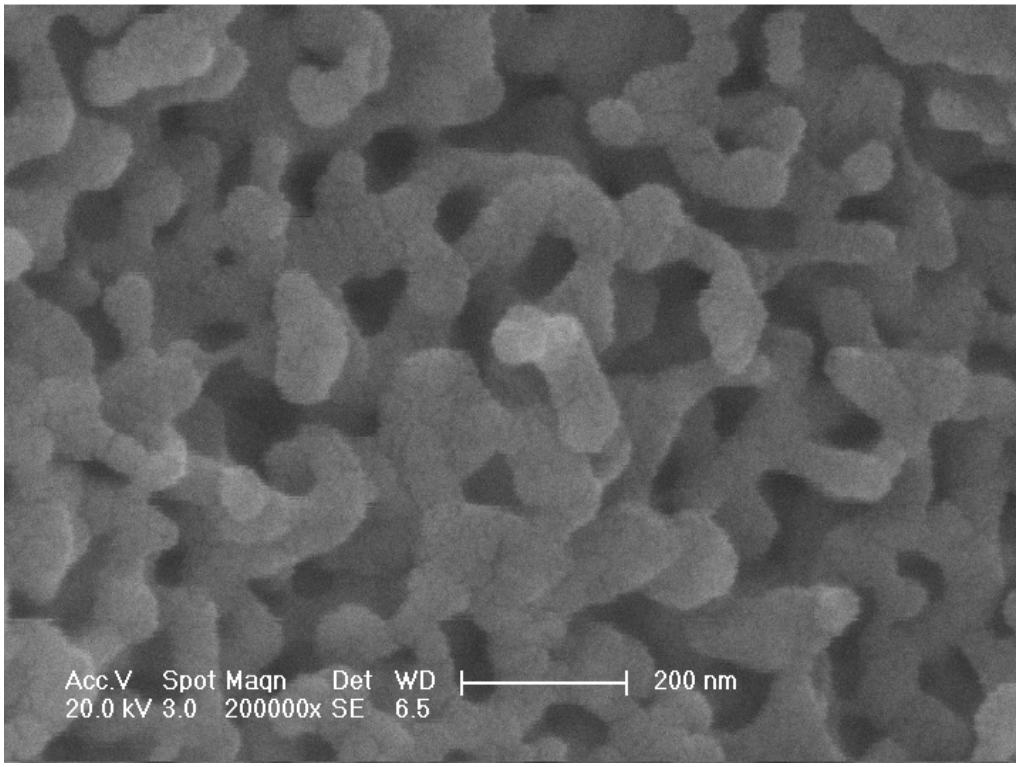

Figure 4.33. SEM image of the CDHA sample after calcination at 700 °C (200000x).

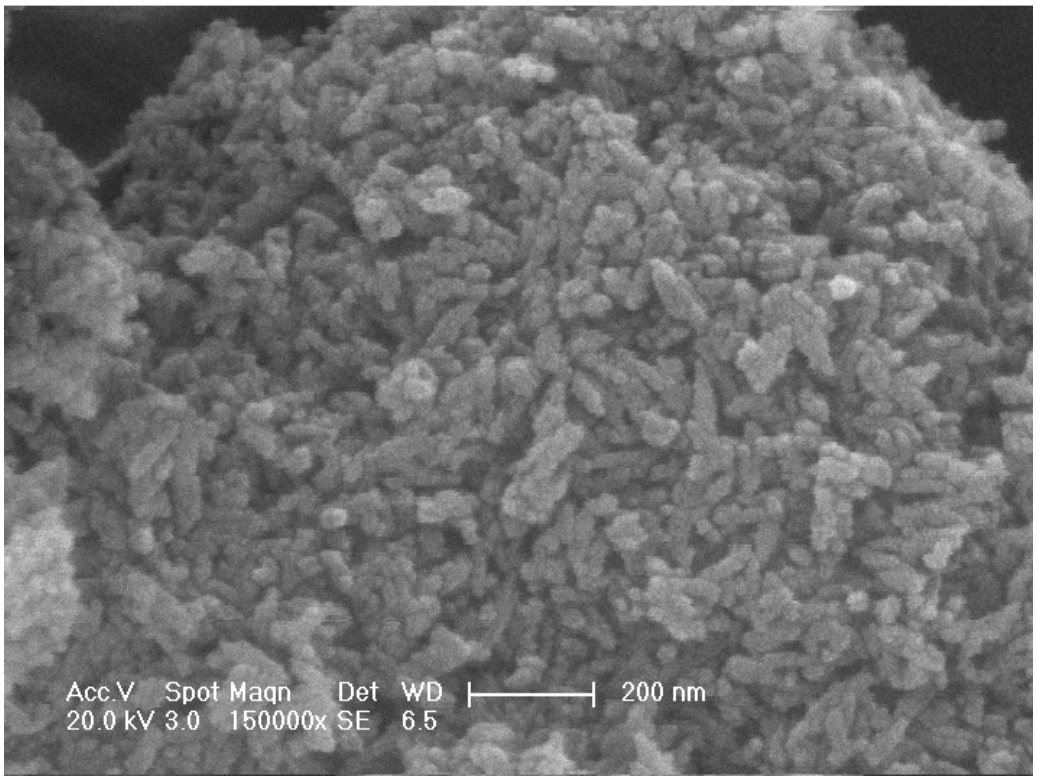

Figure 4.34. SEM image of the 15SCDHA sample prior to calcination (150000x).

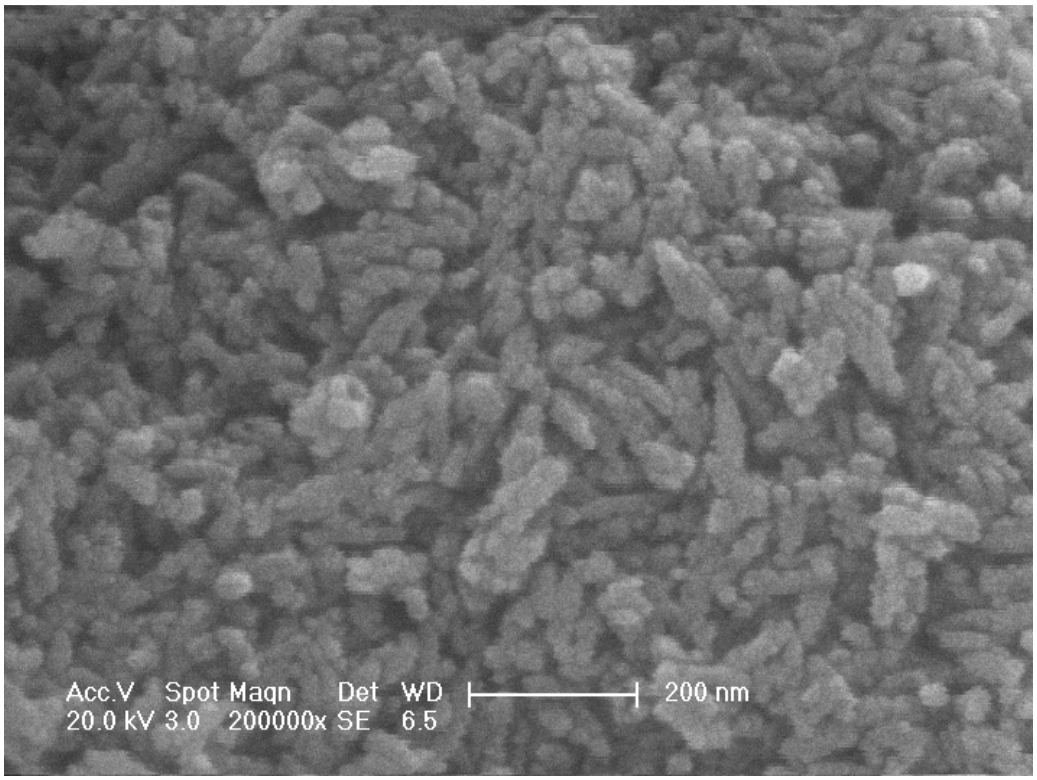

Figure 4.35. SEM image of the 15SCDHA sample prior to calcination (200000x).

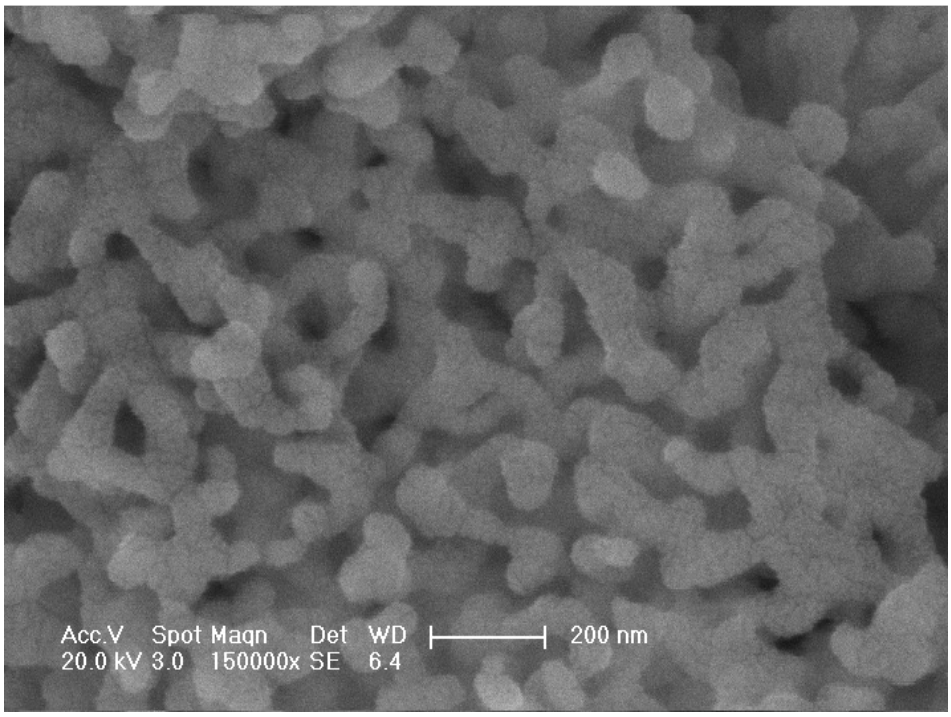

Figure 4.36. SEM image of the 15SCDHA sample after calcination at 700 °C (150000x).

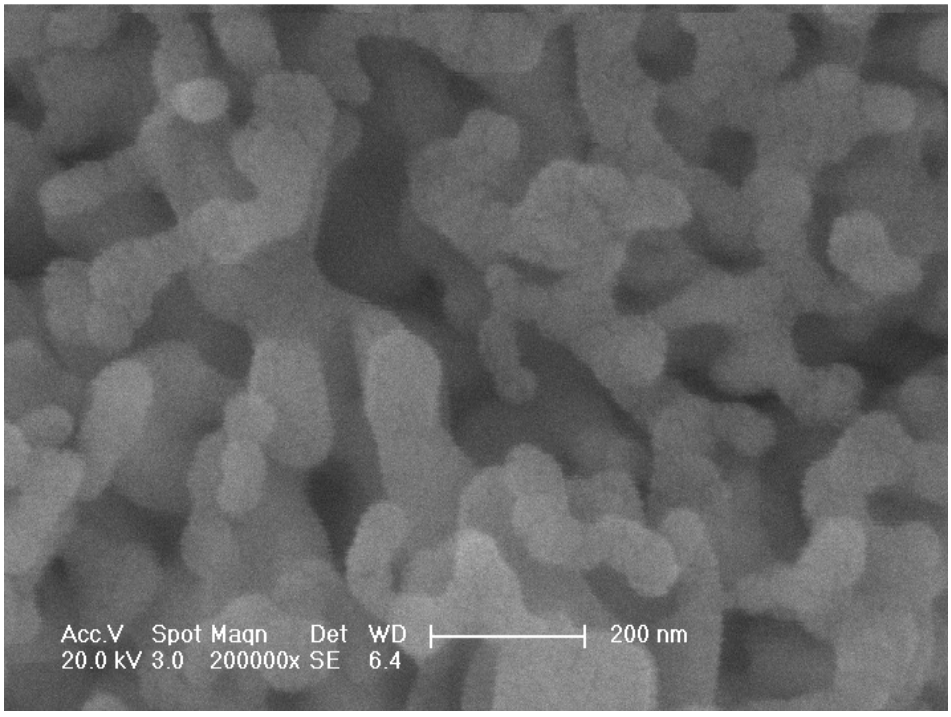

Figure 4.37. SEM image of the 15SCDHA sample after calcination at 700 °C (200000x).

4.2.4. Antibacterial Evaluation of Silver Substituted Nanosized Calcium Deficient Hydroxyapatite

The antibacterial activities of SCDHA samples were tabulated (Table 4.3). The tests were repeated to validate the results (Table 4.4). The antibacterial activity increases with the increasing amount of silver addition. Important to note was the difference in the characteristics of the antibacterial activity of the powders against the two different bacteria. The SCDHA powders greatly reduced the number of E. coli cells in the first 30 min. The same powders showed a weaker antibacterial activity against S. aureus after 30 min. However, the samples were effective against both kinds of bacteria after 24 h. Whereas the 10SCDHA sample was effective against both kinds of bacteria after 24 h, the 15SCDHA sample completely inhibited bacterial activity even after 30 min showing that 15SCDHA powder is potentially a good candidate for antibacterial applications.

Table 4.3. Antibacterial activity of 100 mg SCDHA powder samples with varying silver content in their as-synthesized states against E. coli and S. aureus bacteria in 10 ml bacterial solution with a concentration of 1 x 10^6 cfu/ml.

	E. coli (Gram negative)		S. aureus (Gram positive)	
Sample	Bacterial Load after 30 min (cfu/ml)	Bacterial Load after 24 h (cfu/ml)	Bacterial Load after 30 min (cfu/ml)	Bacterial Load after 24 h (cfu/ml)
15SCDHA	0	0	0	0
10SCDHA	2,000	0	29,000	0
5SCDHA	14,000	9,000	34,000	21,000

Table 4.4. Results of repeated tests of antibacterial activity of 100 mg SCDHA powder samples with varying silver content in their as-synthesized states against E. coli and S. aureus bacteria in 10 ml bacterial solution with a concentration of 1 x 10^6 cfu/ml.

	E. coli (Gram negative)		S. aureus (Gram positive)	
Sample	Bacterial Load after 30 min (cfu/ml)	Bacterial Load after 24 h (cfu/ml)	Bacterial Load after 30 min (cfu/ml)	Bacterial Load after 24 h (cfu/ml)
15SCDHA	0	0	0	0
10SCDHA	0	0	0	0
5SCDHA	0	0	0	0
CDHA	1,07 x 10^5	1,80 x 10^6	1,07 x 10^6	2,27 x 10^6
Control Sample	4,30 x 10^5	3,75 x 10^5	2,00 x 10^6	2,60 x 10^5

Cross-checking of the results revealed that silver incorporation into the calcium deficient hydroxyapatite successfully eliminated bacterial activity. Important to note is that pure CDHA sample without any silver addition allows more bacterial growth than the control sample after 24 h. The increased bacterial activity on the CDHA sample without silver addition after a relatively short adaptation stage (24 h) of the bacteria is thought to be related to the biocompatibility of CDHA.

4.3. Synthesis of Silver Substituted Nanosized Stoichiometric Hydroxyapatite by Microwave

4.3.1. XRD Study of Silver Substituted Nanosized Stoichiometric Hydroxyapatite with and without Silver Substitution

Four different samples with Ag:Ca ratio of 0, 0.3, 0.6 and 0.9 were produced and labeled according to their silver content as HA, 3SHA, 6SHA and 9SHA, respectively. Crystallization and decomposition behavior of nanosized stoichiometric hydroxyapatite with and without silver substitution treated at different temperatures were investigated using XRD (Figures 4.38-4.57). For this purpose, samples were thermally treated at 700, 900, 1000 and 1100 °C for 1 h at open atmosphere using a conventional furnace. In addition to their heat treated states samples were also investigated in their as-synthesized states to understand the effect of thermal treatment to the crystallization and decomposition behavior of the powders.

XRD analyses revealed that the crystallization of the powders regardless of their silver content was improved with the increasing heat treatment temperature. On the other hand, minor β-TCP peaks were observed on the samples heat treated at temperatures above 900 °C and the peak intensities slightly increased with further increasing the heat treatment temperature. The weak peaks around 37.5° found on the samples heat treated above 900 °C may be indicative of minor CaO formation however, there is no further evidence towards this.

The onset temperature of the silver substituted stoichiometric hydroxyapatite decomposition into β-TCP was observed to depend on the silver content of the produced powders. With increasing silver content the onset temperature tends to decrease. This leads to the idea that increasing silver content decreases the thermal stability of the powders. This observation may be justified by the presence of vacancy at the hydroxyl site due to the charge imbalance based on the different charges of Ag^{+} for Ca^{2+} ions [56]. Another fact which might lead to the observed thermal instability of silver containing powders is the great difference of the ionic radii of Ag^{+} (0.128 nm) for Ca^{2+} (0.099 nm) ions [56]. A

similar observation was also made by the investigation of the XRD analyses of calcium deficient hydroxyapatite powders with and without silver substitution, previously.

Considering the stoichiometry of the decomposition reaction of hydroxyapatite into β-TCP water is the by-product of the reaction. This fact might be used to control the decomposition of the silver substituted stoichiometric hydroxyapatite. Carrying out the thermal treatment of silver substituted stoichiometric hydroxyapatite under humid conditions may increase the vapor pressure of water and thus lower the decomposition of the powder [22]. This may be useful for increasing the thermal treatment temperature to improve crystallization of the silver substituted stoichiometric hydroxyapatite without compromising the stability of the powder. However, the negative effect of the charge imbalance and the difference of ionic radii between the Ag^{+} for Ca^{2+} ions as mentioned earlier still remains intact decreasing the overall thermal stability of the powder. Thus, thermal treatment at elevated temperatures is necessary to improve the crystallization of the produced silver substituted stoichiometric hydroxyapatite powders however, this needs to be applied with precaution since it enhances the decomposition into β-TCP of the powder already demonstrating instability due to its silver content.

Neither silver phosphate (Ag_3PO_4) nor silver (Ag) and silver oxide (Ag_2O) peaks were observed in the XRD analyses of the heat treated samples. The observation that neither Ag_3PO_4 nor Ag peaks were detected shows that all of the silver successfully substituted calcium ions in the apatitic structure such that no silver reacted with the phosphate (PO_4^{3-}) ions to form Ag_3PO_4. The observation that no free Ag peaks were found shows that the substituted silver remains in the apaitic structure even after the decomposition of hydroxyapatite into β-TCP at the heat treatment temperatures tested throughout the study. Silver substituted stoichiometric hydroxyapatite preserves its silver content up to 1100 °C.

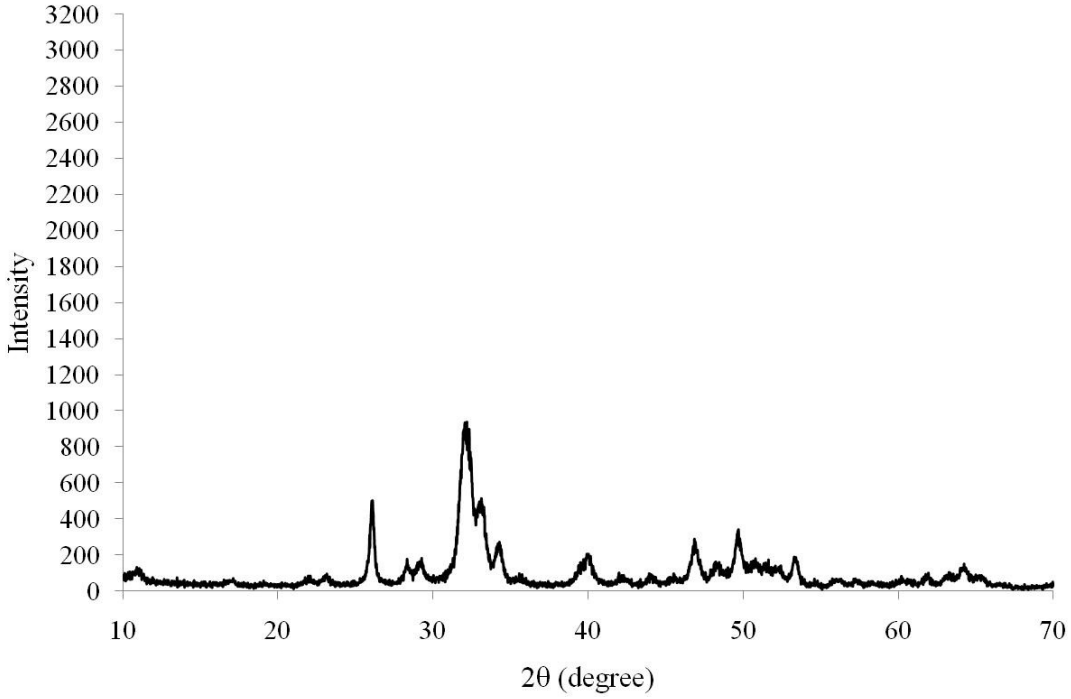

Figure 4.38. XRD spectrum of HA in its synthesized state.

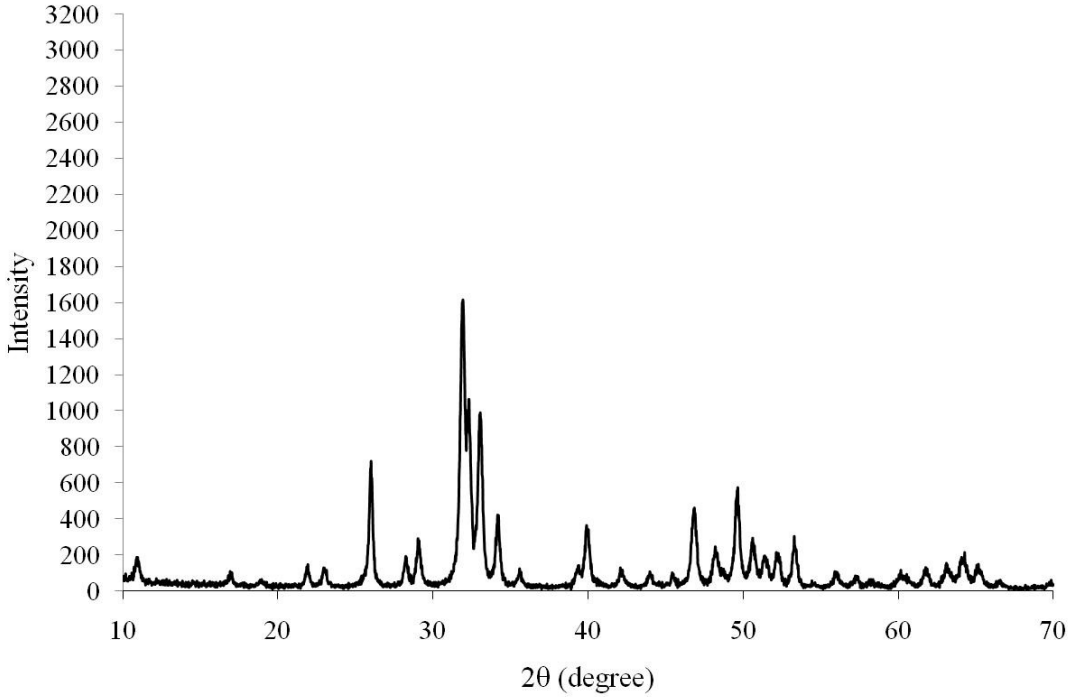

Figure 4.39. XRD spectrum of HA after thermal treatment at 700 °C.

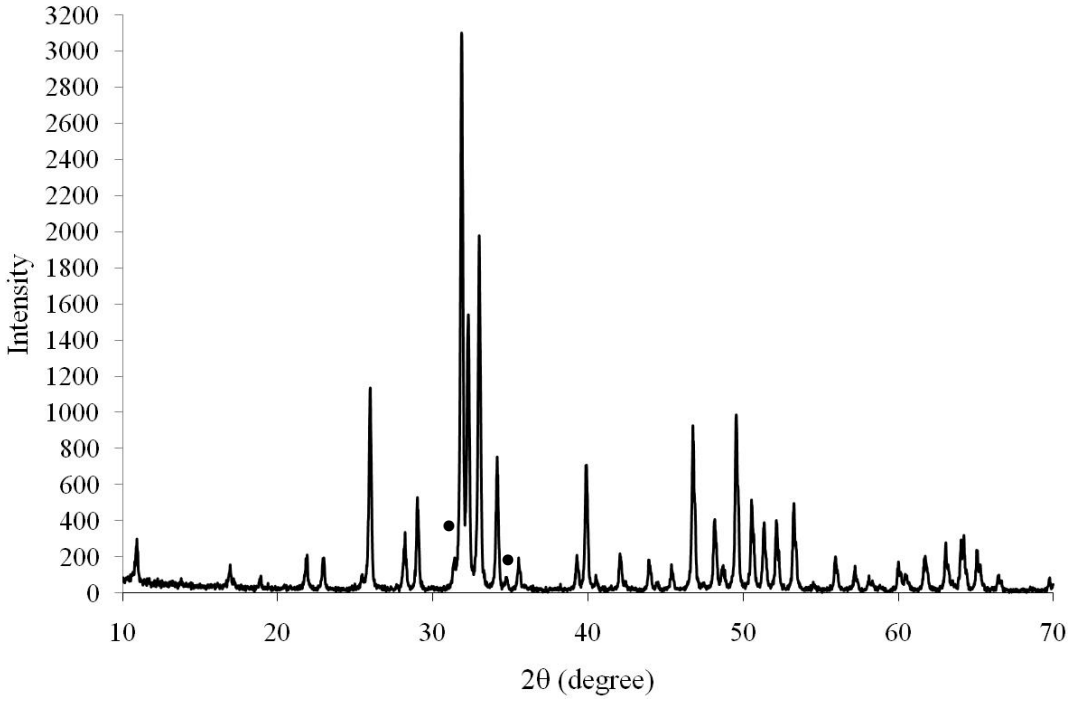

Figure 4.40. XRD spectrum of HA after thermal treatment at 900 °C (•: β-TCP).

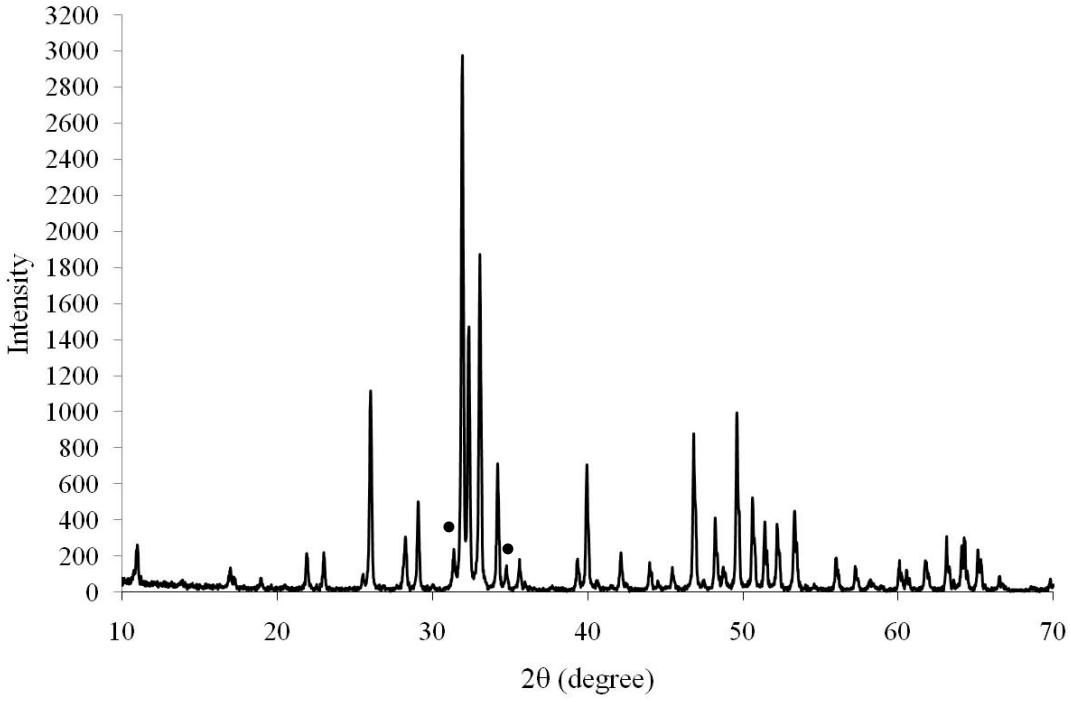

Figure 4.41. XRD spectrum of HA after thermal treatment at 1000 °C (•: β-TCP).

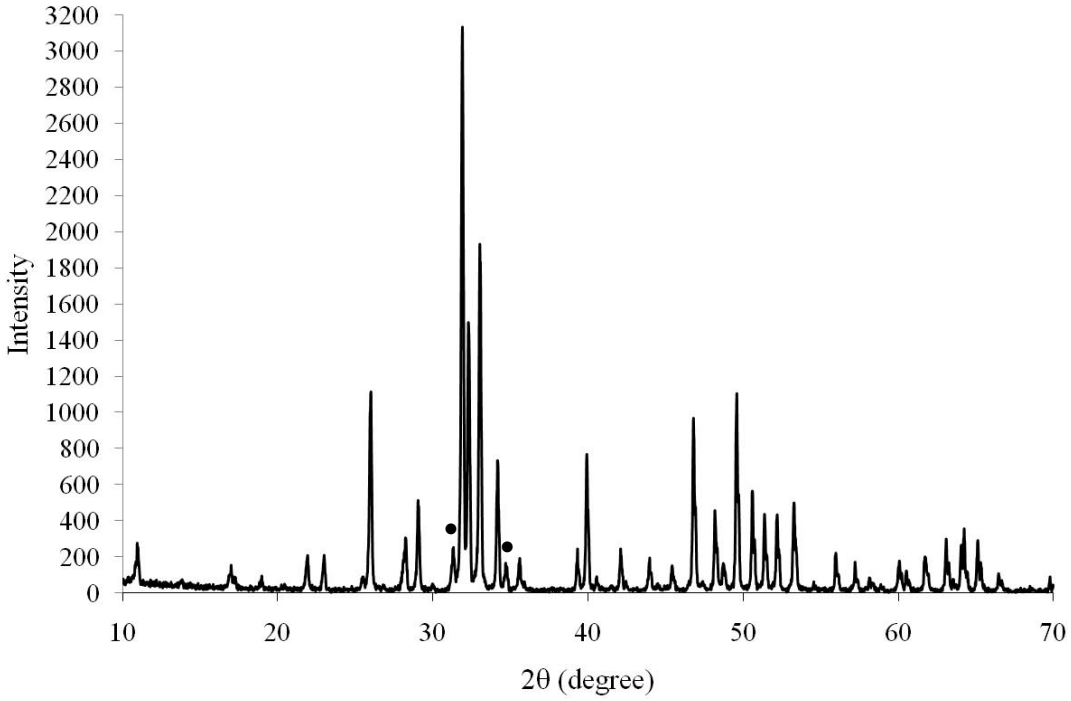

Figure 4.42. XRD spectrum of HA after thermal treatment at 1100 °C (•: β-TCP).

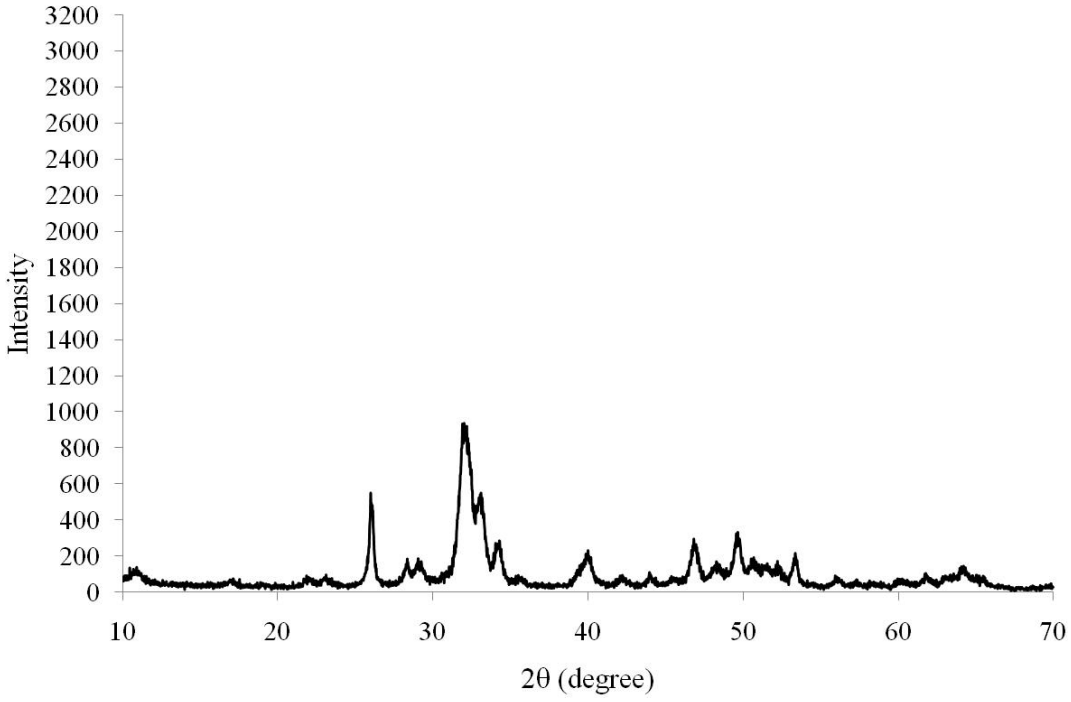

Figure 4.43. XRD spectrum of 3SHA in its synthesized state.

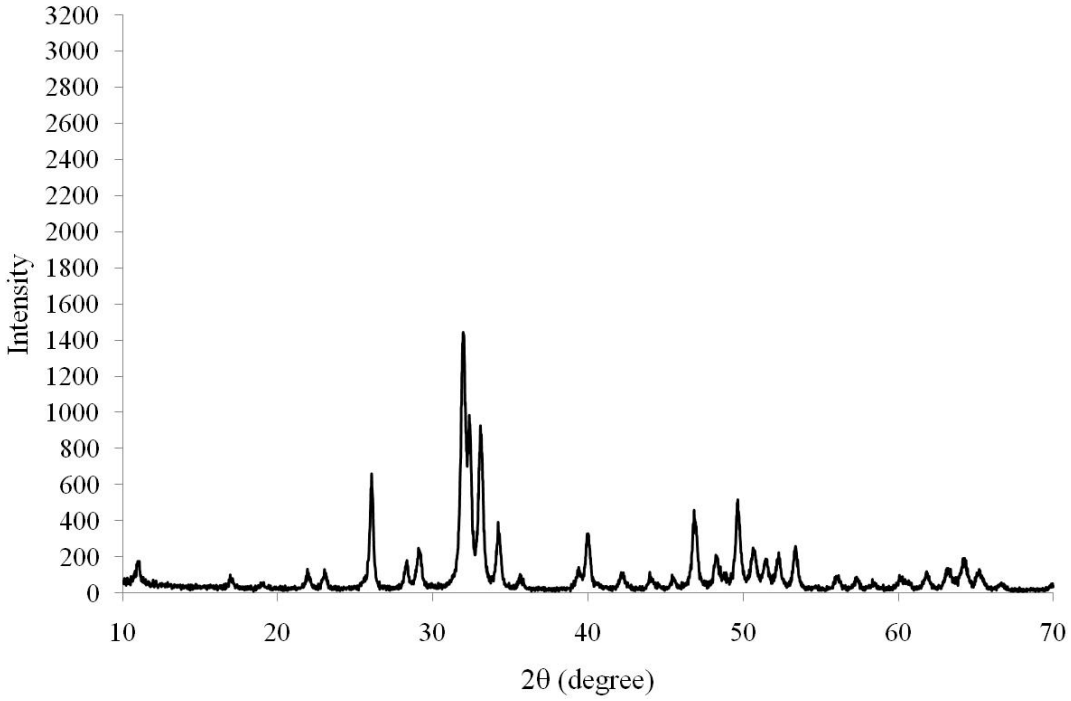

Figure 4.44. XRD spectrum of 3SHA after thermal treatment at 700 °C.

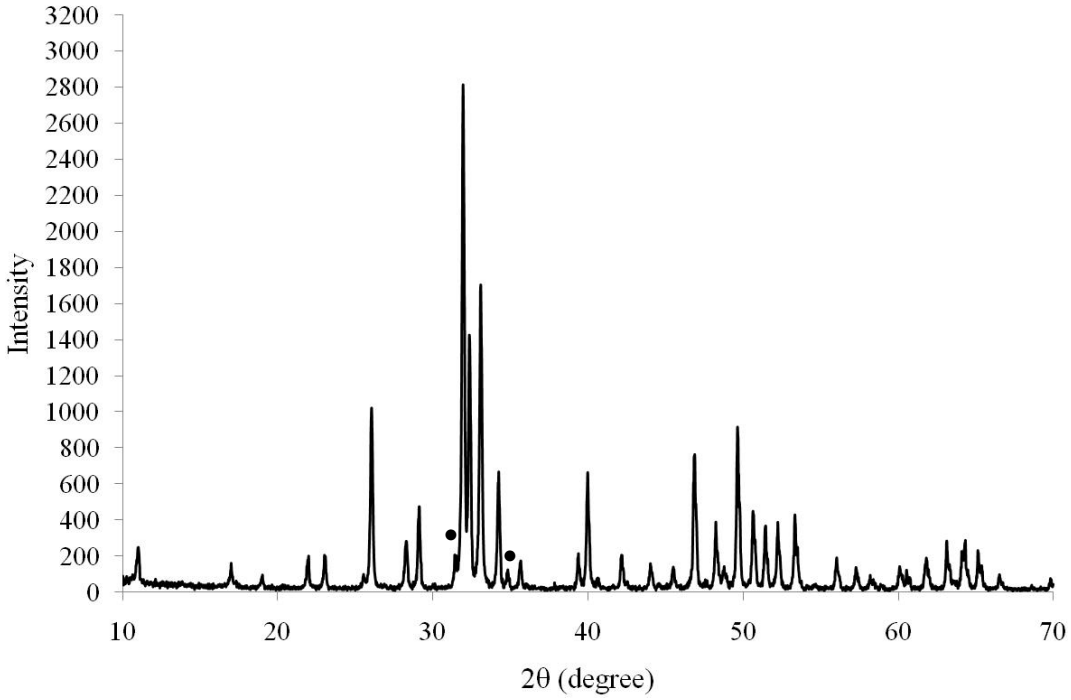

Figure 4.45. XRD spectrum of 3SHA after thermal treatment at 900 °C (•: β-TCP).

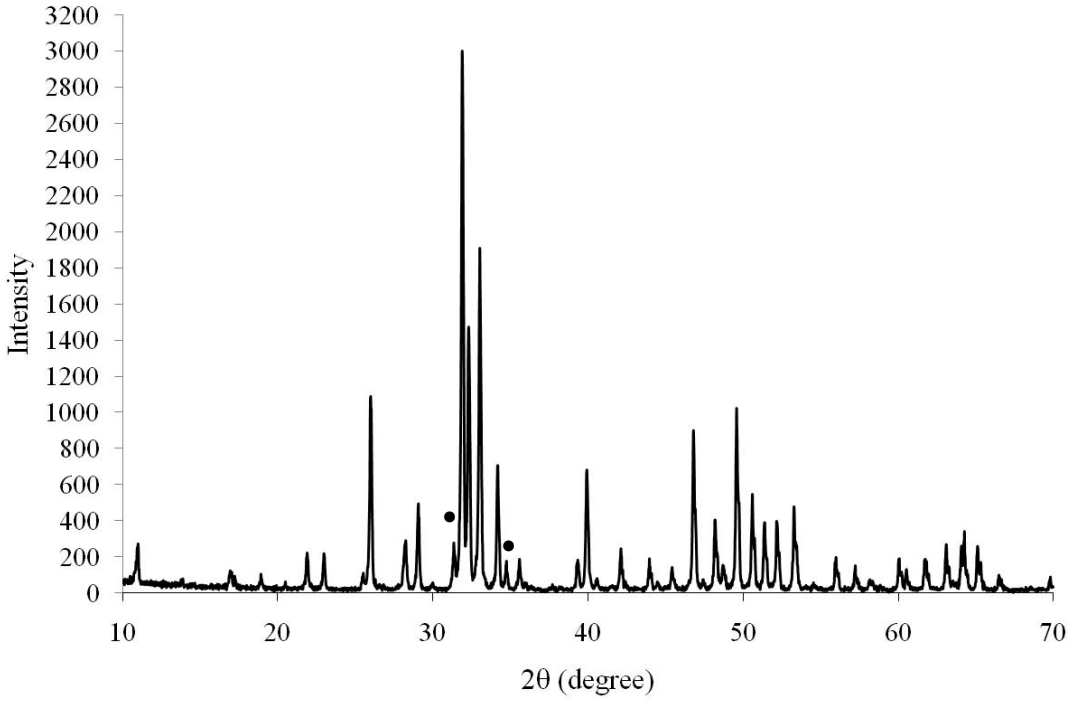

Figure 4.46. XRD spectrum of 3SHA after thermal treatment at 1000 °C (•: β-TCP).

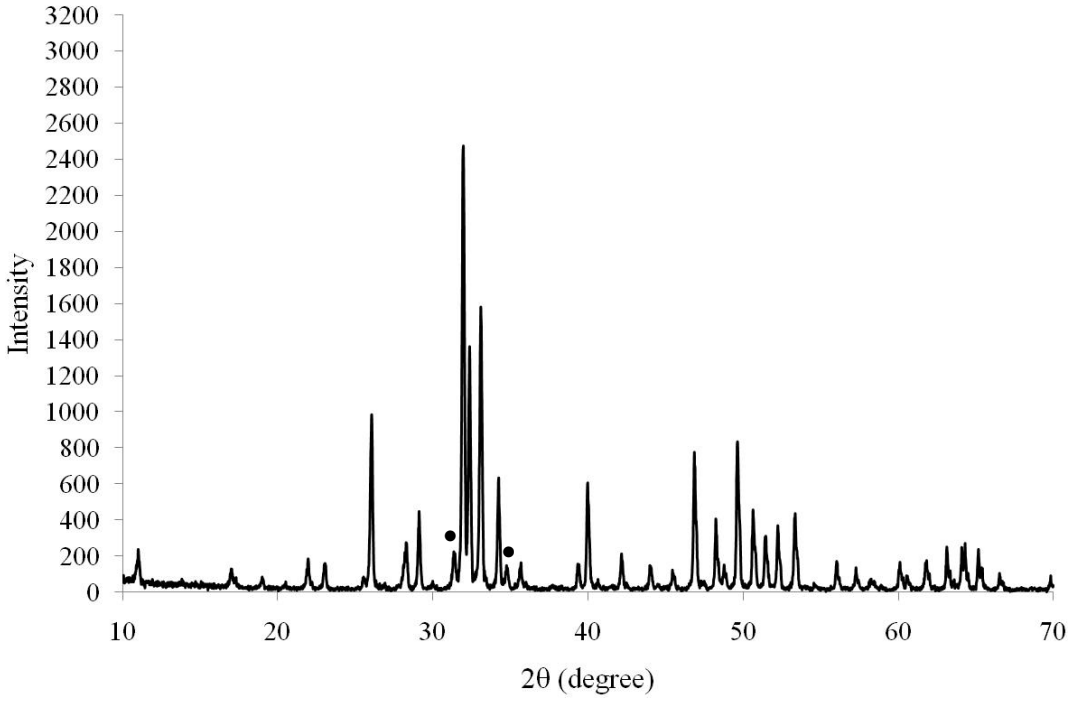

Figure 4.47. XRD spectrum of 3SHA after thermal treatment at 1100 °C (•: β-TCP).

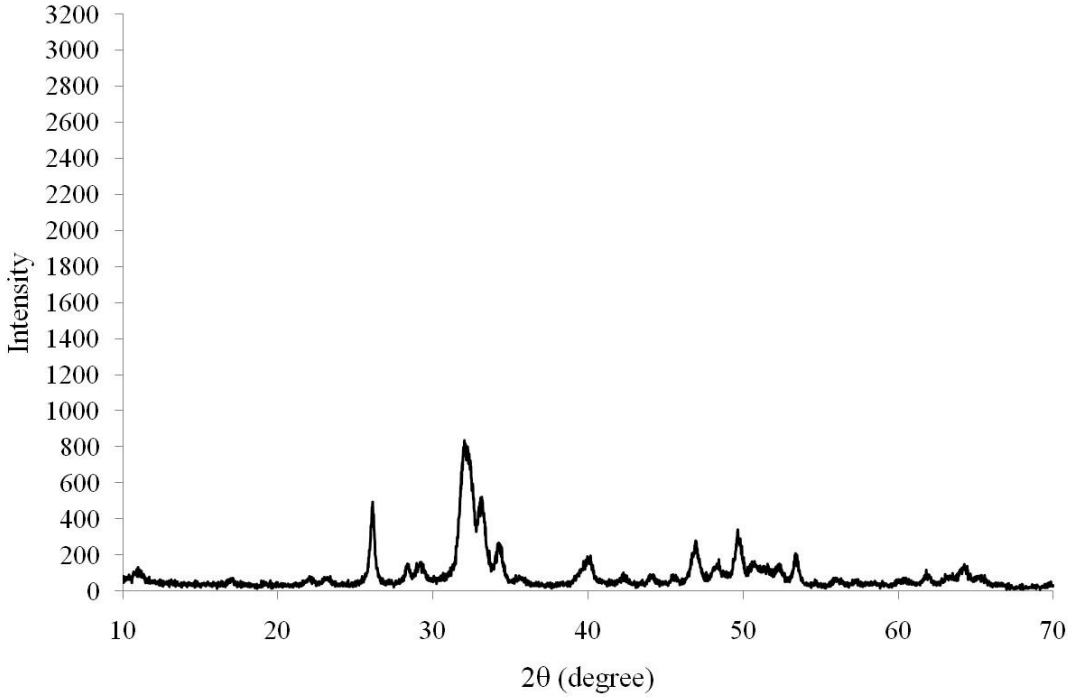

Figure 4.48. XRD spectrum of 6SHA in its synthesized state.

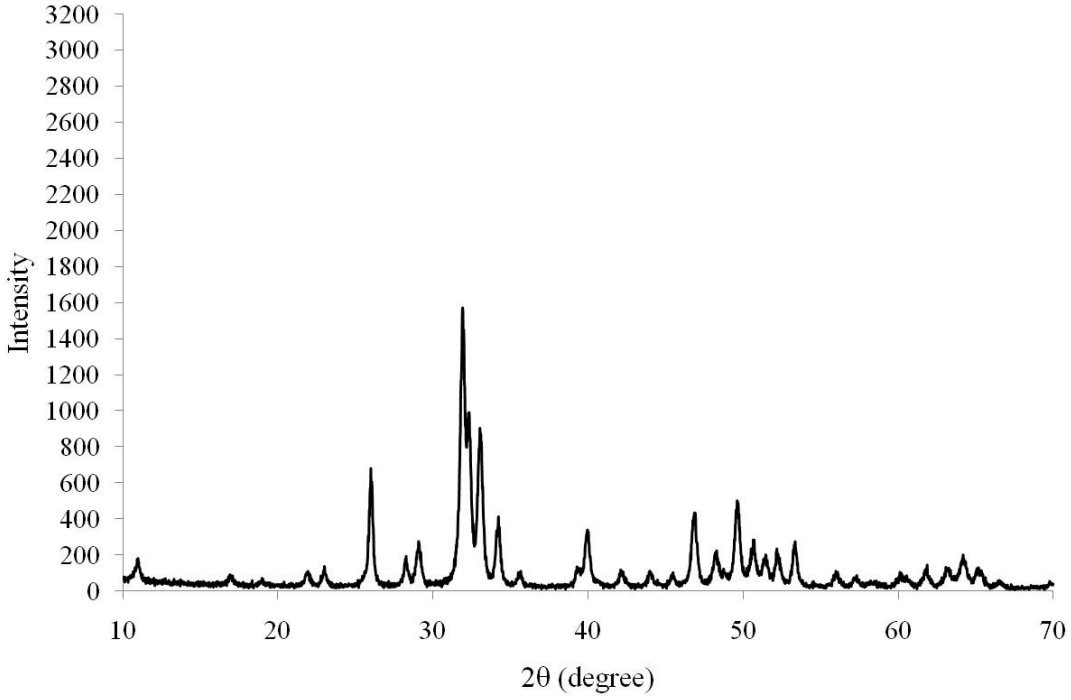

Figure 4.49. XRD spectrum of 6SHA after thermal treatment at 700 °C.

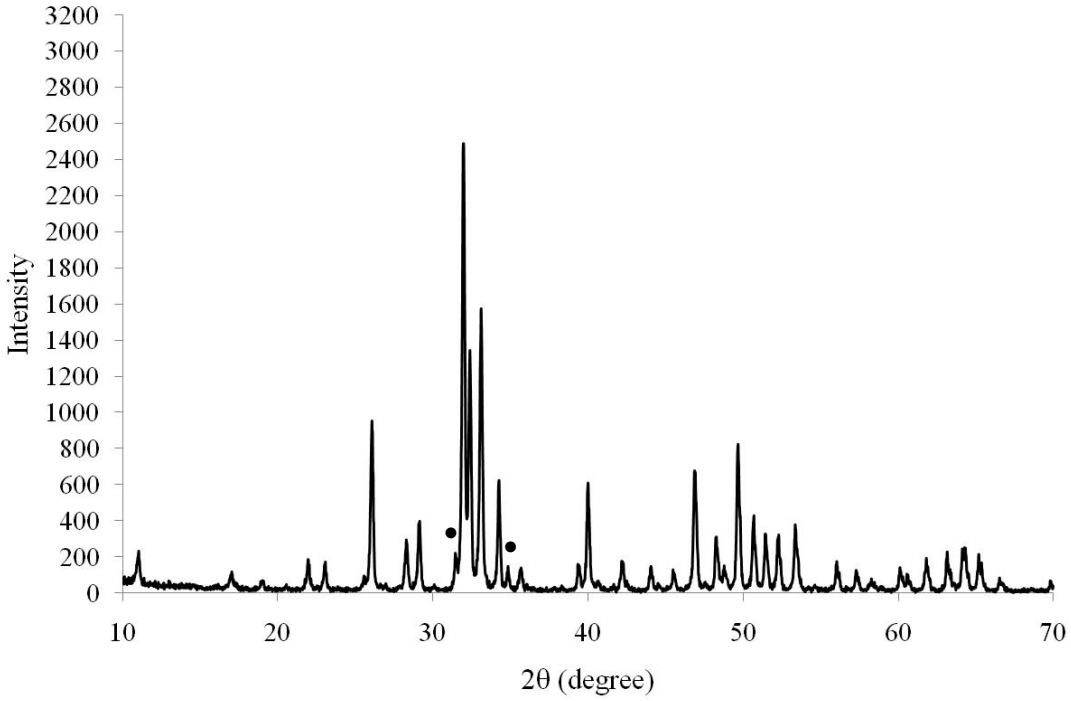

Figure 4.50. XRD spectrum of 6SHA after thermal treatment at 900 °C (•: β-TCP).

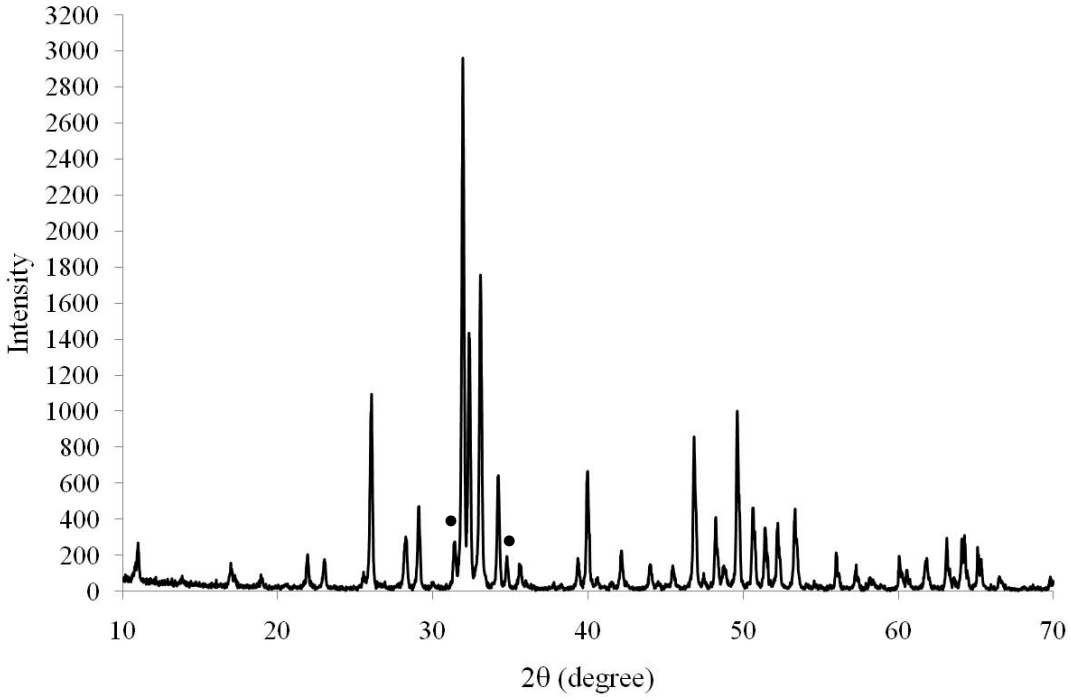

Figure 4.51. XRD spectrum of 6SHA after thermal treatment at 1000 °C (•: β-TCP).

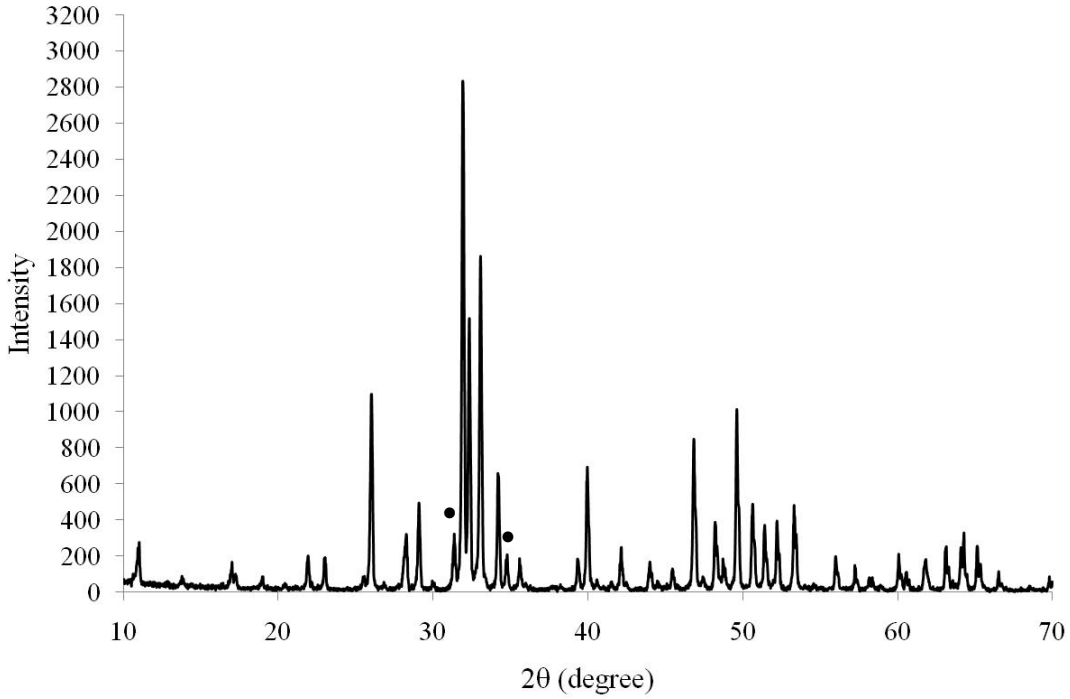

Figure 4.52. XRD spectrum of 6SHA after thermal treatment at 1100 °C (•: β-TCP).

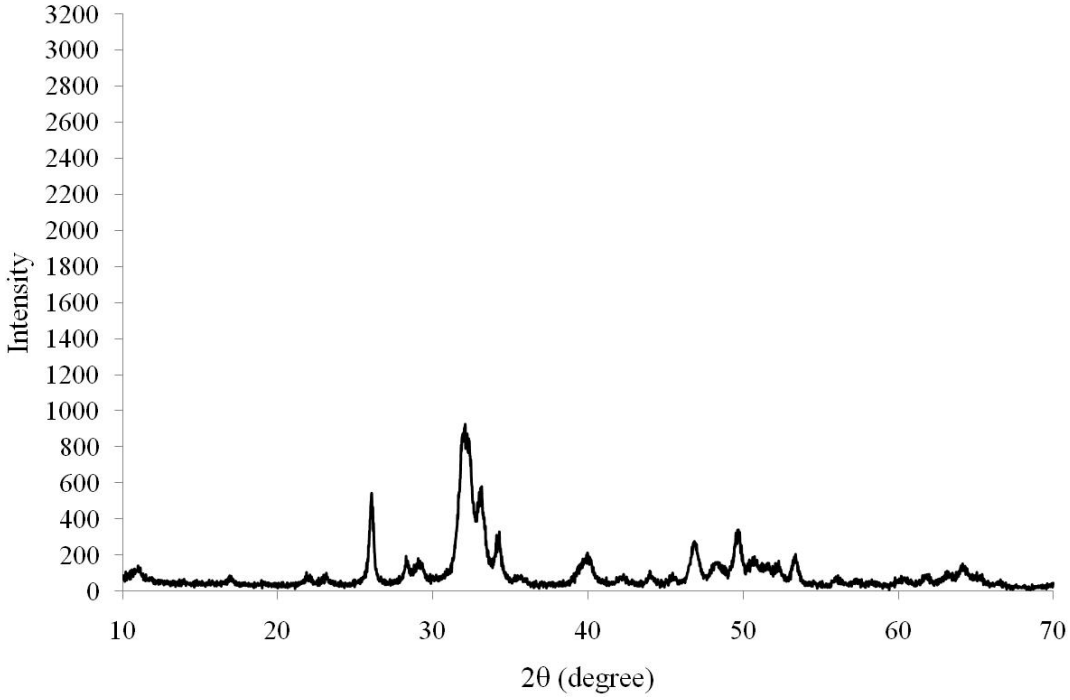

Figure 4.53. XRD spectrum of 9SHA in its synthesized state.

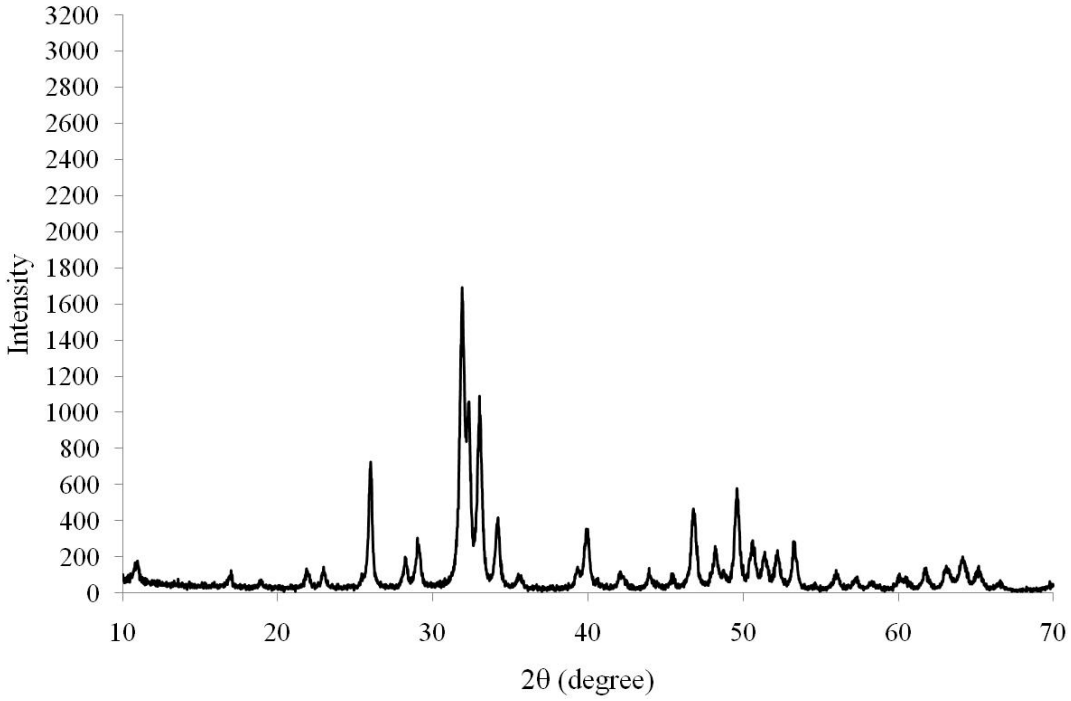

Figure 4.54. XRD spectrum of 9SHA after thermal treatment at 700 °C.

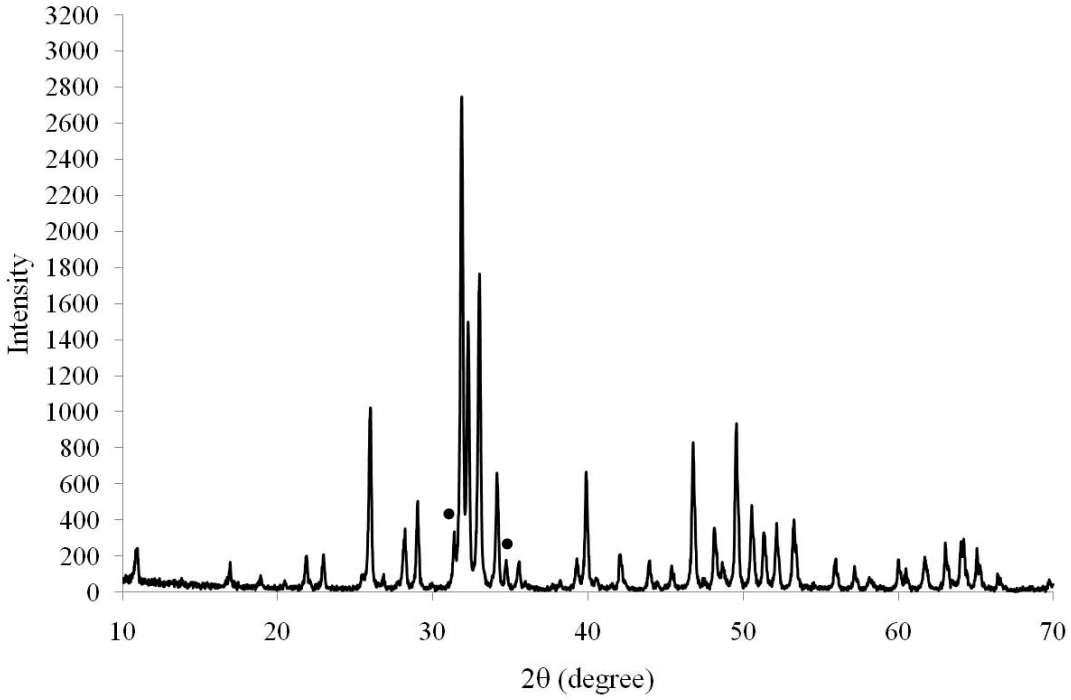

Figure 4.55. XRD spectrum of 9SHA after thermal treatment at 900 °C (•: β-TCP).

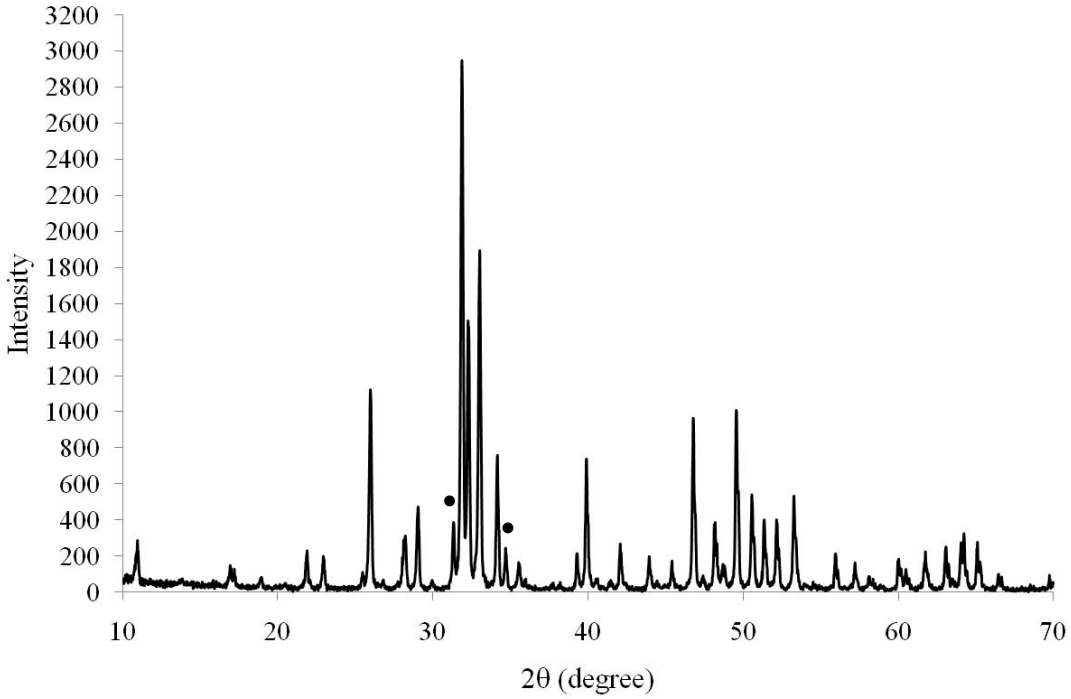

Figure 4.56. XRD spectrum of 9SHA after thermal treatment at 1000 °C (•: β-TCP).

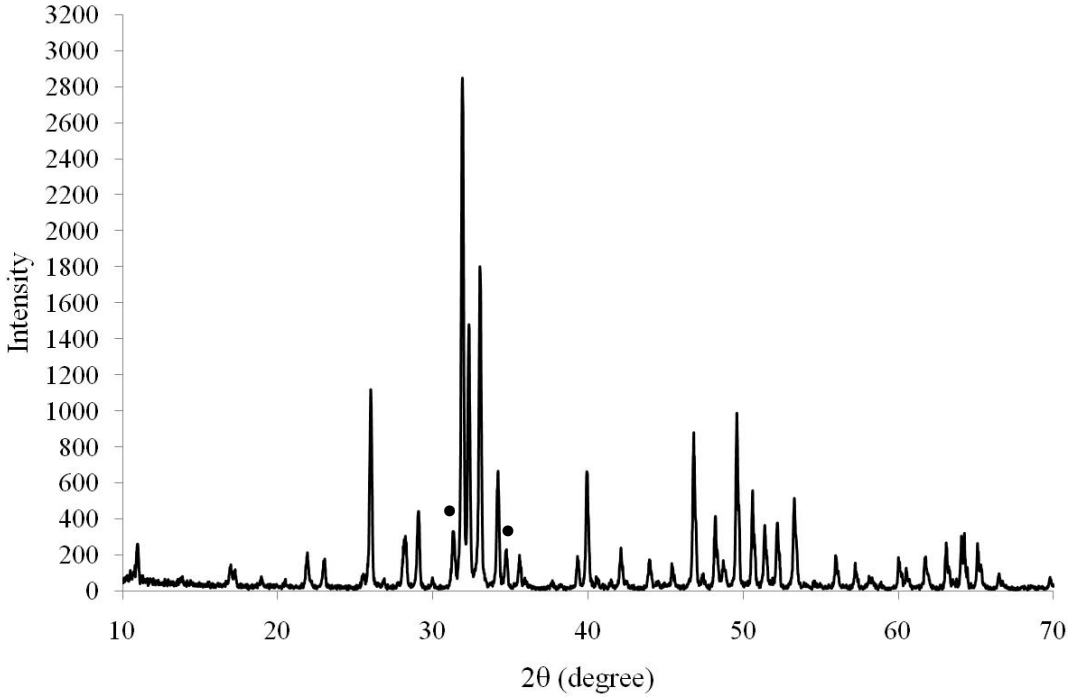

Figure 4.57. XRD spectrum of 9SHA after thermal treatment at 1100 °C (•: β-TCP).

4.3.2. FTIR Study of Silver Substituted Nanosized Stoichiometric Hydroxyapatite with and without Silver Substitution

FTIR analysis of the HA, 3SHA and 6SHA samples were conducted for their heat treated states at 900 and 1100 °C (Figures 4.58-4.63) and of the 9SHA sample for its heat treated states at 900, 1000 and 1100 (Figures 4.64-Figures 4.66) °C. The sharpness of the bands, especially around 560, 600 and 630 cm^{-1}, is a sign of a well crystallized hydroxyapatite [127].

The IR spectra of all of the samples have υ_3 PO_4^{3-} stretching bands around 1086-1087 cm^{-1} and between 1020 and 1028 cm^{-1} [12, 121] and, υ_1 stretching bands of PO_4^{3-} around 960 cm^{-1} [128] which are due to the P–O stretching of the phosphate group and are characteristic for hydroxyapatite. υ_2 bending modes around 470 cm^{-1}, υ_4 bending modes around and 600 cm^{-1}, and υ_4 anti-symmetric bending modes around 560 cm^{-1} due to the O-P-O bending of the PO_4^{3-} group are visible on the spectra of the samples [128]. Peaks found at 628-629 cm^{-1} for all the samples are characteristic for the librational mode of the OH^- group.

Peaks due to the O-H groups in the apatite channel are visualized with the peaks at 628-629 and peaks around 3570 cm^{-1} which are reduced in the spectra of all the samples with the increasing calcination temperature [129].

None of the samples have peaks around 870 and 1460 cm^{-1} indicative for CO_3^{2-} denoting formation of carbonated hydroxyapatite. Similarly, missing peaks around 3400 cm^{-1} show that the adsorbed water was removed due to heat treatment at elevated temperatures [130].

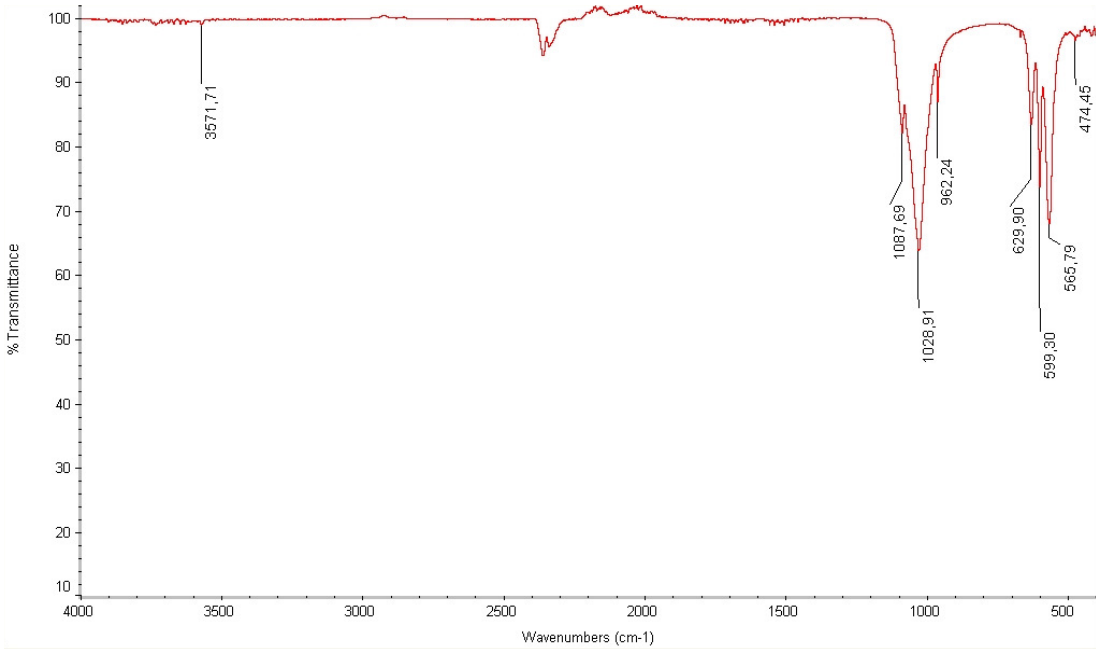

Figure 4.58. FTIR spectrum of the HA sample after thermal treatment at 900 °C.

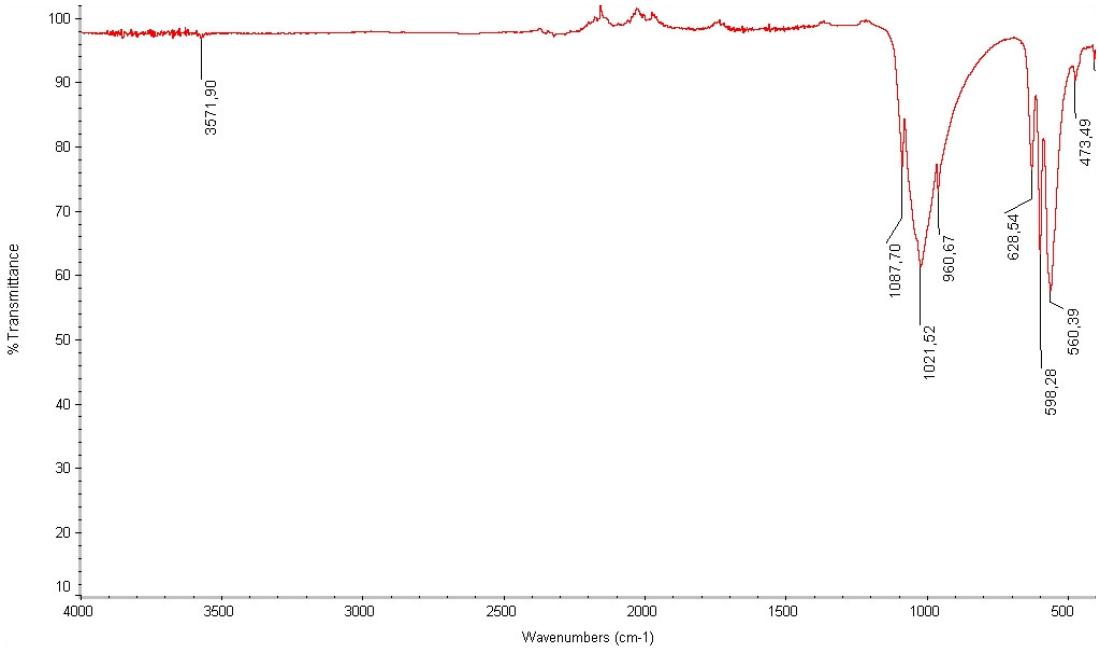

Figure 4.59. FTIR spectrum of the HA sample after thermal treatment at 1100 °C.

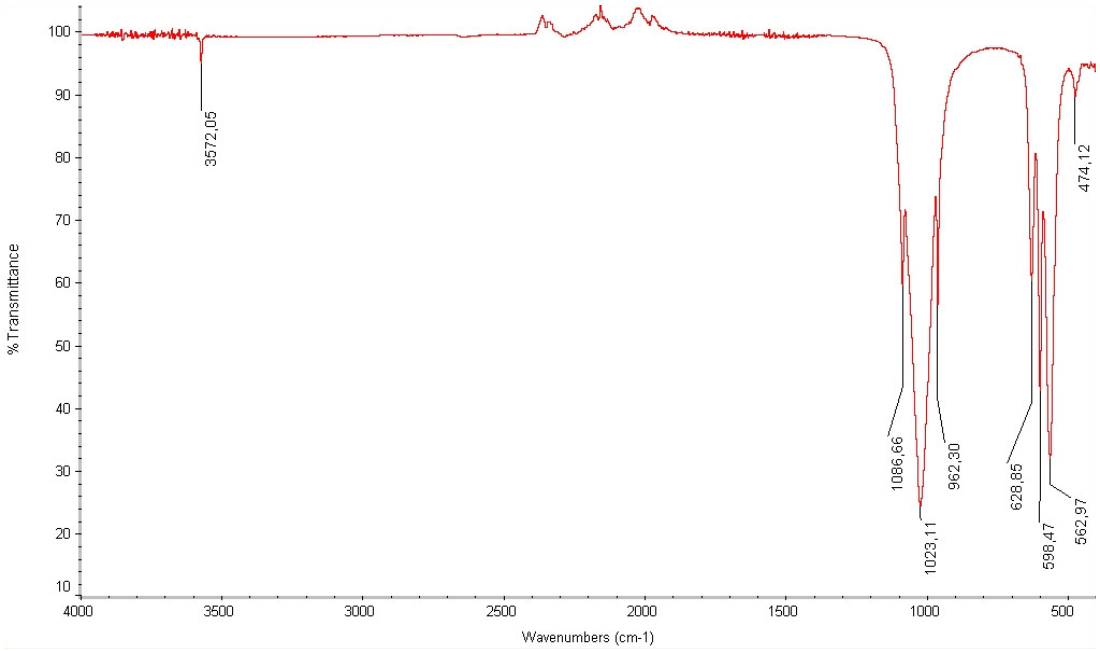

Figure 4.60. FTIR spectrum of the 3SHA sample after thermal treatment at 900 °C.

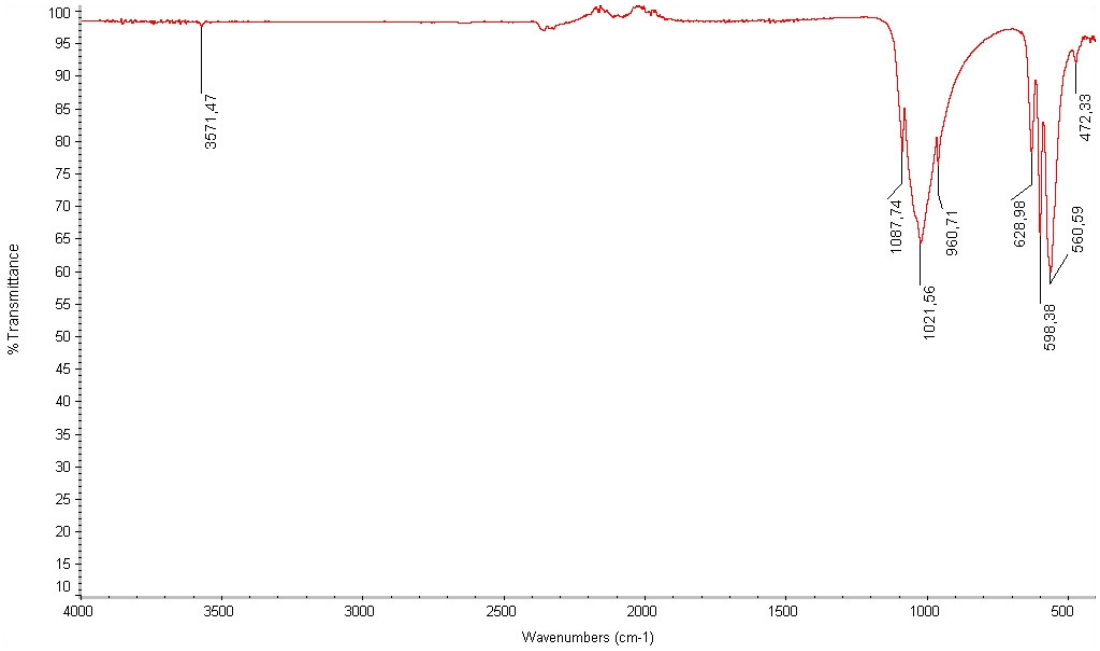

Figure 4.61. FTIR spectrum of the 3SHA sample after thermal treatment at 1100 °C.

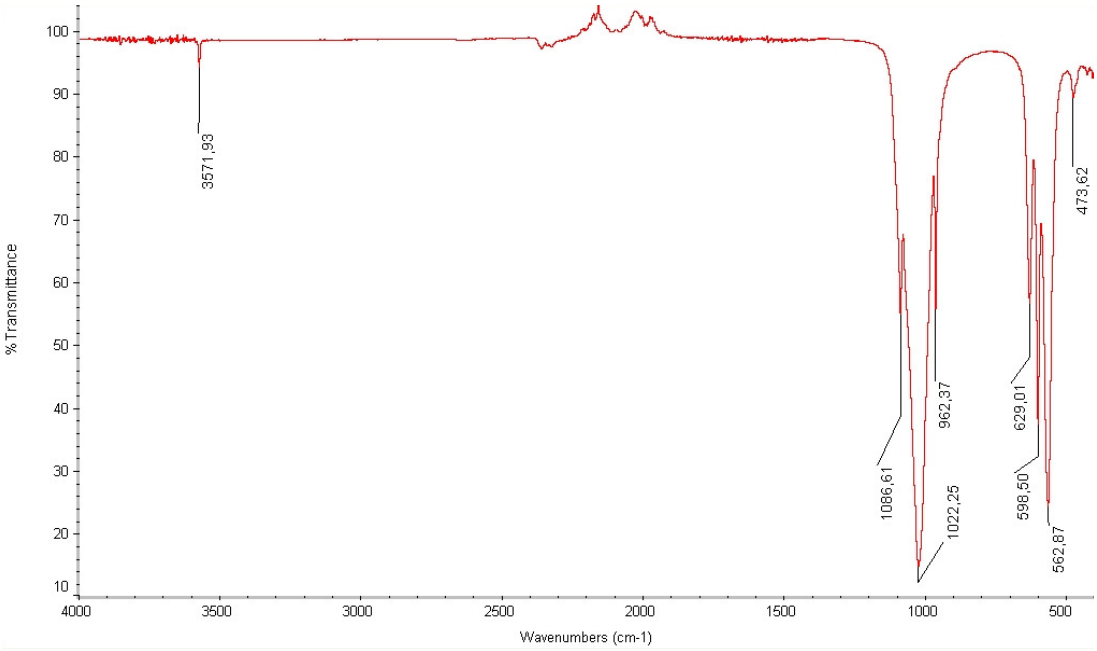

Figure 4.62. FTIR spectrum of the 6SHA sample after thermal treatment at 900 °C.

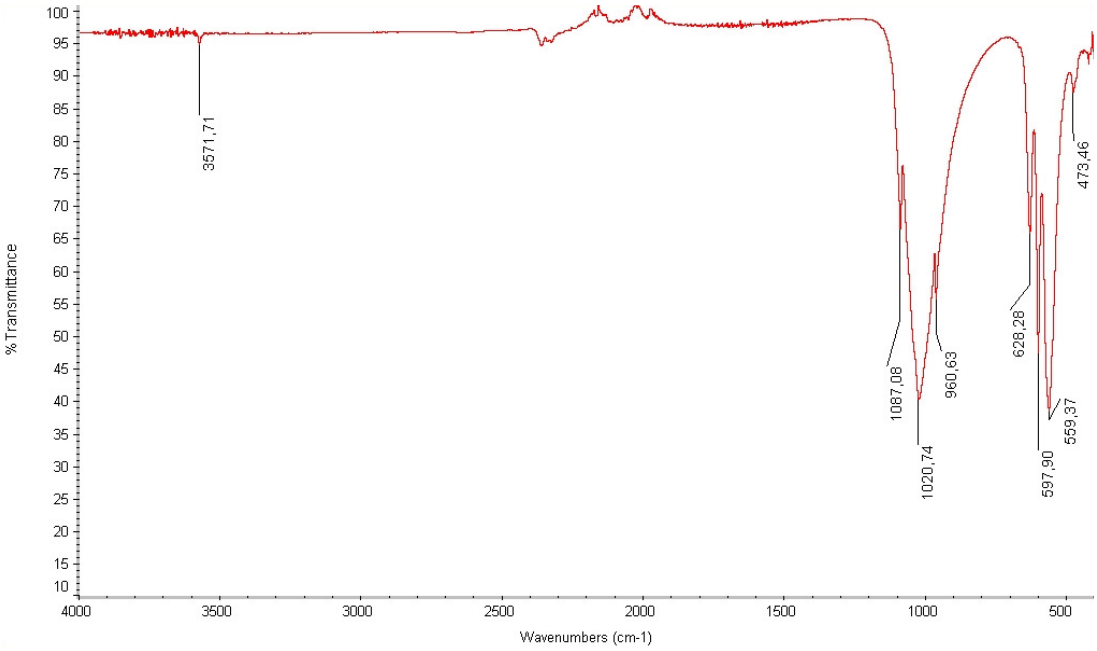

Figure 4.63. FTIR spectrum of the 6SHA sample after thermal treatment at 1100 °C.

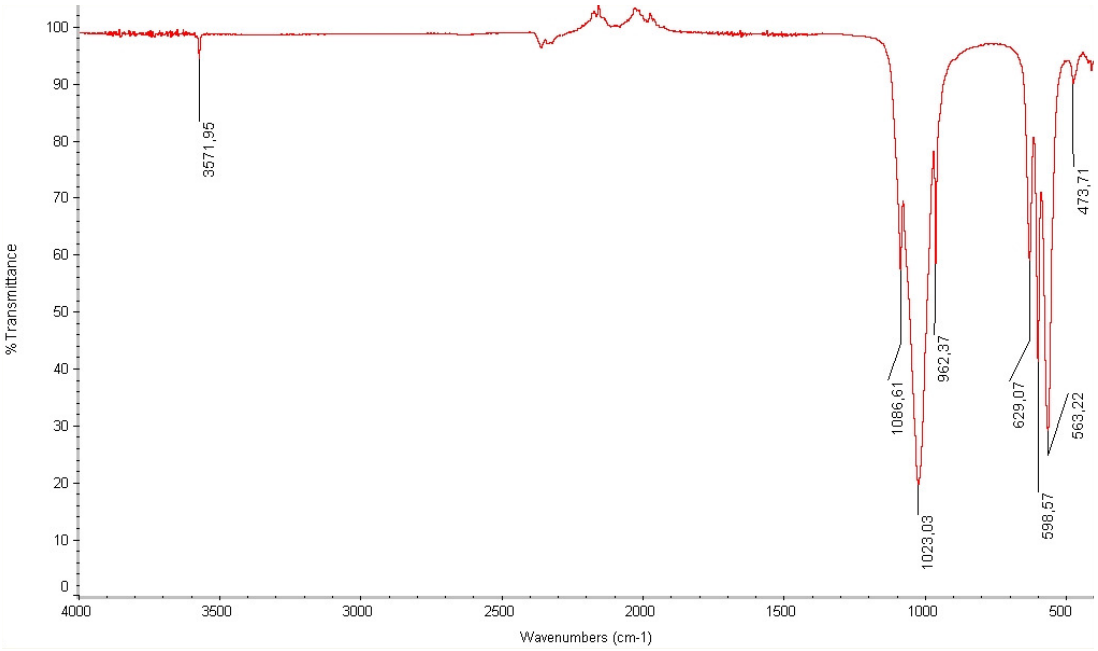

Figure 4.64. FTIR spectrum of the 9SHA sample after thermal treatment at 900 °C.

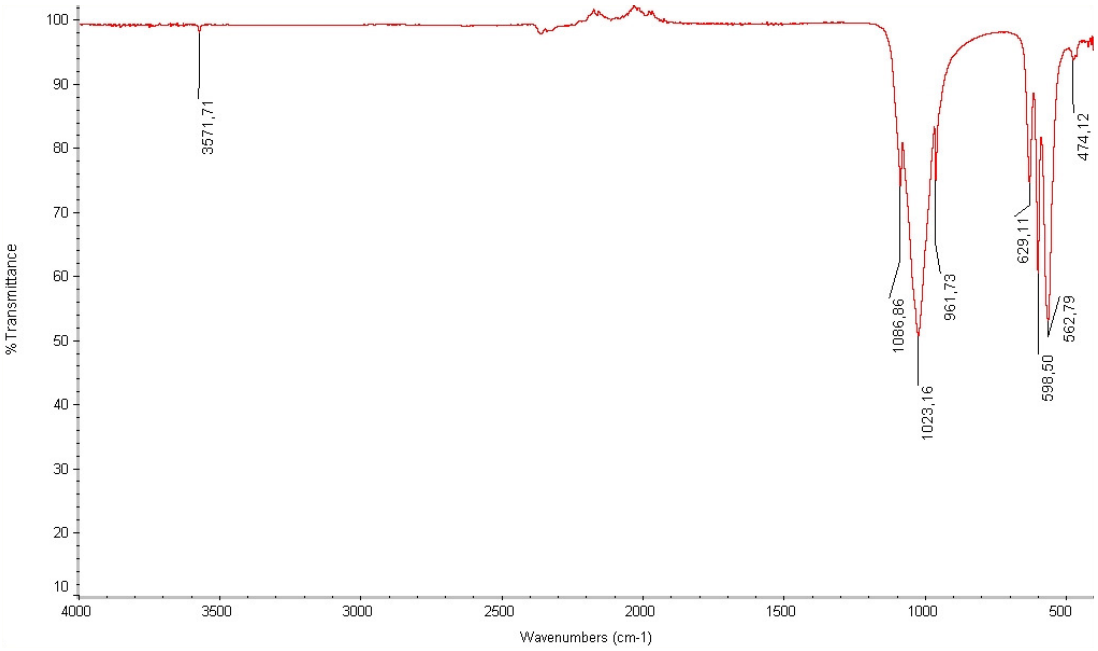

Figure 4.65. FTIR spectrum of the 9SHA sample after thermal treatment at 1000 °C.

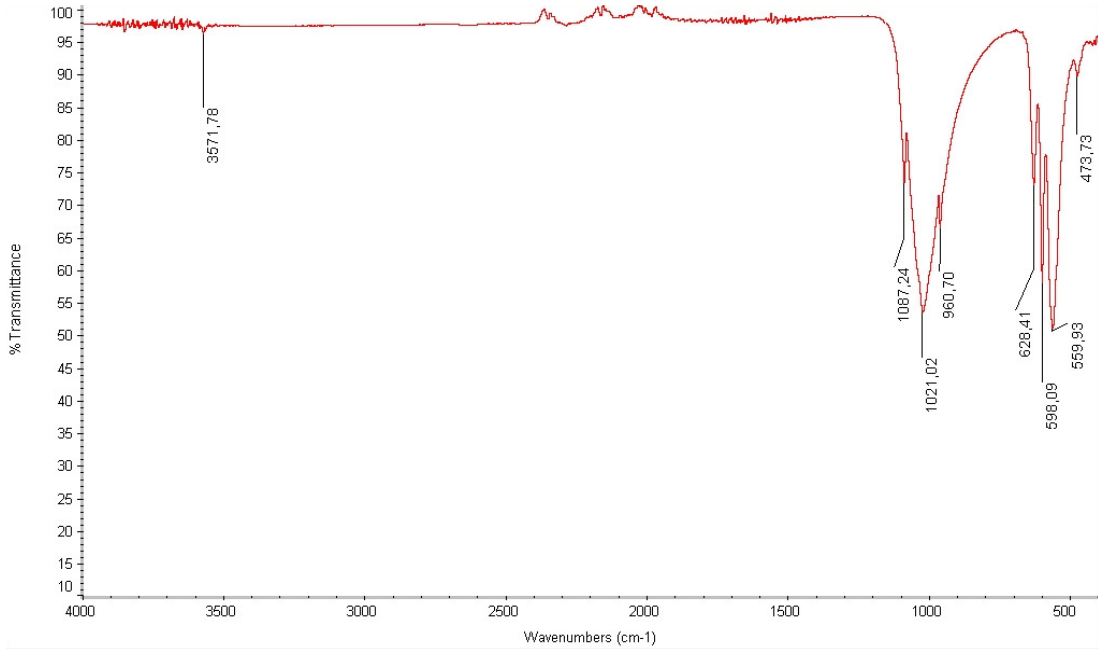

Figure 4.66. FTIR spectrum of the 9SHA sample after thermal treatment at 1100 °C.

4.3.3. Microhardness Measurements and Surface Morphologies of the Pellets Produced from Silver Substituted Nanosized Stoichiometric Hydroxyapatite with and without Silver Substitution

Cracks were not observed on the outside of the pellets after the formation of the compact with the uniaxial press under 80 MPa and after the cold isostatic pressing stage at 350 MPa before the sintering step. The pellets were crack free after sintering at 900, 1000 and 1100 °C at open atmosphere for 1 h. The prepared pellets held at room temperature for further observation indicated no cracks after 15 months. This showed that isostatic pressing is a suitable method in order to prepare solid form structures of silver substituted stoichiometric hydroxyapatite.

The prepared pellets were tested for their microhardness values in order to understand the effect of silver substitution on the hardness of the prepared samples. For this purpose, pellets prepared from HA and 3SHA powders were used. The reason that only HA and 3SHA samples were prepared and no other samples produced from powders of higher silver content were tested for their hardness values arose from the practical aspect of the application of the powders in their solid form. Since solid form structures are

implanted as-is they completely consist of the powder they were produced from. Although, the silver content of the prepared powders were low the overall silver content of the solid form structure is relatively high and increases with the volume of the solid form structure that is going to be implanted. Although, the in vivo biodegradation of hydroxyapatite is relatively low it is not completely bioinert. Therefore, any related dissolution of silver substituted hydroxyapatite in vivo would result in heightened free silver levels in the host organism. To keep the silver levels as low as possible even after slow dissolution of the solid form structures it would be reasonable to use silver substituted stoichiometric hydroxyapatite with possibly lowest content of silver. Therefore, the microhardness measurements were conducted on solid form structures prepared using 3SHA only and compared to HA in order to emphasize the practical limitation of application considering the silver content.

The weight and volume changes and the change in the calculated densities of the pellets are given in Table 4.5. There is a slight difference in the weight change of the samples produced form HA and 3SHA powders after sintering. Although, the weight difference before and after the sintering stage is greater for the 3SHA sample the volume change remains below that of HA at all temperatures studied. It can be stated that silver substituted hydroxyapatite powder has a slightly higher tendency to decompose at elevated heat treatment temperatures based on the observed weight loss of the samples. On the other hand, silver substitution has a negative effect on the compaction behavior of the 3SHA powder as observed by its slightly lower volume change after the sintering stage as compared to the pellets produced from HA. Conclusively, silver substitution enhances the decomposition of the powder and decreases its compactability.

The microhardness values of the pellets produced form HA and 3SHA and sintered 900, 1000 and 1100 °C at open atmosphere for 1 h are visualized in Figure 4.67. The microhardness values of the 3SHA pellets were found to be slightly below that of the HA pellets at all temperatures studied. This decrease in the microhardness values of the 3SHA might be based on the decomposition of the silver substituted samples. Since hydroxyapatite decomposes to β-TCP at elevated temperatures of sintering and since β-TCP phase possesses a lower hardness than hydroxyapatite the 3SHA samples have smaller microhardness. On the other hand, the densification of HA samples were found to

be higher than that of 3SHA which may be another factor effecting the difference in the microhardness values of the HA and 3SHA samples. However, considering the fact that only minor β-TCP were observed on the XRD analyses of the thermally treated silver substituted samples the decrease in the microhardness values of the 3SHA samples might be assumed to be based more on the decreased densification of the 3SHA samples than the β-TCP decomposition.

Table 4.5. Weight, volume and density changes (%) of the pellets produced from HA and 3SHA after sintering.

		% change after sintering	
		HA	3SHA
1100 °C	Weight	-5,95	-6,38
	Volume	-45,97	-43,23
	Density	74,09	64,93
1000 °C	Weight	-5,95	-5,95
	Volume	-37,75	-34,78
	Density	51,08	44,20
900 °C	Weight	-5,51	-5,79
	Volume	-24,56	-20,52
	Density	25,26	18,53

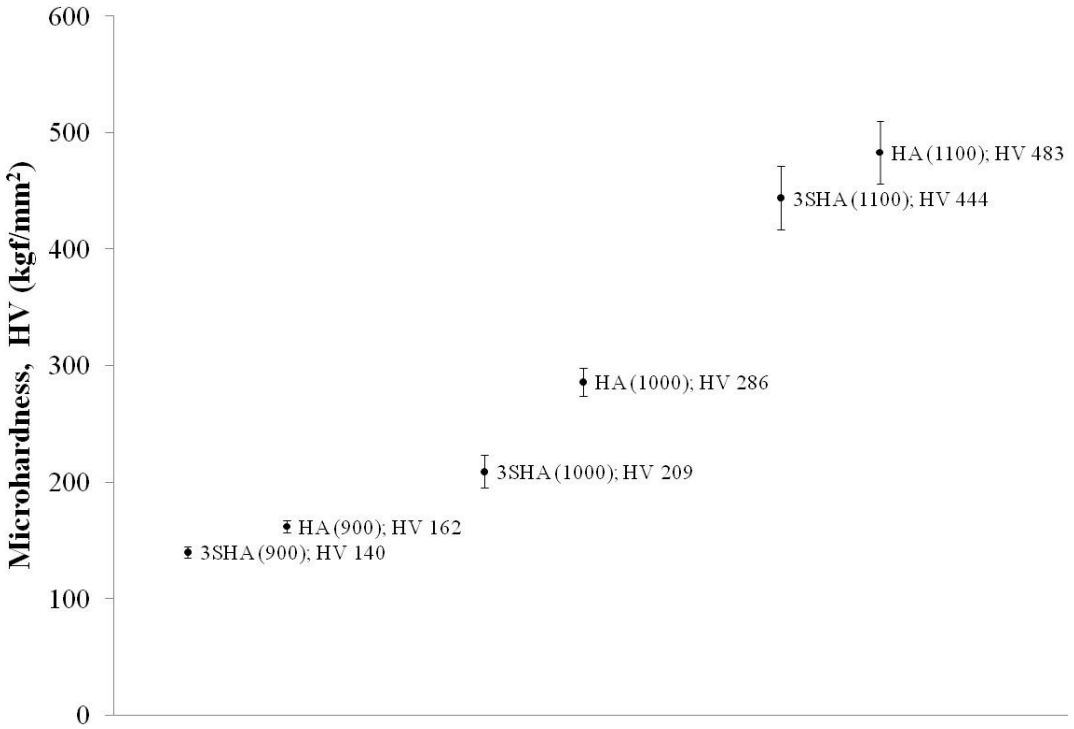

Figure 4.67. Results of the microhardness measurements of the pellets produced using HA and 3SHA powders and sintered at 900, 1000, and 1100 °C.

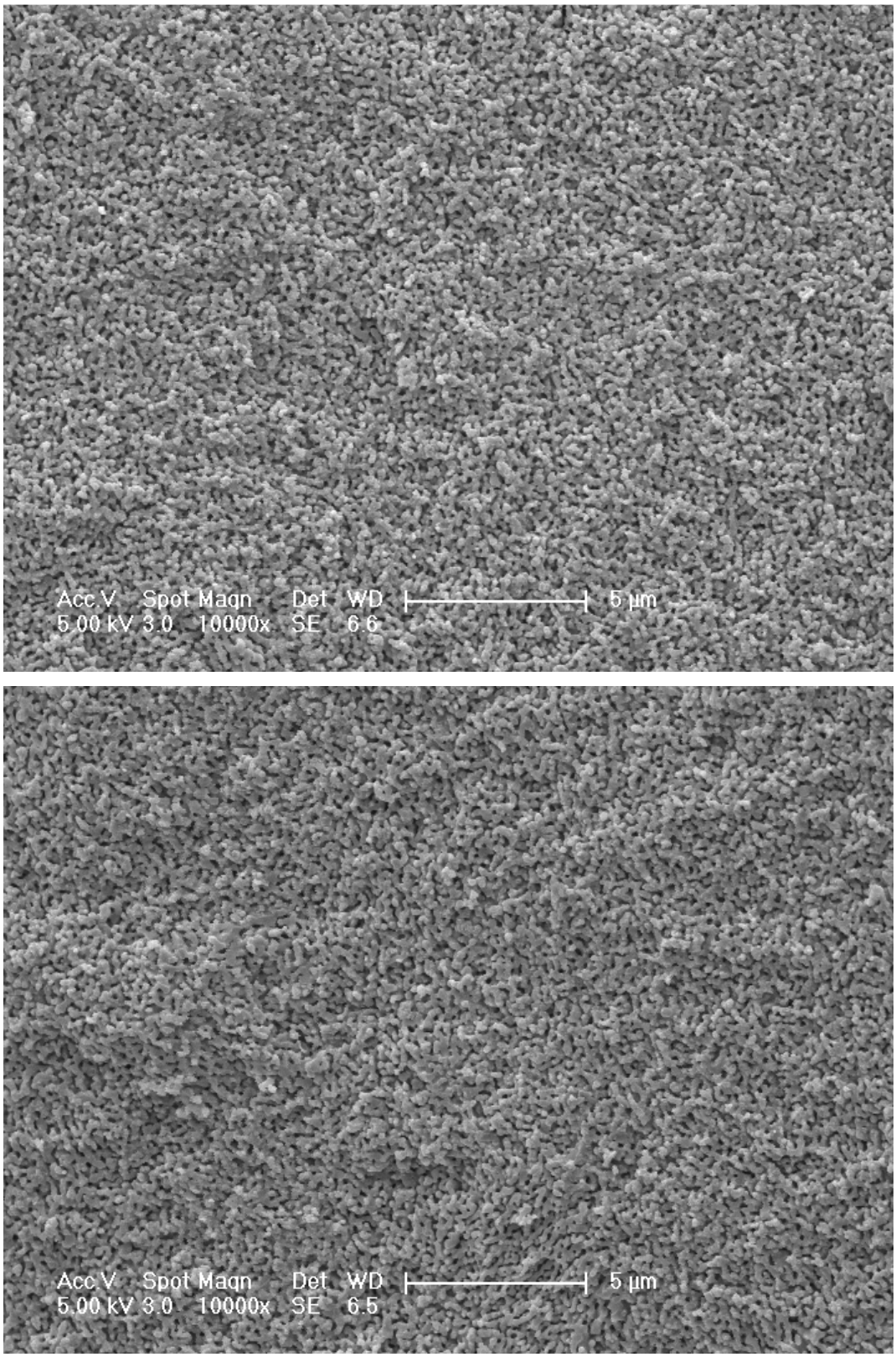

Figure 4.68. Pellets sintered at 900 °C (10000x)

top: HA, bottom: 3SHA.

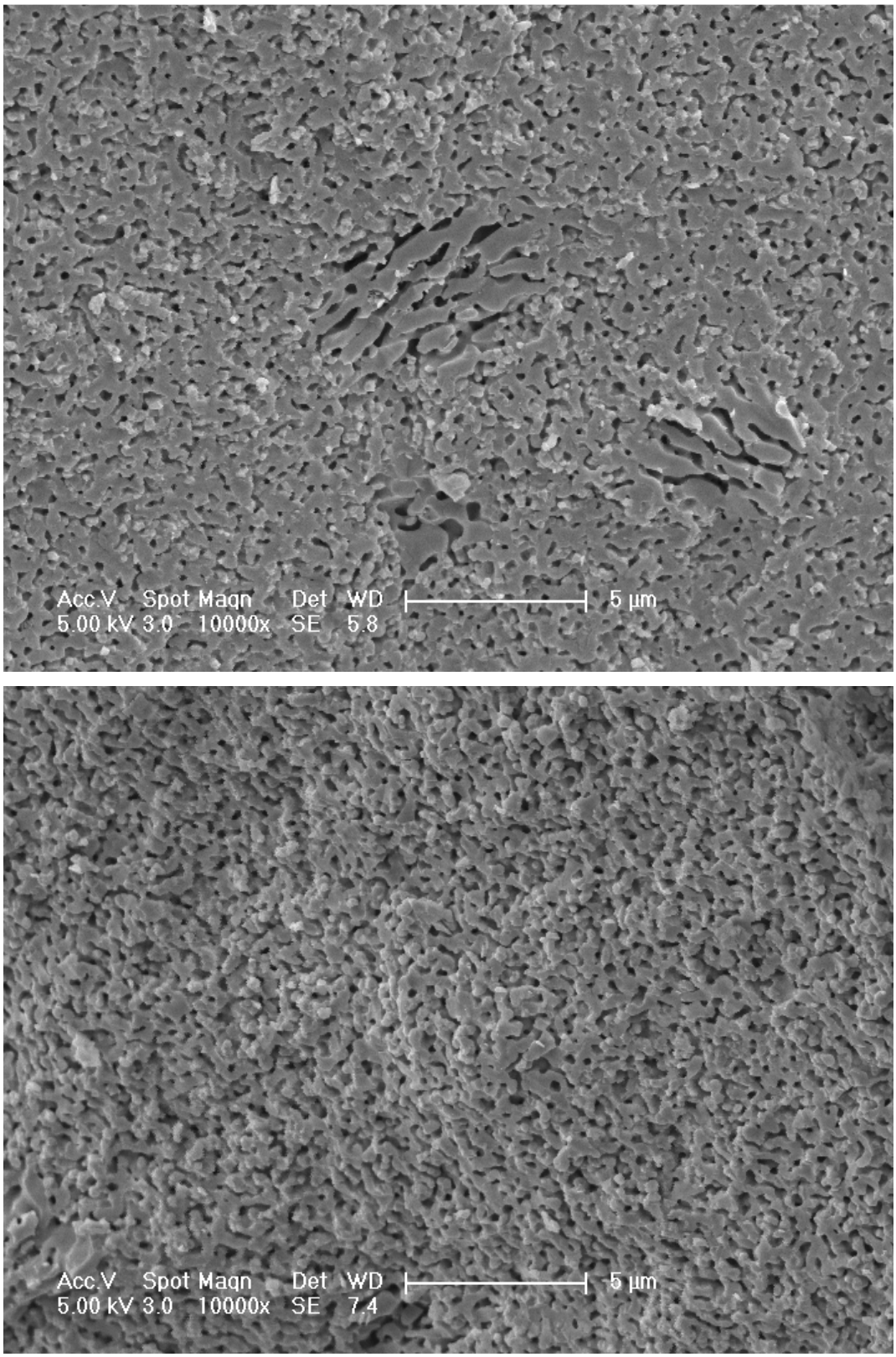

Figure 4.69. Pellets sintered at 1000 °C (10000x)

top: HA, bottom: 3SHA.

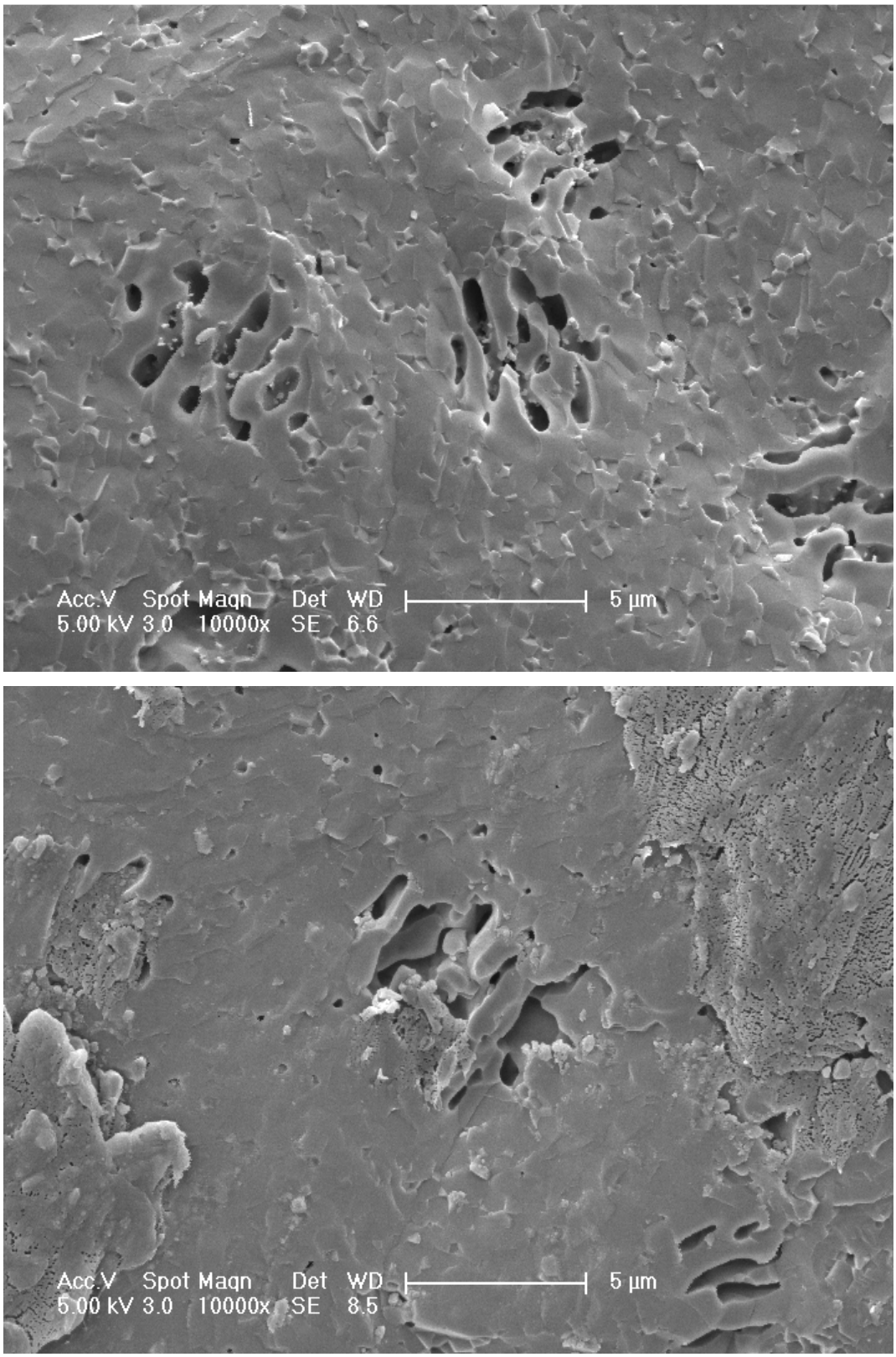

Figure 4.70. Pellets sintered at 1100 °C (10000x)

top: HA, bottom: 3SHA.

SEM images of the sintered pellets produced from HA and 3SHA and sintered at 900, 1000 and 1100 °C (Figures 4.68-4.70) revealed that successful necking of the particles was achieved at 900 °C and a high level of densification was obtained at 1100 °C. These observations are in close correspondence with the microhardness measurements and verified by the changes in the calculated densities of the pelletized samples.

Although similar morphologies were obtained for both of the samples produced using HA and 3SHA powders and sintered at 900 and 1100 °C important to note was the difference between the samples sintered at 1000 °C. Pellets produced from HA showed more densification at 1000 °C whereas the densification of the pellets produced from 3SHA seems to lag at the same temperature. This observed difference in the morphologies can be verified by the relatively high difference of the microhardness values of the samples at 1000 °C. Although pellets sintered from the two different powders and sintered 900 and 1100 °C showed close microhardness values the microhardness values of the pellets of HA and 3SHA powders sintered at 1000 °C deviate greatly due to the difference in the densification behavior at the given temperature.

4.3.4. Antibacterial Evaluation of Silver Substituted Nanosized Stoichiometric Hydroxyapatite

The antibacterial activities of the HA, 3SHA, 6SHA and, 9SHA samples treated at different temperatures are tabulated (Table 4.6). The antibacterial activity of the samples increased with the increasing silver content such that complete elimination of both kinds of bacteria tested could be achieved with the 9SHA samples at 900 °C.

Important to note was the effect of heat treatment temperature on the antibacterial activity of the particular samples. For all of the four samples tested the antibacterial effectiveness decreased with the increased heat treatment temperature regardless of the silver content of the samples. This observation was valid also for the HA samples which did not contain silver which can be explained by considering the results of heat treatment at elevated temperatures. At higher temperatures minor β-TCP peaks were observed on the XRD analyses of the samples. Since antibacterial activity tends to decrease by increasing

temperature and thus by increasing decomposition into β-TCP hydroxyapatite itself might have a higher antibacterial effect than β-TCP. Since with increasing temperature the β-TCP formation is favored which increases the β-TCP content of the sample overall the antibacterial activity of the sample diminishes. However, the increasing β-TCP decomposition alone may not suffice to explain the observed temperature dependent antibacterial activity of the samples since the XRD analyses of the samples revealed only minor β-TCP formation at elevated temperatures. Although no clear free silver peaks were observed in the XRD analyses part of substituted Ag may not exist in apatitic structure any more due to the decomposition of SHA into β-TCP but in form of free Ag which is known have low antibacterial efficiency.

Table 4.6. Antibacterial activity of 100 mg SHA powder samples with varying silver content and thermally treated at different temperatures against E. coli and S. aureus bacteria in 10 ml bacterial solution with a concentration of 1 x 10^6 cfu/ml.

Sample	Temperature (°C)	E. coli (Gram negative) Bacterial Load after 30 min (cfu/ml)	E. coli (Gram negative) Bacterial Load after 24 h (cfu/ml)	S. aureus (Gram positive) Bacterial Load after 30 min (cfu/ml)	S. aureus (Gram positive) Bacterial Load after 24 h (cfu/ml)
9SHA	900	0	0	0	0
9SHA	1000	1,975	40,533	390,000	232
9SHA	1100	357,500	53,833	507,500	235
6SHA	900	10	10	-	-
6SHA	1100	348,000	22,700	-	-
3SHA	900	3,580	10	-	-
3SHA	1100	343,000	66,700	-	-
HA	900	340,000	142,000	-	-
HA	1100	413,000	4,030,000	-	-

The increasing degree of crystallization may also play a role in the observed differences in the antibacterial activity of the samples treated at different temperatures. Since crystallization of the samples is enhanced with the increasing temperature this is thought to effect the antibacterial activity.

The final source for the observed temperature dependent difference of antibacterial activities is considered to be the changing particle and surface morphology of the samples. With the increasing temperature the surface area of the samples decreases which in turn decreases the amount of silver containing surfaces exposed to bacteria which further increases the possibility of the tested organisms to find a suitable site to adhere and multiply. Partial sintering at elevated temperatures achieved by interparticle connections based on the necking of the particles may also effect the antibacterial effectiveness of the powders.

4.4. Production of Silver Substituted Hydroxyapatite Coatings on Titanium Substrates by Electrophoretic Deposition

4.4.1. Coating of Silver Substituted Nanosized Stoichiometric Hydroxyapatite on Titanium Substrates by Electrophoretic Deposition

Titanium substrates were coated by nano sized stoichiometric hydroxyapatite by electrophoretic deposition. Two different coating voltages, 100 and 200 V, were applied for different sets of substrates. The coated samples were sintered in a vacuum furnace under $1x10^{-5}$ mbar at 800 and 900 °C for 1 h at a heating rate of 100 °C/h and a cooling rate of 50 °C/h. SEM analysis was conducted before and after the sintering process.

The SEM analysis of the coatings revealed that there was no distinct difference on the final coating surfaces produced by applying two different coating voltages (Figure 4.71). Although, an increase in the coating voltage was expected to increase the amount of agglomerated particles on the coating surface both coatings produced by 100 and 200 V seemed similar and relatively homogenous in various magnification levels. The series of magnetic stirring and ultrasonication and the following extended duration before

decantation obviously eliminated large agglomerates such that the coating process applied by using different voltages resulted in homogenous coatings and similar results.

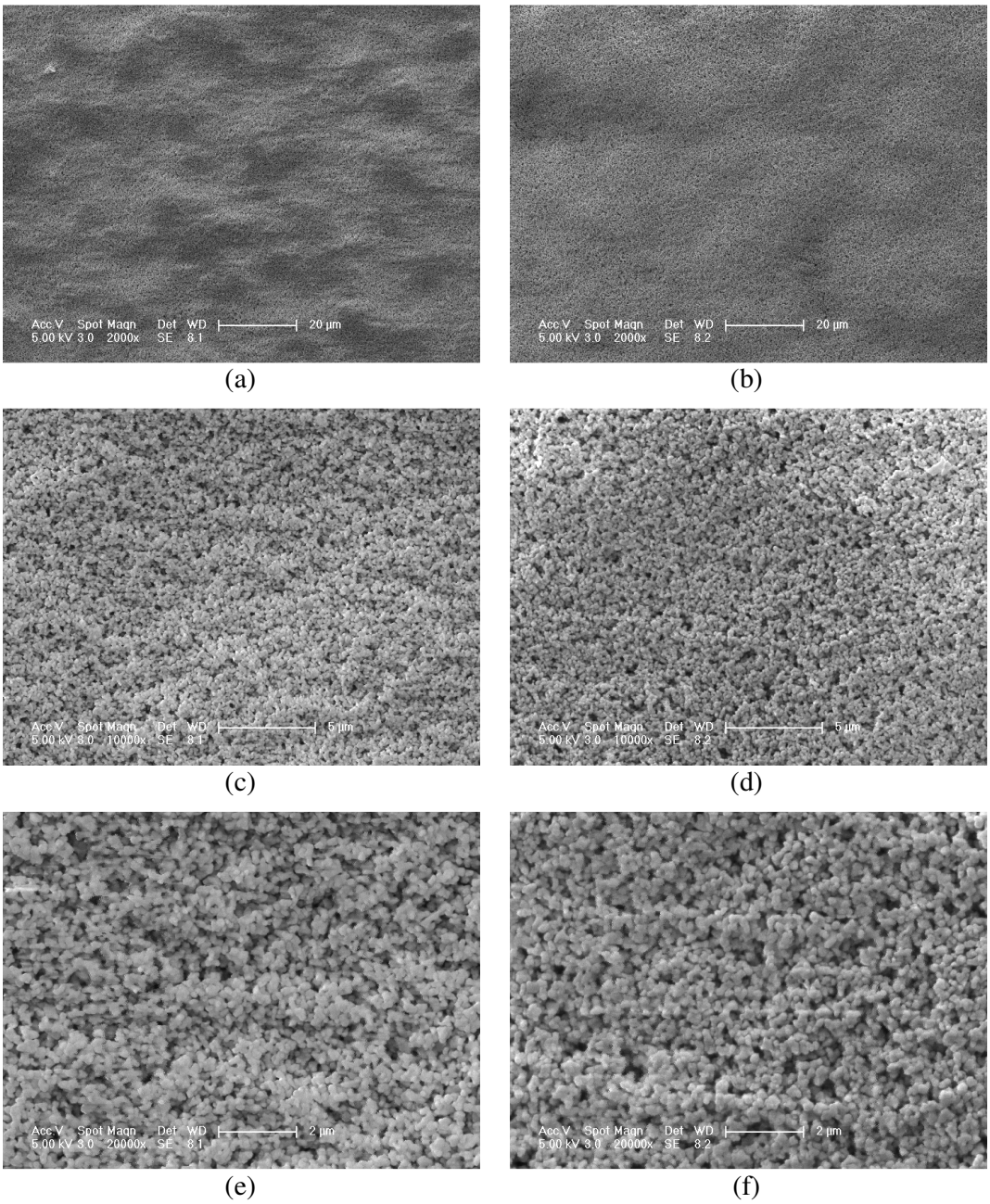

Figure 4.71. SEM images of 9SHA coatings before sintering
(a) 100 V, 60 s (2000x); (b) 200 V, 60 s (2000x); (c) 100 V, 60 s (10000x); (d) 200 V, 60 s (10000x); (e) 100 V, 60 s (20000x); (f) 200 V, 60 s (20000x).

No surface cracks could be observed on the samples dried at open atmosphere after the coating process by electrophoretic deposition. Crack free coating surfaces could be obtained even after sintering the samples at 800 (Figure 4.72) and 900 (Figure 4.73) °C.

Similarities between the results of different coating voltages persisted even after the sintering process at the same temperatures thus indicating the sintering temperature plays a more important role than the coating voltage in obtaining a more dense coating surface structure.

However, differences were observed between the different sintering temperatures. Although, initiation of the necking of the particles could be detected on the coating surfaces of the samples sintered at 800 °C necking goes to completion on the coating surfaces of the samples sintered at 900 °C. Successful necking was obtained at 900 °C resulting in a denser coating surface than those of the samples sintered at 800 °C.

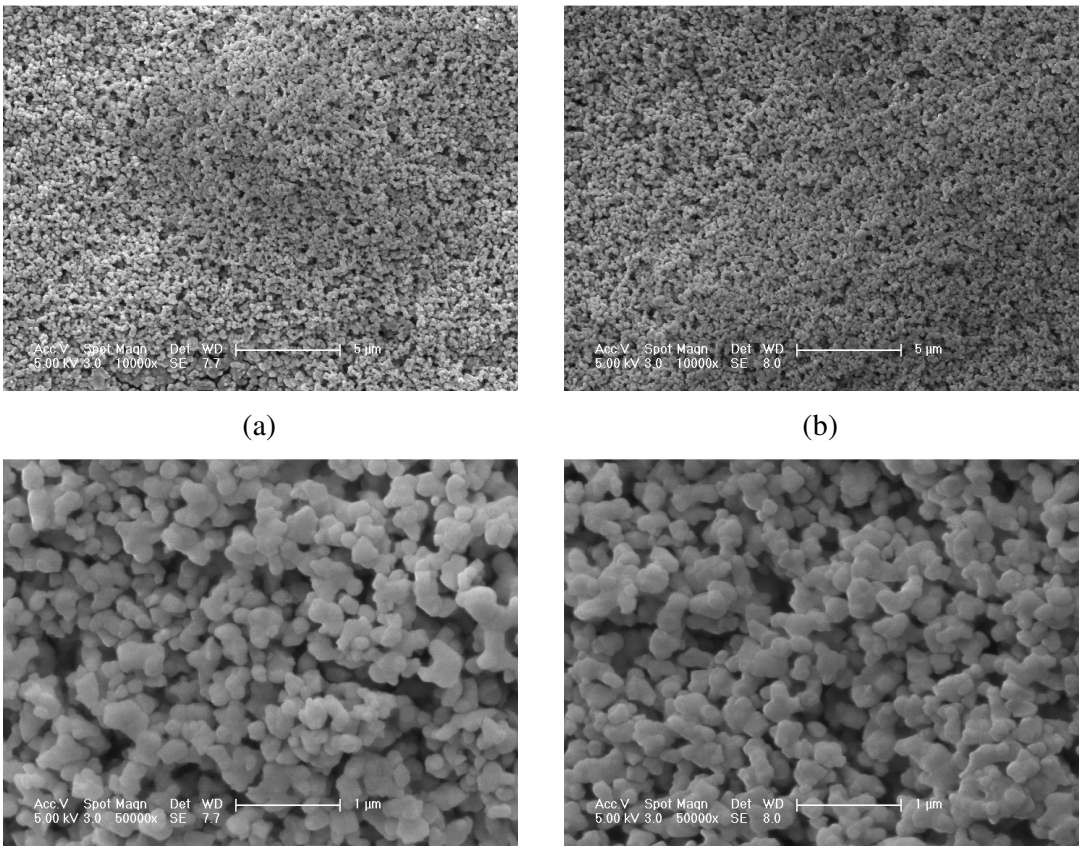

(a) (b)

(c) (d)

Figure 4.72. SEM images of 9SHA coatings after sintering at 800 °C
(a) 100 V, 60 s (10000x); (b) 200 V, 60 s (10000x);
(c) 100 V, 60 s (50000x); (d) 200 V, 60 s (50000x).

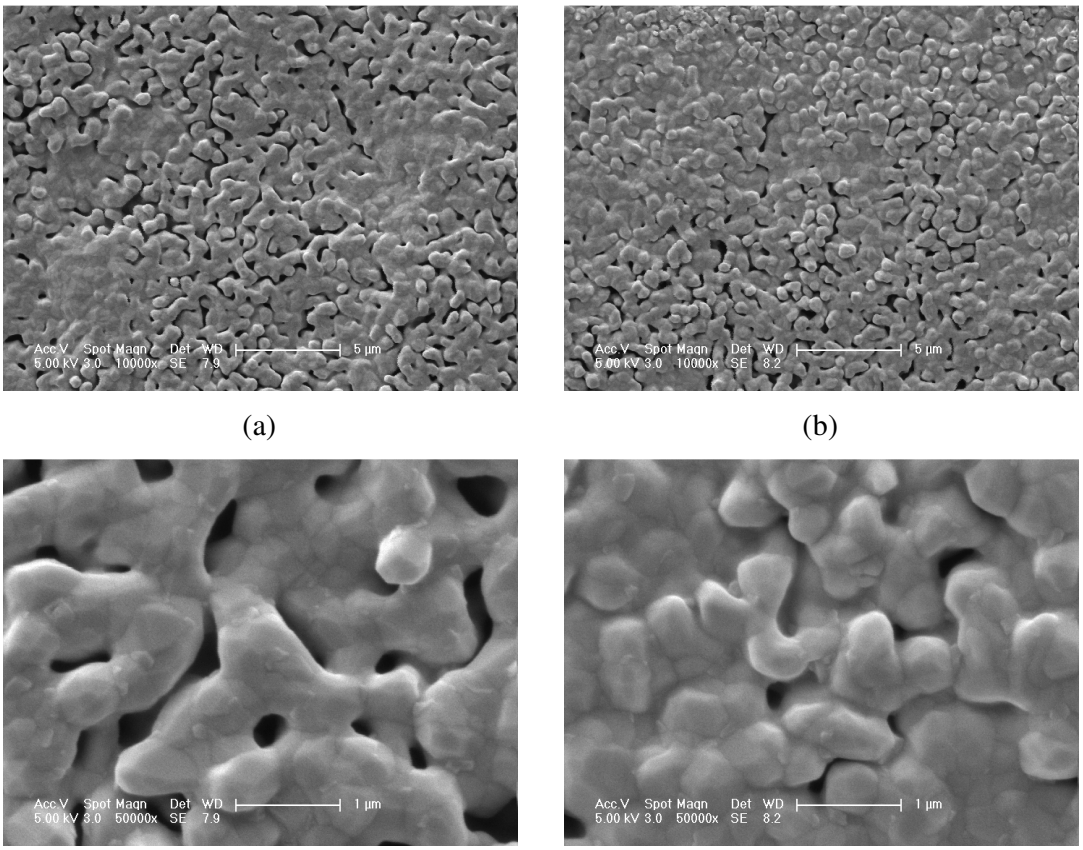

(a) (b)

(c) (d)

Figure 4.73. SEM images of 9SHA coatings after sintering at 900 °C
(a) 100 V, 60 s (10000x); (b) 200 V, 60 s (10000x);
(c) 100 V, 60 s (50000x); (d) 200 V, 60 s (50000x).

4.4.2. Controlling the Decomposition of Silver Substituted Stoichiometric Hydroxyapatite Coatings by the Use of Titanium Dioxide Inner Layer Application

Studies were conducted to detect and control the decomposition of 9SHA in the outer coating layer. For this purpose, samples were prepared in order to determine the effect of the TiO_2 coating voltage and the sintering temperature on the decomposition of 9SHA outer coating layer.

To determine the effect of sintering temperature on the 9SHA decomposition samples were prepared without prior application of TiO_2 by applying 100 V of coating voltage for 60 s and sintered at 900 (Figure 4.74) and 1000 (Figure 4.75) °C. XRD analysis

of the sample sintered at 900 °C indicates β-TCP peaks resulting from the decomposition process as well as clear CaO peaks. On the other hand, no evident hydroxyapatite peaks could be observed on the XRD analysis of the sample sintered at 1000 °C indicating that 9SHA was almost fully decomposed as observed on the analysis.

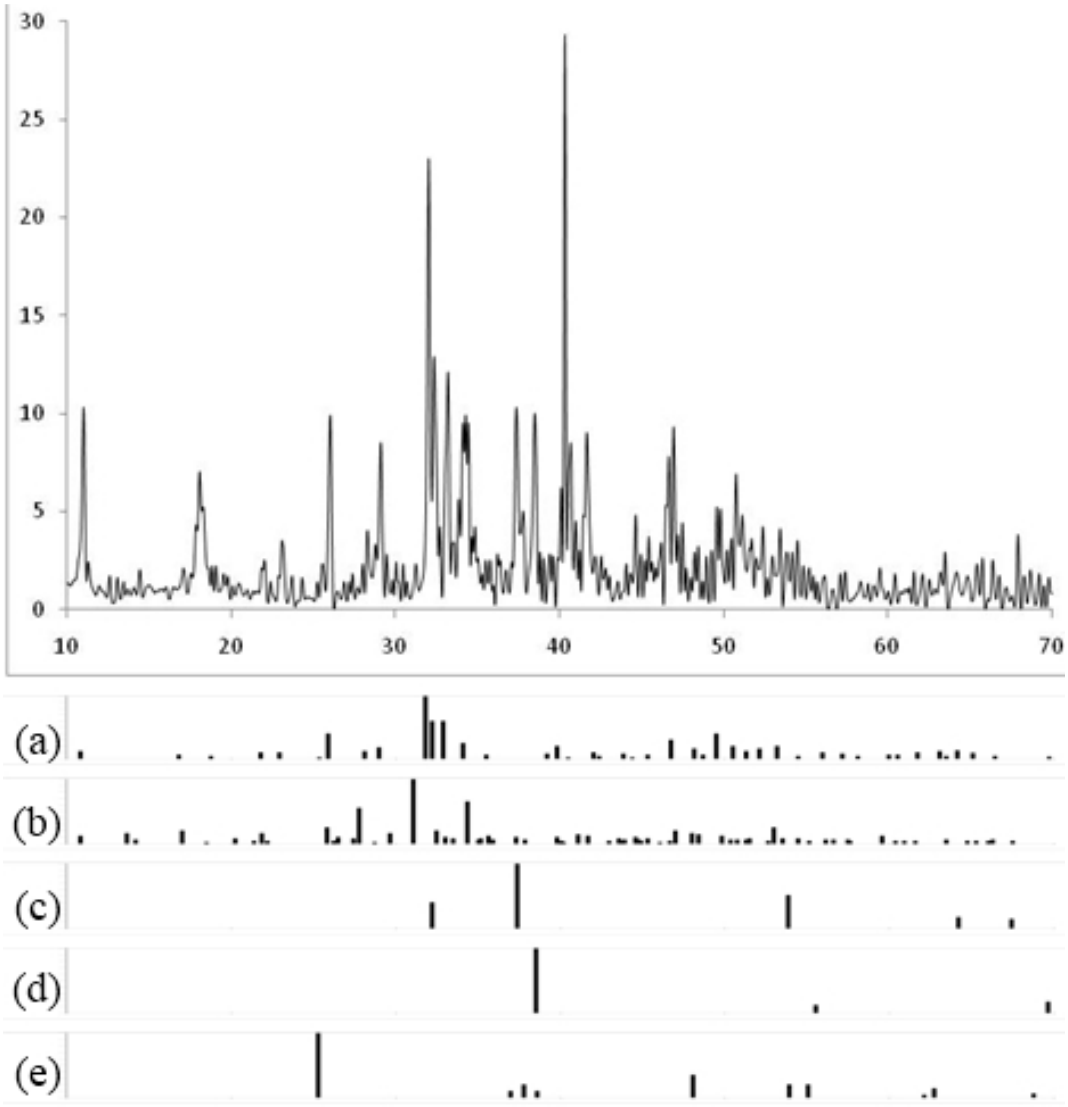

Figure 4.74. XRD analysis of the sample coated with 9SHA (100 V, 60 s) and sintered at 900 °C (no prior TiO_2 inner layer coating)
(a) HA; (b) β-TCP; (c) CaO; (d) Ti; (e) TiO_2.

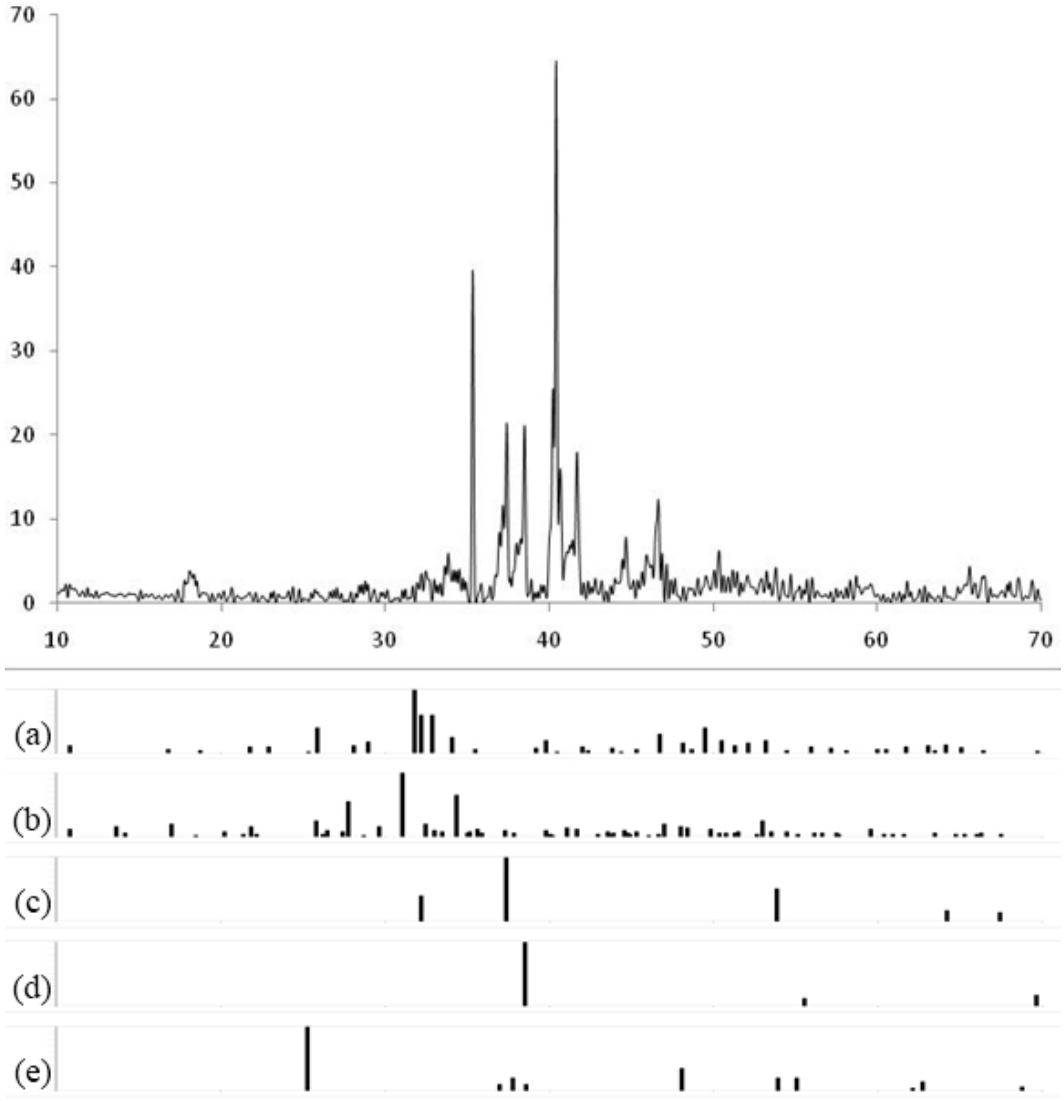

Figure 4.75. XRD analysis of the sample coated with 9SHA (100 V, 60 s) and sintered at 1000 °C (no prior TiO_2 inner layer coating)
(a) HA; (b) β-TCP; (c) CaO; (d) Ti; (e) TiO_2.

This observation showed that samples prepared without prior TiO_2 inner layer coating had significant decomposition such that at an elevated sintering temperature of 1000 °C no 9SHA could be detected in the outer layer. Based on this observation, studies were conducted to control the 9SHA decomposition by applying a TiO_2 inner layer to act as an ion barrier between the titanium substrate and the 9SHA outer layer.

To understand the effect of the TiO_2 inner layer coating voltage on the 9SHA decomposition samples were prepared applying 20 and 40 V of TiO_2 coating voltage for 60 s. The TiO_2 coated samples were further coated with 9SHA by applying 80 V coating voltage for 60 s. The samples were sintered at 900 (Figures 4.76 and 4.78) and 1000 (Figures 4.77 and 4.79) °C.

The samples sintered at 1000 °C showed pronounced CaO peaks accompanied with minor β-TCP peaks. In order to control the decomposition of 9SHA samples were sintered at a lower sintering voltage of 900 °C. This decrease in the sintering temperature resulted in the elimination of the CaO peaks. The samples sintered at 900 °C showed slight indications of β-TCP existence as observed by low intensity peaks.

The apparent shift of major HA peaks to higher degrees as compared to their standard values is thought to be based on the induced internal stresses during the sintering process due to the difference of the thermal expansion coefficients of HA and the underlying metallic substrate.

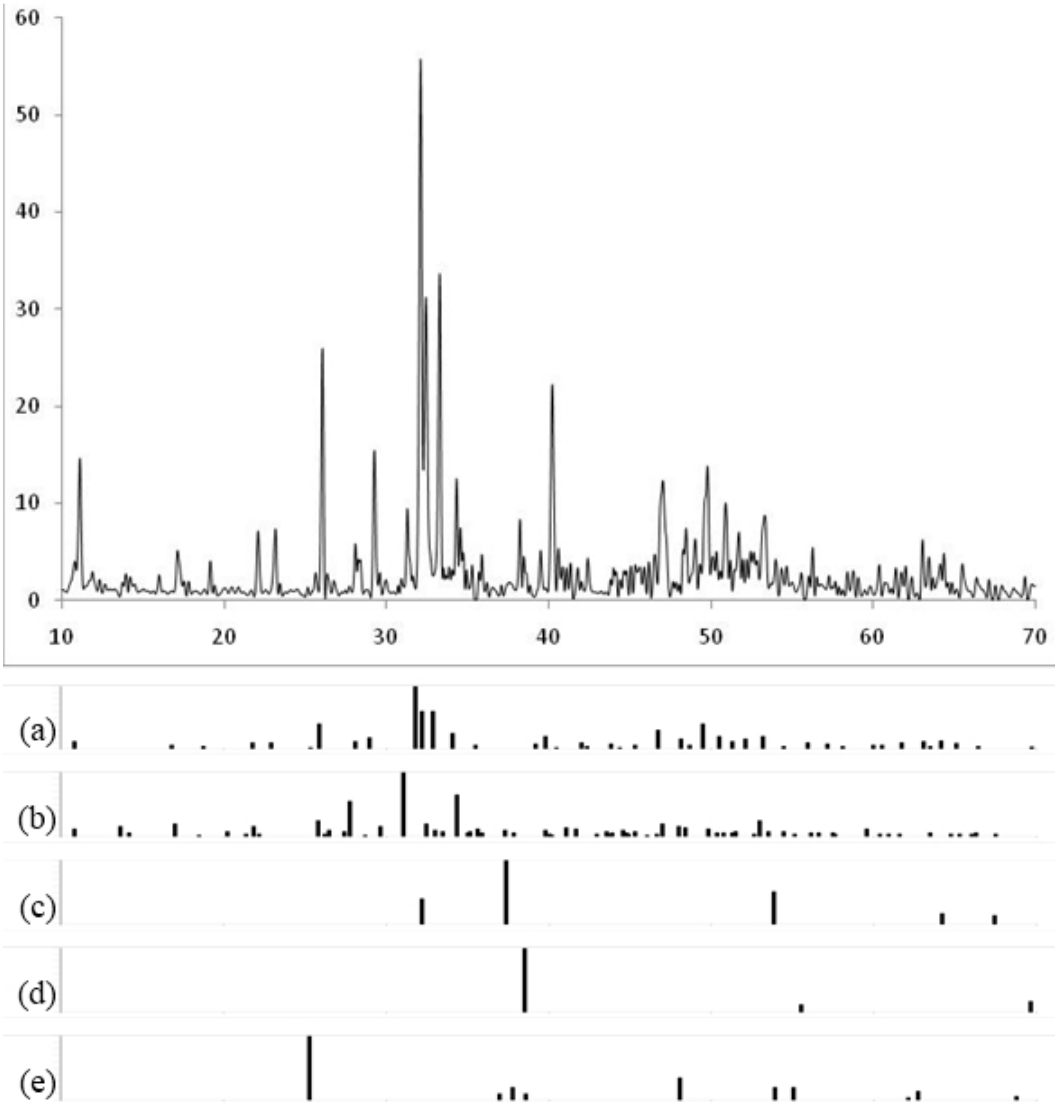

Figure 4.76. XRD analysis of the sample coated with TiO_2 (20 V, 60 s) and with 9SHA (80 V, 60 s) and sintered at 900 °C

(a) HA; (b) β-TCP; (c) CaO; (d) Ti; (e) TiO_2.

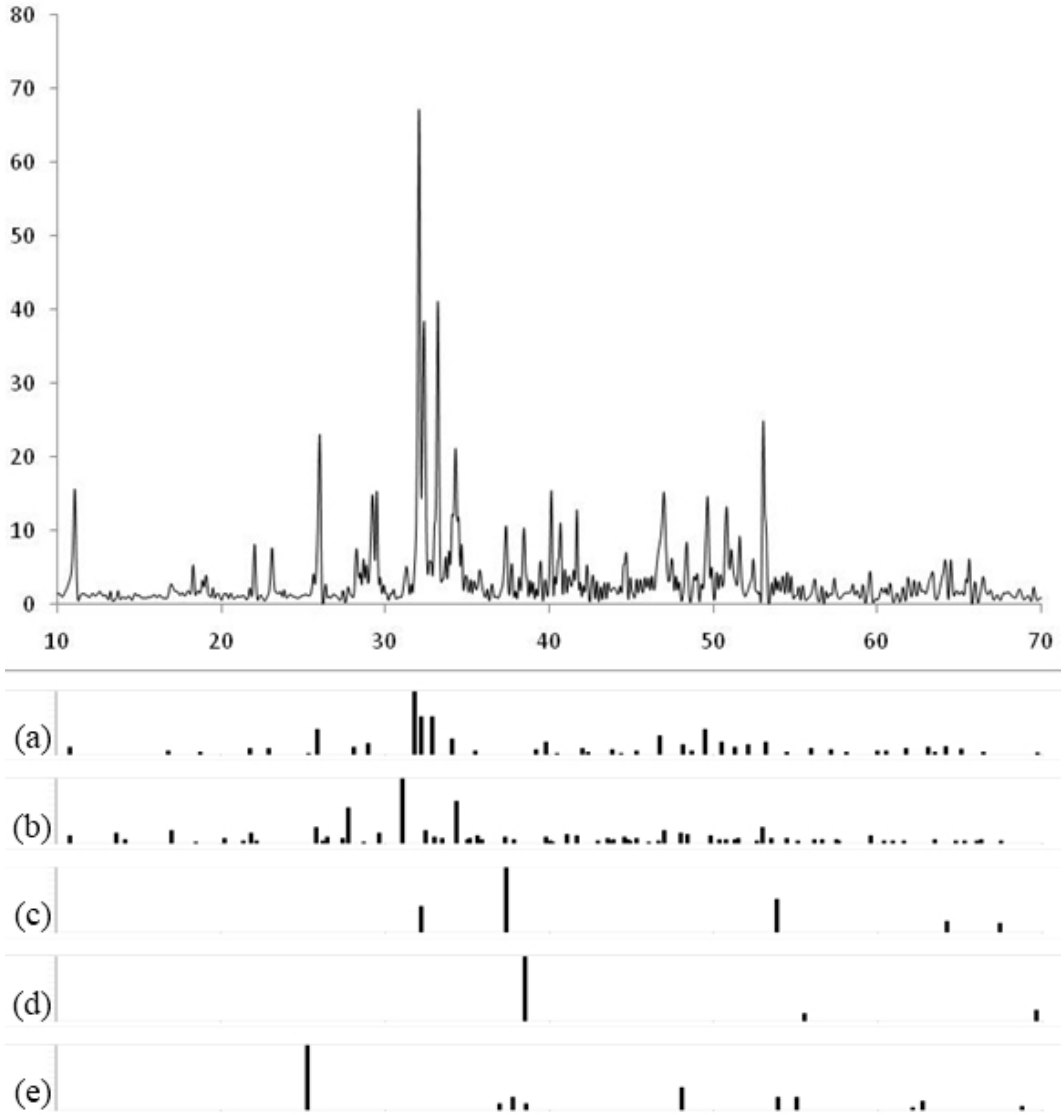

Figure 4.77. XRD analysis of the sample coated with TiO_2 (20 V, 60 s) and with 9SHA (80 V, 60 s) and sintered at 1000 °C

(a) HA; (b) β-TCP; (c) CaO; (d) Ti; (e) TiO_2.

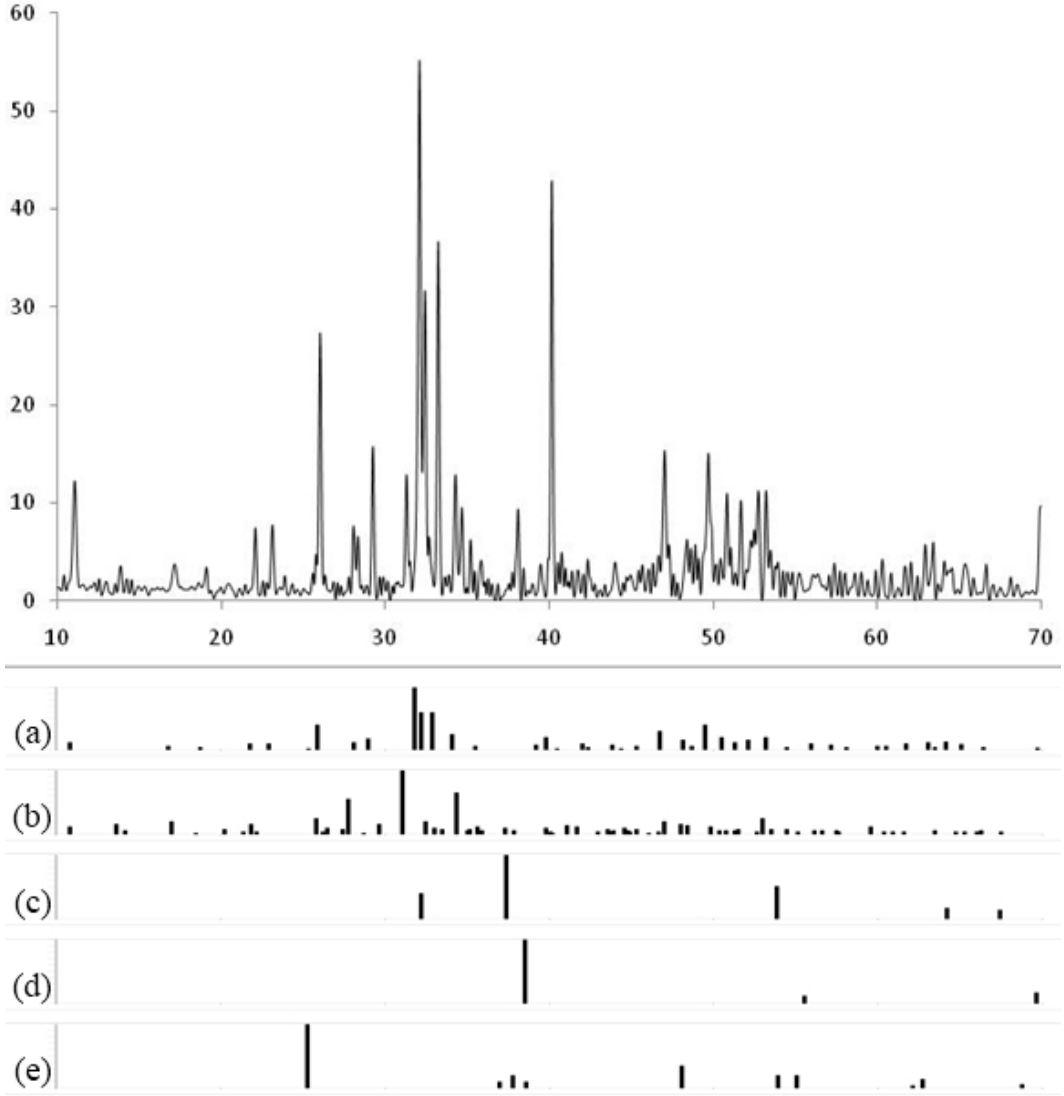

Figure 4.78. XRD analysis of the sample coated with TiO_2 (40 V, 60 s) and with 9SHA (80 V, 60 s) and sintered at 900 °C

(a) HA; (b) β-TCP; (c) CaO; (d) Ti; (e) TiO_2.

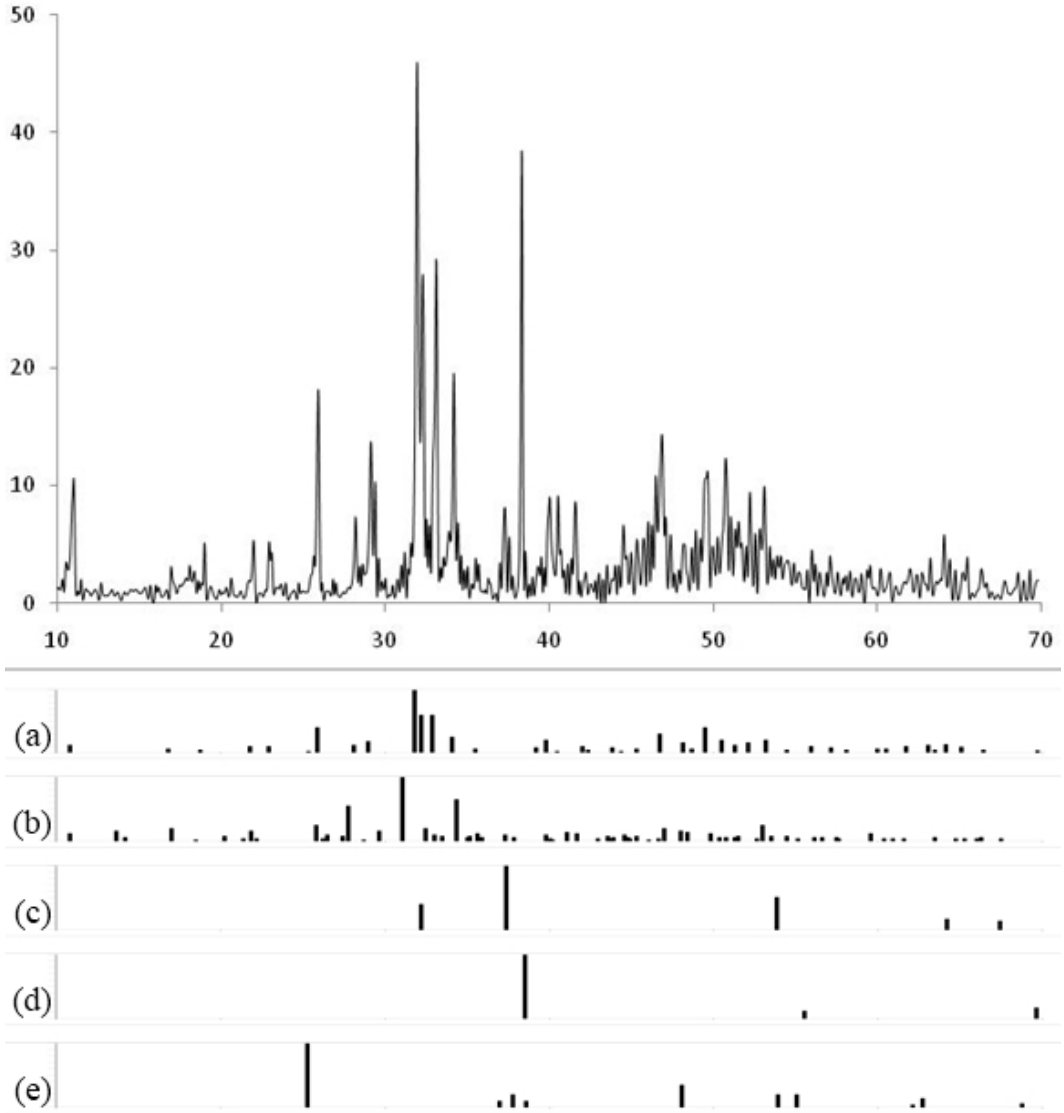

Figure 4.79. XRD analysis of the sample coated with TiO_2 (40 V, 60 s) and with 9SHA (80 V, 60 s) and sintered at 1000 °C

(a) HA; (b) β-TCP; (c) CaO; (d) Ti; (e) TiO_2.

As opposed to the expected result that an increasing TiO_2 would decrease the 9SHA decomposition by imposing a thicker ion barrier between the titanium substrate and the 9SHA outer coating layer samples prepared with 40 V of TiO_2 coating voltage showed more decomposition into β-TCP and CaO than their 20 V counterparts at both sintering temperatures.

To understand the underlying reason of the enhanced decomposition due to the increased TiO_2 coating voltage samples were prepared only with TiO_2 coatings using 20 and 50 V coating voltages and sintered at 800 °C. A lower sintering temperature was selected as compared to 900 and 1000 °C in order to detect the condition of the TiO_2 layer before the necking and densification of the particles, which constitute the layer, occur.

The SEM analysis (Figure 4.80) of the prepared samples showed that increasing the TiO_2 coating voltage resulted in significant cracks in the TiO_2 layer. This could explain the phenomenon that an increasing TiO_2 coating layer voltage results in increased decomposition of the 9SHA layer in the previous experiments. As observed in the SEM images, the crack formation in the TiO_2 layer might have disrupted the role of the TiO_2 inner layer as an ion barrier between the titanium substrate and the 9SHA outer layer and resulted in the decomposition of 9SHA into β-TCP and CaO.

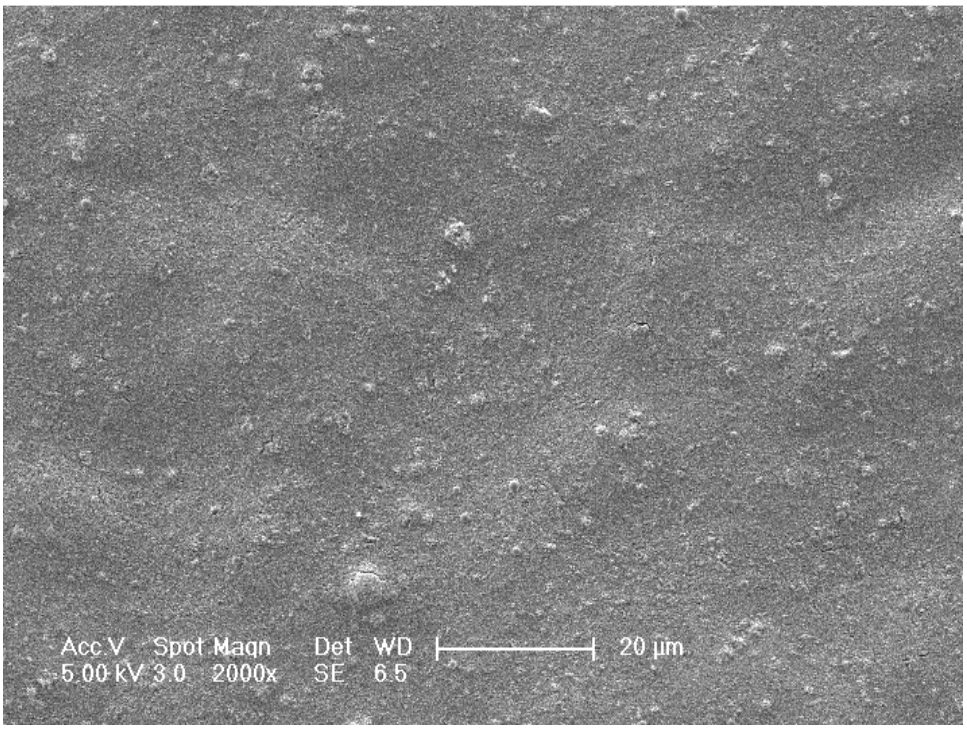

(a)

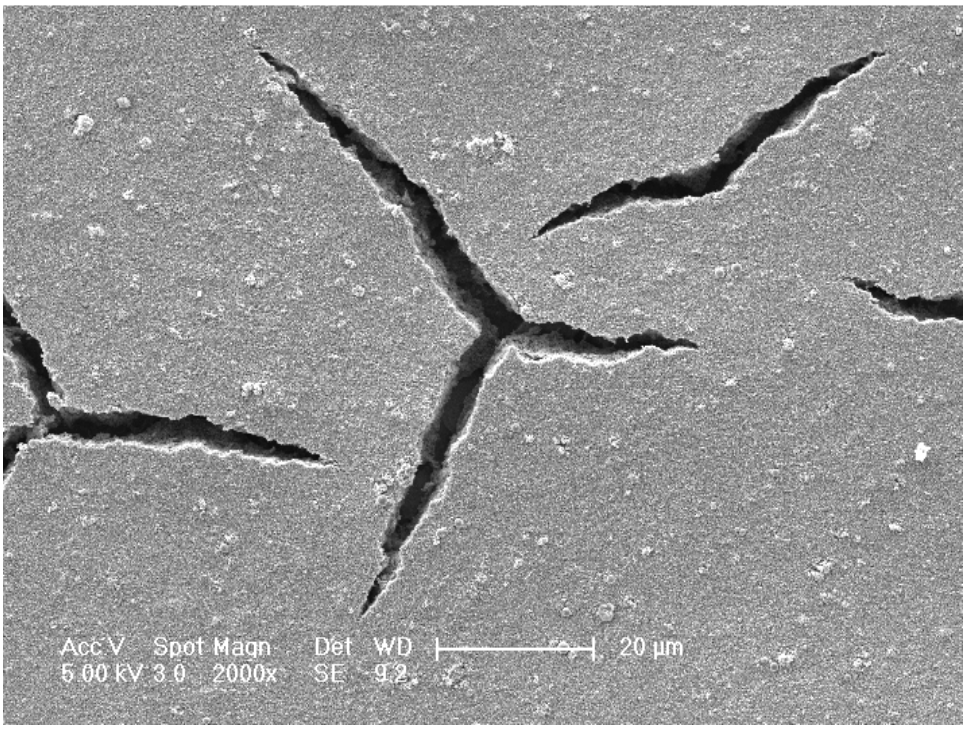

(b)

Figure 4.80. SEM images of the TiO_2 coating layer obtained by applying (a) 20 V for 60 s (2000x); (b) 50 V for 60 s (2000x) and after sintering at 800 °C.

The next approach utilized to control the 9SHA decomposition in the outer layer was to increase the 9SHA coating voltage in order allow formation of a thicker 9SHA layer by electrophoretic deposition. For this purpose, samples were prepared by applying a TiO_2 coating voltage of 50 V for 60 s. The samples were then coated with 9SHA by applying a coating voltage of 200 V for 60 s. The coated samples were sintered at 800 and 900 °C and XRD analysis (Figures 4.81-4.82) was conducted to determine the effect of 9SHA coating voltage on the 9SHA deposition on the sintered samples.

None of the prepared samples showed CaO peaks. On the other hand, very minor β-TCP peaks were observed on the sample sintered at 800 °C whereas the sample sintered at 900 °C showed slightly stronger β-TCP peaks. Shift of major HA peaks due to thermal expansion coefficient mismatch of HA and metallic substrate is evidenced on the XRD spectra.

Experiments showed that TiO_2 inner coating layer application between the titanium substrate and the 9SHA outer coating layer successfully prevented complete decomposition of 9SHA into CaO and β-TCP. Application of a relatively low TiO_2 coating voltage produces a crack free barrier between the metal and the outer coating layer. Increasing the TiO_2 coating voltage increased the tendency of crack formation in the inner layer thus leading to decomposition of the 9SHA in the outer layer.

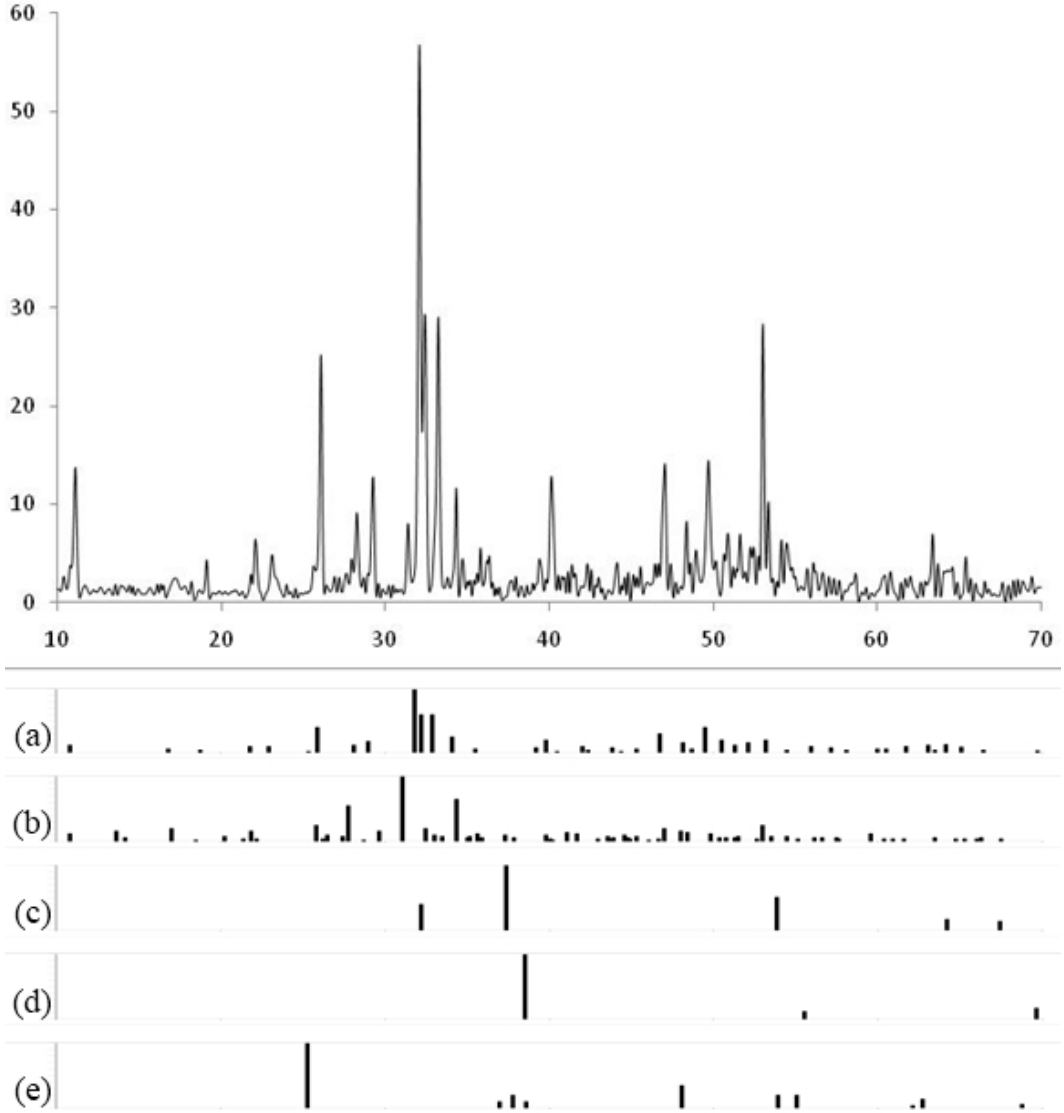

Figure 4.81. XRD analysis of the sample coated with TiO_2 (50 V, 60 s) and with 9SHA (200 V, 60 s) and sintered at 800 °C

(a) HA; (b) β-TCP; (c) CaO; (d) Ti; (e) TiO_2.

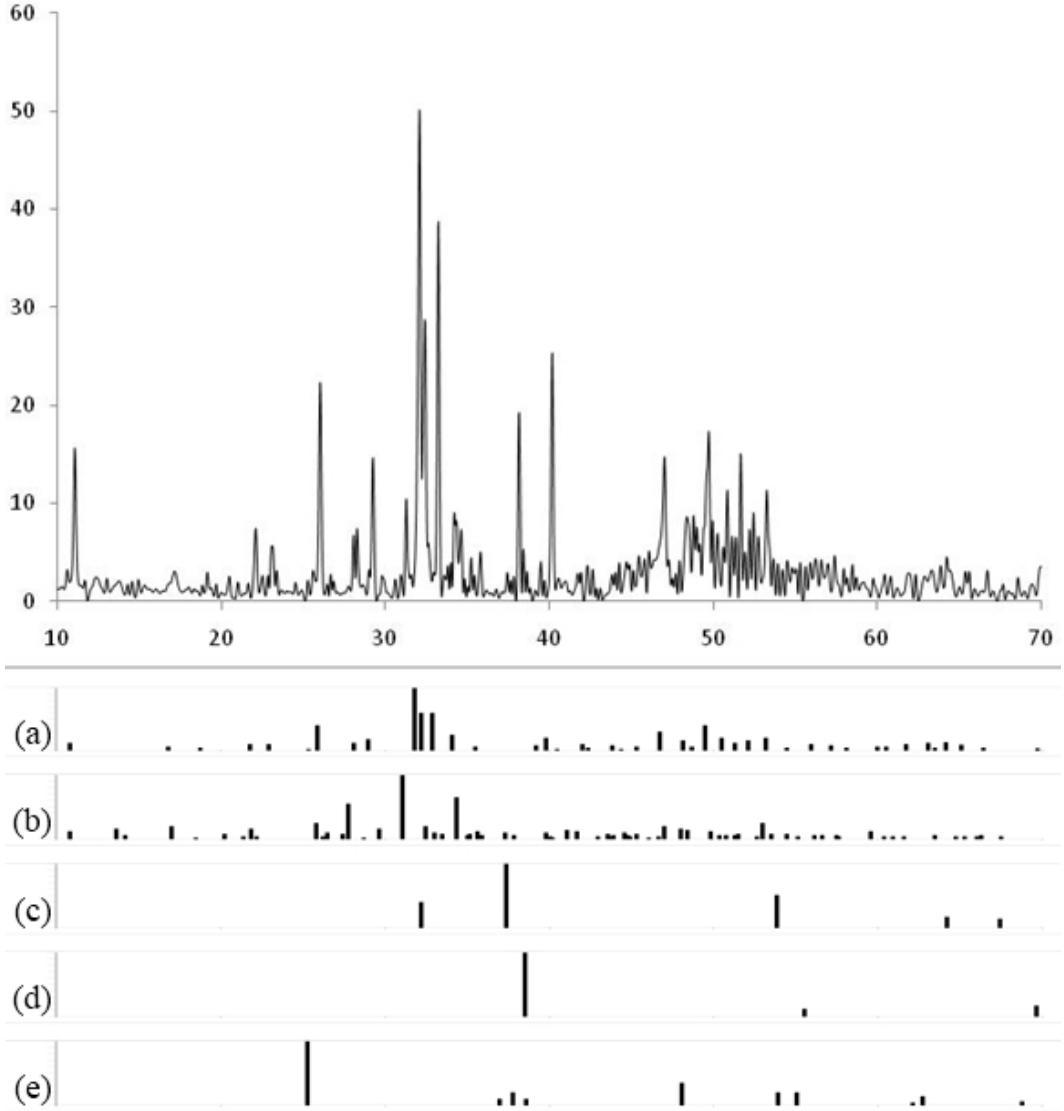

Figure 4.82. XRD analysis of the sample coated with TiO_2 (50 V, 60 s) and with 9SHA (200 V, 60 s) and sintered at 900 °C

(a) HA; (b) β-TCP; (c) CaO; (d) Ti; (e) TiO_2.

4.4.3. Determination of the Effect of Titanium Dioxide Inner Layer Application on the Sintering Characteristics of Silver Substituted Stoichiometric Hydroxyapatite Coatings

TiO_2 inner layer application was performed in order to control the hydroxyapatite decomposition in the coating surface based on the ion transfer from the titanium substrate. For this purpose, the titanium substrate was first coated with TiO_2 and then with 9SHA. The samples were not sintered after each coating step but after drying in open atmosphere the sintering process was conducted in a single step to prevent the negative effect of the relatively high sintering temperatures on the mechanical properties of the underlying titanium substrates.

9SHA coating surfaces were produced both with (Figures 4.83.b, 4.83.d) and without (Figures 4.82.a, 4.83.b) the application of TiO_2 inner layer. The application of the TiO_2 inner layer did not produce any significant difference in the 9SHA coating layer before the sintering stage. This was to be expected since the coated powder in both cases was 9SHA and this resulted in similar coating surface structures in the SEM analysis.

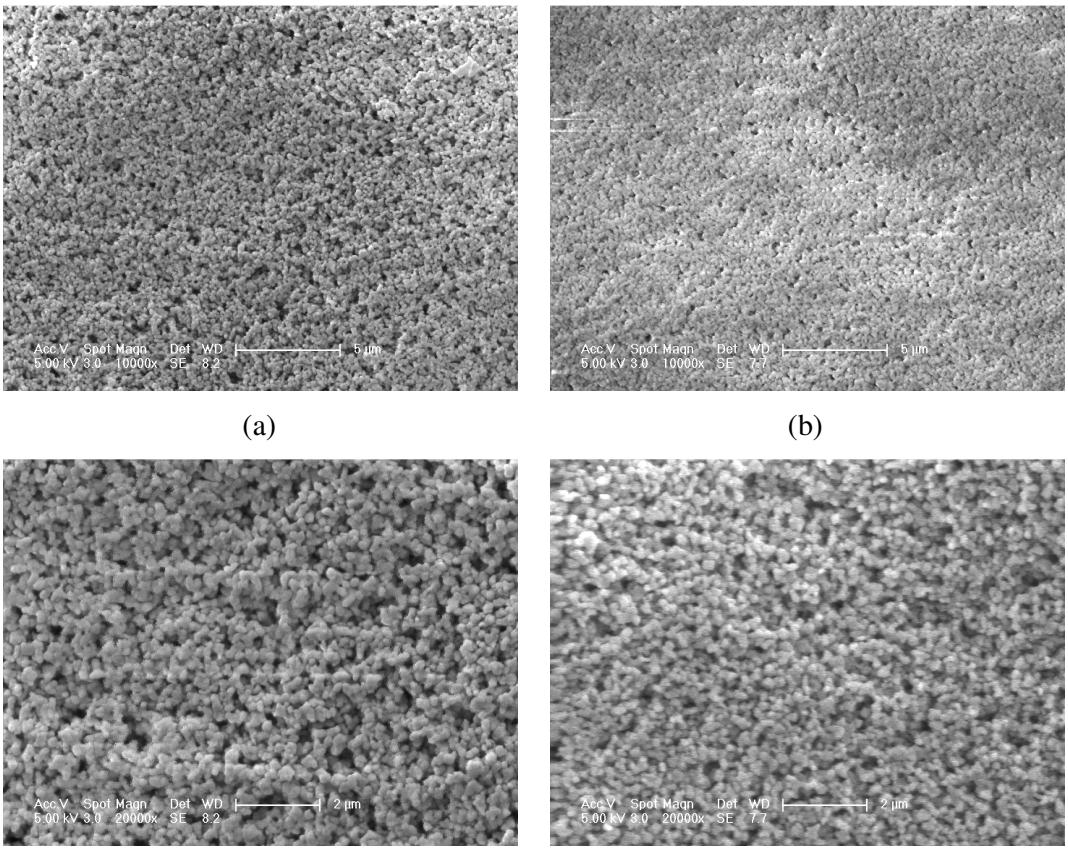

Figure 4.83. Before sintering SEM images of the samples coated with 9SHA (200 V, 60 s) (a) no TiO_2 inner layer (10000x); (b) TiO_2 inner layer applying 20 V, 60 s (10000x); (c) no TiO_2 inner layer (20000x); (d) TiO_2 inner layer applying 20 V, 60 s (20000x).

Samples coated with a TiO_2 inner layer using a coating voltage of 20 V for 60 s and sintered at 800 (Figure 4.84.a) and 900 (Figure 4.84.b) °C revealed that the necking of the 9SHA particles found in the outer coating layer started at 800 °C. However, necking of the particles was enhanced by increasing the sintering temperature to 900 °C.

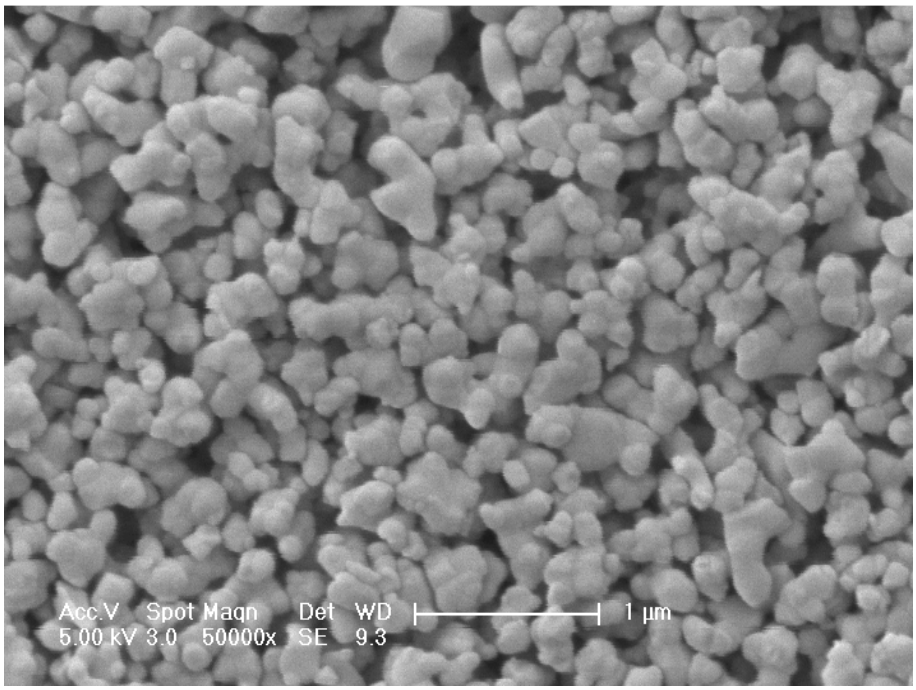

(a)

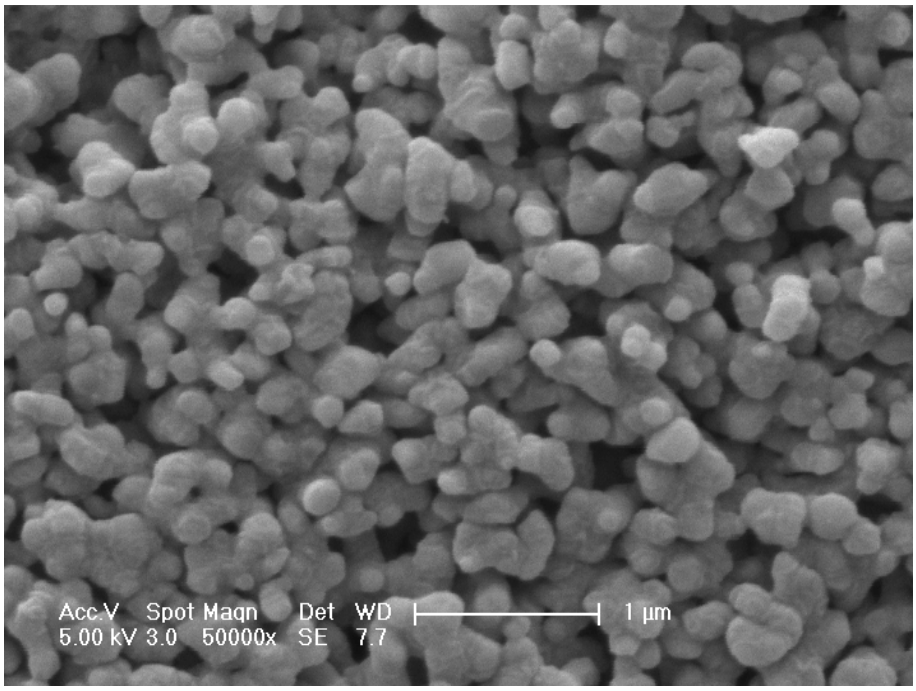

(b)

Figure 4.84. SEM images of samples produced first by coating a TiO_2 inner layer (50 V, 60 s) and then coating 9SHA (200 V, 60 s) and sintered at (a) 800 °C (50000x) and (b) 900 °C (50000x).

Effect of the sintering temperature on the densification of the outer 9SHA coating was more clearly indicated by the SEM analysis of the samples sintered at 900 (Figures 4.85.a, c, e and 4.86.a, c, e) and 1000 (Figures 4.85.b, d, f and 4.86.b, d, f) °C. Increasing the sintering temperature from 800 to 900 °C increased the necking behavior of the 9SHA particles in the outer coating layer. However, increasing the sintering temperature from 900 to 1000 °C led to a more dense coating surface structure where the particles could not be distinguished. Thus, increasing the sintering temperature clearly enhanced the densification of the 9SHA coating layer.

Another important observation noted was that the coating voltage applied to produce TiO_2 inner layer had no significant effect on the 9SHA outer layer after the sintering process based on the observation of the SEM images. Therefore, it can be concluded that TiO_2 coating voltage did not play a role in the surface morphology of the 9SHA outer coating layer.

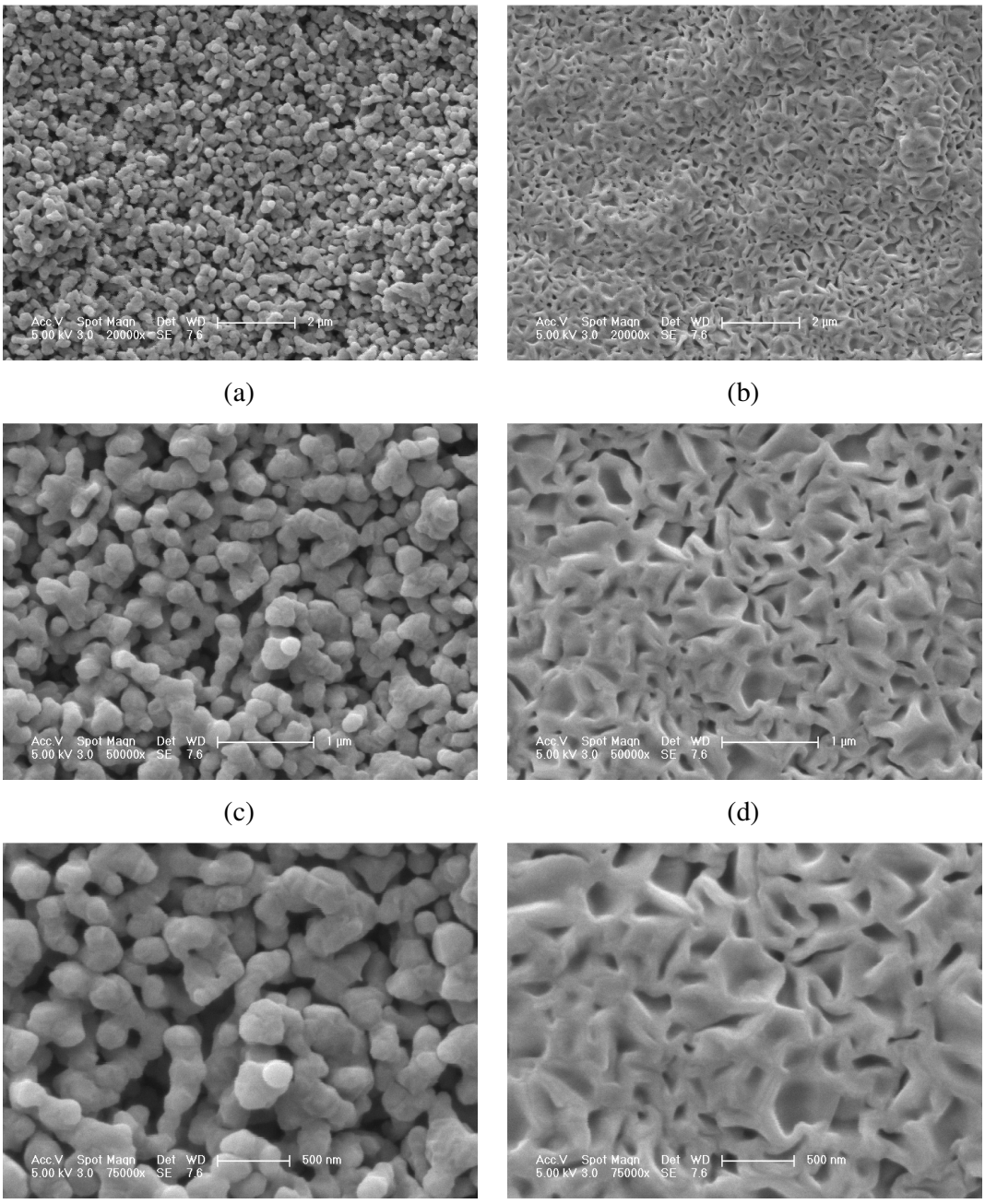

Figure 4.85. SEM images of samples coated first by a TiO_2 inner layer (20 V, 60 s) and then by 9SHA (80 V, 60 s) and sintered at (a) 900 °C (x20000); (b) 1000 °C (20000x); (c) 900 °C (x50000); (d) 1000 °C (50000x); (e) 900 °C (x75000); (f) 1000 °C (75000x).

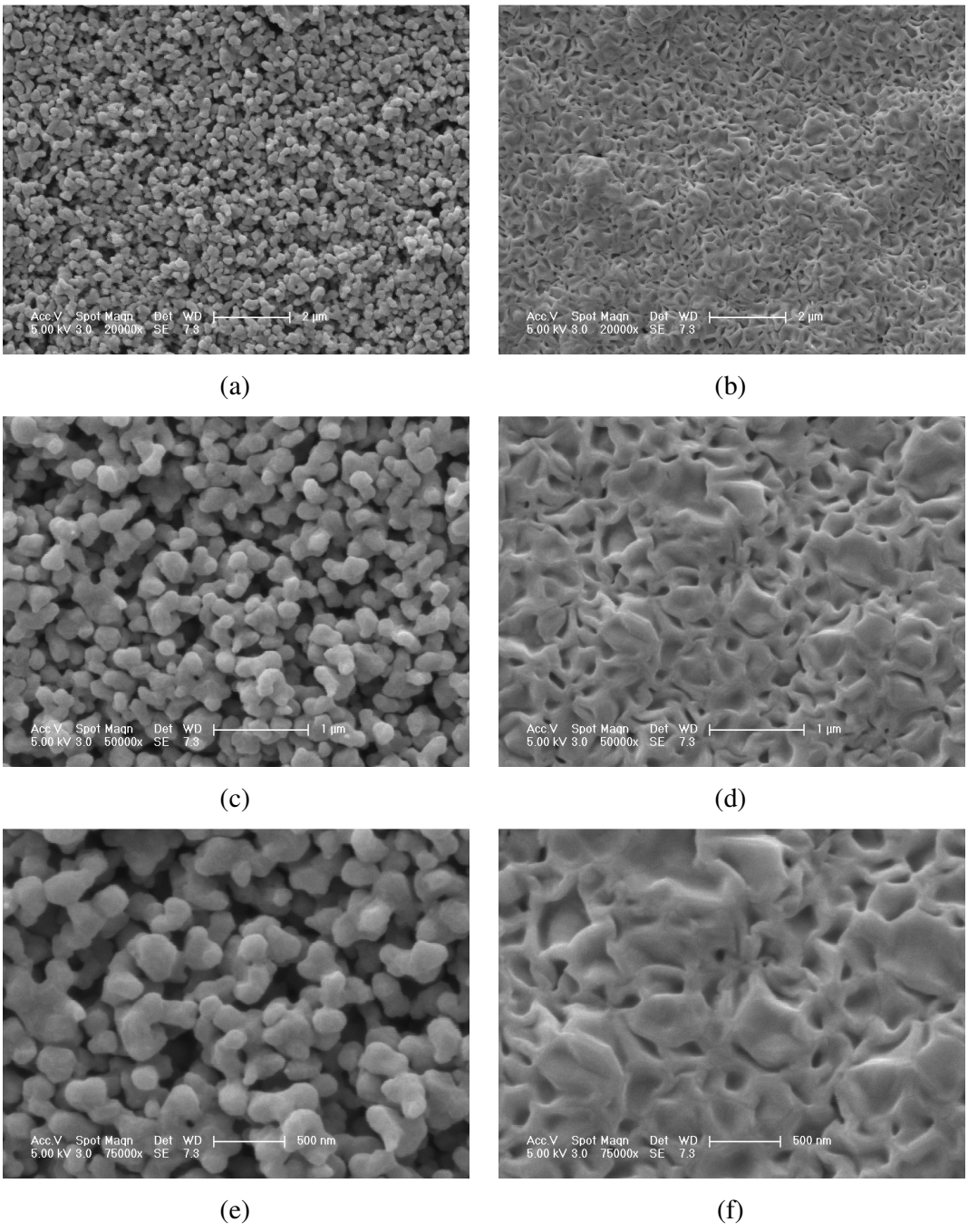

Figure 4.86. SEM images of samples coated first by a TiO_2 inner layer (40 V, 60 s) and then by 9SHA (80 V, 60 s) and sintered at (a) 900 °C (x20000); (b) 1000 °C (20000x); (c) 900 °C (x50000); (d) 1000 °C (50000x);(e) 900 °C (x75000); (f) 1000 °C (75000x).

4.4.4. Mechanical Strengths of the Coatings Produced by the Electrophoretic Deposition of Silver Substituted Stoichiometric Hydroxyapatite on Titanium Substrates with the Use of Titanium Dioxide Inner Layer Application

An epoxy based resin was used to produce test specimen. To determine the strength of the resin two titanium substrates without any coating layer were glued onto each other by using the resin. The shear strength of the resin was determined to be 40 MPa under the specified test conditions.

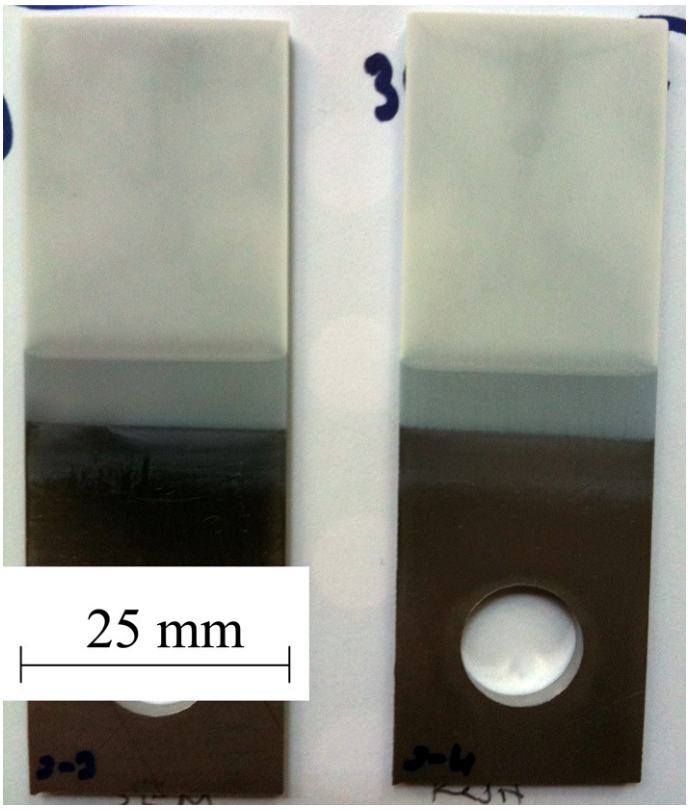

Figure 4.87. Samples prepared for mechanical testing before sintering (light grey areas indicate TiO_2 coating; white areas indicate 9SHA coating).

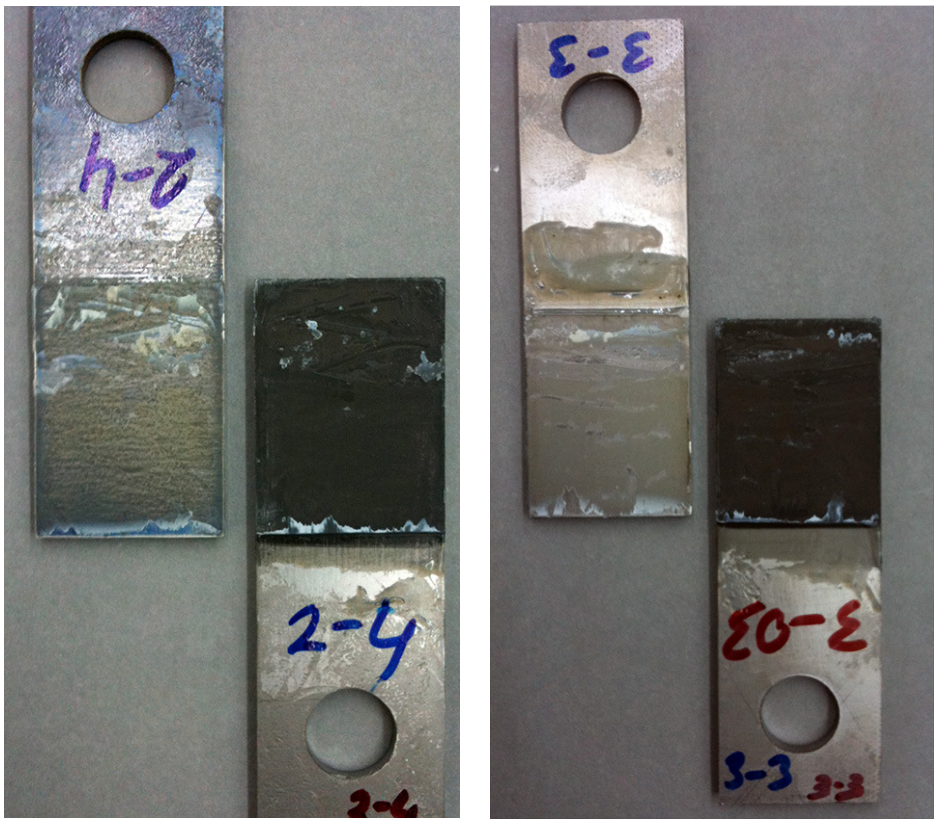

(a) (b)

Figure 4.88. Samples separated after mechanical testing; left substrates with remaining 9SHA coating layers (light) and right substrates with remaining TiO_2 inner coating layers (dark); (a) TiO_2 (10 V, 60 s), (b) TiO_2 (20 V, 30 s) and 9SHA (200 V, 60 s).

Comparing shear strengths of the samples prepared using same coating voltages and durations for the TiO_2 inner layer and 9SHA coating layer and sintered at different temperatures showed that shear strength increased with the increasing sintering temperature (Table 4.7 and Figure 4.89). Based on this observation, increasing the sintering temperature might seem a good method to increase the coating strength. However, XRD analysis of the samples sintered at different temperatures showed that increasing the sintering temperature enhanced the decomposition of the hydroxyapatite in the coating layer. Increasing the sintering temperature thus increases the coating strength of the sample however, decreases the amount of hydroxyapatite found on the outer layer due to the enhanced decomposition of hydroxyapatite into β-TCP. Therefore, increasing the sintering temperature is not a convenient method to obtain higher shear strengths.

Table 4.7. Average shear strengths of the samples prepared for mechanical testing using various coating voltages and durations for the TiO_2 inner layer and 9SHA coating layer and sintered at various temperatures.

TiO_2 Coating		9SHA Coating		Sintering	Average
Voltage (V)	Duration (s)	Voltage (V)	Duration (s)	Temperature (°C)	Shear Strength (MPa)
50	60	200	60	900	4.90
50	60	200	60	1000	8.80
20	60	200	60	900	9.50
20	60	200	60	1000	11.70
10	60	200	60	900	12.82
20	30	200	60	900	13.38

To obtain higher shear strengths the TiO_2 coating voltage was decreased to obtain a thinner layer of TiO_2 inner layer coating. Samples prepared using 20 and 50 V TiO_2 inner layer coating voltages for the same durations and sintered at the same temperatures showed that decreasing the TiO_2 inner layer coating voltage successfully increased the shear strength of the samples. The effect of decreasing the TiO_2 inner layer coating voltage from 50 to 20 V was greater than increasing the sintering temperature from 900 to 1000 °C. Thus, instead of increasing the sintering temperature the TiO_2 inner layer coating voltage might be decreased to obtain higher shear strengths while preventing the decomposition of hydroxyapatite into β-TCP.

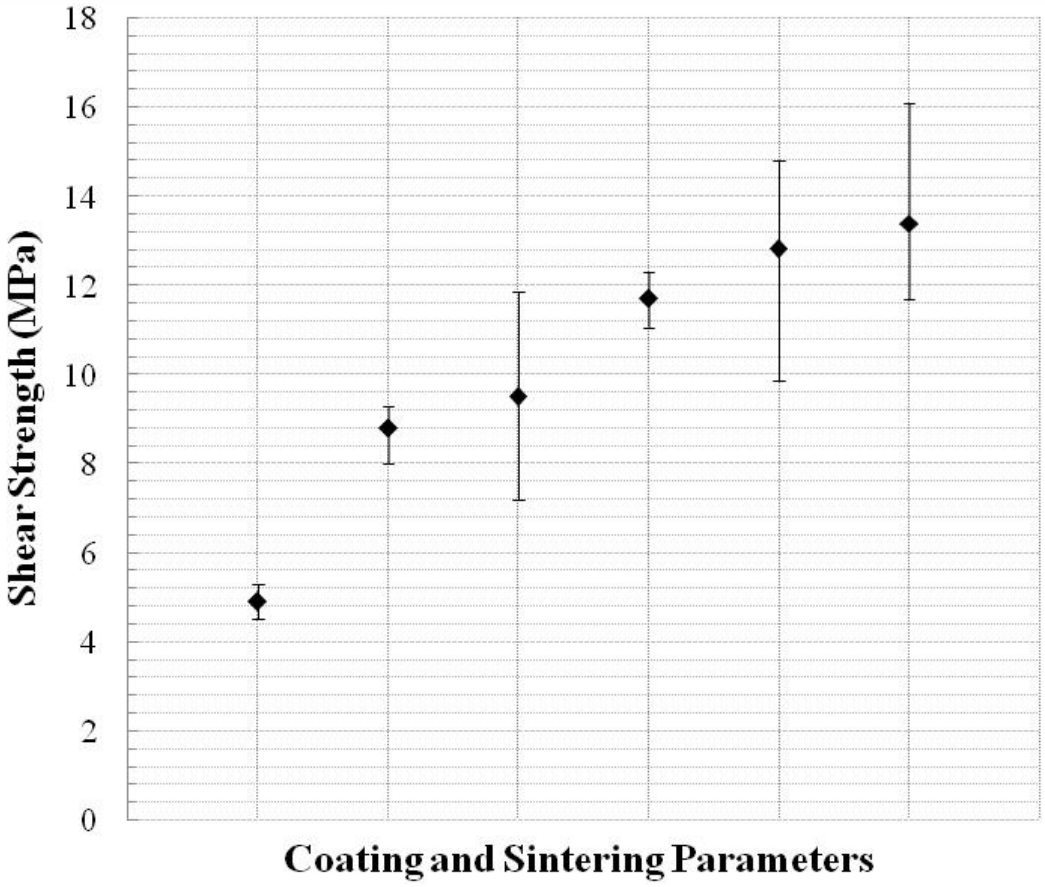

TiO_2 inner layer	50 V, 60 s	50 V, 60 s	20 V, 60 s	20 V, 60 s	10 V, 60 s	20 V, 30 s
9SHA layer	200 V, 60 s	200 V, 60 s	200 V, 60 s	200 V, 60 s	200 V, 60 s	200 V, 60 s
Sint. Temp.	900 °C	1000 °C	900 °C	1000 °C	900 °C	900 °C

Figure 4.89. Shear strengths of the samples prepared for mechanical testing.

To further enhance the shear strength the TiO_2 coating duration was decreased from 60 to 30 s keeping TiO_2 inner layer coating voltage at 20 V and the sintering temperature at 900 °C to prevent decomposition of hydroxyapatite which increased the shear strength from 11.70 to 13.38 MPa. On the other hand, the TiO_2 inner layer coating voltage was decreased from 20 to 10 V while keeping the coating duration to be 60 s which resulted in an increase of the shear strength from 11.70 to 12.82. This showed that the TiO_2 inner layer coating duration also played a significant role in increasing the shear strength of the samples.

The experiments showed that although increasing the sintering temperature increases the shear strength of the samples it is not a suitable method due to the enhanced decomposition of hydroxyapatite at elevated sintering temperatures. On the other hand, decreasing the TiO_2 inner layer coating voltage and choosing shorter TiO_2 inner layer coating durations increase the shear strength without the need of increasing the sintering temperature thus, preventing decomposition of hydroxyapatite. The positive effect of decreasing the TiO_2 inner layer coating voltage and duration on the shear strength of the samples is thought to be based on producing thinner TiO_2 inner layer by using lower coating voltages (10 V vs. 20 V vs. 50 V) and shorter coating durations (30 s vs. 60 s) which further eliminates the risk of crack formation in the TiO_2 inner layer leading to the weakening of the coating.

5. CONCLUSIONS

Calcium deficient hydroxyapatite was produced by use of microwave as a rapid production method. Application of microwave was found to improve the crystallization of the produced calcium deficient hydroxyapatite powders and no phase transformations were detected in the produced samples. Therefore, microwave assisted production is considered to be a time, energy and cost efficient method for the production of calcium deficient hydroxyapatite.

Transformation of calcium deficient hydroxyapatite to β-TCP could be controlled through the use of subsequent heat treatment in the conducted experiments which is particularly important for the application of the produced powders. Since the biodegradability of hydroxyapatite is lower than that of β-TCP powders heat treated powders at higher temperatures are suitable for applications where a high biodegrability is desired which is the case where the implant material is expected to degrade after the implantation. In the opposite case where lower biodegradabiliy is desired powders heat tretated at lower temperatures might be suitable. Selection of the heat treatment temperature enables tailoring the biodegradability of the powders according to the constraints of the particular biomedical application by the modification of the hydroxyapatite to β-TCP transformation.

The amount of silver substitution to the calcium deficient hydroxyapatite was found to increase the β-TCP transformation. Hence, the amount of silver addition plays an important role on the biodegradability of the produced powder. The amount of silver added to the calcium deficient hydroxyapatite must be selected accordingly to keep the bioderadability between desired limits of the particular application.

Microwave power was found to effect the decomposition of silver substituted calcium deficient hydroxyapatite into β-TCP. Use of higher microwave power and longer microwave duration resulted in an increase of β-TCP peak intensities as observed in the XRD analysis of the powders which may accompany formation of free silver at higher temperatures. Therefore, use of lower microwave power to produce silver substituted

calcium deficient hydrxyapatite was found to prevent decomposition into β-TCP as a result of which substituted silver ions would remain in the apatitic structure.

Similar to the results obtained for silver substituted calcium deficient hydroxyapaite powders, heat treatment temperature was found to effect the β-TCP formation of the silver substituted stoichiometric hydroxyapatite. Altough no free silver peaks were observed in the XRD analysis of the heat treated silver substituted stoichiometric hydroxyapatite powders within the considered temperature range data obtained from the heat treatment of silver substituted calcium deficient hydroxyapaite leads to the fact that β-TCP transformation at higher temperatures may accompany free silver formation at higher temperatures. This is particularly important since free silver is reported to have a low antibacterial activity in the literature. Heat treating silver substituted stoichiometric hydroxyapatite may increase the amount of free silver at the extent of silver in the apatitic structure which in turn might decrease the antibacterial activity of the produced powder altough the amount of silver in the produced powder does not change virtually.

The antibacterial activity of the calcium deficient and stoichiometric hydroxyapatite powders were tested against Gram negative E. coli and Gram positive S. aureus bacteria. Conducted experiments showed that calcium deficient as well as stoichiometric hydroxyapatite powders with silver subsitution even at low concentrations possess excellent antibacterial activities against both kinds of bacteria tested even at very low concentrations. Important to note was the difference of the silver substituted hydroxyapatite powder samples heat treated at temperatures between 900-1100 °C. Accordingly, higher heat treatment temperatures had a slightly negative effect on the antibacterial activity of the powders. Altough, no significant β-TCP transformation and thus, no free silver peaks were detected in the XRD analysis of the samples heat treated at elevated temperatures the decrease in the antibacterial activity due to heat treatment at higher temperatures leads to the fact that even minor decomposition accompanied by minor formation of free silver which in turn decreases the amount of silver in apatitic structure may result in the decrease of the antibacterial activity of the powders. Thus, heat treatment or sintering temperatures must be selected accordingly to preserve the antibacterial chracteristics of the silver substituted hydroxyapatite powders.

Increasing the sintering temperature to increase coating strength of the silver substituted stoichiometric hydroxyapatite coated on titanium samples was found to increase the hydroxyapatite decomposition such that no hydroxyapatite peaks could be observed in the XRD analysis of the samples sintered at 1000 °C which is below the decomposition temperature of hydroxyapatite in powder form. This decomposition was considered to be triggered by the increased metal ion mobility from the titanium subtrate during the sintering stage at elevated temperatures. Therefore, titanium dioxide inner layer coating was applied between the titanium substrate and the silver substituted stoichiometric hydroxyapaite coating as an ion barrier. Results showed that titanium inner layer application succesfully prevented hydroxyapatite decomposition at 900 °C and decreased the decomposition at 1000 °C. Therefore, application of titanium dioxide inner layer was found to be an effective method to control and decrease the hydroxyapatite decomposition at elevated sintering temperatures. Titanium substrates which were first coated with a titanium dioxide inner layer and then a silver substituted stoichiometric hydroxyapaite outer layer were sintered in a single step instead of sintering the samples after each coating step to prevent decrease of the mechanical strength of the titanium substrates as subsequent sintering steps were reported to decrease the mechanical strength of titanium as reported in the literature and to eliminate further decomposition of hydroxyapatite.

Altough application of titanium dioxide inner layer was found to successfully prevent hydroxyapatite decomposition on the hydroxyapatite outer layer further experiments showed that thickness of the titanium dioxide inner layer had a profound effect on the decomposition characteristics of the hydroxyapatite outer layer. Increasing the titanium dioxide inner layer coating voltage in order to increase the thickness of the titanium inner layer to further decrease the decomposition of hydroxyapatite resulted in cracks in the titanium dioxide inner layer. Due to the formed cracks the function of the titanium dioxide inner layer as an ion barrier was disturbed which was observed by the increased hydroxyapatite decomposition coated on titanuim dioxide inner layer coated by higher voltages. Therefore, the thickness and thus the coating voltage and coating duration of the titanium dioxide inner layer was found to play an important role in the hydroxyapatite decomposition in the outer layer.

Experiments conducted to determine mechanical srengths of the coatings showed that with increasing sintering temperature from 900 to 1000 °C mechanical strengths of the coated samples increased. However, due to the enhanced decomposition at higher sintering temperatures hydroxyapatite was determined to decompose to a great extent. Therefore, increasing sintering temperature was found to be an inefficient way to increase the mechanical strengths of the coatings.

Preventing the crack formation in the titanium dioxide inner layer was found an efficient method to increase the coating strength without increasing the sintering temperature. For this purpose, application of lower coating voltages and shorter coating durations for the titanium dioxide inner layer were determined to successfully increase the mechanical strength of the coated samples.

Conducted studies showed that application of titanium dioxide inner layer is a simple and efficient method to prevent decomposition of the hydroxyapatite outer layer. Application of the sintering process in a single step eliminates the risk of the decrease in the mechanical stregnth of the coated titanium substrates due to repeated sintering steps. On the other hand, thickness of the titanium dioxide inner layer was found to have a significant role both in the decomposition of the hydroxyapatite outer layer and the mechanical strength of the coated samples. Increasing the titanium dioxide inner layer thickness had a negative effect both on the hydroxyapatite decomposition and the mechanical strength due to the crack formation in the titanium dioxide inner layer coated at higher coating voltages and longer coating durations.

Conclusively, the microwave assisted production of CDHA and HA is a promising technique due to its rapid nature. It is a time saving and energy efficient method since aging and crystallization of the produced powder occurs under microwave in a very short time period. The microwave assisted method goes to completion in 15 to 30 min as compared to acid-base method which requires 24 to 48 hr at 30 to 85 °C [57], to calcium acetate method which requires 3 hr at 40 °C [58] and metathesis method which requires 3 hr at boiling temperature followed by a up to 20 days long aging process [58]. The technique also allows control of the crystallite size of the produced powders by varying the microwave parameters such as microwave treatment time and microwave power. In

addition to that, the specific choice of precursor materials in this work simplifies the production process by guaranteeing that the pH value remains above 9 throughout the reaction without use of any additional chemicals, e.g. ammonium hydroxide.

Silver substitution ensures that the produced powder has antibacterial characteristics, as determined in this study. Silver is added to the powders during the precipitation reaction, which decreases the production time and simplifies the production process as compared to an ion exchange procedure [14] which can alternatively be used to incorporate silver. The proven antibacterial property of the produced powders might play an important role in decreasing the implant related infection possibility. Therefore, use of SCDHA and SHA powders produced may not only eliminate medical concerns due to implant related infections but also the costs resulting from revision surgery because of the infection at the implantation site.

The SCDHA and SHA powders produced in this study may be good candidates as bone filling materials and coating materials for metallic implants. The calcium deficient nature of the SCDHA powder may potentially increase its biodegradability compared to its stoichiometric counterpart which in turn enhances bone remodeling and bone formation at the implantation site. Similarly, the SHA powder produced may be used for coating metallic implant surfaces for enhanced tissue attachment having good biocompatibility where its silver content ensures decreasing bacterial activity at the implantation site.

REFERENCES

1. Vail, N. K. , L. D. Swain, W. C. Fox, T. Lee, B. G. Aufdlemorte, and J. W. Barlow, "Materials for Biomedical Applications", *Materials and Design*, Volume 20, Issue 23, pp. 123-132, 1999.

2. Hench, L. L., "Biomaterials: A Forecast for the Future", *Biomaterials*, Volume 19, Issue 16, pp. 1419-1423, 1998.

3. Murugan, R., K. Panduranga Rao, and T. S. Sampath Kumar, "Heat-Deproteinated Xenogeneic Bone from Slaughterhouse Waste: Physico-Chemical Properties", *Bulletin of Materials Science*, Volume 26, Issue 5, pp. 523-528, 2003.

4. Mittelmeier, H., B. Mittelmeier, and B. Leu, *Bone Substitute Material on the Basis of Natural Bones*, United States Patent No. 4,654,664, 1997.

5. Johnson, G. S., M. R. Mucalo, M. A. Lorier, U. Gieland, and H. Mucha, "The Processing and Characterization of Animal-Derived Bone to Yield Materials with Biomedical Applications. Part II: Milled Bone Powders, Reprecipitated Hydroxyapatite and the Potential Uses of These Materials", *Journal of Materials Science: Materials in Medicine*, Volume 11, Issue 11, pp. 725-741, 2000.

6. Anderson, L.A., M. R. Mucalo, G. S. Johnson, and M. A. Lorier, "The Processing and Characterization of Animal-Derived Bone to Yield Materials with Biomedical Applications. Part III: Material and Mechanical Properties of Fresh and Processed Bovine Cancellous Bone", *Journal of Materials Science: Materials in Medicine*, Volume 11, Issue 11, pp. 743-749 , 2000.

7. Li, J., Y. Dou, J. Yang, Y. Yin, H. Zhang, F. Yao, H. Wang, and K. Yao, "Surface Characterization and Biocompatibility of Micro- and Nano-Hydroxyapatite / Chitosan-Gelatin Network Films", *Materials Science and Engineering C-Biomimetic and Supramolecular Systems*, Volume 29, Issue 4, pp. 1207-1215, 2009.

8. Merrill C. and A. Elixhauser, "Hospital Stays Involving Musculoskeletal Procedures, 1997–2005", *Healthcare Cost and Utilization Project (HCUP)*, Statistical Brief #34, 2007.

9. Gristina, A. G., "Biomaterial-Centered Infection: Microbial Adhesion Versus Tissue Integration", *Science*, Volume 237, pp. 1588-1595, 1987.

10. Berger, T. J., J. A. Spadaro, S. E. Chapin, and R. O. Becker, "Electrically Generated Silver Ions: Quantitative Effects on Bacterial and Mammalian-Cells", *Antimicrobial Agents and Chemotherapy*, Volume 9, Issue 2, pp. 357-358, 1976.

11. Bellantone, M., H. D. Williams, and L. L. Hench, "Broad-Spectrum Bactericidal Activity of Ag_2O-Doped Bioactive Glass", *Antimicrobial Agents and Chemotherapy*, Volume 46, Issue 6, pp. 1940-1945, 2002.

12. Chung, R. J., M. F. Hsieh, K. C. Huang, L. H. Perng, F. I. Chou, and T. S. Chin, "Anti-Microbial Hydroxyapatite Particles Synthesized by a Sol-Gel Route", *Journal of Sol-Gel Science and Technology*, Volume 33, Issue 2, pp. 229-239, 2005.

13. Chen, W., Y. Liu, H. S. Courtney, M. Bettenga, C. M. Agrawal, J. D. Bumgardner, and J. L. Ong, "In Vitro Anti-Bacterial and Biological Properties of Magnetron Co-Sputtered Silver-Containing Hydroxyapatite Coating", *Biomaterials*, Volume 27, Issue 32, pp. 5512-5517, 2006.

14. Feng, Q. L., T. N. Kim, J. Wu, E. S. Park, J. O. Kimi, D. Y. Limi, and F. Z. Cui, "Antibacterial Effects of Ag-HAp Thin Films on Alumina Substrates", *Thin Film Solids*, Vol. 335, Issues 1-2, pp. 214-219, 1998.

15. Opalchenova, G., E. Dyulgerova, and O. E. Petrov, "A Study of the Influence of Biphase Calcium Phosphate Ceramics on Bacterial Strains: In Vitro Approach", *Journal of Biomedical Materials Research*, Volume 31, Issue 2, pp. 219-226, 1996.

16. Zimmerli, W., A. Trampuz, and P. E. Ochsner, "Current Concepts: Prosthetic-Joint Infections", *The New England Journal of Medicine*, Volume 351, Issue 16, pp. 1645–1654, 2004.

17. Malchau, H., G. Garelick, and P. Herberts, "The Evidence from the Swedish Hip Register", *The Well-Cemented Total Hip Arthroplasty: Theory and Practice*, S. Breusch and H. Malchau (Ed.), 291-301, Springer, Berlin, Germany, 2006.

18. Trampuz, A. and W. Zimmerli, "Prosthetic Joint Infections: Update in Diagnosis and Treatment", *Swiss Medical Weekly*, Volume 135, Issues 17-18, pp. 243-251, 2005.

19. Darouiche, R. O., "Current Concepts - Treatment of Infections Associated with Surgical Implants", *The New England Journal of Medicine*, Volume 350, Issue 14, pp. 1422-1429, 2004.

20. Chen, S. and I. Darby, "Dental Implants: Maintenance, Care and Treatment of Peri-Implant Infection", *Australian Dental Journal*, Volume 48, Issue 4, pp. 212-220, 2003.

21. King, P. H. and R. C. Fries, *Design of Biomedical Devices and Systems*, Marcel Dekker, New York, USA, 2003.

22. Ratner, B. D., A. S. Hoffman, F. J. Schoen, and J. E. Lemons (Ed.), *An Introduction to Materials in Medicine*, Academic Press, New York, USA, 1996.

23. Park, J. B. and R. S. Lakes, *Biomaterials: An Introduction*, John Wiley & Sons, New York, USA, 1992.

24. Szycher, M., "Biomaterials", , *Handbook of Biomedical Engineering*, J. Kline (ed.), pp. 441-457, Academic Press, California, USA, 1988.

25. Dee, K. C., D. A. Puleo, and R. Bizios, *An Introduction to Tissue-Biomedical Interactions*, John Wiley & Sons, New Jersey, USA, 2002.

26. Best, S. M., A. E. Porter, E. S. Thian, and J. Huang, "Bioceramics: Past, Present and for the Future", *Journal of the European Ceramic Society*, Volume 28, Issue 7, pp. 1319-1327, 2008.

27. Katz, J. L., L. L. Latta, S. Singh, and H. S. Yoon, "Biomechanics of Orthopedics and Rehabilitation of the Musculoskeletal System", *Handbook of Biomedical Engineering*, J. Kline (ed.), pp. 459-524, Academic Press, California, USA, 1988.

28. Sykaras, N., A. M. Iacopino, V. A. Marker, R. Triplett, and R. D. Woody, "Implant Materials, Design, and Surface Topographies: Their Effect on Osseointegration. A Literature Review", *The International Journal of Oral & Maxillofacial Implants*, Volume 15, Issue 5, pp. 675-690, 2000.

29. Thamaraiselvi, T. V. and S. Rajeswari, "Biological Evaluation of Bioceramic Materials - A Review", *Trends in Biomaterials and Artificial Organs*, Volume 18, Issue 1, pp. 9-17, 2004.

30. Daoud, W. A. and Y. H. Zhang, "Surface Functionalization of Cellulose Fibers with Titanium Dioxide Nanoparticles and Their Combined Bactericidial Activities", *Surface Science*, Volume 599, Issues 1-3, pp. 69-75, 2005.

31. Nonami, T. and K. Funakoshi, "Apatite-Coated Titanium Dioxide Photocaalyst for Air Purification", *Catalysis Today*, Volume 96, Issue 3, pp. 113-118, 2004.

32. Ozeki, K., H. Aoki, and Y. Fukui, "Photocatalytic Hydroxyapatite/Titanium Dioxide Multilayer Thin Film Deposited onto Glass Using an RF Magnetron Sputtering Technique", *Applied Surface Science*, Volume 253, Issue 7, pp. 3397-3401, 2007.

33. Raynaud, S., E. Champion, D. Bernache-Assollant, and P. Thomas, "Calcium Phosphate Apatites with Variable Ca/P Ratio – I. Synthesis, Characterization and Thermal Stability of Powders", *Biomaterials*, Volume 23, Issue 4, pp. 1065-1072, 2002.

34. Tas, A. C., M. Timucin, and N. Akkas, "An Investigation of the Chemical Synthesis and High-Temperature Sintering Behaviour of Calcium Hydroxyapatite (HA) and Tricalcium Phosphate (TCP) Bioceramics", Journal *of Materials Science: Materials in Medicine*, Volume 8, Issue 2, pp. 91-96, 1997.

35. Daculsi, G., O. Laboux, O. Malard, and P. Weiss, "Current State of the Art of Biphasic Calcium Phosphate Bioceramics", *Journal of Materials Science: Materials in Medicine*, Volume 14, Issue 3, pp. 195-200, 2003.

36. Wang, H., J. K. Lee, A. Moursi, and J. J. Lannutti, "Ca/P Ratio on the Degradation of Hydroxyapatite In Vitro", *Journal of Biomedical Materials Research: Part A*, Volume 67A, Issue 2, pp. 599-608, 2003.

37. Fujita, R., A. Yokoyama, T. Kawasaki, and T. Kohgo, "Bone Augmentation Osteogenesis Using Hydroxyapatite and β-TCP Phosphate Blocks", *Journal of Oral and Maxillofacial Surgery*, Volume 61, Issue 9, pp. 1045-1053, 2003.

38. Hench, L. L. and J. Wilson, Bioceramics, *MRS Bulletin*, Volume 16, Issue 9, pp. 62-74, 1991.

39. Dubok, V. A., "Bioceramics - Yesterday, Today, Tomorrow", *Powder Metallurgy and Metal Ceramics*, Volume 39, Issues 7-8, pp. 381-394, 2000.

40. Bagambisa, F. B., U. Joos, and W. Schilli, "Mechanisms and Structure of the Bond between Bone and Hydroxyapatite Ceramics, *Journal of Biomedical Materials Research*, Volume 27, Issue 8, pp. 1047-1055, 1993.

41. Ipekoglu, M., *Effects of Calcination and Particle Size on the Sintering of Natural Hydroxyapatite*, M.S. Thesis, Bogazici University, 2004.

42. Oktar, F. N., *Characterization of Processed Tooth Hydroxyapatite and Bioglass for Potential Applications in Dentistry*, Ph.D. Thesis, Bogazici University, 1999.

43. Goren, S., *Production of Hydroxylapatite from Animal Bone*, M.S. Thesis, Bogazici University, 2003.

44. Gokbayrak, H., *Production of Hydroxyapatite Ceramics*, M.S. Thesis, Bogazici University, 1996.

45. Tas, A. C., "Participation of Calcium Phosphate Bone Substitutes in the Bone Remodeling Process: Influence of Materials Chemistry and Porosity", *Key Engineering Materials*, Volumes 264-268, pp. 1969-1972, 2004.

46. Sivakumar, M., T. S. Sampath Kumar, K.L. Shanta, and K. Panduranga Rao, "Development of Hydroxyapatite Derived from Indian Coral," *Biomaterials,* Volume 17, Issue 17 , pp. 1709-1714, 1996.

47. Kweh, S. W. K., K. A. Khor, and P. Cheang, "The Production and Characterization of Hydroxyapatite (HA) Powders", *Journal of Materials Processing Technology*, Volume 90, Special Issue, pp. 373-377, 1999.

48. Kumta, P. N., C. Sfeir, D. Lee, D. Colton, and D. Choi, "Nanostructured Calcium Phosphates for Biomedical Applications: Novel Synthesis and Characterization", *Acta Biomaterialia*, Volume 1, Issue 1, pp. 65-83, 2005.

49. Narasaraju, T. S. B. and D. E. Phebe, "Some Physicochemical Aspects of Hydroxylapatite", *Journal of Materials Science*, Volume 31, Issue 1, pp. 1-21, 1996.

50. O. Ertorer, E. Fakioglu, I. Sirer, C. Oncel, and M. A. Gulgun, "Microwave Assisted Processing of Ceramics", *Key Engineering Materials*, Volumes 264-268, pp. 765-768, (2004).

51. Kannan, S. and R. V. Jasra, "Microwave Assisted Rapid Crystallization of Mg-M(III) Hydrotalcite Where M(III) = Al, Fe or Cr", *Journal of Materials Chemistry*, Volume 10, Issue 10, pp. 2311-2314, 2000.

52. Katsuki, H, S. Furuta, and S. Komarneni, "Microwave- versus Conventional-Hydrothermal Synthesis of Hydroxyapatite Crystals from Gypsum", *Journal of American Ceramic Society*, Volume 82, Issue 8, pp. 2257-2259, 1999.

53. Vijayan, S. and H. Varma, "Microwave Sintering of Nanosized Hydroxyapatite Powder Compacts", *Materials Letters*, Volume 56, Issue 5, pp. 827-831, 2002.

54. Rameshbabu, N., K. Prassad Rao, and T. S. Sampath Kumar, "Accelerated Microwave Processing of Nanocrystalline Hydroxyapatite", *Journal of Materials Science*, Volume 40, Issue 23, pp. 6319-6323, 2005.

55. Siddharthan, A., S. K. Seshadri, and T. S. Sampath Kumar, "Microwave Accelerated Synthesis of Nanosized Calcium Deficient Hydroxyapatite", *Journal of Materials Science: Materials in Medicine*, Volume 15, Issue 12, pp. 1279-1284, 2004.

56. Rameshbabu, N., T. S. Sampath Kumar, T. G. Prabhakar, V. S. Sastry, K. V. G. K. Murty, and K. Prasad Rao, "Antibacterial Nanosized Silver Substituted Hydroxyapatite: Synthesis and Characterization", *Journal of Biomedical Materials Research Part A*, Volume 80A, Issue 3, pp. 581-591, 2007.

57. Albayrak, O, *Hydroxyapatite Coating on Metallic Substrates by Using Electrophoretic Deposition Method*, Ph.D. Thesis, Bogazici University, 2008.

58. Wei, M., *Electrophoresis of Hydroxyapatite on Metal Substrates*, Ph.D. Thesis, University of New South Wales, 1997.

59. Wnek, G. E. and G. L. Bowlin, *Encyclopedia of Biomaterials and Biomedical Engineering*, 2nd Ed., Volume 1, pp. 462-463, Informa HealthCare, 2008.

60. Mazor, Z., M. Peleg, A. K. Garg, and G. Chaushu, "The Use of Hydroxyapatite Bone Cement for Sinus Floor Augmentation with Simultaneous Implant Placement in the Atrophic Maxilla. A Report of 10 Cases", *Journal of Periodontology*, Volume 71, Issue 7, pp. 1187-1194, 2000.

61. Yamamoto, T., T. Onga, T. Marui, and K. Mizuno, "Use of Hydroxyapatite to Fill Cavities after Excision of Benign Bone Tumours - Clinical Results", *The Journal of Bone and Joint Surgery*, Volume 82B, Issue 8, pp. 1117-1120, 2000.

62. Reddy R. and M. K. S. Swamy, "The Use of Hydroxyapatite as a Bone Graft Substitute in Orthopaedic Conditions", *Indian Journal of Orthopaedics*, Volume 39, Issue 1, pp. 52-54, 2005.

63. Natarajan, M., R. Dhanapal, S. Kumarawel, J. Hussain, R. Selvaraj, and N. R. Uvaraj, "The Use of Bovine Calcium-Hydroxy-Apatite in Filling Defects Following Curettage of Benign Bone Tumours", *Indian Journal of Orthopaedics*, Volume 37, Issue 3, pp. 15 , 2003.

64. De Almeida, C. C., L. A. Sena, M. Pinto, C. A. Muller, J. H. C. Lima, and G. de Almeida Soares, "In Vivo Characterization of Titanium Implants Coated with Synthetic Hydroxyapatite by Electrophoresis", *Brazilian Dental Journal*, Volume 16, Issue 1, pp 75-81 , 2005.

65. Darimont, G. L., R. Cloots, E. Heinen, L. Seidel, and R. Legrand, "In Vivo Behaviour of Hydroxyapatite Coatings on Titanium Implants: A Quantitative Study in the Rabbit", *Biomaterials*, Volume 23, Issue 12, pp. 2569-2575, 2002.

66. De Sena, L. A., M. C. de Andrade, A. M. Rossi, and G. de Almeida Soares, "Hydroxyapatite Deposition by Electrophoresis on Titanium Sheets with Different Surface Finishing", *Journal of Biomedical Materials Research Part B: Applied Biomaterials*, Volume 60, Issue 1, pp. 1-7, 2002.

67. Ma, J., C. H. Liang, L. B. Kong, and C. Wang, "Colloidal Characterization and Electrophoretic Deposition of Hydroxyapatite on Titanium Substrate", *Journal of Materials Science: Materials in Medicine*, Volume 14, Issue 9, pp. 797-801, 2003.

68. Gomez-Vega, J.M., E. Saiz, A. P. Tomsia, T. Oku, K. Suganuma, G. W. Marshall, and S. J. Marshall, "Novel Bioactive Functionally Graded Coatings on Ti6Al4V", *Advanced Materials*, Volume 12, Issue 12, pp. 894-898, 2000.

69. Stoch, A., A. Brozek, S. Blazewicz, W. Jastrzebski, J. Stoch, A. Adamczyk and I. Roj, "FTIR Study of Electrochemically Deposited Hydroxyapatite Coatings on Carbon Materials", *Journal of Molecular Structure*, Volumes 651-653, pp. 389-396, 2003.

70. Bharati, S., M. K. Sinha, and D. Basu, "Hydroxyapatite Coating by Biomimetic Method on Titanium Alloy Using Concentrated SBF", *Bulletin of Materials Science*, Volume 28, Issue 6, pp. 617-621, 2005.

71. Shirkhanzadeh, M., "Bioactive Calcium Phosphate Coatings Prepared by Electrodeposition", *Journal of Materials Science Letters*, Volume 10, Issue 23, pp. 1415-1417, 1991.

72. Redepenning, J. and J. P. Mc Isaac, "Electrocrystallization of Brushite Coatings on Prosthetic Alloys", *Chemistry of Materials*, Volume 2, Issue 6, pp. 625-627, 1990.

73. Royer, P. and C. Rey, "Calcium Phosphate Coatings for Orthopaedic Prosthesis", *Surface and Coatings Technology*, Volume 45, Issues 1-3, pp. 171-177, 1991.

74. Melvin, M., *Electrophoresis, Analytical Chemistry by Open Learning*, John Wiley & Sons, New York, USA, 1987.

75. Wang, C., J. Ma, W. Cheng, and R. Zhang, "Thick Hydroxyapatite Coatings by Electrophoretic Deposition", *Materials Letters*, Volume 57, Issue 1, pp. 99-105, 2002.

76. Heavens, S. N., "Electrophoretic Deposition as a Processing Route for Ceramics", J. G. P. Binner (ed.), *Advanced Ceramic Processing and Technology*, Volume 1, pp. 255-283, Noyes Publications, New Jersey, USA, 1990.

77. Martin-Molina, A., M. Quesada-Peres, F. Galisteo-Gonzales, and R. Hidalgo-Alvarez, "Primitive Models and Electrophoresis: An Experimental Study", *Colloids and Surfaces A. Physicochemical and Engineering Aspects*, Volume 222, Issues 1-3, pp. 155-164, 2003.

78. Windes, W. E., J. Zimmerman, and I. E. Reimanis, "Electrophoretic Deposition Applied to Thick Metal-Ceramic Coatings", *Surface and Coatings Technology*, Volume 157, Issues 2-3, pp. 267-273, 2002.

79. Shaw, D. J., *Introduction to Colloid & Surface Chemistry*, Reed Educational and Professional Publishing, New York, USA, 1992.

80. Kopeliovich, D., "Stabilization of Colloids", http://www.substech.com/dokuwiki/doku.php?id=stabilization_of_colloids, 2011.

81. Ma. J., C. Wang, and K. W. Peng, "Electrophoretic Deposition of Porous Hydroxyapatite Scaffold", *Biomaterials*, Volume 24, Issue 20, pp. 3505-3510, 2003.

82. Van der Biest, O., S. Put, G. Anne, and J. Vleugels, "Electrophoretic Deposition for Coating and Free Standing Objects", *Journal of Materials Science*, Volume 39, Issue 3, pp. 779-785, 2004.

83. Wei, M., A. J. Ruys, B. K. Milthorpe, C. C., J. H. Evans, and Sorrell, "Electrophoretic Deposition of Hydroxyapatite Coatings on Metal Substrates: A Nanoparticulate Dual-Coating Approach", *Journal of Sol-Gel Science and Technology*, Volume 21, Issues 1-2, pp. 39-48, 2001.

84. Meng, X., T. Y. Kwon, Y. Yang, J. L. Ong, and K. H. Kim, "Effects of Applied Voltages on Hydroxyapatite Coating of Titanium by Electrophoretic Deposition", *Journal of Biomedical Materials Research Part B: Applied Biomaterials*, Volume 78B, Issue 2, pp. 373–377, 2006.

85. Chen, F., W. M. Lam, C. J. Lin, G. X. Qiu, Z. H. Wu, K. D. K. Luk and W. W. Lu, "Biocompatibility of Electrophoretical Deposition of Nanostructured Hydroxyapatite Coating on Roughen Titanium Surface: In Vitro Evaluation Using Mesenchymal Stem Cells", *Journal of Biomedical Materials Research B Applied Biomaterials*, Volume 82, Issue 1, pp. 183-191, 2007.

86. Sridhar, T. M., U. Kamachi Mudali, and M. Subbaiyan, "Sintering Atmosphere and Temperature Effects on Hydroxyapatite Coated Type 316L Stainless Steel", *Corrosion Science*, Volume 45, Issue 10, pp. 2337-2359, 2003.

87. Javidi, M., S. Javadpour, M. E. Bahrololoom, and J. Ma, "Electrophoretic Deposition of Natural Hydroxyapatite on Medical Grade 316L Stainless Steel", *Materials Science and Engineering C*, Volume 28, Issue 8, pp. 1509-1515, 2008.

88. Mondragon-Cortez, P. and G. Vargas-Gutierrez, "Electrophoretic Deposition of Hydroxyapaite Submicron Particles at High Voltages", *Materials Letters*, Volume 58, Issues 7-8, pp. 1336-1339, 2004.

89. Zhitomirsky, I. and L. Gal-Or, "Electrophoretic Deposition of Hydroxyapatite", *Journal of Materials Science: Materials in Medicine*, Volume 8, Issue 4, pp. 213-219, 1997.

90. Ducheyne, P., P. D. Bianco, and C. Kim, "Bone Tissue Growth Enhancement by Calcium Phosphate Coatings on Porous Titanium Alloys: The Effect of Shielding Metal Dissolution Product", *Biomaterials*, Volume 13, Issue 9, pp. 617-624, 1992.

91. Albayrak, O., C. Oncel, M. Tefek, and S. Altintas, "Effects of Calcination on Electrophoretic Deposition of Naturally Derived and Chemically Synthesized Hydroxyapatite", *Review on Advanced Materials Science*, Volume 15, pp. 10-15, 2007.

92. Albayrak, O., O. El-Atwani, and S. Altintas, "Hydroxyapatite Coating on Titanium Substrate by Electrophoretic Deposition Method: Effects of Titanium Dioxide Inner Layer on Adhesion Strength and Hydroxyapatite Decomposition", *Surface and Coatings Technology*, Volume 202, Issue 11, pp. 2482-2487, 2008.

93. Ravaglioli, A. and A. Krajewski, *Bioceramics: Materials, Properties, Applications*, Chapman & Hall, London, UK, 1992.

94. Talaro, K. P. and A. Talaro, *Foundations in Microbiology*, 4th Ed., McGraw-Hill, New York, USA, 1992.

95. Tortora, G. J., B. R. Funke, and C. L. Case, *Microbiology An Introduction*, 10th Ed. Pearson Education Inc., San Francisco, USA, 2010.

96. Ingraham, J. L. and C. A. Ingraham, *Introduction to Microbiology: A Case-History Study Approach*, 3rd Ed., Brooks/Cole, Kentucky, USA, 2003.

97. Hudson, M. C., W. K. Ramp, and K. P. Frankenburg, "Staphylococcus Aureus Adhesion to Bone Matrix and Bone-Associated Biomaterials", *FEMS Microbiology Letters*, Volume 173, Issue 2, pp. 279-284, 1999.

98. Kitano, T., Y. Yutani, A. Shimazu, I. Yano, H. Ohashi, and Y. Yamano, "The Role of Physicochemical Properties of Biomaterials and Bacterial Cell Adhesion In Vitro", *The International Journal of Artificial Organs*, Volume 19, Issue 6, pp. 353-358, 1996.

99. An, Y. H. and R. J. Friedman, "Concise Review of Mechanisms of Bacterial Adhesion to Biomaterial Surfaces", *Journal of Biomedical Materials Research*, Volume 43, Issue 3, pp. 338-48, 1998.

100. Katsikogianni, M. and Y.F. Missirlis, "Concise Review of Mechanisms of Bacterial Adhesion To Biomaterials and of Techniques Used in Estimating Bacteria Material Interactions", *European Cells and Materials*, Volume 8, pp. 37-57, 2004.

101. Reid, C., "Biofilms in Infectious Disease and on Medical Devices", *International Journal of Antimicrobial Agents*, Volume 11, Issue 3, pp. 223-226, 1999.

102. Woodson, L. P., *Biofilm Reduction Sterilizer*, United States Patent No. 6,004,438, 1999.

103. Lee, I. S., C. N. Whang, K. S. Oh, J. C. Park, K. Y. Lee, G. H. Lee, S. M. Chung, and X. D. Sun, "Formation of Silver Incorporated Calcium Phosphate Film for Medical Applications", *Nuclear Instruments and Methods in Physics Research B*, Volume 242, pp. 45-47, 2006.

104. Chen, W., S. Oh., A. P. Ong, N. Oh, Y. Liu, H. S. Courtney, M. Appleford, and J. L. Ong, "Antibacterial and Osteogenic Properties of Silver-Containing Hydroxyapatite Coatings Produced Using a Sol-Gel Process", *Journal of Biomedical Materials Research Part A*, Volume 82, Issue 4, 899-906, 2007.

105. Feng, Q.L. and F. Z. Cui, "Ag-Substituted Hydroxyapatite Coatings with Both Antimicrobial Effects and Biocompatibility", *Journal of Materials Science Letters*, Volume 18, Issue 7, pp. 559-561, 1999.

106. Kim, T. N., Q. L. Feng, J. O. Kim, J. Wu, H. Wang, G. C. Chen, and F. Z. Cui, "Antimicrobial Effects of Metal Ions (Ag+, Cu2+, Zn2+) in Hydroxyapatite", *Journal of Materials Science: Materials in Medicine*, Volume 9, Issue 3, pp. 129-134, 1998.

107. Han, D. W., M. S. Lee, M. H. Lee, M. Uzawa, and J. C. Park, "The Use of Silver-Coated Ceramic Beads for Sterilization of Sphingonomas sp. in Drinking Mineral Water", *World Journal of Microbiology & Biotechnology*, Volume 21, Issues 6-7, pp. 921-924, 2005.

108. Nishioka, M, T. Nishimura, and M. Taya, "Kinetic Evaluation of Bactericidial Activity of Silver-Loaded Zirconium Phosphate Combined with Hydroxyapatite in the Presence of Chloride Ion", *Biochemical Engineering Journal*, Volume 20, Issue 1, pp. 79-84, 2004.

109. Feng, Q. L., J. Wu, G. Q. Chen, F. Z. Cui, T. N. Kim, and J. O. Kim, "A Mechanistic Study of the Antibacterial Effect of Silver Ions on Escherichia Coli and Staphylococcus Aureus", *Journal of Biomedical Materials Research*, Volume 52, Issue 4, pp. 662-668, 2000.

110. Scales, J. T. and M. J. Wilkinson, *Antimicrobial Surgical Implants*, United States Patent No. 4,615,705, 1986.

111. Faust, R. A., *Toxicity Summary for Silver*, Oak Ridge National Laboratory, December 1992.

112. Asmus, S. M. F., S. Sakakura, and G. Pezzotti, "Hydroxyapatite Toughened by Silver Inclusions", *Journal of Composite Materials*, Volume 37, Issue 23, pp. 2117-2129, 2003.

113. Zhang, X., G. H. M. Gubbels, R. A. Terpstra, and R. Metselaar, "Toughening of Calcium Hydroxyapatite with Silver Particles", *Journal of Materials Science*, Volume 32, Issue 1, pp. 235-243, 1997.

114. Manjubala, I. and T. S. Sampath Kumar, "Effect of TiO2-Ag2O Additives on the Formation of Calcium Phosphate Based Functionally Graded Bioceramics", *Biomaterials*, Volume 21, Issue 9, pp. 1995-2002, 2000.

115. Shirkhanzadeh, M. and M. Azadegan, "Formation of Carbonate Apatite on Calcium Phosphate Coatings Containing Silver Ions", *Journal of Materials Science: Materials in Medicine*, Volume 9, Issue 7, pp. 385-391, 1998.

116. Yang, L., X. Ning, Q. Xiao, K. Chen, and H. Zhou, "Development and Characterization of Porous Silver-Incorporated Hydroxyapatite Ceramic for Separation and Elimination of Microorganisms", *Journal of Biomedical Materials Research Part B: Applied Biomaterials*, Volume 81, Issue 1, pp. 50-56, 2007.

117. Onay, A. S., *Production of Ni-Zn Ferrite Transformer Cores*, M.S. Thesis, Bogazici University, 2002.

118. ASTM Standard F1044-99, *Standard Test Method for Shear Testing of Calcium Phosphate Coating and Metallic Coatings*, American Society for Testing and Materials, 1999.

119. Bouyer, E., F. Gitzhofer, and M. I. Boulos, "Morphological Study of Hydroxyapatite Nanocrystal Suspension", *Journal of Materials Science: Materials in Medicine*, Volume 11, Issue 8, pp. 523-532, 2000.

120. Santos, M. H., M. de Oliviera, L. P. de Freitas Souza, H. S. Mansur, and W. L. Vasconcelos, "Synthesis Control and Characterization of Hydroxyapatite Prepared by Wet Precipitation Process", *Materials Research*, Volume 7, Issue 4, pp. 625-630, 2004.

121. Gibson, I. R., S. M. Best, W. Bonfield, "Chemical Characterisation of Silicon-Substituted Hydroxyapatite", *Journal of Biomedical Materials Research*, Volume 44, Issue 4, pp. 422-428, 1999.

122. Manafi, S. A., B. Yazdani, M. R. Rahimiopour, S. K. Sadrnezhaad, M. H. Amin, and M. Razavi, "Synthesis of Nano-Hydroxyapatite under a Sonochemical /Hydrothermal Condition", *Biomedical Materials*, Volume 3, Issue 2, Article ID 025002, DOI:10.1088/1748-6041/3/2/025002, 2008.

123. Stoch, A., W. Jastrzebski, A. Brozek, B. Trybalska, M. Cichocinska, E. Szarawara, "FTIR Monitoring of the Growth of the Carbonate Containing Apatite Layers from Simulated and Natural Body Fluids", *Journal of Molecular Structure*, Volumes 511-512, pp. 287-294, 1999.

124. Phillips, M. J., J. A. Darr, Z. B. Luklinska, I. Rehman, "Synthesis and Characterization of Nano-Biomaterials with Potential Osteological Applications", *Journal of Materials Science: Materials in Medicine*, Volume 14, Issue 10, pp. 875-882, 2003.

125. Nayak, Y., R. Rana, S., S. Pratihar, and S. Bhattacharyya, "Low-Temperature Processing of Dense Hydroxyapatite-Zirconia Composites", *International Journal of Applied Ceramic Technology*, Volume 5, Issue 1, pp. 29-36, 2008.

126. Pramanik, N., D. Mishra, I. Banerjee, T.apas K. Maiti, P. Bhargava, and P. Pramanik, "Chemical Synthesis, Characterization, and Biocompatibility Study of Hydroxyapatite/Chitosan Phosphate Nanocomposite for Bone Tissue Engineering Applications", *International Journal of Biomaterials*, Volume 2009, Article ID 512417, DOI:10.1155/2009/512417, 2009.

127. Kumar, A. P., K. K. Mohaideen, S. A. S. Alariqi, and R. P. Singh, "Preparation and Characterization of Bioceramic Nanocomposites Based on Hydroxyapatite (HA) and Carboxymethyl Cellulose (CMC)", *Macromolecular Research*, Volume 18, Issue 12, pp. 1160-1167, 2010.

128. Kannan, S., J. M. G. Ventura, A. F. Lemos, A. Barba, and J. M. F. Ferreira, "Effect of Sodium Addition on the Preparation of Hydroxyapatites and Biphasic Ceramics", *Ceramics International*, Volume 34, Issue 1, pp. 7-13, 2008.

129. Fellah, B. H., and P. Layrolle, "Sol–Gel Synthesis and Characterization of Macroporous Calcium Phosphate Bioceramics Containing Microporosity", *Acta Biomaterialia*, Volume 5, Issue 2, pp. 735-742, 2009.

130. Reyes-Gasga, J., R. Garcia-Garcia, M. J. Arellano-Jimenez, E. Sanchez-Pastenes, G. E. Tiznado-Orozco, I. M. Gil-Chavarria, and G. Gomez-Gasga, "Structural and Thermal Behaviour of Human Tooth and Three Synthetic Hydroxyapatites from 20 to 600 °C", Journal of Physics D: Applied Physics, Volume 41, Issue 22, Article ID 225407, DOI:10.1088/0022-3727/41/22/225407, 2008.

REFERENCES NOT CITED

Clark, D. E., D. C. Folz, C. E. Folgar, and M. M. Mahmoud (Ed.), *Microwave Solutions for Ceramic Engineers*, The American Ceramic Society, Ohio, USA, 2005.

El-Soufi, W. M. A., *Bacterial Adhesion to Solid Surfaces and Its Prevention by the Application of Silver*, M.S. Thesis, Bogazici University, 2001.

Fung, Y. C., N. Perrone, and M. Anliker (Ed.), *Biomechanics Its Foundations and Objectives*, Prentice-Hall Inc., New Jersey, USA, 1972.

Gan, L., *Calcium Phosphate Sol-Gel-Derived Coatings on Ti6Al4V Substrate for Biomedical Applications*, Ph.D. Thesis, University of Toronto, 2003.

Namazu, T., S. Inoue, D. Ano, and K. Koterazawa, "Direct Measurement Technique of Strain in XRD Tensile Test for Evaluating Poisson's Ratio of Micron-Thick TiN Films", *Proceedings of the 17th IEEE International Conference on Micro Electro Mechanical Systems (MEMS)*, pp. 157-160, DOI: 10.1109/MEMS.2004.1290546, 2004.

Park, J. B., *Biomaterials Science and Engineering*, Plenum Press, New York, USA, 1984.

Prescott, L. M., J. P. Harley, and D. A. Klein, *Microbiology*, 5th Ed., McGraw-Hill, Ohio, USA, 2002.

Reed, J. S., *Introduction to the Principles of Ceramic Processing*, John Wiley & Sons, New York, USA, 1987.

Shrivastava, S. (Ed.), *Medical Device Materials*, ASM International, Ohio, USA, 2004.

Tredwin, C. J., *Sol-Gel Derived Hydroxyapatite, Fluorhydroxyapatite and Fluorapatite Coatings for Titanium Implants*, Ph.D. Thesis, University College London, 2009.